THE SCATTERING OF HIGH FREQUENCY ELECTROMAGNETIC RADIATION FROM THE OCEAN SURFACE: AN ANALYSIS BASED ON A BISTATIC GROUND WAVE RADAR CONFIGURATION

ERIC WILLIAM GILL

The Scattering of High Frequency Electromagnetic Radiation from the Ocean Surface: An Analysis Based on a Bistatic Ground Wave Radar Configuration

by

©Eric William Gill, B.Sc., B.Ed., M.Eng.

A thesis submitted to the School of Graduate Studies

in partial fulfillment of the requirements for the

degree of Doctor of Philosophy

Faculty of Engineering and Applied Science

Memorial University of Newfoundland

January, 1999

St. John's Newfoundland Canada

Abstract

The scattering of high frequency (HF) radiation from rough surfaces is addressed with a view to developing bistatic cross sections of the ocean surface. The analysis starts with an expression for the normal component of the electric field in the form of a two-dimensional spatial convolution involving the spatially Fourier transformed source field and the appropriate Green's function for the region of interest. This expression is reduced to integrals which are analyzed to second order in scatter. The reception point of the scattered field is kept general, and, initially, the good-conducting, slightly rough surface is chosen to be time invariant. The excitation of the assumed vertical dipole source is also kept general at the outset. Reduction of the resulting integrals is accomplished primarily via asymptotic techniques.

The analysis leads to a first-order field component and a second-order solution consisting of three separate components. The latter account for (1) double scattering from a surface region remote from both the source and the receiver and (2) fields arising from single scattering near either the source or receiver which is followed or preceded, respectively, by a single remote scatter. These bistatic forms are shown to reduce to existing monostatic results with the introduction of the appropriate scattering configuration.

Using the general field expressions, the source is next specified to be a vertical dipole with a pulsed sinusoidal excitation. This is done with a view to extending the analysis to obtain bistatic cross section expressions for the ocean surface when interrogation is carried out with a pulsed radar. Before this can be accomplished, time variation for the randomly rough surface is also introduced into the model. It is assumed that the surface varies much less slowly than the time necessary to obtain a single measurement of the scattered field.

The HF bistatic Doppler cross section of the time varying surface is effected via Fourier transformation of the ensemble-averaged electric field and subsequent com-

parison with the radar range equation. This standard technique gives first- and second-order cross section models which are calculated and depicted by introducing an appropriate directional representation of the ocean spectrum. It is shown that all of the essential characteristics of the previous monostatic formulations are contained in these cross sections as a special case.

Finally, a technique is developed for modelling the expected pulse radar spectrum when signal reception is externally noise limited. It is assumed that both the ocean echo and noise voltage may be represented as zero-mean Gaussian random variables. The resulting models are shown to compare very favourably with available monostatic spectra.

The bistatic cross sections and the noise model for pulsed HF radar provide a means of setting the appropriate specifications of particular systems which may be used for ocean surface parameter estimation. Additionally, the properties of the scattering as manifested in the theory should be relevant to further developments of clutter suppression schemes for use in hard-target detection.

Acknowledgements

The author wishes to thank the Faculty of Engineering and Applied Science for affording him the opportunity of conducting this work. Particularly, the supervision provided by Dr. John Walsh and the interest and patience which he has shown throughout the research period have been singular. His suggestions and insights regarding the fundamentals of this topic have been invaluable. The approach to independent study which he has sought to instill, I believe, was not only an encouragement for the task at hand but should prove very useful in future research stemming from the ideas developed here.

Also, Supervisory Committee members, Drs. Jim Helbig and Rafaat Khan, are to be commended for their agreement to critically review this document. At the early stages, discussions with Dr. Khan gave the author opportunity to air ideas related to the general character of the work at hand.

Present and former personnel of Northern Radar Systems Limited, St. John's have all been a help at various stages of this work. The author's software and hardware enquiries and demands were well attended to by Desmond Power, Sherri-Lynn Lewis, Bill Hunt, and Barry Dawe. Former president, Fraser Eaton, and current president, Barry Dawe, are to be thanked for the company's support of the research by providing office space and supplies.

The author is grateful to the administration of the College of the North Atlantic (formerly, Cabot College) for granting two years of unpaid Educational Leave so that the ongoing research could be completed.

This effort was supported by (1) a two-year Graduate Award from the Career Development Fund overseen by the provincial Department of Career Development and Advanced Studies and (2) graduate student support from a Natural Sciences and Engineering Research Council (NSERC) Grant to Dr. John Walsh.

Finally, this work could not have been completed without the unfailing patience,

understanding, and support of the author's wife, Susan, and family, Nicola and Erika. In particular, Susan's extensive effort in LaTeXing a major portion of the original manuscript and her subsequent detailed initial proofreading have been crucial in bringing a timely conclusion to the project.

Contents

List of Figures

Table of Symbols

The page numbers here indicate the place of first significant reference. There are numerous symbols used throughout the text other than those given below. For example, associated with the bistatic scattering problem, there are many displacement parameters required. These appear as $\vec{\rho}$'s with various subscripts. Their directions are similarly subscripted θ's. The early ones are given in this table as examples, but many of the others are not explicitly referenced. However, the definitions of these variables and others are obvious from the context.

σ° : Peake's average scattering cross section for a slightly rough surface (p. 8).

$z = \xi(x, y)$: Two-dimensionally rough (i.e in x and y directions) surface (p. 15).

$h(\cdot)$: Heaviside function (p. 16).

σ , σ_0 : Conductivities above and below (or on) the rough surface, respectively (p. 16).

ϵ : Electrical permittivity (p. 16).

ϵ_0 , ϵ_1 : Permittivities above (free space) and below (or on) the rough surface, respectively (p. 16).

$\vec{\nabla}$: $\hat{x}\frac{\partial}{\partial x} + \hat{y}\frac{\partial}{\partial y} + \hat{z}\frac{\partial}{\partial z}$ with the hat vectors being the unit vectors along the coordinate axes (p. 17).

t : Time (p. 17).

$\vec{E}$: Electric field vector (p. 17).

$\sqrt{j}$: $\sqrt{-1}$ (p. 17).

ω : Angular frequency of the electric field (p. 17).

$\vec{B}$: Magnetic flux density (p. 17).

$\vec{H}$: Magnetic field intensity (p. 17).

$\vec{D}$: Electric flux density (p. 17).

$\vec{J}$: Current density including conduction currents $\left(\vec{J}_c\right)$ and source currents $\left(\vec{J}_s\right)$ (p. 17).

ρ : Charge density (p. 17).

μ_0 : Magnetic permeability for entire space (p. 17).

k : Radiation wavenumber $(= \omega\sqrt{\mu_0\epsilon_0})$ (p. 17).

η_r : Refractive index of the scattering medium (p. 17).

γ_0^2 : $k^2\left[h + (1-h)\eta_r^2\right]$ (p. 17).

$\vec{n}$: Normal of magnitude $|\vec{n}|$ to the surface in direction of increasing z (p. 17).

$\delta(\cdot)$: Dirac delta function (p. 17).

T_{sE} : Electrical source operator $\left(\frac{1}{j\omega\epsilon_0}\left[\vec{\nabla}\left(\vec{\nabla}\cdot\right) + k^2\right]\right)$ (p. 17).

$\vec{E}^+$: Electric field immediately above the surface (p. 17).

$\frac{e^{-jkr}}{4\pi r}$, $\frac{e^{-j\gamma r}}{4\pi r}$: Green's functions above and below the surface, respectively, with $r = \sqrt{x^2+y^2+z^2}$ and $\gamma^2 = k^2\eta_r^2$ (p. 18).

$\frac{\partial}{\partial n}$: Partial derivative with respect to the surface normal (p. 18).

$\vec{K}$: Surface wave vector of magnitude K and planar components K_x and K_y (p. 18).

$\underline{\vec{E}}_s(K_x, K_y)^{z^-}$: Free space source field Fourier transformed in the plane $z = z^- < \xi(x, y)$ (p. 19).

G : Free space Green's function (p. 19).

$\vec{\nabla}_{xy}$: $\hat{x}\frac{\partial}{\partial x} + \hat{y}\frac{\partial}{\partial y}$ (p. 19).

u : $\begin{cases} \sqrt{K^2 - k^2}, & \text{for real roots} \\ j\sqrt{k^2 - K^2}, & \text{for imaginary roots (p. 19).} \end{cases}$

R^+ : A function of the $\vec{E}^+$ field as defined on p. 19.

$\underline{I}$: Identity matrix (p. 20).

$\sum$: Summation symbol (p. 20).

T_1 , T_2 : Electric field operators (pp. 21–22).

$\vec{E}_m^+$: m^{th} order of the field $\vec{E}^+$ where $m = 0, 1, 2, \ldots$ (p. 22).

$\hat{n}$: Unit normal to the scattering surface (p. 23).

$F(\rho)$: Sommerfeld attenuation function with $\rho = \sqrt{x^2 + y^2}$ (p. 23).

$\overset{xy}{*}$: Two-dimensional spatial convolution symbol (p. 23).

$\mathcal{F}_{xy}^{-1}$: Two-dimensional spatial inverse Fourier transform (p. 23).

$(E_{0_n}^+)_1$: First order of the normal component of E_0^+. The next two orders are $(E_{0_n}^+)_2$ and $(E_{0_n}^+)_3$ (p. 23).

$\Delta\rho$: Width of a scattering patch for a pulsed radar (monostatic) (p. 25).

ξ_{rms} : Total root mean square waveheight of scattering surface (p. 30).

E^s : Magnitude of the propagating field without scatter (p. 32).

$\mathcal{T}_1$, $\mathcal{T}_2$: Field operators as defined on p. 32.

I : Arbitrary source current (p. 32).

$\Delta\ell$: Length of vertical dipole (p. 32).

$C_0\left(=\frac{I\Delta\ell k^2}{j\omega\epsilon_0}\right)$: Dipole constant in the temporal Fourier transform domain (p. 32).

U : Wind speed in m/s (p. 33).

g : Gravitational acceleration ($= 9.8$ m/s^2) (p. 33).

Δ : Surface impedance of a smooth plane (p. 34).

$\vec{\rho}_1$, $\vec{\rho}_2$: Displacements associated with the first-order scatter (p. 35).

N : Fundamental surface wavenumber $\left(=\frac{2\pi}{L}\right)$ where L is the fundamental spatial period (p. 35).

P_{mn} : Fourier coefficient of a surface component whose wave vector is $\vec{K}_{mn} = Nm\hat{x} + Nn\hat{y}$ (p. 36).

$P_{\vec{K}_{mn}}$: Same as P_{mn} (p. 36).

θ_{mn} : Direction of $\vec{K}_{mn}$ (p. 36).

θ_1 : Direction of $\vec{\rho}_1$ (p. 36).

θ : Direction of $\vec{\rho}$ as measured from transmitter to receiver (p. 36).

(μ, δ) : Elliptical coordinates (p. 38).

I_j : Various intermediate integrations and convolutions in the electric field equations. The j takes different forms, its first being "δ" (p. 39).

$\vec{N}$, $\vec{T}$: Normal and tangent vectors, respectively, to the scattering ellipse, and θ_N is the direction of $\vec{N}$ (p. 40).

ϕ : Bistatic angle (p. 41).

ρ_s : $\frac{\rho_1 + \rho_2}{2}$ where ρ_1 and ρ_2 are given on p. 35 (p. 41).

$\vec{K}_{pq}$: Wave vector of surface component analogous to $\vec{K}_{mn}$ (p. 46).

$\Phi_j(\mu, \delta)$: Functions used in the stationary phase analyses of the second-order electric fields. The j is dependent on the particular field component under consideration, its first value being "12" (p. 47).

$\gamma_{E12F,1}$: Preliminary electromagnetic coupling coefficient for patch scatter (p. 54).

$\vec{K}_{rs}$: Sum $\left(\vec{K}_{mn} + \vec{K}_{pq}\right)$ of the scattering wave vectors whose direction is θ_{rs} (p. 55).

$\hat{N}$: Unit normal to the scattering ellipse (p. 57).

$\gamma_{E12F,2}$: Preliminary electromagnetic coupling coefficient involving scatter at the transmitter (p. 61).

$\gamma_{E12B,1}$: Preliminary electromagnetic coupling coefficient involving scatter at the receiver (p. 70).

c : Free space speed of light $= 3 \times 10^8$ m/s (p. 77).

η_0 : Intrinsic impedance of free space (p. 77).

$\mathcal{F}$, $\mathcal{F}^{-1}$: Temporal Fourier transform and its inverse (p. 77).

I_0 : Peak current on a pulsed dipole (p. 78).

ω_0 : Angular (radian) frequency of a pulsed sinusoid (p. 78).

τ_0 : Transmit pulse length (p. 78).

$k_0 \left(= \frac{\omega_0}{c}\right)$: Wavenumber of the dipole excitation current (p. 78).

$\Delta\rho_s \left(= \frac{c\tau_0}{2}\right)$: Patch width as viewed by pulse radar (p. 81).

ϕ_0 : Representative value of the bistatic angle (p. 83).

${}_E\Gamma_P$: Revised electromagnetic coupling coefficient for "patch" scatter (p. 86).

t_0 : A time which determines a particular scattering ellipse (p. 86).

${}_E\Gamma_T$: Revised electromagnetic coupling coefficient involving scatter at the transmitter (p. 88).

${}_E\Gamma_R$: Revised electromagnetic coupling coefficient involving scatter at the receiver (p. 89).

$W\left(\frac{2\pi}{T}\right)$: Fundamental radian frequency of the surface with T being the fundamental period (p. 95).

$P_{\vec{K},\omega}$: Random Fourier coefficient of the surface associated with the component whose wave vector is $\vec{K}$ and whose angular frequency is ω (p. 95).

$R(\cdot)$: Autocorrelation of the surface function (p. 96).

$< \cdot >$: Ensemble average (p. 96).

$S(\vec{K},\omega)$: Surface power spectral density (i.e. the surface spectrum) (p. 97).

λ_w : Ocean wavelengths (p. 98).

$S_1(\vec{K},\omega)$: First-order ocean wave spectrum (p. 99).

${}_1P_{\vec{K},\omega}$, ${}_2P_{\vec{K},\omega}$: First- and second-order surface Fourier coefficients (p. 100).

${}_H\Gamma$: Hydrodynamic coupling coefficient (p. 100).

$\mathcal{R}(\tau)$: Autocorrelation of the received electric field (p. 110).

A_r : Effective free space aperature of the receiving antenna (p. 110).

λ_0 : Free space wavelength of the transmitted signal (p. 110).

G_r : Free space gain of the receiving antenna (p. 110).

P_r^0 : Average received power (p. 110).

$\mathcal{P}(\omega_d)$: Doppler power spectral density of the received electric field where ω_d is the (radian) Doppler frequency (p. 111).

f_d : Doppler frequency in hertz $\left(= \frac{\omega_d}{2\pi}\right)$ (p. 112).

$_s\Gamma_P$: Symmetricized coupling coefficient for patch scatter (p. 116).

$\mathcal{K}$: Curvature of a smooth curve (p. 120).

$\hat{T}$: Unit tangent to a smooth curve at a distances s along the curve (p. 121).

ρ_c : Radius of curvature (p. 121).

dA : Elemental area of scattering surface (p. 122).

P_t : Transmitted power (p. 123).

G_t : Free space gain of the transmitting antenna (p. 123).

$\sigma(\omega_d)$: Doppler cross section per unit area of surface whose components are variously subscripted in equation (3.69) (pp. 122-123).

$G(\theta_{\vec{K}})$: Directional characteristic of the ocean surface (p. 127).

$S_J(K)$: JONSWAP spectrum (p. 127).

$S_F(K)$: JONSWAP fetch parameter (p. 127).

$S_{PM}(K)$: Pierson-Moskowitz spectrum (p. 128).

$\alpha_{PM}(K)$: Non-dimensional parameter in the Pierson-Moskowitz spectrum. Its value is 0.0081 (p. 128).

$s(K)$: Spread function for ocean wave directional characteristics (p. 129).

$\bar{\theta}$: Mean wind direction (p. 129).

Γ : Gamma function (p. 129).

ω_B : (Radian) Bragg frequency $(= \sqrt{2gk_0 \cos\phi_0})$ (p. 131).

B : Receiver bandwidth (p. 173).

$n_a(t)$: Ambient noise voltage as a function of time (p. 173).

$\epsilon(\omega')$: Random phase of frequencies in $n(t)$ (p. 173).

$S_N(\omega')$: Power spectral density of the ambient noise as a function of radian frequency, ω' (p. 173).

T_L : Pulse repetition period (p. 173).

$n(t)$: Noise voltage as observed by a pulse radar (p. 174).

$\mathcal{R}_{N_f}$: Noise autocorrelation of a finite pulse train (p. 174).

$\mathcal{P}_{N_f}$: Noise power spectral density of a finite pulse train (p. 174).

$d\left(=\frac{\tau_0}{T_L}\right)$: Radar duty cycle (p. 176).

$\mathcal{P}_N$: Noise power spectral density of an infinite pulse train (p. 179).

$\mathcal{R}_{N_{ns}}$: Autocorrelation for non-stationary noise (p. 187).

$\mathcal{P}_{N_{ns}}$: Power spectral density for non-stationary noise (p. 188).

$c_a(t)$: Ocean clutter signal (p. 192).

$S_c(\omega_c')$: Power spectral density of ocean clutter signal (p. 192).

B_c : Ocean clutter bandwidth (p. 192).

$\epsilon(\omega_c')$: Random phase of frequencies in $c_a(t)$ (p. 192).

$c(t)$: Gated ocean clutter signal (p. 193).

$\mathcal{P}_c$: Doppler power spectral density of gated ocean clutter signal (p. 193).

$(SNR)_c$: Clutter signal to noise ratio (p. 194).

f_a : External noise factor (p. 195).

T_0 : Reference temperature taken as 290 K (p. 195).

$k = 1.38 \times 10^{-23} J/K$: Boltzmann's constant (p. 195).

F_a : External noise figure ($= 10 \log f_a$) (p. 195).

F_{am} : Median external noise figure (p. 195).

d_s : Element spacing in receiving antenna (p. 197).

$BW_{\frac{1}{2}}$: Half-power beamwidth of receiving antenna (p. 197).

A : Scattering patch area (p. 197).

Chapter 1

Introduction

1.1 Research Rationale

An ever-increasing interest in marine-related enterprise is bringing with it a corresponding need to accurately and quickly provide comprehensive oceanographic information. A detailed description of the ocean surface would require knowledge of such parameters as directional wave height spectra, surface currents and wind fields. Consumers of this information encompass (1) scientists interested in the dynamics of the upper ocean and in environmental concerns; (2) governments defending national ocean-related interests; (3) search and rescue personnel; and (4) commercial and industrial users involved in navigation, renewable resource development (eg. fisheries operations), and non-renewable resource exploration and development (eg. the mining and petroleum industries).

Conventionally, oceanographic information has been provided by a variety of instruments including wave staffs, pressure sensors, wave buoys, current meters, and drogued and undrogued surface drifters. Wind data near the ocean surface has typically been provided by surface buoys and ships' anemometers. With the exception of drifters used for surface current measurement, these devices are limited to providing data from very small regions of ocean – i.e., they are essentially point sensors. In addition to this limitation, deployment, retrieval and data transmission, especially in rough seas when the required information may be most useful, can be both difficult

and expensive.

In recent decades, a variety of remote sensing techniques for ocean surface parameter estimation using radar have emerged. Microwave radars, limited to line-of-sight measurement, have been successful in providing information on spectral shape, dominant wave directions, wave periods, and, to some extent, surface currents (Tucker [1], Chapter 8). However, microwaves interact primarily with short ocean waves (wavelengths < 15 cm), while most of the wave energy is found in the much longer gravity wave portion of the spectrum (wavelengths of tens to hundreds of metres). Determining the energy content of these long waves by considering their modulation of the short waves has proven to be a very difficult process. As a result, producing calibrated wave energy spectra using microwave radar has not been achieved to date.

Over the last twenty years, high frequency (HF) radars, operating between 3 and 30 MHz, have been used to measure ocean surface characteristics. Unlike microwave systems, these radars are not limited to line-of-sight operation. They have been used successfully in both sky wave and ground wave modes to "look" well beyond the horizon. They have the potential for viewing thousands of square kilometres (eg. Gill *et al.*, [2]), even in single-site operations. The resolution of such systems when used in oceanic measurements is typically from a few hundred metres to a few kilometres, depending on the application. The wavelengths associated with HF electromagnetic (e-m) radiation are of the same order of magnitude as those of the ocean waves carrying the bulk of the spectral energy. The information mapped to the HF radar signal by the ocean surface therefore lends itself to interpretation more easily than is the case for microwaves.

As ocean waves are moving targets, they cause Doppler shifts in any radiation which is scattered from them. It is well known that the chief mechanism of the interaction between the incident e-m radiation and the ocean waves is that of Bragg scattering. This means that, for grazing incidence, the first-order interaction is between

the e-m wave and ocean waves of wavelength one-half that of the incident radiation. Second- and higher-order interactions also occur, but the effective mapping of the ocean spectrum to the radar spectrum is correspondingly more complicated. The nature of the scattered signal is known to depend on radar frequency, beam width, polarization and configuration (monostatic or bistatic). In order to determine ocean surface features from the scattered radiation, the scattering mechanism itself must be investigated. That is, the scattering cross section at HF for the ocean must be developed. The scattering cross section is defined as "that area which, when multiplied by the power flux density of the incident wave, would yield sufficient power that could produce by isotropic radiation, the same radiation intensity as that in a given direction from the scattering surface" [3]. In the case of the ocean, development of such a cross section is complicated by the random roughness of the surface.

As is indicated in Section 1.2, several formulations of the HF radar cross sections of random, slightly rough, surfaces already exist. However, extensive treatment has been carried out only for the case of co-location of transmitter and receiver – i.e. a *monostatic* (or backscatter) configuration. Such cross sections, in general, yield ambiguous directional information, this problem being overcome by using two or more complete radar installations. The development of the *bistatic* cross sections will provide a description of the scattering as viewed from a site remote from the source of the radiation (i.e. the transmitter and receiver are not co-located). For radar operation in a marine environment, such cross sections will provide meaningful relationships between the actual received signal for a bistatic configuration and the ocean surface conditions responsible for the scatter. This would mean that with a single transmitter and two widely separated receivers (one possibly at the transmit location) directional information could be obtained without the use of two full radar systems. Thus, an understanding of the bistatic scattering problem will provide a basis for facilitating a more economical way of measuring directional ocean surface characteristics. Ad-

ditionally, knowledge of the bistatic interaction mechanism will be essential to the development of bistatic clutter suppression schemes. Such algorithms, which already exist for monostatic operation [4], are important in hard-target detection and tracking when the targets being interrogated lie in regions of the radar spectrum which are highly contaminated with radiation scattered from the ocean surface.

The aim of this research is to address the fundamental scattering problems associated with bistatic operation of HF radars in an ocean setting. It is desired that the models formulated here should provide a foundation for future experimental investigations, not only of the ocean itself but also of targets of interest travelling on its surface.

1.2 Literature Review

The development of the radar cross-section of the ocean surface during the last two and one half decades has relied necessarily on existing theories of e-m scattering from rough surfaces. Classically, these theories have been grouped into two broad categories, namely, (1) perturbation and (2) the Kirchhoff (or tangent-plane) method. As is discussed below, combinations of these techniques have been implemented also.

Since the 1960's, other models of e-m scatter have begun to show promising applications. The most widely documented of these include (1) the composite-surface scattering or wave-facet model; (2) the full-wave technique and, most recently, (3) a generalized function approach, finding its roots in the work of Walsh [5]. Barrick's "unified modal representation" [6] has not been applied to two-dimensionally rough surfaces and is not addressed here.

Valenzuela [7] has provided a concise review of the classical models as well as the wave-facet model. The following sections provide a brief discussion of the various rough-surface scattering techniques listed above. Particular emphasis is placed on the Walsh developments ([5], [8], [9]) on which the research in this thesis is based.

Application papers relating these techniques to the ocean surface are also considered.

1.2.1 Perturbation

1.2.1.1 Methodologies

Perturbation scattering theory was presented by Lord Rayleigh (see Strutt, [10]) to investigate acoustic scattering from corrugated surfaces having a sinusoidal profile. This method, briefly reviewed below, was subsequently implemented by other investigators in the study of the scattering of planar e-m waves from statistically "slightly rough" surfaces. The condition of being "slightly rough" dictates that the product of the incident e-m radiation wavenumber (k) and any surface deviation, $\xi(x, y)$, from the mean must be very much less than unity (i.e., $k\xi << 1$).

Rice [11] presented an extensive perturbation methodology for e-m scattering from non-time-varying two-dimensionally-rough surfaces. The surface randomness is introduced by expanding a "real" two-dimensional surface, $\xi(x, y)$, periodic in both x and y, into a Fourier series in which the coefficients are taken to be independent random variables. The mean surface is taken to be planar, i.e. flat. The (x, y, z) scattered electric field ($\vec{E}$) components, resulting from plane wave incidence on such surfaces, are also written in series form. The terms of the latter represent discrete angular modes for the scattered field. The problem is to determine the coefficients of these modes. The coefficients of the components are related through the divergence relation, $\vec{\nabla} \cdot \vec{E} = 0$.

In order to solve for the coefficients of the various spectral terms, the electric field boundary condition must be imposed. For a perfectly conducting surface, as Rice treats initially, the condition is simply that the tangential component, $\vec{E}_T$, of $\vec{E}$ must be zero on the surface. Of course, it is through the boundary condition that the surface and its derivatives (or slopes), ξ_x and ξ_y, enter into the $\vec{E}$-field expressions. Rice retains only terms up to second order in $k\xi$ in the equations resulting from

$\vec{E}_T = 0$. As is the case for $k\xi$, it is assumed that ξ_x , $\xi_y << 1$. The coefficients of the spectral modes are expanded in a perturbational series, again up to second order. The first-order E_x and E_y coefficients are seen to follow immediately from the boundary conditions. These results are then used to obtain the next highest order, and so on. Using the E_x and E_y coefficients, the coefficients of E_z terms are obtained from the divergence relation.

Rice completed the analysis up to second order for a perfectly conducting surface for both horizontal and vertical polarization of the incident plane wave. Determining first the mean and then the variance of the scattered fields, Rice provided a kind of "roughness" spectrum for the scatter. In addition to the results for a perfectly conducting surface, he explicitly presented first-order scattered fields for the case of a horizontally polarized plane wave incident on a rough dielectric surface.

Wait [12] presented a perturbation technique for the case of reflection of a vertically polarized e-m plane wave from a two-dimensional periodic surface, rough in x only (i.e., $\xi(x)$ rather than $\xi(x,y)$). Initially, the angle of incidence is kept arbitrary. Beginning with an impedance boundary condition, sometimes referred to as the Leontovich boundary condition (see, for example, Ishimaru [13]) in which Wait used a surface impedance normalized to that of free space, the Rice procedure was followed. That is, a series expansion of the $\vec{E}$-field is substituted into the boundary condition and the coefficients, treated in a perturbational sense, are determined to second order. Using these coefficients, Wait also derived expressions for the "effective" normalized surface impedance for the case of specular reflection, with special emphasis on near-grazing incidence. Wait's results, consistent with corresponding formulae obtained by Rice [11] and Barrick [14], show that, even when a sinusoidal surface is perfectly conducting, the effective impedance of the surface will have a non-zero real part when the surface wavelength is greater than half the radiation wavelength.

The Barrick [14] analysis uses the same vein of argument as that of Rice. The

nature of the field is that of wave being "guided" by a rough, highly-conducting surface. The Rayleigh hypothesis, i.e. the assumption that the field can be represented in terms of only upgoing (away from the surface) waves, is invoked. Having developed expressions for the effective impedance, Barrick then makes application to propagation across the rough sea surface, examining the increased losses in the field due to sea state.

Rosich and Wait [15] extended and generalized Wait's [12] perturbation analysis to include all spectral orders of the scattered field. No upper limit was imposed on the perturbation order. Again, the analysis was limited to vertical polarization and a two-dimensional periodic surface, rough in one direction. The results were shown to be consistent with the analysis of the special cases, i.e. specular reflection and grazing incidence, examined earlier.

Mitzner [16] developed a general perturbation formulation for an arbitrarily shaped mean surface, as opposed to Rice's flat mean surface. The small height and slope assumptions are maintained. Mitzner writes the basic e-m field equations in terms of dyadic Green's functions and effective currents on the mean surface. These surface currents are determined by substituting the surface perturbation expansion, to second order, into the tangential boundary conditions. Once the dyadic Green's function for a particular geometrical configuration is found, the perturbed fields may be calculated. Mitzner gives dyadic Green's functions for the cases of an unbounded medium, a circular cylinder surrounded by another medium (and similarly for a sphere), and the half-space problem ($z < 0$ filled with one medium and $z > 0$ filled with another). While Mitzner gives the general formulation for these various cases, calculated fields are presented only for scattering from a cylinder with sinusoidal irregularities.

More recently, Rodríguez and Kim [17] have presented a so-called "unified perturbation expansion" for surface scattering. Starting with the "extinction theorem", a perturbation parameter is chosen such that the analysis becomes applicable to the

small height, small momentum transfer, and two-scale regimes (see Section 1.2.3). By invoking the small height approximation, the results reduce to those of the Rice method, and by splitting the surface into smooth and rough components, the analysis is shown to lead to the composite surface cross section (Section 1.2.3). The results of the second-order cross sections are seen to deteriorate as angle of incidence or surface height increases, especially for vertical polarization.

1.2.1.2 Applications of Perturbation to E-M Scattering from the Ocean

In principle, once the scattered fields have been calculated, radar cross sections of the scattering surface may be obtained. Peake [18] appears to have been the first to reduce Rice's [11] perturbation theory to the average scattering cross section, σ°, for a slightly rough surface. The general form of this cross section is

$$\sigma^\circ = 4\pi \frac{\text{average power scattered per unit solid angle per area of surface}}{\text{incident power at unit area of surface}} . \quad (1.1)$$

Peake's analysis was applied, in particular, to roadways and other random, slightly varying rough surfaces, as well as to surfaces with vegetation, characterized as thin lossy cylinders.

Valenzuela [19], as part of his investigation of the depolarization of e-m waves by slightly rough surfaces, developed a HF cross section of the sea surface to second order assuming a Neumann spectrum (Kinsman [20]) and a cosine-squared directional distribution for a fully developed sea wave regime.

Barrick [14], Part 2, on developing expressions for the effective surface impedance at grazing incidence, then makes application to propagation across the rough sea surface, examining the increased losses at HF and VHF (very high frequency) due to sea state. Continuing with the Rice [11] theory, Barrick [21] developed a first-order HF scattering cross section – the restrictions of the first-order perturbation theory are generally met by the sea surface when the e-m wave lies in the HF band. In carrying out this analysis, Barrick introduced the sea surface as a time-varying quantity

(i.e., $\xi(x, y, t)$ rather than simply $\xi(x, y)$). Barrick's results verified Crombie's [22] experimental deductions that Bragg scattering was the physical mechanism responsible for e-m scatter from the ocean surface. The effect on the received monostatic radar spectrum (eg., Figure 1.1) is to produce two large peaks at frequencies of $\pm\sqrt{2gk}$, where g is the acceleration due to gravity and k is the radio wavenumber. These shifts correspond uniquely with deviations which would be produced by ocean waves having lengths exactly one-half the radio wavelength and moving directly toward or away from the radar.

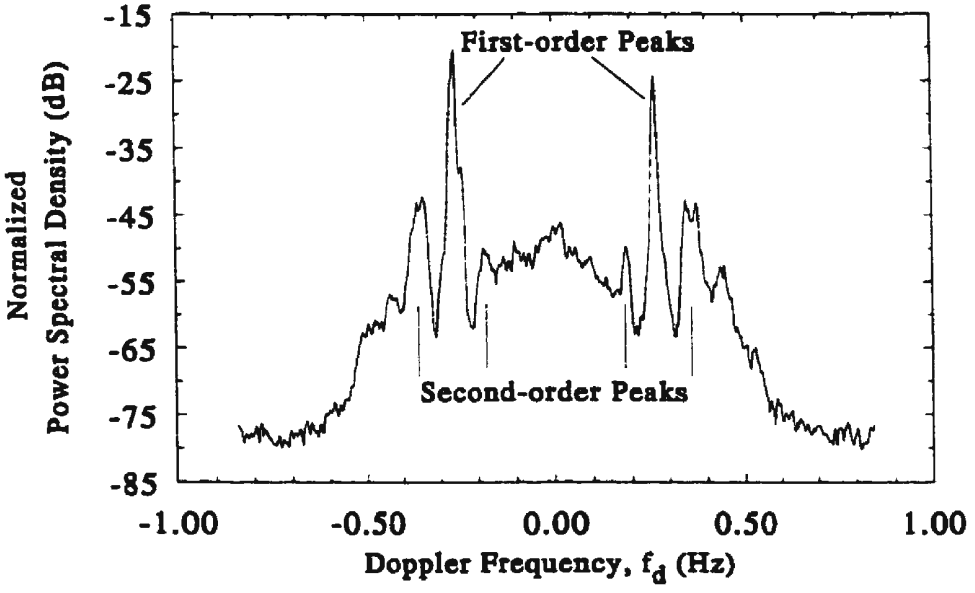

Figure 1.1: Typical monostatic HF ground wave radar spectrum. Operating frequency is 6.75 MHz.

Doppler spectra of e-m backscatter from the ocean, such as seen in Figure 1.1, invariably contain a continuum beyond and between the first-order Bragg peaks. Hasselmann [23] proposed that this continuum arises due to higher-order hydrodynamic and electromagnetic interactions. Then, Barrick [24], assuming vertical polarization and grazing incidence, derived expressions for the average second-order backscatter cross section and the first-order bistatic cross section. The second-order electromagnetic and hydrodynamic effects appeared in Barrick's second-order formulation in the

form of a coupling coefficient. The higher-order mechanisms are well summarized by Shearman [25]. Also, Kinsman [20] elaborates on the second-order terms appearing in the hydrodynamic equations describing the water surface height.

Since Barrick's initial efforts in developing ocean cross sections at HF using the perturbation technique, he has published widely in refining and extending the work. Barrick [26] verified the proper use of the gravity-wave dispersion relation in the cross section equations, and Barrick and Lipa [27] presented the hydrodynamic coupling coefficient for shallow water applications. Also, Lipa and Barrick [28] have neatly summarized techniques to extract sea state from monostatic HF radar sea echo. Others (eg., Wyatt *et al.* [29], Gill and Walsh [30], Howell and Walsh [31], Hickey *et al.* [32]) have extended and modified these techniques with very good success in determining non-directional ocean spectra, significant wave heights, and surface currents. Such favourable results stemming from the use of the monostatic cross sections lend credibility to the perturbation technique initially used in deriving them.

Subsequent to Barrick's cross section work, Johnstone [33], proceeding with a similar perturbation analysis, developed ocean surface cross sections to second order. Johnstone also gave a preliminary expression for the second-order bistatic case but made no attempt to evaluate the resulting integrals.

1.2.2 Physical Optics

1.2.2.1 Methodology

Whenever a body or surface is smooth (i.e. the radius of curvature is much greater than the wavelength of the incident radiation) the surface fields may be approximated by the fields that would be present were a conducting tangent plane introduced at each surface point. The technique is referred to as the Kirchhoff method or tangent-plane approximation. When the surface fields are used in the Stratton-Chu integral equations (Stratton [34], Section 8.14) to obtain the scattered fields, the procedure is

referred to as the Kirchhoff or *physical optics* method in scattering. As the incident wavelengths become vanishingly small, the physical optics method approaches *geometrical optics*, in which the e-m waves may be treated as rays, and the scattering reduces to *specular reflection*.

Details of the physical optics method are presented by Beckmann and Spizzichino [35], Chapter 3. The technique assumes plane wave incidence and does not account for multiple scattering. As noted by Ishimaru [13], the physical optics approximation, unlike the geometrical optics approximation, contains wavelength dependence by virtue of the same being found in the Fresnel reflection coefficients appearing in the former.

1.2.2.2 Applications of Physical Optics

The process of obtaining the radar cross sections of a perfectly conducting rough time invariant surface using the physical optics approach is presented by Kodis [36]. The integrals for the scattered field are evaluated asymptotically by the method of stationary phase. It is shown that specular reflection makes the principal contribution to the cross section. Kodis' approach appeared superior to older analyses in that the physical optics integral is evaluated before averaging over an ensemble of surfaces instead of afterwards, thus allowing more insight into the physical mechanism responsible for the scatter.

Barrick [37] generalized the Kodis analysis to the bistatic case, including finite surface conductivity. Also, Barrick and Bahar [38] showed that the same results may be obtained independent of the order of the averaging and the stationary phase integration processes. Their procedure, unlike the Kodis' work, explicitly accounted for shadowing.

The physical optics approach has been applied to scattering from the sea surface (eg. Barrick [39]) and more recently has appeared in geoscience applications (eg. Ulaby and Elachi [40]).

While the physical optics method has proven useful for short e-m radiation (wavelengths on the order of centimetres or smaller), its constraint on the radii of surface curvatures and its inability to properly account for multiple scattering precludes its application to HF scattering from the ocean surface.

1.2.3 Composite Surface Scattering and Related Theory

Some surfaces may be characterized by multiple roughness scales. Of particular interest is a surface which may be considered as being composed of a small-scale roughness (i.e. small heights and slopes) superimposed on an underlying, gently undulating (i.e. large-scale surface heights), unperturbed surface. That is, the total surface is *composite* in nature. Wright [41] developed a first-order microwave cross section of such a surface, but his results did not account for a transition between small- and large-scale effects. Brown [42] treated the scattering of e-m waves from the large-scale surface using the physical optics technique, while the small-scale features were analyzed from a perturbational viewpoint. Again, Brown's results were given to first order for a perfectly conducting time invariant surface, but, unlike Wright's, provided for a continuous transition between the near-specular physical optics and wide-angle tilted-plane Bragg solutions.

Brown [43] applied the integral equation method of smoothing (IEMS) to random surface scattering. Plane wave incidence and perfect conductivity were assumed. The general approach consists of an attempt to first find the current induced on the surface by the incident field and then to compute the scattered field from the knowledge of that current. The smoothing technique involves (1) multiplying the surface current appearing in the magnetic field equation by an exponential factor involving the surface height and slopes, (2) expressing that product as the sum of an average value and a zero-mean fluctuating part, (3) generating and solving an integral equation for the fluctuating part in terms of the average and (4) using the result of

step (3) in the equation of step (1) to determine the indicated product, from which may be determined the average field scattered by the surface. While the formulation is mathematically exact, Brown notes that evaluation of the resulting expressions is formidable and stops short of a numerical study. The smoothing analysis is extended by Brown [44] to include perfectly conducting random rough surfaces having small height but large slopes, curvatures, etc.. He notes that, due to the applicability of the theory to large slopes, it might be possible to use it in determining when the Rice theory becomes invalid. However, while the general formulation is developed, no application is actually carried out.

Brown's work during the 1980's appears to have led him to an extension of his 1978 composite surface analysis (see Brown [45]). In the latter, an approach based on combining normalization and the method of smoothing is developed. The normalization, which allows for more relaxed constraints on the surface heights and slopes, consists of dividing the integral equation that models the current induced on a perfecting conducting rough surface by a phase factor whose presence normally invalidates the smoothing process as surface height increases. The IEMS is then applied to this normalized equation with the phase factor being reintroduced subsequently by multiplication in the spatial domain or convolution in the Fourier transform domain. The latter is used to determine the scattered field. Brown concludes that the method works best when large slopes are concentrated in a portion of the spectrum having small heights or when large heights corresponds to relatively small slopes. The analysis is also an improvement on the Kirchhoff approximation in that it implies some degree of accounting for diffraction and multiple scattering from the large-scale surface features. Again, while the general expressions for the scatter are developed, no calculations are carried out and no cross sections are presented.

1.2.4 Full-wave Technique

The evaluation of the electric field integral for an e-m wave being scattered from a rough surface must be accomplished by approximate techniques (a concise discussion is found in Ishimaru [13], Chapter 15). A complete analysis leads to (1) a radiation field – when the observation point is a large distance from the image point of the source but not near the reflecting surface; (2) a surface field; and (3) a lateral wave resulting when the incident field impinges a boundary where the relative index of refraction is less than unity. When all three fields are included in the analysis, the method is referred to as the *full-wave* technique.

Development and application of the full-wave technique to rough surface scatter appears to have been initiated by Bahar as early as 1972, [46]. Bahar and Rajan [47] used the full-wave analysis, maintaining the condition of small slope, in investigating e-m scattering for arbitrary incident and scatter angles. Collin [48] showed this "regular" full-wave theory to be accurate beyond the range accounted for by first-order perturbation theory. Bahar [49] extended his previous work to include surfaces of arbitrary slope in an attempt to bridge the gap between the small perturbation regime and the Kirchhoff regime. Subsequently, Bahar and Barrick applied this "extended" full-wave analysis to obtain the scattering cross sections of composite surfaces (see Section 1.2.3) which cannot be decomposed into a two-scale model without violating the conditions of either the perturbation theory or the physical optics theory. Neglecting the effects of multiple scattering, cross section expressions for specular and Bragg scattering were developed, but numerical evaluations were not pursued. Bahar [50] presented an analysis which, unlike his previous work, accounted for the correlation between rough surface heights and slopes. For one-dimensionally rough surfaces with small heights and slopes, the full-wave solutions again appeared to reduce to the Rice theory. Still, multiple scatter was not considered. Expanding Bahar's full-wave analysis to two-dimensionally rough surfaces, Bahar and Lee [51] presented solutions

for bistatic radar cross sections. However, in order to compare these results with previously published work, calculations were carried out for one-dimensionally rough surfaces only. Bahar found that agreement between the Rice perturbation analysis and the full-wave technique decreased with decreasing slope for the case of backward scattering. Subsequently, Bahar *et al.* [52], continuing with the full-wave theory, presented bistatic cross sections for non-time-varying rough surfaces. All of their examples were calculated for the visible region, albeit for different roughness scales.

An extensive numerical evaluation and analysis of Bahar's full-wave theory was carried out by Collin [53]. Collin's detailed numerical results for microwave frequencies conclusively show that Bahar's initial assumption of uncorrelated slopes and heights was a very bad one, leading to physical optics cross sections up to an order of magnitude greater than those predicted by the Kirchhoff theory. As well, Bahar's 1980 results [49] were shown not to conform to the perturbation theory, while his 1991 analysis [50] did reduce to the perturbation results when rms slopes and heights are small. Private communication between Bahar and Collin (see Collin [53]) seems to indicate possible continued advancement of the full-wave theories that have been reported in the open literature to date.

1.2.5 The Walsh Technique

1.2.5.1 Methodologies

Walsh [5] presented an analysis for e-m scattering from rough surfaces based on the concept of "generalized functions". As this and subsequent works by Walsh and his colleagues (cited below) form the basis of the research proposed here, a somewhat detailed description of this approach follows.

The two dimensional surface, $z = \xi(x, y)$ (see Figure 1.2), is assumed to be defined and bounded for all x and y and forms the boundary of the lower medium. Using the

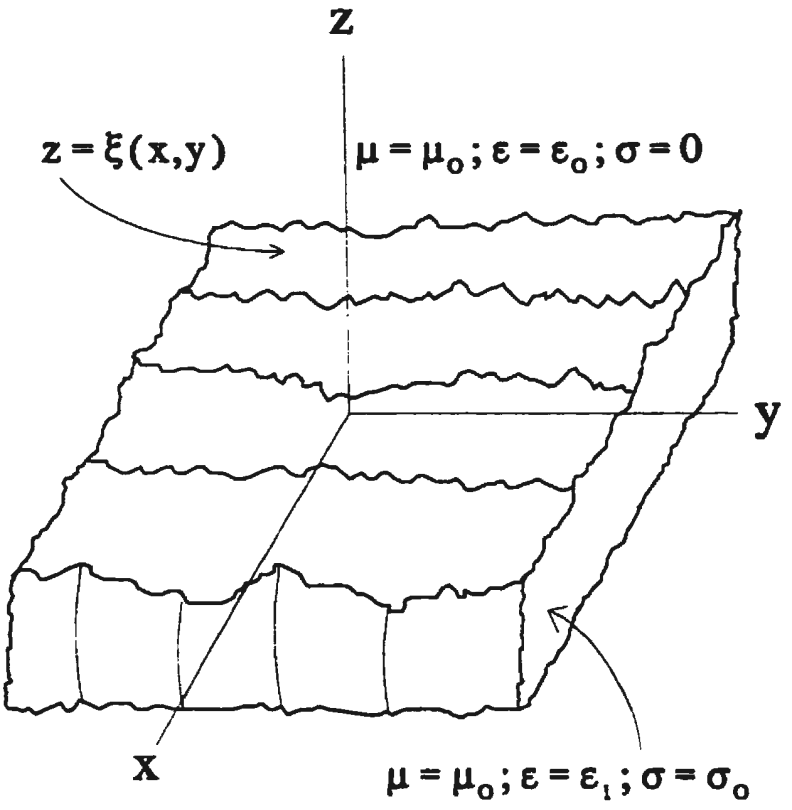

Figure 1.2: Rough surface used in Walsh's analysis. Parameters are as defined in the text.

Heaviside function given by

$$h(z-\xi(x,y)) = \begin{cases} 0, & z \leq \xi(x,y) \\ 1, & z > \xi(x,y) \end{cases} , \tag{1.2}$$

the electrical properties of the entire space may be written as

$$\sigma = (1-h)\sigma_0 \tag{1.3}$$

$$\epsilon = \epsilon_0 h + \epsilon_1(1-h) \tag{1.4}$$

where it is assumed that the conductivity, σ, is zero above the surface and that below the surface, $\sigma = \sigma_0$. Above the surface, the permittivity, ϵ, is ϵ_0 and below the surface $\epsilon = \epsilon_1$, it being understood that ϵ_0 is the free space value of that parameter. The permeability is taken to be the free space value, μ_0, above and below the surface. The analysis is not confined to this particular choice of e-m parameters.

Maxwell's equations for the space described above are written in point form, assuming $e^{j\omega t}$ time (t) dependency, ω being angular frequency, as

$$\vec{\nabla} \times \vec{E} = -j\omega\vec{B} \tag{1.5}$$

$$\vec{\nabla} \times \vec{H} = j\omega\vec{D} + \vec{J} \tag{1.6}$$

$$\vec{\nabla} \cdot \vec{B} = 0 \tag{1.7}$$

$$\vec{\nabla} \cdot \vec{D} = \rho \tag{1.8}$$

where $\vec{E}$ is the electric field intensity, $\vec{B}$ is the magnetic flux density, $\vec{D}$ is the electric flux density, $\vec{H}$ is the magnetic field intensity, $\vec{J}$ is the current density consisting of conduction currents ($\vec{J}_c$) and source currents ($\vec{J}_s$), and ρ is the charge density. In view of the parameter description above, the so-called constitutive relations may be simply written as

$$\begin{aligned} \vec{D} &= [\epsilon_0 h + \epsilon_1(1-h)]\,\vec{E} \quad (a) \\ \vec{J}_c &= \sigma_0(1-h)\vec{E} \quad (b) \\ \vec{B} &= \mu_0\vec{H}\,. \quad (c) \end{aligned} \tag{1.9}$$

From equations (1.5)-(1.8), and using equations (1.9a–1.9c), Walsh writes the basic equation for the electric field intensity of the entire space as

$$\nabla^2\vec{E} + \gamma_0^2\vec{E} = \frac{\eta_r^2 - 1}{\eta_r^2}\vec{\nabla}\left[\vec{n}\cdot\vec{E}^{+} + \delta(z-\xi)\right] - T_{sE}(\vec{J}_s) \tag{1.10}$$

where

- ξ is the same as $\xi(x,y)$ and is the upper boundary of the lower medium.
- $\eta_r^2 = \dfrac{\epsilon_1}{\epsilon_0} + \dfrac{\sigma_0}{j\omega\epsilon_0}$ is the square of the refractive index of the lower medium.
- $\gamma_0^2 = k^2\left[h + (1-h)\eta_r^2\right]$ with $k^2 = \omega^2\mu_0\epsilon_0$.
- $\vec{n} = -\dfrac{\partial\xi}{\partial x}\hat{x} - \dfrac{\partial\xi}{\partial y}\hat{y} + \hat{z}$ is the normal to $z = \xi(x,y)$ in the direction of increasing z, $\hat{x}$, $\hat{y}$, $\hat{z}$ being the unit vectors along the respective coordinate axes.
- $\delta(\cdot)$ is the Dirac delta function.

- $T_{sE} = \frac{1}{j\omega\epsilon_0}\left[\vec{\nabla}(\vec{\nabla}\cdot) + k^2\right]$ is known as *the electrical source operator.*

- $\vec{J}_s$ is an arbitrary source current, herein assumed to lie in the region $z > \xi(x,y)$.

- $\vec{E}^+$ is the value of $\vec{E}$ immediately above the surface; i.e.

$$\vec{E}^+ = \lim_{z \to \xi(x,y)^+} \vec{E}(x,y,z) = \vec{E}^+(x,y).$$

Walsh then decomposes the $\vec{E}$-field as

$$\vec{E} = h\vec{E} + (1-h)\vec{E} \tag{1.11}$$

and computes from this $\nabla^2\vec{E} + \gamma_0^2\vec{E}$ required in (1.10). The result gives three differential equations: (1) one for the field above the surface; (2) one for the field below the surface; and (3) an equation stipulating the conditions which $\vec{E}$ must satisfy at the boundary. The first two of these are reduced to integral equations through a three-dimensional convolution with the Green's functions appropriate to the particular spaces (i.e. $\frac{e^{-jkr}}{4\pi r}$ and $\frac{e^{-j\gamma r}}{4\pi r}$ above and below the surface, respectively; $r = \sqrt{x^2+y^2+z^2}$ and $\gamma^2 = k^2\eta_r^2$).

The basic problem of determining the scattered field reduces to finding the field, $\vec{E}^+$, immediately above the surface, along with the derivative of $\vec{E}$, $\frac{\partial\vec{E}}{\partial n}$, with respect to the normal to the surface. This is facilitated by Fourier transforming the two integral equations referred to above. The field below the surface is transformed (with respect to x and y) in a horizontal plane $z > \xi(x,y)$ and the equation for the field above the surface is similarly transformed in a plane $z < \xi(x,y)$. The transformed variables are K_x and K_y, the surface wavenumber, $K(= |\vec{K}|)$, being given by $K^2 = K_x^2 + K_y^2$ (note: $\vec{K} = K_x\hat{x} + K_y\hat{y}$). The first of these equations is solved approximately on the assumption that the functions of the integrand are spatially band-limited and that the bandwidth is much less than $|\eta_r k|$. This is essentially the same as the impedance boundary condition, Ishimaru [13]. Using this solution in the second transformed

equation results in

$$2\underline{\vec{E}}_s(K_x,K_y)^{z^-}e^{-z^-u} = \int_{x'}\int_{y'}\left[|\vec{n}(x',y')|^2\,\vec{E}^+(x',y') - \frac{1}{u}\,\vec{R}^+(x',y')\right]e^{-\xi(x',y')u}e^{-j(K_xx'+K_yy')}dx'dy' \tag{1.12}$$

with

$$\vec{R}^+ = -\frac{\eta_r^2-1}{\eta_r^2}\vec{\nabla}_{xy}(\vec{n}\cdot\vec{E}^+) - jk\eta_r\left[|\vec{n}|^2\,\vec{E}^+ - \frac{\eta_r^2-1}{\eta_r^2}\left(\vec{n}\cdot\vec{E}^+\right)\vec{n}\right].$$

We note

- $\underline{\vec{E}}_s(K_x,K_y)^{z^-}$ is the free space source field (or incident field) Fourier transformed in the spatial sense in the plane $z = z^- < \xi(x,y)$. It may be derived from the source current ($\vec{J}_s$) according to

$$\begin{aligned}\underline{\vec{E}}_s(K_x,K_y)^{z^-} &= \vec{T}_{sE}(\vec{J}_s) * G \\ &= \int_{x'}\int_{y'}\int_{z'}\vec{T}_{sE}\left(\vec{J}_s(x',y',z')\right)G(x-x',y-y',z-z')dx'dy'dz'\end{aligned}$$

  where $*$ denotes a spatial convolution. G is the free space Green's function as defined above.

- $\vec{\nabla}_{xy} = \hat{x}\frac{\partial}{\partial x} + \hat{y}\frac{\partial}{\partial y}$

- $u = \begin{cases}(K^2-k^2)^{\frac{1}{2}} & \text{, for real roots} \\ j(k^2-K^2)^{\frac{1}{2}} & \text{, for imaginary roots.}\end{cases}$

In general, a solution of (1.12) for $\vec{E}^+$ (using $\vec{R}^+$) allows calculation of the scattering above, below, and on the surface. For the case of present interest, namely *ground wave* propagation and scatter, an expression for $\vec{E}^+$ is therefore necessary. During the last decade, a substantial effort has been expended by Walsh and his colleagues in seeking efficient means of generating a solution of (1.12). The most relevant parts of that extensive research constitute the subject of the next few paragraphs.

Srivastava [54] presented the first expression for the surface field which led to the HF cross section of the ocean surface being developed from Walsh's theory. Assuming the surface to be a good conductor, Srivastava reduced (1.12) to a summation

equation, aided by expressing the surface as a two-dimensional Fourier series. The equation is formally inverted in the form of a Neumann series, i.e.

$$(\underline{\underline{I}} + T)^{-1} = \sum_{m=0}^{\infty} (-T)^m = \underline{\underline{I}} - T + T^2 - T^3 + \ldots$$

where $\underline{\underline{I}}$ is the identity matrix and T is a linear operator resulting, in this case, from converting the integral to a sum. In the analysis, $\underline{\underline{I}}$ operating on the *source* field provides the zero-order *surface* field. Corrections to this term are also gathered from relevant higher terms of the series. Similarly, T, and corresponding corrections to it appearing in subsequent terms, allow calculation of the first-order field, and so on. Srivastava takes the analysis to second order in this sense. Each of the T operators themselves consist of a series of matrices, and to facilitate the analysis each T is approximated by its first term.

Srivastava's solution for the surface field of a two-dimensional periodic surface first assumes a general source. Next, the source is taken to be an elementary vertical dipole located close to the surface and having a pulsed sinusoidal excitation. It is additionally assumed that $|\eta_r| >> 1$ and that the surface slopes, $\xi_x, \xi_y << 1$. Furthermore, attention is confined to the vertical component of the surface field as this constitutes the dominant mode of e-m propagation for antennas being close to a good conducting surface. The solution may be interpreted as 1) a ground wave propagating outward from the source, the surface impedance being modified by the surface roughness and 2) ground waves, again with modified surface impedances, propagating in different directions due to scattering. The required integral inversions in the spatial transform domain, along with the evaluation of the resulting convolution integrals, are accomplished through stationary phase/steepest descent techniques. The backscattered surface field, to second order, is calculated assuming a narrow beam receiving antenna. It is also of significance that Srivastava's results for the scattered field, under the assumptions of small height and slope, reduce to those of Rice [11].

Walsh and Donnelly [55] extend the scattering analysis to determine the e-m field due to a finite current source which is located in a vacuum outside of two electrically different media. For the special case of rough surface scattering, where the medium above the surface is free space, their approach reduces to that of Srivastava [54] and Walsh and Srivastava [56].

Walsh and Dawe [57] present a modification of the Walsh [5] and Srivastava [54] techniques. As already indicated, Srivastava expands the integrand of equation (1.12) by immediately introducing the Fourier series of the surface profile and its slopes and continues the analysis in the K_x , K_y domain. In the new approach, equation (1.12) is presented in operator form and, upon simplification, the results are returned to the x, y domain *before* the surface profile is considered. The procedure, as briefly outlined below, considerably reduces some of the algebraic tedium associated with finding a suitable expression for the surface field.

Using underbars (__) to denote two-dimensional (x, y) Fourier transformation, (1.12) may be written as

$$2\underline{\vec{E}_s^{z^-}} e^{-z^- u} = (\underline{|\vec{n}|^2 \vec{E}^+} - \frac{1}{u}\underline{\vec{R}^+}) - \Big[\underline{|\vec{n}|^2 \vec{E}^+(1 - e^{-\xi u})} - \frac{1}{u}\underline{\vec{R}^+(1 - e^{-\xi u})}\Big] \tag{1.13}$$

where the arguments of the various functions have been omitted for the sake of clarity. Using $|\eta_r| >> 1$, $\vec{R}^+$ may be written as

$$\vec{R}^+(x, y) = -\vec{\nabla}_{xy}(\vec{n} \cdot \vec{E}^+) - jk\eta_r |\vec{n}|^2 \vec{E}_t^+ - \frac{jk}{\eta_r} |\vec{n}|^2 \vec{E}_n^+ \tag{1.14}$$

where the subscripts t and n denote tangential and normal components, respectively.

Noting from (1.14) that $\vec{R}^+$ is a linear function of $\vec{E}^+$, equation (1.13) may be written as

$$2\underline{\vec{E}_s^{z^-}} e^{-z^- u} = T_1(\vec{E}^+) - T_2(\vec{E}^+) \tag{1.15}$$

where T_1 and T_2 are defined as

$$T_1(\vec{E}^+) = \underline{|\vec{n}|^2 \vec{E}^+} - \frac{1}{u}\underline{\vec{R}^+(\vec{E}^+)}$$

and

$$T_2(\vec{E}^+) = \underline{|\vec{n}|^2\,\vec{E}^+(1-e^{-\xi u})} - \frac{1}{u}\underline{\vec{R}^+(\vec{E}^+)(1-e^{-\xi u})}\,.$$

$\vec{R}^+(\vec{E}^+)$ is defined by (1.14). Assuming that T_1 has an inverse, equation (1.15) becomes

$$T_1^{-1}(2\underline{\vec{E}_s^{z^-}}\,e^{-z^-u}) = \vec{E}^+ - T_1^{-1}T_2(\vec{E}^+) \quad , \tag{1.16}$$

the general formal solution of which is

$$\vec{E}^+ = \sum_{m=0}^{\infty} \vec{E}_m^+ \tag{1.17}$$

where

$$\vec{E}_0^+ = T_1^{-1}(2\underline{\vec{E}_s^{z^-}}\,e^{-z^-u}) \tag{1.18}$$

and

$$\vec{E}_m^+ = (T_1^{-1}T_2)^m\vec{E}_0^+ \quad . \tag{1.19}$$

By virtue of (1.14) and the definition of T_1, the zero-order estimate (i.e. equation (1.18)) includes surface slopes but ignores the height effect, $e^{-\xi u}$. The latter is accounted for in (1.19) with $m = 1, 2, \ldots$. To date, equation (1.19) has not been addressed, while equation (1.18) has been analyzed in detail by Walsh and Dawe [57] and Walsh *et al.* [8]. Determining the zero-order estimate in (1.18) (i.e. $\vec{E}^+ \approx \vec{E}_0^+$) requires, on the basis of the definition of $T_1(\vec{E}_0^+)$, the solution of the equation

$$T_1(\vec{E}_0^+) = \underline{|\vec{n}|^2\,\vec{E}_0^+} - \frac{1}{u}\underline{\vec{R}^+(\vec{E}_0^+)} = 2\underline{\vec{E}_s^{z^-}}\,e^{-z^-u}\,. \tag{1.20}$$

Making the "good conductor" approximation ($u + jk\eta_r) \approx jk\eta_r$ and $jk(\eta_r - \frac{1}{\eta_r}) \approx jk\eta_r$), Walsh and Dawe [57] eliminate the tangential component, $\vec{E}_{0_t}^+$, and write a scalar equation for the normal component as

$$\begin{aligned} E_{0_n}^+ + \frac{\hat{n}}{|\vec{n}|^2}\cdot\left[\hat{n}\hat{n}\cdot\vec{\nabla}_{xy}(|\vec{n}|\,E_{0_n}^+) \overset{xy}{*} F(\rho)\frac{e^{-jk\rho}}{2\pi\rho}\right] \\ = \frac{\hat{n}}{|\vec{n}|^2}\cdot\left[\hat{n}\hat{n}\cdot\mathcal{F}_{xy}^{-1}(2u\underline{\vec{E}_s^{z^-}}e^{-z^-u}) \overset{xy}{*} F(\rho)\frac{e^{-jk\rho}}{2\pi\rho}\right] \end{aligned} \tag{1.21}$$

where $\overset{xy}{*}$ denotes 2-d (x,y) convolution, $\mathcal{F}_{xy}^{-1}$ is the inverse Fourier transform, $F(\rho)$ is the Sommerfeld attenuation function, and $\rho = (x^2+y^2)^{\frac{1}{2}}$ is the plane polar distance variable. Implicit in this expression is the constraint that $k\xi \ll 1$. Equation (1.21) may be "solved" by the method of Neumann series or "successive approximations".

In 1990, Walsh *et al.* [8] revisited equation (1.21). Writing the unit normal vector $\hat{n}$ as

$$\hat{n} = \frac{\vec{n}}{|\vec{n}|} = \frac{\hat{z} - \vec{\nabla}\xi}{|\vec{n}|} \quad ; \quad |\vec{n}| = \sqrt{1 + \left|\vec{\nabla}\xi\right|^2} \ .$$

equation (1.21) was rewritten as

$$\begin{aligned} E_{0_n}^{+} - \frac{1}{|\vec{n}|^3}\left[\frac{\vec{\nabla}\xi}{|\vec{n}|^2}\cdot\vec{\nabla}_{xy}(|\vec{n}|\,E_{0_n}^{+}) \overset{xy}{*} F(\rho)\frac{e^{-jk\rho}}{2\pi\rho}\right] \\ -\frac{\vec{\nabla}\xi}{|\vec{n}|^3}\cdot\left[\frac{\vec{\nabla}\xi\vec{\nabla}\xi}{|\vec{n}|^2}\cdot\vec{\nabla}_{xy}(|\vec{n}|\,E_{0_n}^{+}) \overset{xy}{*} F(\rho)\frac{e^{-jk\rho}}{2\pi\rho}\right] \\ = \frac{\vec{n}}{|\vec{n}|^3}\cdot\left[\frac{\vec{n}\vec{n}}{|\vec{n}|^3}\cdot\mathcal{F}_{xy}^{-1}(2u\underline{\vec{E}_s^{z^-}}e^{-z^- u}) \overset{xy}{*} F(\rho)\frac{e^{-jk\rho}}{2\pi\rho}\right] . \end{aligned} \tag{1.22}$$

Walsh *et al.* [8] then make the simplifying assumption on the surface slope that $\left|\vec{\nabla}\xi\right| \ll 1$. which means that

$$|\vec{n}|^2 = 1 + \left|\vec{\nabla}\xi\right|^2 \approx 1 \ .$$

Subsequently, assuming a pulsed-dipole source, the first-, second-, and third-order *backscattered* fields (i.e. $(E_{0_n}^{+})_1$, $(E_{0_n}^{+})_2$, $(E_{0_n}^{+})_3$ monostatic formulations) from a rough surface are calculated via a Neumann series approach.

1.2.5.2 Applications of Walsh's Scattering Analysis

As intimated in the previous section, Srivastava [54], starting with equation (1.12), developed expressions for the backscattered surface field to second order. Initially, this was done for a time invariant surface. Then, a time varying, statistically rough surface was introduced into the equations for the backscattered field so that application could be made to the ocean surface. The surface randomness was effected by treating the

Fourier coefficients of the ocean surface as random variables after the manner of Rice [11]. A second-order hydrodynamic effect (arising from wave-wave interaction, Hasselmann [23]) was also included in the second-order solution for the backscattered field. Assuming a periodic pulsed sinusoid dipole source, a narrow beam receiving antenna, and the linear dispersion relation for deep water gravity waves (Kinsman [20]), Srivastava derived the first- and second-order HF monostatic cross sections of the ocean surface. Srivastava's first order is identical to that of Barrick referred to in Section 1.2.1.2. The second order, however, contains three portions: (1) double scattering occuring on the scattering patch; (2) scattering due to the interaction of the incident field and the surface along the path from the source to scattering patch; and (3) a double scattering consisting of two single scatters neither of which is on the patch. Srivastava shows the second term to be very pronounced at higher Doppler frequencies, while the third term may be neglected if a narrow beam transmitting antenna is used.

Walsh and Dawe [57] reduce equation (1.21) to a Volterra type integral equation which could be solved for $E^{+}_{0_n}$ by a Neumann series. Subsequently, the first-order cross section of the ocean was determined under the assumption that the source was a time-pulsed radar. As usual, the surface was considered to be slowly varying with respect to the propagation times. The result differs from Srivastava's [54] first-order cross section by a factor dependent on the wind speed. The factor becomes smaller as the wind speed increases. This effect is in addition to the usual increase in first-order power as the sea spectrum increases. Additionally, [57] addresses the problem of multipathing, reaching the conclusion that this phenomenon does not add significant power to most of the Doppler spectrum.

Using the fields generated by the approximation, $|\vec{n}| \approx 1$, discussed in Section 1.2.5.1, Walsh *et al.* [8] developed monostatic cross sections of the ocean surface to third order in slope. The first-order result reduces to that of Barrick [24] for the

limiting case of $\Delta\rho \rightarrow \infty$ where $\Delta\rho$ is the width of the scattering patch. The second order, which bears many of the properties of the Barrick result, differs from the latter in the form of the electromagnetic coupling coefficient (see Gill and Walsh [30]). The general features of the second order conforms to those of observed radar spectra as well as to those of other models (Howell [58]). Results of wave data interpretation algorithms (see Gill and Walsh [30], Howell and Walsh [31] and Gill *et al.* [2]) based on the 1990 cross sections of Walsh *et al.* [8] have been shown to compare favourably with data collected from *in situ* devices. These experimental studies have thus provided a significant degree of confidence in the basic scattering theory on which they are based.

The 1990 analysis by Walsh *et al.* [8] shows that for increasing sea state and/or radar operating frequency, the third-order backscattering cross section may dominate the second order for large Doppler. This modelling result may partially explain why in reality the radar spectrum for sea echo falls off at a slower rate for increasing Doppler shift than is predicted by the classical first- and second-order theories alone.

1.3 The Scope of the Thesis

As discussed in Section 1.2.5, the primary content of this thesis is established on the theoretical foundations developed by Walsh over nearly two decades. The rudiments of the rough surface scattering technique alluded to above are used to derive the bistatic cross sections of the ocean surface to second order for incident radiation in the HF band.

In Chapter 2, the focus is on equation (1.21). This equation is written in an operator form which clearly delineates the various orders of scatter from a rough, time invariant surface under the assumption of a vertical dipole source. The randomly rough surface is assumed to be representable by a two-dimensional Fourier series whose coefficients are time-independent random variables. Using approximations for

the surface slope, the convolutions involved in the first- and second-order scattering are reduced to integral form. The direction from which the scattered field is observed is kept general. The integrals are approximated largely via the stationary phase method.

In addressing the second-order field, the development of the field integrals, which involves dual two-dimensional spatial convolutions, may proceed in two separate, but equivalent ways. That is, there are two physically meaningful approaches to the order of convolution. It transpires that each of these processes is necessary to reveal potentially important features of the scattered second-order field. It is shown that the most interesting aspects of the second-order scatter involve (1) a double scattering from first-order surface components which are near each other on the scattering surface, (2) a scatter near the transmitter followed by another at a surface point which is remote from both the source and the point of observation and (3) a single scatter, again from first-order surface components, followed by a second near the observation position. Subsequently, the first two of these fields along with the first-order result are shown to reduce , in their essential characteristics, to those which exist for monostatic reception. No previous monostatic result was developed for the third aspect of the second-order scattering phenomenon. Also, the case of scatter at the transmitter presented here is seen to better represent physical reality than that derived in [54].

In the final sections of Chapter 2, a pulsed sinusoid is considered as the current excitation on a vertical dipole source. The fields, modified appropriately for this source, are then suitable for developing the bistatic HF cross sections of the ocean surface when the interrogation instrument is a pulsed Doppler radar.

The goal in Chapter 3 is to develop the actual expressions for the bistatic HF cross sections of the ocean surface. This necessitates a modification of the surface to include a time variation. The model chosen dictates that the ocean surface be represented by a zero-mean stationary Gaussian random process. Only the gravity wave portion of the

ocean wave spectrum is considered. For analysis purposes, deep water is assumed, although the results are easily extendable to general depth. The surface features include wave-wave interaction and the derivations, in this sense, incorporate second-order surface characteristics. It is eventually shown that signal interaction with these so-called second-order waves gives rise to a major portion of the second-order bistatic cross section. Extensive use is made of the linear dispersion relationship (eg., see [20]) and Hasselmann's model [59] for nonlinear energy transfer in the gravity wave spectrum.

With the appropriate assumptions on the time variability of the surface as compared to a single interrogation time by an HF signal, the electric field equations derived in Chapter 2 are reformulated for application to the ocean. Subsequently, the auto- and cross-correlations of the various electric field components, via ensemble averaging, are derived with a view to developing the Doppler power spectral density associated with the scattered signal. Many of the approximations and important properties of these derivations are detailed throughout Appendices B.1–B.6.

Once the power spectral densities have been obtained, the remainder of Chapter 3 is devoted to calculating the bistatic cross section components. In so doing, a model of the ocean surface must be chosen. Here, it is assumed that it can be reasonably characterized as the product of the Pierson-Moskowitz (PM) [60] non-directional spectrum and a cardioid directional parameter. It is asserted in the chapter and proven in Appendix B.7 that the proper spectral form to be introduced into the cross section calculations when using the PM model involves a factor of $\frac{1}{2}$ which is not used by previous investigators. Once the cross sections are derived, the effects of such parameters as operating frequency, bistatic angle and ocean surface conditions are examined in some detail.

Cross section models presented to date have not, in detail, considered the effects of noise. Chapter 4 is dedicated to this cause. External noise limitation is

assumed. Initially, the external noise is modelled as a single-variable zero-mean stationary Gaussian process after the scheme of Pierson [61]. The proper form of this noise as it is interrogated by a pulsed Doppler radar is then determined, first for a finite number and then an infinite number of pulses. This model is seen to account for the aliasing of the noise signal into the limited bandwidth of the receiving system. For completeness, non-stationary noise is also addressed.

Following the noise model, the proper form of the transmit power to be used in the radar range equation for calculating the power density of the signal (i.e. clutter) received from the ocean is derived. Then, again using Pierson's model [61] for a stationary Gaussian process, a means of estimating the Doppler power spectrum of the combined clutter and noise is deduced. The details of this are given in Appendix C.2 with illustrations and comparison with actual data being addressed in Section 4.5.

In Chapter 5, the fundamental conclusions reached from the research presented in the previous three chapters are summarized. There, too, based on the many questions generated by the present analysis, a few obvious suggestions for future work are indicated.

Chapter 2

The Electric Field Equations for Scattering From a Surface Representable by a Fourier Series – Bistatic Form

2.1 Introduction

The starting point of this analysis is equation (1.21). As pointed out there, the work of Walsh and Dawe [57] which produced this equation was used by Walsh *et al.* [8] to develop monostatic cross sections of the ocean surface. Some of the simplifying features legitimately associated with the monostatic calculations either do not exist or must be used in a modified form for the more general bistatic case.

In this chapter, we seek to analyze equation (1.21) to give the first- and second-order bistatic electric field when the source is a vertical dipole and the scattering surface is time invariant and is represented by a Fourier series. It should be noted that Walsh and Dawe [9] have already developed a result for the first-order case, but this does not appear in readily available open literature. Therefore, with some minor modifications in notation and procedure and more extensive referencing and discussion, this analysis is detailed here for readability and completeness.

The convolutions in equation (1.21) theoretically lead to integral expressions for the vertical component of all orders of the scatter field, the first two of which will

be considered in this chapter. A physical interpretation of these convolutions will be given.

Bearing in mind that the theory will be subsequently applied to the ocean surface, it will be seen that justifiable constraints on the surface slopes will lead to more tractable forms of the equations. The simplifications of the integrals are effected via a stationary phase approach. It is shown that, for second-order scattering, modification of this asymptotic integral evaluation scheme is required. Much of the detail associated with the theoretical framework is found in various appendices cited throughout the chapter.

2.2 The Normal Component of the Surface Wave Field Assuming a Vertical Dipole Source

For the sake of completeness, we rewrite equation (1.21) for the normal component, $E_{0_n}^{+}$, of the surface wave,

$$E_{0_n}^{+} + \frac{\hat{n}}{|\vec{n}|^2} \cdot \left[\hat{n}\hat{n} \cdot \vec{\nabla}_{xy} \left(|\vec{n}| E_{0_n}^{+} \right) \overset{xy}{*} F(\rho) \frac{e^{-jk\rho}}{2\pi\rho} \right] \tag{2.1}$$
$$= \frac{\hat{n}}{|\vec{n}|^2} \cdot \left[\hat{n}\hat{n} \cdot \mathcal{F}_{xy}^{-1} \left(2u \underline{\vec{E}_s}^{z^-} e^{-z^- u} \right) \overset{xy}{*} F(\rho) \frac{e^{-jk\rho}}{2\pi\rho} \right] ,$$

where the various symbols have been defined throughout Chapter 1. It was briefly noted in the previous chapter that implicit in this equation is the assumption that $k\xi \ll 1$ – i.e., it deals with what Walsh *et al.* [8] refer to as "the small height analysis". In fact, with reference to the ocean, it has been proposed by Barrick [26], based on the careful analysis of monostatic HF second-order Doppler echo, that $k\xi_{\rm rms} < \frac{1}{2}$ is a suitable cut-off condition beyond which the radar spectrum saturates. That is, the second-order monostatic models will overpredict the echo energy beyond a *total root mean square* (rms) wave height, $\xi_{\rm rms}$, of $\frac{1}{2k}$, where k is the wavenumber of the transmitted radiation. For example, for a 25 MHz signal (i.e. $k = 0.524$ m^{-1}), the maximum allowable $\xi_{\rm rms}$ is just under 1 m, while for a 5.75 MHz signal (i.e.

$k = 0.120\ \mathrm{m}^{-1}$) it is approximately 4.15 m. From Earle and Bishop [62] this translates to significant wave heights of approximately 3.8 m and 16.5 m, respectively, or, correspondingly, wind speeds of approximately 15 m/s and 25 m/s. These considerations must be borne in mind when illustrating models of the radar spectra (Chapter 3) which are based on the formulations of this chapter.

It is well known that for a surface $\mathbf{F}(x, y, z) = 0$, $\vec{\nabla}\mathbf{F}$ is the normal at any arbitrary surface point. Then, noting that $z = \xi(x, y)$ may be written as $\mathbf{F}(x, y, z) = z - \xi(x, y) = 0$, we have

$$\vec{n} = \hat{z} - \vec{\nabla}_{xy}\xi(x, y)$$

so that

$$\hat{n} = \frac{\vec{n}}{|\vec{n}|} = \frac{\hat{z} - \vec{\nabla}_{xy}\xi(x, y)}{|\vec{n}|} \tag{2.2}$$

with

$$|\vec{n}| = \sqrt{1 + \left|\vec{\nabla}_{xy}\xi(x, y)\right|^2}\ . \tag{2.3}$$

Substituting $\hat{n}$ from equation (2.2) into the left member of equation (2.1) and noting that $\hat{n}\hat{n} = \dfrac{\vec{n}\vec{n}}{|\vec{n}|^2}$,

$$E_{0_n}^{+} + \frac{(\hat{z} - \vec{\nabla}_{xy}\xi(x, y))}{|\vec{n}|^3} \cdot \left[\frac{\left(\hat{z} - \vec{\nabla}_{xy}\xi(x, y)\right)\left(\hat{z} - \vec{\nabla}_{xy}\xi(x, y)\right)}{|\vec{n}|^2} \cdot \vec{\nabla}_{xy}\left(|\vec{n}| E_{0_n}^{+}\right) \right.$$
$$\left. \overset{xy}{*}\ F(\rho)\frac{e^{-jk\rho}}{2\pi\rho} \right] = \frac{\hat{n}}{|\vec{n}|^2} \cdot \left[\frac{\vec{n}\vec{n}}{|\vec{n}|^2} \cdot \mathcal{F}_{xy}^{-1}\left(2u\underline{\vec{E}_s}^{z^-} e^{-z^- u}\right) \overset{xy}{*}\ F(\rho)\frac{e^{-jk\rho}}{2\pi\rho} \right]\ . \tag{2.4}$$

Since $\hat{z} \cdot \vec{\nabla}_{xy}(\,\cdot\,) = 0$, equation (2.4), on dropping the argument of ξ to facilitate compactness, becomes

$$E_{0_n}^{+} - \frac{1}{|\vec{n}|^3}\left\{ \frac{\vec{\nabla}_{xy}\xi}{|\vec{n}|^2} \cdot \vec{\nabla}_{xy}\left(|\vec{n}| E_{0_n}^{+}\right) \overset{xy}{*}\ F(\rho)\frac{e^{-jk\rho}}{2\pi\rho} \right\}$$
$$- \frac{\vec{\nabla}_{xy}\xi}{|\vec{n}|^3} \cdot \left\{ \frac{\vec{\nabla}_{xy}\xi\vec{\nabla}_{xy}\xi}{|\vec{n}|^2} \cdot \vec{\nabla}_{xy}\left(|\vec{n}| E_{0_n}^{+}\right) \overset{xy}{*}\ F(\rho)\frac{e^{-jk\rho}}{2\pi\rho} \right\}$$
$$= \frac{\vec{n}}{|\vec{n}|^3} \cdot \left\{ \frac{\vec{n}\vec{n}}{|\vec{n}|^2} \cdot \mathcal{F}_{xy}^{-1}\left(2u\underline{\vec{E}_s}^{z^-} e^{-z^- \mu}\right) \overset{xy}{*}\ F(\rho)\frac{e^{-jk\rho}}{2\pi\rho} \right\}$$

or, equivalently, in operator form

$$E_{0_n}^{+} - \mathcal{T}_1\left(E_{0_n}^{+}\right) - \mathcal{T}_2\left(E_{0_n}^{+}\right) = E^s \tag{2.5}$$

where

$$\begin{aligned}
\mathcal{T}_1 &= \frac{1}{|\vec{n}|^3} \cdot \left\{ \frac{\vec{\nabla}_{xy}\xi}{|\vec{n}|^2} \cdot \vec{\nabla}_{xy}\left(|\vec{n}|\cdot\right) \overset{xy}{*} F(\rho)\frac{e^{-jk\rho}}{2\pi\rho} \right\} , \\
\mathcal{T}_2 &= \frac{\vec{\nabla}_{xy}\xi}{|\vec{n}|^3} \cdot \left\{ \frac{\vec{\nabla}_{xy}\xi\vec{\nabla}_{xy}\xi}{|\vec{n}|^2} \cdot \vec{\nabla}_{xy}\left(|\vec{n}|\cdot\right) \overset{xy}{*} F(\rho)\frac{e^{-jk\rho}}{2\pi\rho} \right\} , \\
E^s &= \frac{\vec{n}}{|\vec{n}|^3} \cdot \left\{ \frac{\vec{n}\vec{n}}{|\vec{n}|^2} \cdot \mathcal{F}_{xy}^{-1}\left(2u\underline{\vec{E}_s}^{z^-} e^{-z^- u}\right) \overset{xy}{*} F(\rho)\frac{e^{-jk\rho}}{2\pi\rho} \right\} .
\end{aligned} \tag{2.6}$$

Before further analysis of equation (2.5), a source field, $\vec{E}_s$, must be considered. We shall assume that this field is provided by a vertical dipole located at the (x, y, z) origin but infinitesimally elevated; that is, the dipole is at the point whose coordinates are $(x, y, z) \equiv (0, 0, 0^+)$. It is well known (eg. Collin [63]) that the far field of such a source is given by

$$\vec{E}_s = \frac{I\Delta\ell k^2}{j4\pi\omega\epsilon_0 r} e^{-jkr}\hat{z} \tag{2.7}$$

where I is the current on the dipole of length $\Delta\ell$, and k, ω, ϵ_0 and r have been defined following equation (1.10). Of course the radial distance, r, may also be cast as $r = \sqrt{\rho^2 + z^2}$ where ρ is the plane polar distance variable given by $\sqrt{x^2 + y^2}$. Spatially Fourier transforming $\vec{E}_s$ and setting

$$\frac{I\Delta\ell k^2}{j\omega\epsilon_0} = C_0 ,$$

results in

$$\underline{\vec{E}_s} = \frac{C_0 e^{-|z|u}}{2u}\hat{z}$$

or using a plane, z^-, where $z < 0$,

$$\underline{\vec{E}_s}^{z^-} = \frac{C_0 e^{z^- u}}{2u}\hat{z} . \tag{2.8}$$

Rearranging (2.8) and carrying out the spatial inverse Fourier transform, it is evident that

$$\mathcal{F}_{xy}^{-1}\left(2u\underline{\vec{E}_s}^{z^-}e^{-z^-u}\right) = C_0\delta(x)\delta(y)\hat{z}\ , \tag{2.9}$$

$\delta(x)\delta(y)$ being the two-dimensional Dirac delta function. If the surface in the vicinity of the source is assumed to be flat such that $\vec{\nabla}_{xy}\xi(x,y)|_{x=y=0} = 0$, then, from equation (2.2), $\vec{n} = \hat{z}$ there. Using this assumption and the replicating property of the delta function, it is readily seen that substitution from equation (2.9) into E^s of equation (2.6) yields

$$E^s = \frac{C_0}{|\vec{n}|^3}F(\rho)\frac{e^{-jk\rho}}{2\pi\rho}\ . \tag{2.10}$$

Again, it should be noted that the arguments (ρ) for the field, E^s, and $(\vec{K})$ for the transformed source field, $\underline{\vec{E}_s}^{z^-}$, as discussed following equation (1.11), have been suppressed here. Before attempting a solution to equation (2.5) for the normal component of the surface wave field, the condition that surface slope is small, i.e. $|\vec{\nabla}_{xy}\xi(x,y)|^2 << 1$, is imposed. This procedure is carried out with a view to the fact that the results of the analysis are to be applied to ocean surface gravity waves. The validity of this assumption for that case is well documented. For example, Phillips [64] gives the mean square slope, in the notation here, as

$$\overline{|\vec{\nabla}_{xy}\xi(x,y)|^2} = 0.46\times 10^{-2}\log\frac{2\pi U^2}{0.3g} \tag{2.11}$$

where U is wind speed in m/s and g is the acceleration due to gravity. Thus, if $U = 15$ m/s, for example, $|\vec{\nabla}_{xy}\xi(x,y)|^2 \approx 0.012$. The imposition of this constraint in equation (2.3) leads to

$$|\vec{n}|^2 = 1 + |\vec{\nabla}_{xy}\xi(x,y)|^2 \approx 1\ . \tag{2.12}$$

If, it is agreed to neglect powers of $\vec{\nabla}_{xy}\xi(x,y)$ which are greater than one in a single scatter, then, from equations (2.10) and (2.12), equation (2.5) becomes

$$E_{0_n}^+ - \left\{\vec{\nabla}_{xy}\xi\cdot\vec{\nabla}_{xy}(E_{0_n}^+)\overset{xy}{*}F(\rho)\frac{e^{-jk\rho}}{2\pi\rho}\right\} = C_0F(\rho)\frac{e^{-jk\rho}}{2\pi\rho}$$

or, in operator form,

$$E^+_{0_n} - \mathcal{T}_1\left(E^+_{0_n}\right) = E^s \,. \tag{2.13}$$

Writing (2.13) as

$$\begin{aligned} E^+_{0_n} &= E^s + \mathcal{T}_1(E^+_{0_n}) \\ &= E^s + \mathcal{T}_1\left(E^s + \mathcal{T}_1(E^+_{0_n})\right) \\ &= E^s + \mathcal{T}_1(E^s) + \mathcal{T}_1^2(E^+_{0_n}) \\ &= E^s + \mathcal{T}_1(E^s) + \mathcal{T}_1^2(E^s) + \mathcal{T}_1^3(E^+_{0_n}) \\ &= \ldots \end{aligned}$$

shows that by successive approximation (Neumann Series) the solution to equation (2.13) is

$$E^+_{0_n} = \sum_{m=0}^{\infty} \mathcal{T}_1^m(E^s) \,. \tag{2.14}$$

From (2.10) and (2.14) we see that the zeroth-order term, $(E^+_{0_n})_0 = \mathcal{T}_1^0(E^s) = E^s$, is simply the expression for propagation, without scattering, over a plane whose surface impedance, Δ, is incorporated into the attenuation function $F(\rho)$; that is, $(E^+_{0_n})_0$ is the "direct" wavefield.

2.2.1 The First-order Solution for a Time Invariant Surface

2.2.1.1 Reduction to Integral Form

The term in equation (2.14) for which $m = 1$ represents a first-order scatter, $(E^+_{0_n})_1$; that is, a single scatter from the rough surface. Considering this term in conjunction with $\mathcal{T}_1$ of equations (2.6) and (2.13) and E_s of equation (2.10),

$$\begin{aligned} (E^+_{0_n})_1 &= \mathcal{T}_1(E^s) \\ &= \vec{\nabla}_{xy}\xi \cdot \vec{\nabla}_{xy}\left(C_0 F(\rho)\frac{e^{-jk\rho}}{2\pi\rho}\right) \overset{xy}{*} F(\rho)\frac{e^{-jk\rho}}{2\pi\rho} \,. \end{aligned} \tag{2.15}$$

In Appendix A.1.1 it is shown that, on converting $\vec{\nabla}_{xy}(\cdot)$ to its polar equivalent,

an asymptotic integral form of equation (2.15) is

$$(E_{0_n}^{+})_1 \approx -jkC_0\frac{1}{(2\pi)^2}\int_{y_1}\int_{x_1}\hat{\rho}_1\cdot\vec{\nabla}_{x_1y_1}(\xi(x_1,y_1)) \cdot F(\rho_1)F(\rho_2)\cdot\frac{e^{-jk(\rho_1+\rho_2)}}{\rho_1\rho_2}dx_1dy_1\ . \tag{2.16}$$

This represents a single scattering as illustrated in Figure 2.1. It should be recalled

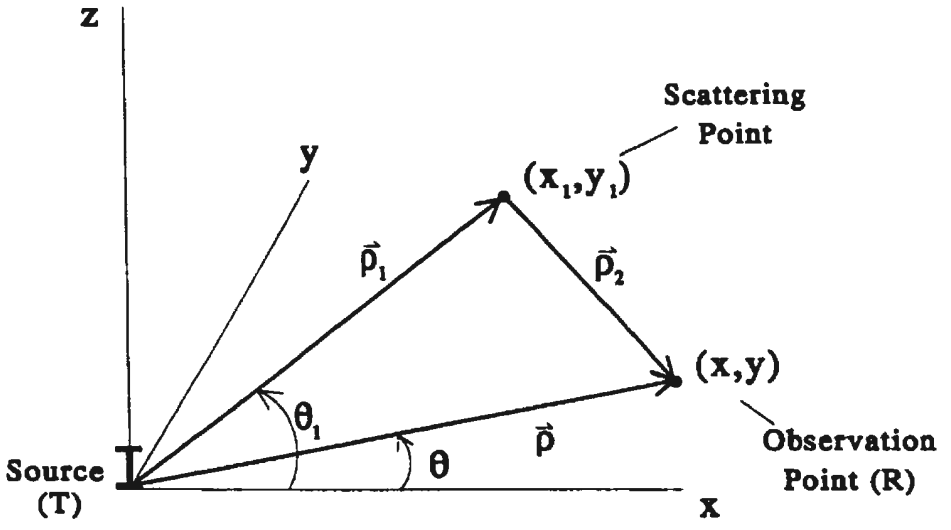

Figure 2.1: The geometry of the first-order scatter.

that the source is at the origin and the scatter occurs at point (x_1, y_1). Of course the scattered radiation travels in all directions over the scattering surface, but it is "observed" at position (x, y). The distances ρ, ρ_1 and ρ_2 are from source to reception point, from source to scatter point, and from scatter point to reception point, respectively. The integration limits are over the entire $x - y$ plane.

It is now required that the surface, $\xi(x, y)$, be characterized in some fashion, the choice here taking the form of a two-dimensional Fourier series. We shall assume that the fundamental surface wavenumber, N, is the same in both the x and y directions. Thus, $N = \frac{2\pi}{L}$ where L is the fundamental spatial "period", again in both directions.

The appropriate series is

$$\xi(x,y) = \sum_{m,n} P_{mn} e^{jN(mx+ny)} \ . \tag{2.17}$$

The indices m, n span the set of integers and P_{mn} is the Fourier coefficient corresponding to the wavenumber components Nm and Nn. The randomness of the surface is included by specifying the coefficients to be zero-mean Gaussian random variables. We may, therefore, express the mn^{th} surface wave vector component as

$$\vec{K}_{mn} = Nm\hat{x} + Nn\hat{y} \ ,$$

$\hat{x}$ and $\hat{y}$ being the usual unit vectors. Since a general planar displacement vector, $\vec{\rho}$, on the surface may be written as

$$\vec{\rho} = x\hat{x} + y\hat{y} \ ,$$

equation (2.17) is, equivalently,

$$\begin{aligned} \xi(x,y) &= \sum_{m,n} P_{\vec{K}_{mn}} e^{j\vec{\rho}\cdot\vec{K}_{mn}} \\ &= \sum_{m,n} P_{\vec{K}_{mn}} e^{j\rho K_{mn}\cos(\theta_{mn}-\theta)} \end{aligned} \tag{2.18}$$

where θ_{mn} is the direction of $\vec{K}_{mn}$ and θ $(= \tan^{-1}\left(\frac{y}{x}\right))$ is the direction of $\vec{\rho}$. Writing equation (2.18) for the scattering point (x_1, y_1) of Figure 2.1 and substituting into equation (2.16) is shown in Appendix A.1.1 to lead to

$$\begin{aligned} \left(E_{0_n}^{+}\right)_1 \approx\ & \frac{kC_0}{(2\pi)^2} \sum_{m,n} P_{\vec{K}_{mn}} K_{mn} \int_{y_1}\int_{x_1} \cos(\theta_{mn}-\theta_1) \frac{F(\rho_1)F(\rho_2)}{\rho_1\rho_2} \\ & \cdot\ e^{j\rho_1[K_{mn}\cos(\theta_{mn}-\theta_1)-k]} e^{-jk\rho_2}\ dx_1 dy_1 \end{aligned} \tag{2.19}$$

for the first-order field.

Equation (2.19) represents the integral form of the field observed at a general point (x, y) or (ρ, θ) when a single scatter occurs at a point (x_1, y_1) far from the source and the surface profile is not a function of time. The simplification of this expression is the subject of the next section.

2.2.1.2 A Stationary Phase Result for the First-Order Field

King [65] has shown in his treatment of the surface field produced by an elementary vertical dipole on an impedance plane that an integration, whose form is similar to equation (2.19), may be performed by a stationary phase process (see, for example, Bleistein and Handelsman [66]). The stationary phase integration is most simply accomplished via an elliptic coordinate transformation. With reference to Figures 2.1 and 2.2, the desired transformation is effected as follows:

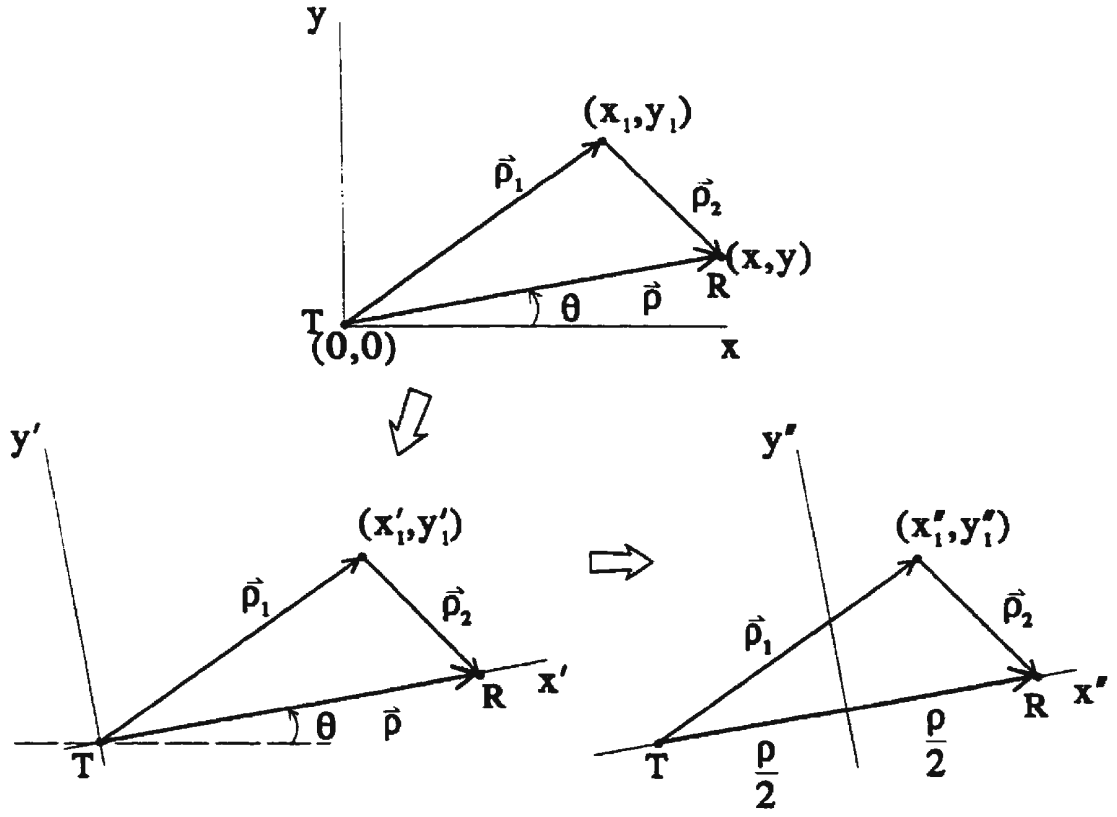

Figure 2.2: Coordinate transformation for analysis of the first-order scatter.

1. the $x - y$ coordinate system is rotated through angle θ. This gives (x_1, y_1) in terms of the new primed coordinates, (x_1', y_1'), as

$$x_1 = x_1' \cos\theta - y_1' \sin\theta$$

$$y_1 = x_1' \sin\theta + y_1' \cos\theta$$

2. noting that, eventually, use will be made of the fact that radiation from a source at position (0,0) will be received at (x, y) simultaneously from an elliptical locus whose foci are at those points, the origin of the primed coordinate system is shifted to the centre of the line segment defined by the transmitting and receiving points. This gives in the new double-primed notation,

$$x_1'' = x_1' - \frac{\rho}{2} \; ; \quad y_1'' = y_1'$$

Transformations (1) and (2) together give

$$x_1 = (x_1'' + \frac{\rho}{2}) \cos\theta - y_1'' \sin\theta$$

$$y_1 = (x_1'' + \frac{\rho}{2}) \sin\theta + y_1'' \cos\theta$$

3. thirdly, we introduce elliptic coordinate variables μ, δ (see, for example, Jeffrey [67]) and note that constant μ corresponds, in the planar sense, to a particular ellipse. Thus,

$$x_1'' = \frac{\rho}{2} \cosh\mu \cos\delta$$

$$y_1'' = \frac{\rho}{2} \sinh\mu \sin\delta$$

where cosh and sinh are the usual hyperbolic cosine and sine functions, respectively. Combining this step with the transformation of Step (2) yields

$$\begin{aligned} x_1 &= \frac{\rho}{2} [(1 + \cosh\mu \cos\delta) \cos\theta - \sinh\mu \sin\delta \sin\theta] \\ y_1 &= \frac{\rho}{2} [(1 + \cosh\mu \cos\delta) \sin\theta + \sinh\mu \sin\delta \cos\theta] \; . \end{aligned} \tag{2.20}$$

From the obvious relationships between the distance vectors and their defining coordinates appearing in Figure 2.1 or 2.2 and invoking equation (2.20), it is easily shown that

$$\rho_1 = \frac{\rho}{2}(\cosh\mu + \cos\delta)$$

$$\begin{aligned}\rho_2 &= \frac{\rho}{2}(\cosh\mu - \cos\delta) \\ \theta_1 &= \tan^{-1}\left(\frac{y_1}{x_1}\right) \\ &= \tan^{-1}\left[\frac{(1+\cosh\mu\cos\delta)\sin\theta + \sinh\mu\sin\delta\cos\theta}{(1+\cosh\mu\cos\delta)\cos\theta - \sinh\mu\sin\delta\sin\theta}\right] .\end{aligned} \tag{2.21}$$

Additionally, the Jacobian of the transformation is $\rho_1\rho_2$ so that $dx_1dy_1 = \rho_1\rho_2 d\mu d\delta$. As well, $\rho_1\cos\theta_1 = x_1$ and $\rho_1\sin\theta_1 = y_1$. Therefore, expanding $\cos(\theta_{mn} - \theta_1)$ in the exponential of equation (2.19) and applying (2.20) leads to, in elliptic coordinates,

$$\begin{aligned}(E_{0_n}^+)_1 \approx \frac{kC_0}{(2\pi)^2}\sum_{m,n} P_{\vec{K}_{mn}} K_{mn}\int_0^{2\pi}\int_0^{\infty}\cos(\theta_{mn}-\theta_1)F(\rho_1)F(\rho_2) \\ \cdot\, e^{j\frac{\rho}{2}\{K_{mn}[(1+\cosh\mu\cos\delta)\cos(\theta_{mn}-\theta)+\sinh\mu\sin\delta\sin(\theta_{mn}-\theta)]-2k\cosh\mu\}}\, d\mu d\delta .\end{aligned} \tag{2.22}$$

Equation (2.22) is, formally, the expression for the scattered field at the observation point (ρ,θ). Now, with reference to Figure 2.1, it will be useful to consider the equation (2.22) for constant $(\rho_1+\rho_2)$ which corresponds to a fixed ellipse in the spatial sense and a fixed time in the temporal sense. To this end, we note from (2.21) that, for fixed μ,

$$(\rho_1+\rho_2) = \rho\cosh\mu \tag{2.23}$$

will yield the desired components of the received signal at a particular instant. If it is thus agreed to hold μ constant, the δ-integration may be effected. To aid in the visualization of this process, equation (2.22) may be presented as

$$\begin{aligned}(E_{0_n}^+)_1 &= \frac{kC_0}{(2\pi)^2}\sum_{m,n} P_{\vec{K}_{mn}} K_{mn} e^{j\frac{\rho K_{mn}}{2}\cos(\theta_{mn}-\theta)} \\ &\quad\cdot\int_0^{\infty} e^{-jk\rho\cosh\mu}\left\{\int_0^{2\pi}\cos(\theta_{mn}-\theta_1)F(\rho_1)F(\rho_2)\right. \\ &\quad\left.\cdot\, e^{j\frac{\rho K_{mn}}{2}[\cosh\mu\cos\delta\cos(\theta_{mn}-\theta)+\sinh\mu\sin\delta\sin(\theta_{mn}-\theta)]}d\delta\right\} d\mu ,\end{aligned} \tag{2.24}$$

from whence we write for the δ-integral

$$\begin{aligned}I_\delta &= \int_0^{2\pi}\cos(\theta_{mn}-\theta_1)F(\rho_1)F(\rho_2) \\ &\quad\cdot\, e^{j\frac{\rho K_{mn}}{2}[\cosh\mu\cos\delta\cos(\theta_{mn}-\theta)+\sinh\mu\sin\delta\sin(\theta_{mn}-\theta)]}d\delta .\end{aligned} \tag{2.25}$$

Of course, it is understood from equation (2.21) that ρ_1, ρ_2 and θ_1 are functions of (μ, δ). In equation (2.25), K_{mn} is a typical wavenumber associated with the scattering surface. Keeping in mind that eventually the analysis will be applied to a surface representative of ocean gravity waves, K_{mn} will be of order approximately 10^1 to $10^{-2}\mathrm{m}^{-1}$ (see Kinsman [20], Chapter 1). If we agree that, for bistatic operation, ρ will likely be several 10's of kilometres, then $\left(\frac{\rho K_{mn}}{2}\right)$ in the phase term of equation (2.25) will be a large parameter. From the plots of the attenuation functions given by Wait [12] it is seen that $F(\rho_1)$ and $F(\rho_2)$ are slowly varying quantities, especially for highly conductive surfaces such as sea water (conductivity $\sim 4\mho/\mathrm{m}$). Under these conditions, I_δ may be determined via a stationary phase integration, the details of which are found in Appendix A.1.2.1. The result is

$$I_\delta \approx \sqrt{2\pi}\cos(\theta_{mn}-\theta_1)F(\rho_1)F(\rho_2) \cdot \frac{e^{j\frac{\rho K_{mn}}{2}[\cosh\mu\cos\delta\cos(\theta_{mn}-\theta)+\sinh\mu\sin\delta\sin(\theta_{mn}-\theta)]}}{\left[j\frac{\rho K_{mn}}{2}\left[\cosh\mu\cos\delta\cos(\theta_{mn}-\theta)+\sinh\mu\sin\delta\sin(\theta_{mn}-\theta)\right]\right]^{\frac{1}{2}}} \quad (2.26)$$

where, in addition to (2.21), a stationary phase condition on δ as given by

$$\tan\delta = \tanh\mu\tan(\theta_{mn}-\theta) \quad (2.27)$$

applies. We note that θ and ρ (see Figure 2.1) are considered constant during the δ integration. This corresponds to fixed positions for the source and the receiver, and the integration is actually a sum over the values of δ satisfying equation (2.27).

In Appendix A.1.2.2, it is shown that the stationary phase condition on δ appearing in equation (2.27) leads to the conclusion that at the stationary scattering point the surface wave vector $\vec{K}_{mn}$ is normal to the scattering ellipse. This is depicted in Figure 2.3 where the ellipse of constant $(\rho_1+\rho_2)$ is shown (i.e. constant μ) . Without loss of generality, the direction of $\vec{\rho}$ from the transmitter, T, (relabeled from 0 of Figure 2.2) to the receiver, R, has been set to zero (i.e. $\theta = 0$). Vectors $\vec{N}$ and $\vec{T}$ shown in the

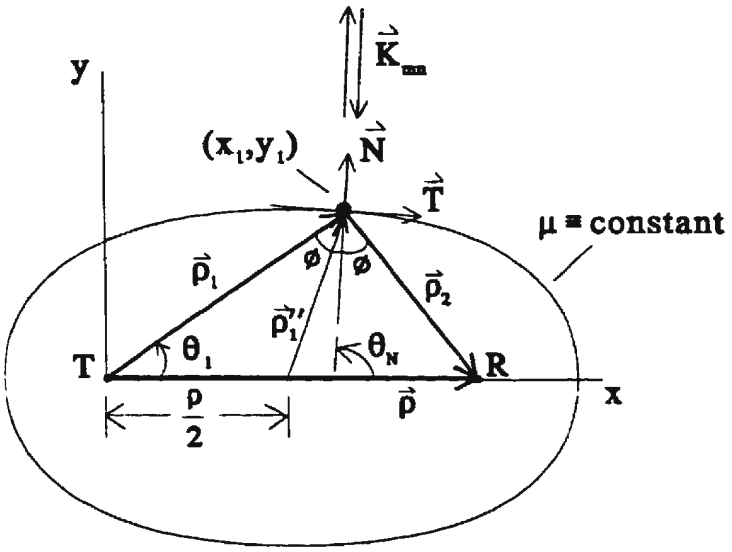

Figure 2.3: Depiction of the geometry associated with the first-order stationary phase condition. R and T are receiver and transmitter, respectively.

figure are the normal and the tangent vectors, respectively, at the point of scatter. They are used in Appendix A.1.2.2 to interpret the direction of $\vec{K}_{mn}$. It is also shown there that the angle between the transmitter and receiver as viewed from the scattering point is bisected by the ellipse normal at that point. Each portion of this bisection is seen in Figure 2.3 as angle ϕ, hereafter referred to as the *bistatic angle*. Appendix A.1.2.2 concludes by using the ideas and results stated in this paragraph to write a final asymptotic form for I_δ of equation (2.26) as

$$I_\delta \approx \sqrt{2\pi}(\pm(\sqrt{\cos\phi})\frac{F(\rho_1)F(\rho_2)}{\sqrt{K_{mn}\rho_s}}e^{\pm jK_{mn}\rho_s\cos\phi}e^{\mp j\frac{\pi}{4}} \tag{2.28}$$

with

$$\rho_s = \frac{\rho_1+\rho_2}{2} = \frac{\rho}{2}\cosh\mu\ .$$

Substituting I_δ from (2.28) into equation (2.24), it is seen that the first-order surface field may now be expressed as a single integral over μ given by

$$\begin{aligned}(E_{0_n}^+)_1 \;=\; & \frac{kC_0}{(2\pi)^{\frac{3}{2}}}\sum_{m,n}P_{\vec{K}_{mn}}\sqrt{K_{mn}}\,e^{j\frac{\vec{\rho}}{2}\cdot\vec{K}_{mn}}\int_0^\infty e^{-jk\rho\cosh\mu} \\ & \cdot e^{\mp j\frac{\pi}{4}}(\pm\sqrt{\cos\phi})\frac{F(\rho_1)F(\rho_2)}{\sqrt{\rho_s}}e^{\pm jK_{mn}\rho_s\cos\phi}\,d\mu\ .\end{aligned} \tag{2.29}$$

Next, it is desirable to write this $\mu-$integral in terms of the actual bistatic parameters of Figure 2.3. Noting, again, that $\rho_s = \frac{\rho}{2}\cosh\mu$,

$$d\rho_s = \frac{\rho}{2}\sinh\mu d\mu = \frac{\rho}{2}\sqrt{\cosh^2\mu - 1}\; d\mu$$

$$\Rightarrow \quad d\rho_s = \frac{\rho}{2}\sqrt{\frac{4\rho_s^2}{\rho} - 1}\; d\mu = \sqrt{\rho_s^2 - \left(\frac{\rho}{2}\right)^2}\; d\mu\,.$$

Since $\rho_s|_{\mu=0} = \frac{\rho}{2}$, equation (2.29), in view of the intervening change of variables, becomes

$$\begin{aligned}(E_{0_n}^+)_1 \;=\; & \frac{kC_0}{(2\pi)^{\frac{3}{2}}}\sum_{m,n} P_{\vec{K}_{mn}}\sqrt{K_{mn}}\, e^{j\frac{\vec{\rho}}{2}\cdot\vec{K}_{mn}} \int_{\frac{\rho}{2}}^{\infty} \frac{F(\rho_1)F(\rho_2)}{\sqrt{\rho_s[\rho_s^2 - \left(\frac{\rho}{2}\right)^2]}} \\ & \cdot\, e^{\mp j\frac{\pi}{4}}\left(\pm\sqrt{\cos\phi}\right) e^{j\rho_s[\pm K_{mn}\cos\phi - 2k]}\; d\rho_s\,. \end{aligned} \tag{2.30}$$

Equation (2.30) is the vertical component of the electric field observed at $\vec{\rho} = (\rho, 0°)$ after a single scatter from all points on the Fourier surface. We note that all surface points are included since $\rho_s = \frac{\rho_1 + \rho_2}{2}$ (see Figure 2.2) is the parameter over which the integration is being carried out. It should be reiterated also that this is the field for a continuously excited vertical dipole source. In Section 2.2.5 this field will be appropriately modified to include a pulsed or gated source and subsequently in Section 3.3 to include a time varying scattering surface.

2.2.2 The Second-order Solution for a Time Invariant Surface – Forward Analysis

Many of the ideas used in the first-order problem form the basis of extending the analysis to obtain an expression for the second-order field, $(E_{0_n}^+)_2$. However, as might be expected, this is a more complex result and several modifications to the procedures of Section 2.2.1 are necessitated.

Using equation (2.14), the second-order field may be written as

$$(E_{0_n}^+)_2 = \mathcal{T}_1^2(E_s) = \mathcal{T}_1[\mathcal{T}_1(E_s)] \tag{2.31}$$

which, from equation (2.15), becomes

$$(E_{0_n}^{+})_2 = \mathcal{T}_1 \left\{ \vec{\nabla}_{xy}(\xi) \cdot \vec{\nabla}_{xy} \left(C_0 F(\rho) \frac{e^{-jk\rho}}{2\pi\rho} \right) \overset{xy}{*} F(\rho) \frac{e^{-jk\rho}}{2\pi\rho} \right\} . \tag{2.32}$$

Then, using the asymptotic form of $\vec{\nabla}_{xy} \left(C_0 F(\rho) \frac{e^{-jk\rho}}{2\pi\rho} \right)$ given in equation (A.3), along with equations (2.6) and (2.12) ,

$$\begin{aligned} (E_{0_n}^{+})_2 \approx & -jkC_0 \left\{ \vec{\nabla}_{xy}(\xi) \cdot \vec{\nabla}_{xy} \left[\hat{\rho} \cdot \vec{\nabla}_{xy}(\xi) F(\rho) \frac{e^{-jk\rho}}{2\pi\rho} \overset{xy}{*} \right. \right. \\ & \left. \left. F(\rho) \frac{e^{-jk\rho}}{2\pi\rho} \right] \overset{xy}{*} F(\rho) \frac{e^{-jk\rho}}{2\pi\rho} \right\} . \end{aligned} \tag{2.33}$$

Equation (2.33) provides the foundation for all further discussion of the second-order scattering theory throughout this work. The convolutions therein may be generally interpreted according to Figure 2.4. The radiation from the transmitter position, $T(0,0)$, scatters in all directions from a general point (x_1, y_1). Some of this energy

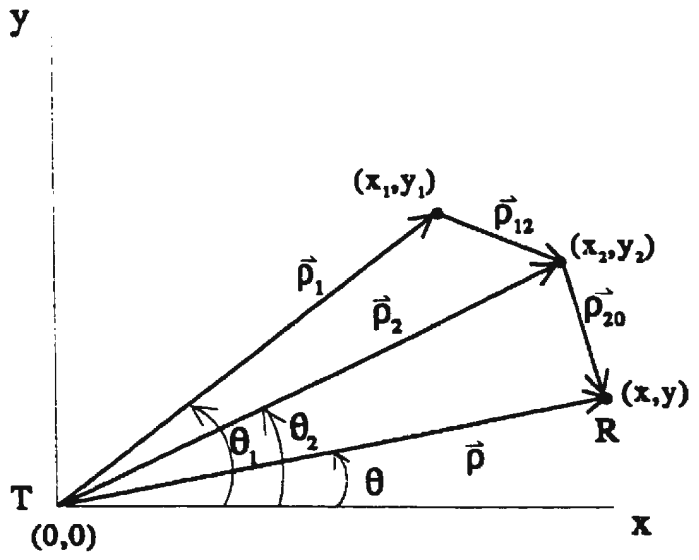

Figure 2.4: The geometry associated with the second-order scatter.

scatters again at point (x_2, y_2) and a portion of this is, in turn, received at $R(x, y)$. the field scattering from (x_1, y_1) and reaching (x_2, y_2) is represented by the inner

convolution of (2.33). The dot product of the gradient ($\vec{\nabla}_{xy}$) of this convolution with the surface gradient ($\vec{\nabla}_{xy}(\xi)$) represents the scatter from (x_2, y_2) so that the final convolution gives the received field at $R(x, y)$. At this stage of the analysis, (x_1, y_1) and (x_2, y_2) are general points and equation (2.33) therefore includes two scatters from any and all points on the surface. In what follows, an examination of the most significant components of the second-order field at R is carried out. In the following subsections, the convolutions in equation (2.33) will be carried out in the order in which they appear and hence the term "Forward Analysis" in the title of this section.

2.2.2.1 Reduction to Partial Integral Form

Cursory examination of equation (2.33) reveals that the convolutions may be approached in a variety of ways. For example, Gill and Walsh [68] presented a result for the components of the second-order field which arises when the two scatters occur near each other but far from both transmitter and receiver. In that work, the inner convolution was carried out before its gradient, $\vec{\nabla}_{xy}$, was applied. A suitable result which reduced nicely to the monostatic formulation by Walsh *et al.* [8] was obtained. However, during subsequent analysis it was found that the route taken precluded the possibility of obtaining what could be significant second-order components. With this in mind, an alternate approach is taken here.

Two important features of the convolution of functions $f_n(x, y)$ are

$$\vec{\nabla}_{xy}[f_1(x,y) * f_2(x,y)] = \vec{\nabla}_{xy}(f_1(x,y)) * f_2(x,y) = f_1(x,y) * \vec{\nabla}_{xy}(f_2(x,y)) \qquad (2.34)$$

and the convolution is associative, i.e.

$$\begin{aligned} f_1(x,y) * f_2(x,y) * f_3(x,y) &= [f_1(x,y) * f_2(x,y)] * f_3(x,y) \\ &= f_1(x,y) * [f_2(x,y) * f_3(x,y)] \,. \end{aligned} \qquad (2.35)$$

From property (2.34), equation (2.33) may be written as

$$\begin{aligned} (E_{0_n}^{+})_2 \approx\; & -jkC_0 \left\{ \vec{\nabla}_{xy}(\xi) \cdot \left[\vec{\nabla}_{xy}(\xi) \cdot \hat{\rho} \left(F(\rho) \frac{e^{-jk\rho}}{2\pi\rho} \right) \overset{xy}{*} \vec{\nabla}_{xy} \left(F(\rho) \frac{e^{-jk\rho}}{2\pi\rho} \right) \right] \right. \\ & \left. \overset{xy}{*} F(\rho) \frac{e^{-jk\rho}}{2\pi\rho} \right\} \,. \end{aligned} \qquad (2.36)$$

Using the same asymptotic argument as that leading to equation (A.3),

$$\vec{\nabla}_{xy}\left(F(\rho)\frac{e^{-jk\rho}}{2\pi\rho}\right) \approx -jkF(\rho)\frac{e^{-jk\rho}}{2\pi\rho}\hat{\rho}\ ,$$

so that, on noting $\hat{\rho}\cdot\vec{\nabla}_{xy}(\xi)$ is a scalar, equation (2.36) may be cast as

$$\begin{aligned}(E_{0_n}^{+})_2 \approx\ & \frac{-k^2C_0}{(2\pi)^3}\left\{\left[\vec{\nabla}_{xy}(\xi)\cdot\hat{\rho}\left(F(\rho)\frac{e^{-jk\rho}}{\rho}\right)\right]_1\right. \\ & \overset{xy}{*}\ \left[\vec{\nabla}_{xy}(\xi)\cdot\hat{\rho}\left(F(\rho)\frac{e^{-jk\rho}}{\rho}\right)\right]_2 \overset{xy}{*}\left.\left[F(\rho)\frac{e^{-jk\rho}}{\rho}\right]_3\right\} \qquad (2.37)\end{aligned}$$

The subscripted square brackets in (2.37) may again be referenced to Figure 2.4 as follows: $[\cdots]_1$ accounts for propagation from T along $\vec{\rho}_1$ and scattering at (x_1, y_1); $[\cdots]_2$ similarly accounts for propagation from (x_1, y_1) along $\vec{\rho}_{12}$ and scattering at (x_2, y_2); and $[\cdots]_3$ involves propagation from (x_2, y_2) along $\vec{\rho}_{20}$ to the point of reception, R.

In the course of the analysis, we shall have cause to consider equation (2.36) according to the two separate groupings indicated in equation (2.35). As an initial approach to finding the important parts of $(E_{0_n}^{+})_2$, the convolutions will be done in the order in which they appear, i.e. the first form in equation (2.35).

From equation (2.37) the first convolution may be denoted by

$$I_{12F} = \left[\vec{\nabla}(\xi)\cdot\hat{\rho}F(\rho)\frac{e^{-jk\rho}}{\rho}\right]_1 \overset{xy}{*}\left[\vec{\nabla}(\xi)\cdot\hat{\rho}F(\rho)\frac{e^{-jk\rho}}{\rho}\right]_2 \qquad (2.38)$$

where the subscript $_{12F}$ indicates the forward convolution describing the scattering explained above. The first dot product of (2.38) appears as equation (A.7) in Appendix A.1.1 . That is,

$$\begin{aligned}(\vec{\nabla}(\xi)\cdot\hat{\rho})_1 &= \vec{\nabla}(\xi(x_1, y_1))\cdot\hat{\rho}_1 \\ &= j\sum_{m,n} P_{\vec{K}_{mn}} K_{mn}\cos(\theta_{mn}-\theta_1)\cdot\ e^{j\rho_1 K_{mn}\cos(\theta_{mn}-\theta_1)} \qquad (2.39)\end{aligned}$$

where $P_{\vec{K}_{mn}}$, K_{mn}, and θ_{mn} are the Fourier coefficient, wavenumber, and direction of wave vector $\vec{K}_{mn}$ associated with the surface at the first scattering point, (x_1, y_1), and θ_1 is the direction of $\vec{\rho}_1$ as given in Figure 2.4. In the same fashion, since $\hat{\rho}_{12}\cdot\hat{\rho}_2$

$= \cos(\theta_{12} - \theta_2)$ and $\hat{\rho}_{12} \cdot \hat{\theta}_2 = \sin(\theta_{12} - \theta_2)$, it is easy to show that the second dot product in equation (2.38) may be characterized as

$$\begin{aligned}(\vec{\nabla}(\xi) \cdot \hat{\rho})_2 &= \vec{\nabla}(\xi(x_2, y_2)) \cdot \hat{\rho}_{12} \\ &= j \sum_{p,q} P_{\vec{K}_{pq}} K_{pq} \cos(\theta_{pq} - \theta_{12}) \cdot e^{j\rho_2 K_{pq} \cos(\theta_{pq} - \theta_2)} \end{aligned} \tag{2.40}$$

where the pq subscripts designate, at the second scattering point, (x_2, y_2), the same kind of quantities as the mn subscripts denote at (x_1, y_1). Note that $\hat{\rho}_{12}$ is the unit vector in the direction of propagation from (x_1, y_1) to (x_2, y_2) and θ_{12} is its direction.

Proceeding in the same way as for the first-order convolution of equation (2.15), equation (2.38) in integral form becomes

$$\begin{aligned}I_{12F} &= -\sum_{m,n} \sum_{p,q} P_{\vec{K}_{mn}} K_{mn} P_{\vec{K}_{pq}} K_{pq} \int_{x_1} \int_{y_1} \cos(\theta_{mn} - \theta_1) e^{j[\rho_1 K_{mn} \cos(\theta_{mn} - \theta_1) - k\rho_1]} \\ &\quad \cdot \cos(\theta_{pq} - \theta_{12}) e^{j[\rho_2 K_{pq} \cos(\theta_{pq} - \theta_2) - k\rho_2]} \cdot \frac{F(\rho_1) F(\rho_{12})}{\rho_1 \rho_{12}} \, dx_1 dy_1 \, . \end{aligned} \tag{2.41}$$

In view of equation (2.37) and the intervening analysis, the former is then

$$(E_{0_n}^+)_2 \approx \frac{-k^2 C_0}{(2\pi)^3} I_{12F} \overset{xy}{*} \left[F(\rho) \frac{e^{-jk\rho}}{\rho} \right]_3 \, . \tag{2.42}$$

Before attempting the final convolution, we seek a stationary phase result for I_{12F} as described in the next section.

2.2.2.2 A Stationary Phase Approach to the Second-order Field

As in the first-order case, it is convenient to change to elliptic coordinates in order to seek a stationary phase approximation of I_{12F} in equation (2.41). This is accomplished in a way completely analogous to the three steps outlined in Section 2.2.1.2. Referencing Figure 2.4, (1) rotate the coordinate axis by θ_2, (2) shift the origin halfway along ρ_2 and (3) introduce elliptic coordinates. Corresponding to equations (2.20) and (2.21) we then have

$$\begin{aligned} x_1 &= \frac{\rho_2}{2} \{(\cosh\mu \cos\delta + 1)\cos\theta_2 - \sinh\mu \sin\delta \sin\theta_2\} \\ y_1 &= \frac{\rho_2}{2} \{(\cosh\mu \cos\delta + 1)\sin\theta_2 + \sinh\mu \sin\delta \cos\theta_2\} \end{aligned} \tag{2.43}$$

and

$$\begin{aligned}
\rho_1 &= \sqrt{x_1^2 + y_1^2} = \frac{\rho_2}{2}(\cosh\mu + \cos\delta) \\
\rho_{12} &= \sqrt{(x_2 - x_1)^2 + (y_2 - y_1)^2} = \frac{\rho_2}{2}(\cosh\mu - \cos\delta) \qquad (2.44) \\
\theta_1 &= \tan^{-1}\frac{y_1}{x_1} = \tan^{-1}\left[\frac{(1+\cosh\mu\cos\delta)\sin\theta_2 + \sinh\mu\sin\delta\cos\theta_2}{(1+\cosh\mu\cos\delta)\cos\theta_2 - \sinh\mu\sin\delta\sin\theta_2}\right] .
\end{aligned}$$

From (2.43), $dx_1 dy_1 = \rho_1\rho_{12}d\mu d\delta$. Additionally, from (2.44), $\rho_1 + \rho_{12} = \rho_2\cosh\mu$ giving

$$e^{j(-k\rho_1 - k\rho_2)} = e^{j\frac{\rho_2}{2}(-2k\cosh\mu)} . \qquad (2.45)$$

Expanding $\cos(\theta_{mn} - \theta_1)$ in the exponential of equation (2.41), noting that $x_1 = \rho_1\cos\theta_1$ and $y_1 = \rho_1\sin\theta_1$ along with equations (2.43) and (2.45) then permits (2.41) to be written as

$$\begin{aligned}
I_{12F} &= -\sum_{m,n}\sum_{p,q} P_{\vec{K}_{mn}} K_{mn} P_{\vec{K}_{pq}} K_{pq} \int_{\delta=0}^{2\pi}\int_{\mu=0}^{\infty} \cos(\theta_{mn} - \theta_1)\cos(\theta_{pq} - \theta_{12}) \\
&\quad \cdot e^{j\rho_2 K_{pq}\cos(\theta_{pq} - \theta_2)} F(\rho_1)F(\rho_{12}) e^{j\frac{\rho_2}{2}\Phi_{12}(\mu,\delta)}\, d\mu d\delta \qquad (2.46)
\end{aligned}$$

where

$$\begin{aligned}
\Phi_{12}(\mu,\delta) &= K_{mn}[(1+\cosh\mu\cos\delta)\cos(\theta_{mn} - \theta_2) \\
&\quad + \sinh\mu\sin\delta\sin(\theta_{mn} - \theta_2)] - 2k\cosh\mu . \qquad (2.47)
\end{aligned}$$

It must be emphasized that during the $x_1 - y_1$ integration, or equivalently the $\mu - \delta$ integration, ρ_2 and θ_2 along with the variables subscripted by mn and pq are considered fixed.

The significant contributions to I_{12F} in equation (2.46) are determined via a modification of a two-dimensional stationary phase method, the theory of which is found in Bleistein and Handelsman [66], Chapter 8 or Friedman [69], Chapter 3. According to this theory, the stationary points of the integral in (2.46) are the solutions to the simultaneous equations

$$\frac{\partial\Phi_{12}(\mu,\delta)}{\partial\mu} = 0$$

and (2.48)

$$\frac{\partial \Phi_{12}(\mu,\delta)}{\partial \delta} = 0 .$$

Therefore, from (2.46) the solution to the pair of transcendental equations

$$\begin{aligned} K_{mn}[\sinh\mu\cos\delta\cos(\theta_{mn}-\theta_2)+\cosh\mu\sin\delta\sin(\theta_{mn}-\theta_2)]-2k\sinh\mu &= 0 \\ K_{mn}[-\cosh\mu\sin\delta\cos(\theta_{mn}-\theta_2)+\sinh\mu\cos\delta\sin(\theta_{mn}-\theta_2)] &= 0 \end{aligned} \quad (2.49)$$

is required. After some algebra, the solutions are found to be

$$\begin{aligned} &(1)\quad \mu=0 \quad \delta=0 \\ &(2)\quad \mu=0 \quad \delta=\pm\pi \text{ (only one of the pair is distinct)} \\ &(3)\quad \tan\delta=\frac{\sqrt{K_{mn}^2-4k^2\cos^2(\theta_{mn}-\theta_2)}}{2k\cos(\theta_{mn}-\theta_2)} \end{aligned} \quad (2.50)$$

$$\tanh\mu=\frac{\sqrt{K_{mn}^2-4k^2\cos^2(\theta_{mn}-\theta_2)}}{2k\sin(\theta_{mn}-\theta_2)} .$$

In (3) of (2.50), the restriction $2k|\cos(\theta_{mn}-\theta_2)| < K_{mn} < 2k$ obviously applies. Furthermore, $\theta_{mn} \neq \theta_2$, $\theta_2 \neq \theta_{mn} \pm \frac{\pi}{2}$ in the points designated by (3), but these values are covered by the first two stationary points.

Prior to determining the form of I_{12F} of (2.46) for each of the three cases in (2.50), it is desirable to give some physical meaning to these stationary values:

1. Stationary Point $(\mu,\delta) \equiv (0,0)$

   From the first two equations in (2.44), $(\mu,\delta) \equiv (0,0)$ means that $\rho_1 = \rho_2$ and $\rho_{12} = 0$. With reference to Figure 2.4, it is seen that this indicates a double scatter at (x_1, y_1) (i.e.$(x_2, y_2) \equiv (x_1, y_1)$). For reasons that will become evident when this analysis is applied to a pulse radar (Section 2.2.5.2), it is customary to refer to this phenomenon as "patch scatter". The geometry appears in Figure 2.5a.

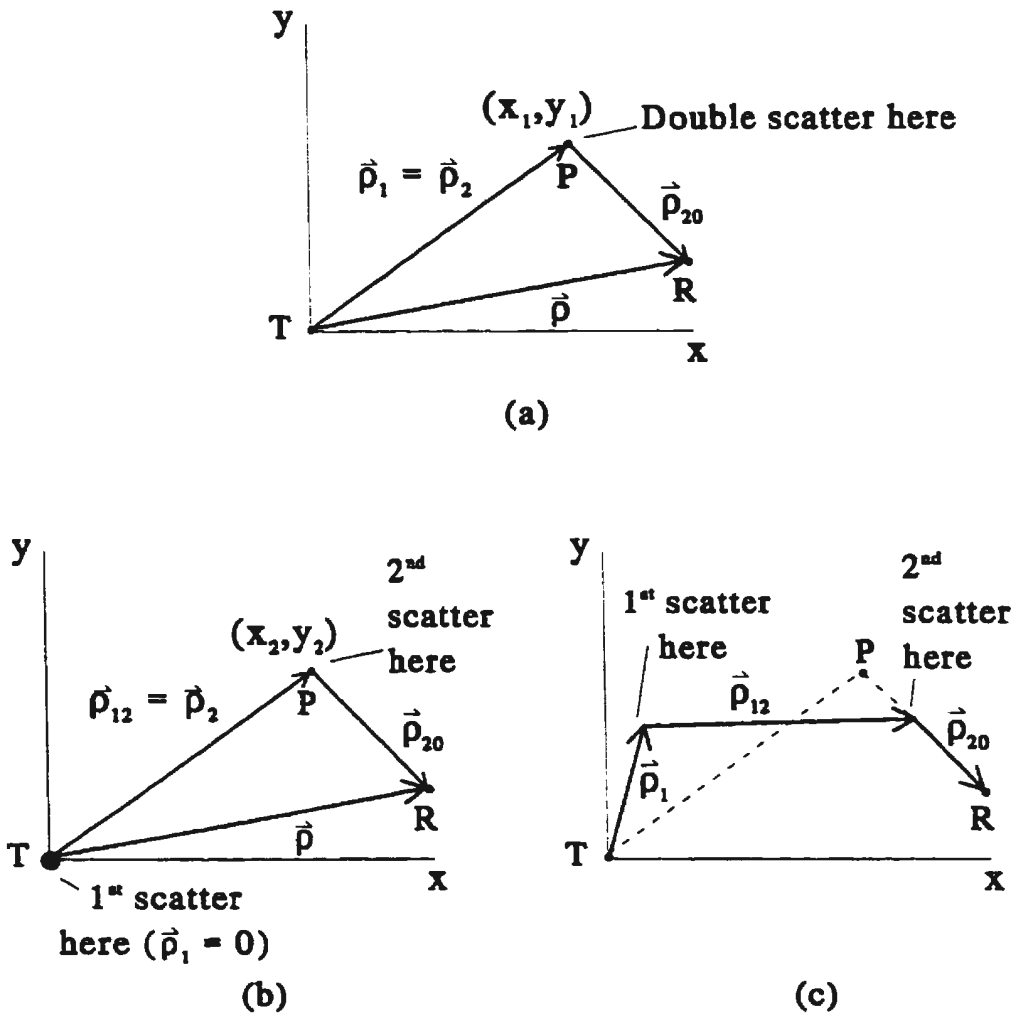

Figure 2.5: Possible occurrences of second-order scatter showing (a) both scatters on a remote "patch", (b) one scatter near the transmitter followed by another on the remote patch and (c) two scatters off the patch.

2. Stationary Point $(\mu, \delta) \equiv (0, \pi)$

For the $(0, \pi)$ stationary point the first two equations of (2.44) reduce to $\rho_1 = 0$, $\rho_{12} = \rho_2$. This time, Figure 2.4 indicates that point (x_1, y_1) has shifted to the transmitting sight, T, and the second scatter occurs remotely from T at (x_2, y_2). Given that $\theta_{12} = \tan^{-1}\left[\frac{y_2 - y_1}{x_2 - x_1}\right]$ it is easy to show that $\theta_{12} \rightarrow \theta_2$ uniquely as $(\mu, \delta) \rightarrow (0, \pi)$. Thus, the $(0, \pi)$ represents a first scatter near the transmitter and a second on a patch of ocean which is "viewed" from R. See Figure 2.5b. When using a narrow beam receiver, the second scatter must be on the same

"patch" as (x_1, y_1) was above if this component is received at the same time as that from (1).

3. Stationary Point From (3) in Equation (2.50)

The restrictions on the third stationary "point" (which is really a set of points) stated following (2.50) make it distinct from the previous two points. Thus, the scatter for the third "point" must occur elsewhere than at the transmitter or at the remote patch whereon (x_1, y_1) or (x_2, y_2) resides. However, to be received at R simultaneously with the other two components, the total scatter path length must be the same as for the other two points. Referring to Figure 2.5(c) it is clear that for this case the double scatter will always involve two single bistatic scatters. From Equation (2.30), it is seen from the $\sqrt{\cos\phi}$ factor, that a single scatter will be strongest when the bistatic angle, ϕ, is 0, i.e. the backscatter condition. This will not occur for this "off-patch" scatter, even if R is moved to T. Consequently, off-patch scatter will not be as strong as that represented by the first two stationary points for which one of the scatters can indeed be a backscatter. In fact, for monostatic operation, Srivastava [54] shows that, in relation to the other two, this third case is not significant. It will, therefore, not be further addressed in this thesis. As a final point in this discussion, it should be mentioned that the receiver will later be considered to be of the narrow beam type (this is implied in Figure 2.5 in that the final scatter is shown to travel along the direction from a distant patch point, P, to the receiver position, R).

2.2.2.3 A Modified Stationary Phase Solution for Patch Scatter

In the previous section, it was concluded that the stationary point $(0, 0)$ corresponded to a double scatter on a surface patch remote from both the transmitter and receiver. With reference to Figures 2.4 and 2.5a and equations (2.43) and (2.44), the following

hold:

$$\begin{aligned}
\rho_1 &= \rho_2 \\
\rho_{21} &= 0 \\
\theta_1 &= \theta_2 \\
\theta_{12} &= \tan^{-1}\left[\frac{y_2 - y_1}{x_2 - x_1}\right] \\
&= \tan^{-1}\left[\frac{(1+\cosh\mu\cos\delta)\sin\theta_2 - \sinh\mu\sin\delta\cos\theta_2}{(1+\cosh\mu\cos\delta)\cos\theta_2 - \sinh\mu\sin\delta\sin\theta_2}\right] .
\end{aligned} \tag{2.51}$$

An extremely important matter here concerns the value of θ_{12} at the stationary point. In fact, it can be shown that as $(\mu,\delta) \to (0,0)$, θ_{12} is not unique, but takes a different value for each direction of approach towards the stationary point. The physical significance of this point is that radiation from the first scatter may occur in *any* direction before scattering the second time. One way to verify this is to let $\mu = m\delta$ (to distinguish different lines of approach for different m's) in θ_{12} given above. Using L'Hopital's Rule it then transpires that

$$\lim_{\delta\to 0}\theta_{12}(\delta) = \tan^{-1}\left[\frac{(1-m^2)\sin\theta_2 - 2m\cos\theta_2}{(1-m^2)\cos\theta_2 + 2m\sin\theta_2}\right] ,$$

and the assertion of non-uniqueness is established. Because of this, the standard two-dimensional stationary phase technique cannot be applied directly to equation (2.46) since $\cos(\theta_{pq} - \theta_{12})$ found there is not unique at $(\mu,\delta) \equiv (0,0)$. The modification to the usual approach constitutes the remainder of this section.

In finding the stationary points of the integral in equation (2.46), ρ_2 and θ_2 were fixed. This fact, along with the ρ and θ relationships of (2.51), gives for (2.46)

$$\begin{aligned}
I_{12F,1} &= -\frac{1}{2}\sum_{m,n}\sum_{p,q} P_{\vec{K}_{mn}} K_{mn} P_{\vec{K}_{pq}} K_{pq} e^{j\rho_2 K_{pq}\cos(\theta_{pq}-\theta_2)} \cos(\theta_{mn}-\theta_2) F(\rho_2) F(0) \\
&\quad \cdot \int_0^{2\pi}\int_0^{\infty} \cos(\theta_{pq}-\theta_{12}) e^{j\frac{\rho_2}{2}\Phi_{12}(\mu,\delta)}\, d\mu d\delta
\end{aligned} \tag{2.52}$$

with $\Phi_{12}(\mu,\delta)$ as defined in (2.47) and $I_{12F,1}$ being the component of I_{12F} considered at the first stationary point. The factor of $\frac{1}{2}$ in front of the summations appears

because the stationary point $(0,0)$ is on the boundary of integration (see Friedman [69], Chapter 3).

An approximation of the double integral in (2.52) is sought by expanding $\Phi_{12}(\mu,\delta)$ in a double Taylor series to second order about the stationary point $(0,0)$. From equation (2.48) it is obvious that the first-order term in this expression is 0, leaving

$$\Phi_{12}(\mu,\delta) \approx \Phi_{12}(0,0) + \frac{1}{2}\left[\frac{\partial^2\Phi_{12}}{\partial\mu^2}\mu^2 + \frac{2\partial^2\Phi_{12}}{\partial\mu\partial\delta}\mu\delta + \frac{\partial^2\Phi_{12}}{\partial\delta^2}\right]_{(0,0)} ,$$

which is easily shown to give

$$\begin{aligned}\Phi_{12}(\mu,\delta) \approx\ & [2K_{mn}\cos(\theta_{mn}-\theta_2)-2k] \\ & + \frac{1}{2}\{[K_{mn}\cos(\theta_{mn}-\theta_2)-2k]\mu^2 + 2K_{mn}\sin(\theta_{mn}-\theta_2)\mu\delta \\ & - K_{mn}\cos(\theta_{mn}-\theta_2)\delta^2\} . \end{aligned} \tag{2.53}$$

The first term in (2.53) is constant with respect to the integration variables and therefore $I_{12F,1}$ of equation (2.52) may be written from (2.51) and (2.53) in the form

$$\begin{aligned} I_{12F,1} \approx\ & -\frac{1}{2}\sum_{m,n}\sum_{p,q} P_{\vec{K}_{mn}} K_{mn} P_{\vec{K}_{pq}} K_{pq}\, e^{j\rho_2 K_{pq}\cos(\theta_{pq}-\theta_2)} \\ & \cdot e^{j\frac{\rho_2}{2}[2K_{mn}\cos(\theta_{mn}-\theta_2)-2k]}\cos(\theta_{mn}-\theta_2)F(\rho_2)F(0) \\ & \cdot \int_0^{2\pi}\int_0^{\infty}\cos(\theta_{pq}-\theta_{12})e^{j\frac{\rho_2}{4}Q(\mu,\delta)}\, d\mu d\delta \end{aligned} \tag{2.54}$$

with

$$\begin{aligned} Q(\mu,\delta) =\ & [K_{mn}\cos(\theta_{mn}-\theta_2)-2k]\mu^2 + 2K_{mn}\sin(\theta_{mn}-\theta_2)\mu\delta \\ & - K_{mn}\cos(\theta_{mn}-\theta_2)\delta^2 . \end{aligned} \tag{2.55}$$

The analysis becomes algebraically intensive at this point and the details associated with the results given in the remainder of this section appear in Appendix A.2.1.

As a first step, we write the double integral of (2.54) separately as

$$I_m = \int_0^{2\pi}\int_0^{\infty}\cos(\theta_{pq}-\theta_{12})e^{j\frac{\rho_2}{4}Q(\mu,\delta)}\, d\mu d\delta . \tag{2.56}$$

This integration is more easily effected with a change of variables which eliminates the cross term (i.e. the $\mu\delta$ term) of $Q(\mu,\delta)$ in (2.55). All of the details are in the appendix referred to above. Following a general procedure given in DeRusso *et al.* [70], Section 4.9, the starting point is to cast $Q(\mu,\delta)$ as

$$Q(\mu,\delta) = \begin{bmatrix} \mu & \delta \end{bmatrix} \begin{bmatrix} K_{mn}\cos(\theta_{mn}-\theta_2) - 2k & K_{mn}\sin(\theta_{mn}-\theta_2) \\ K_{mn}\sin(\theta_{mn}-\theta_2) & -K_{mn}\cos(\theta_{mn}-\theta_2) \end{bmatrix} \begin{bmatrix} \mu \\ \delta \end{bmatrix} . \tag{2.57}$$

It can then be shown that in (ψ,χ) coordinates

$$Q(\psi,\chi) = \lambda_1\psi^2 + \lambda_2\chi^2 , \tag{2.58}$$

where λ_1 and λ_2 are the eigenvalues of the large matrix in (2.57) and are given by

$$\begin{aligned} \lambda_1 &= -k + \sqrt{k^2 + K_{mn}^2 - 2kK_{mn}\cos(\theta_{mn}-\theta_2)} \\ &\text{and} \\ \lambda_2 &= -k - \sqrt{k^2 + K_{mn}^2 - 2kK_{mn}\cos(\theta_{mn}-\theta_2)} \end{aligned} \tag{2.59}$$

and

$$\begin{aligned} \psi &= \left[\frac{(\lambda_1 + K_{mn}\cos(\theta_{mn}-\theta_2))\mu + (K_{mn}\sin(\theta_{mn}-\theta_2))\delta}{[(\lambda_1 + K_{mn}\cos(\theta_{mn}-\theta_2))^2 + (K_{mn}\sin(\theta_{mn}-\theta_2))^2]^{\frac{1}{2}}} \right] \\ &\text{while} \\ \chi &= \left[\frac{(K_{mn}\sin(\theta_{mn}-\theta_2))\mu + (\lambda_2 - K_{mn}\cos(\theta_{mn}-\theta_2) + 2k)\delta}{[(\lambda_2 - K_{mn}\cos(\theta_{mn}-\theta_2) + 2k)^2 + (K_{mn}\sin(\theta_{mn}-\theta_2))^2]^{\frac{1}{2}}} \right] . \end{aligned} \tag{2.60}$$

In terms of ψ and χ, $\cos(\theta_{pq}-\theta_{12})$ in equation (2.56) may be written as outlined in Appendix A.2.1.2 (to second order in μ and δ) as

$$\cos(\theta_{pq}-\theta_{12}) \approx \frac{1}{c_1[\psi^2+\chi^2]} \cdot \left\{ c_2\psi^2 - c_2\chi^2 + c_3\psi\chi \right\} \tag{2.61}$$

where

$$\begin{aligned} c_1 &= (\lambda_1 + K_{mn}\cos(\theta_{mn}-\theta_2))^2 + (K_{mn}\sin(\theta_{mn}-\theta_2))^2 \\ c_2 &= [(K_{mn}\sin(\theta_{mn}-\theta_2))^2 - (\lambda_1 + K_{mn}\cos(\theta_{mn}-\theta_2))^2]\cos(\theta_{pq}-\theta_2) \\ &\quad -[(2K_{mn}\sin(\theta_{mn}-\theta_2))(\lambda_1 + K_{mn}\cos(\theta_{mn}-\theta_2)]\sin(\theta_{pq}-\theta_2) \\ c_3 &= -2\{(2K_{mn}\sin(\theta_{mn}-\theta_2))(\lambda_1 + K_{mn}\cos(\theta_{mn}-\theta_2)]\cos(\theta_{pq}-\theta_2) \\ &\quad + [(K_{mn}\sin(\theta_{mn}-\theta_2))^2 - (\lambda_1 + K_{mn}\cos(\theta_{mn}-\theta_2))^2]\sin(\theta_{pq}-\theta_2)\} . \end{aligned}$$

Utilizing equations (2.58) through (2.61) and observing that the Jacobian of the transformation from (μ, δ) to (ψ, χ) is unity, equation (2.56) appears in the new coordinates as

$$I_m \approx \int_{-\infty}^{\infty}\int_{-\infty}^{\infty} \frac{c_2(\psi^2-\chi^2)+c_3\psi\chi}{c_1[\psi^2+\chi^2]} e^{j\frac{\rho_2}{4}[\lambda_1\psi^2+\lambda_2\chi^2]}\, d\psi d\chi \,. \tag{2.62}$$

The exponential immediately suggests a change of variables to polar coordinates (r, ν) so that $\psi = r\cos\nu$ and $\chi = r\sin\nu$ with the Jacobian obviously given as $rdrd\nu$. Implementing this change, again as detailed in Appendix 2.1.3, it is shown that

$$I_m \approx \frac{-4\pi j}{\rho_2}\left[\frac{c_2\sqrt{\lambda_1\lambda_2}+c_2 k}{c_1\sqrt{k^2+K_{mn}^2-2kK_{mn}\cos(\theta_{mn}-\theta_2)}\sqrt{\lambda_1\lambda_2}}\right] .$$

From the definition of the various constants in equations (2.59) and (2.61) and multiplying I_m by the factors $K_{pq}K_{mn}\cos(\theta_{mn}-\theta_2)$ of equation (2.54), the latter is shown to reduce to

$$\begin{aligned} I_{12F,1} \;\approx\; & -2\pi\sum_{m,n}\sum_{p,q} P_{\vec{K}_{mn}} P_{\vec{K}_{pq}} e^{j\rho_2 K_{pq}\cos(\theta_{pq}-\theta_2)} \frac{F(\rho_2)}{\rho_2} \cdot \gamma_{E12F,1} \\ & \cdot e^{j\frac{\rho_2}{2}[2K_{mn}\cos(\theta_{mn}-\theta_2)-2k]} , \end{aligned} \tag{2.63}$$

where $F(0) = 1$ has been used and

$$\gamma_{E12F,1} = \left\{\frac{j\sqrt{\vec{K}_{mn}\cdot[\vec{K}_{mn}-2k\hat{\rho}_2]}+k}{k^2+\vec{K}_{mn}\cdot[\vec{K}_{mn}-2k\hat{\rho}_2]}\right\} \cdot \left\{\frac{(\vec{K}_{mn}\cdot\hat{\rho}_2)[\vec{K}_{pq}\cdot(\vec{K}_{mn}-k\hat{\rho}_2)]}{\sqrt{\vec{K}_{mn}\cdot(\vec{K}_{mn}-2k\hat{\rho}_2)}}\right\} . \tag{2.64}$$

The parameter $\gamma_{E12F,1}$, whose subscripts have been chosen to link it to the integration at this first stationary point, clearly involves the interaction of the transmit wave vector, $\vec{k}$, with the surface wave vectors $\vec{K}_{pq}$ and $\vec{K}_{mn}$. It has been customary in other analysis, (e.g. Srivastava [54], Walsh *et al.* [8]), to refer to such a parameter as an *electromagnetic coupling coefficient.* Here, then, $\gamma_{E12F,1}$ is the electromagnetic coupling coefficient for "patch scatter". This quantity is examined in detail when the analysis is applied to the ocean surface (Section 3.6.3, note 4). Prior to applying the convolution indicated by equation (2.42), consider that the exponentials in equation

(2.63) may be written as

$$e^{j\rho_2[K_{pq}\cos(\theta_{pq}-\theta_2)+K_{mn}\cos(\theta_{mn}-\theta_2)-k]} = e^{j\rho_2[(\vec{K}_{pq}\cdot\hat{\rho}_2+\vec{K}_{mn}\cdot\hat{\rho}_2)-k]}$$
$$= e^{j\rho_2[(\vec{K}_{pq}+\vec{K}_{mn})\cdot\hat{\rho}_2-k]} = e^{j\rho_2[K_{rs}\cos(\theta_{rs}-\theta_2)-k]} \qquad (2.65)$$

where $K_{rs} = |\vec{K}_{mn} + \vec{K}_{pq}|$ and θ_{rs} is the direction of $(\vec{K}_{mn} + \vec{K}_{pq})$. Then, to indicate the contribution of the first stationary point to the E-field of (2.42), equations (2.63) and (2.65) may be used to write

$$(E_{0_n}^+)_{2,F,1} \approx \frac{-k^2 C_0}{(2\pi)^3} I_{12F,1} \overset{xy}{*} \left[F(\rho)\frac{e^{-jk\rho}}{\rho}\right]_3 . \qquad (2.66)$$

That is, $(E_{0_n}^+)_{2,F,1}$ is the contribution to the second-order field received at R (of Figure 2.4) from a double scatter on a surface patch remote from both the transmitter, T, and the receiver, the analysis being executed in the forward (F) sense as mentioned following equation (2.38).

Synthesizing equations (2.63), (2.65) and (2.66),

$$(E_{0_n}^+)_{2,F,1} \approx \frac{-kC_0}{(2\pi)^2}\sum_{m,n}\sum_{p,q} P_{\vec{K}_{mn}} P_{\vec{K}_{pq}}(-k\gamma_{E12F,1})$$
$$\cdot \frac{F(\rho_2)}{\rho_2} e^{j\rho_2[K_{rs}\cos(\theta_{rs}-\theta_2)-k]} \overset{xy}{*} \left[F(\rho)\frac{e^{-jk\rho}}{\rho}\right]_3 . \qquad (2.67)$$

Noting from Figure 2.4 that the appropriate distance parameter in $[\cdots]_3$ is ρ_{20}, it is clear from Appendix A.1.1 that equation (2.67) may be written in the form

$$(E_{0_n}^+)_{2,F,1} \approx \frac{-kC_0}{(2\pi)^2}\sum_{m,n}\sum_{p,q} P_{\vec{K}_{mn}} P_{\vec{K}_{pq}} \int_{y_2}\int_{x_2}(-k\gamma_{E12F,1})$$
$$\cdot \frac{F(\rho_2)F(\rho_{20})}{\rho_2\rho_{20}} e^{j\rho_2[K_{rs}\cos(\theta_{rs}-\theta_2)]} \cdot e^{-j(\rho_2+\rho_{20})k}\, dx_2 dy_2 . \qquad (2.68)$$

The double integral here is seen to be of the same *form* as for the first-order result in equation (2.19). Thus, an elliptic coordinate approach may again be taken. Since the concepts involved are not new, the procedure as it pertains to the second-order scatter and the propagation along $\vec{\rho}_{20}$ in Figure 2.4 may be summarized as follows: (1) rotate the coordinate axis through angle θ; (2) shift the origin halfway along $\vec{\rho}$;

(3) write the rotated/translated coordinates in terms of the usual elliptic coordinates so that then

$$\begin{aligned}
\rho_2 &= \frac{\rho}{2}(\cosh\mu + \cos\delta) \\
\rho_{20} &= \frac{\rho}{2}(\cosh\mu - \cos\delta) \\
\rho_2 + \rho_{20} &= \rho\cosh\mu \\
x_2 &= \frac{\rho}{2}[(1+\cosh\mu\cos\delta)\cos\theta - \sinh\mu\sin\delta\sin\theta] = \rho_2\cos\theta_2 \\
y_2 &= \frac{\rho}{2}[(1+\cosh\mu\cos\delta)\sin\theta + \sinh\mu\sin\delta\cos\theta] = \rho_2\sin\theta_2 \\
\theta_2 &= \tan^{-1}\left(\frac{y_2}{x_2}\right) = \tan^{-1}\left[\frac{(1+\cosh\mu\cos\delta)\sin\theta + \sinh\mu\sin\delta\cos\theta}{(1+\cosh\mu\cos\delta)\cos\theta - \sinh\mu\sin\delta\sin\theta}\right] \\
dx_2dy_2 &= \rho_2\rho_{20}d\mu d\delta
\end{aligned} \tag{2.69}$$

Consequently, equation (2.68) becomes in elliptical coordinates

$$\begin{aligned}
(E_{0_n}^{+})_{2,F,1} \approx\ & \frac{-kC_0}{(2\pi)^2}\sum_{m,n}\sum_{p,q} P_{\vec{K}_{mn}}P_{\vec{K}_{pq}} \\
& \cdot e^{j\frac{\rho}{2}(K_{rs}\cos(\theta_{rs}-\theta))}\int_0^{\infty} e^{-jk\rho\cosh\mu}\left\{\int_0^{2\pi}(-k\gamma_{E12F,1})\right. \\
& \cdot e^{j\frac{\rho K_{rs}}{2}[\cosh\mu\cos\delta\cos(\theta_{rs}-\theta)+\sinh\mu\sin\delta\sin(\theta_{rs}-\theta)]} \\
& \left.\cdot F(\rho_2)F(\rho_{20})d\delta\right\}d\mu\ .
\end{aligned} \tag{2.70}$$

As with the first order, it is desirable to consider equation (2.70) in terms of scatter at constant $(\rho_2 + \rho_{20})$ since this will correspond to a fixed time when the analysis is taken to that domain. Again, this means that the integration will proceed over δ while fixing μ (i.e. scatter will occur from an elliptical locus as before) and ρ and θ are held constant. Since the form of the exponential term containing the hyperbolic functions is exactly the same as in the first-order term of (2.24), the stationary phase analysis and its interpretation for equation (2.70) may be written down directly using Appendices A.1.2.1 and A.1.2.2. Thus, comparing equations (2.70) and (A.9) we identify

$$Z = \rho\frac{K_{rs}}{2}, \text{ the "large" positive real number,}$$

$$f(\delta) = \cosh\mu\cos\delta\cos(\theta_{rs}-\theta) + \sinh\mu\sin\delta\sin(\theta_{rs}-\theta)\ , \tag{2.71}$$

$$F(\delta) = (k\gamma_{E12F,1})F(\rho_2)F(\rho_{20})\ ,$$

and from equation (A.12) the stationary points, δ_s, are given by

$$\tan\delta_s = \tanh\mu\tan(\theta_{rs}-\theta)\ . \tag{2.72}$$

Replacing (x_1'', y_1'') of equations (A.15) through (A.16) with (x_2'', y_2'') and, without loss of generality, again setting $\theta = 0$, leads for equation (A.19) in the present case to

$$\vec{K}_{rs} = \pm K_{rs}\hat{N}\ . \tag{2.73}$$

Furthermore, since $\vec{\rho}_1$ and $\vec{\rho}_2$, of the first order are replaced by $\vec{\rho}_2$ and $\vec{\rho}_{20}$ respectively, in this second order, equation (A.22) may be written analogously as

$$\hat{\rho}_{20}\cdot\hat{N} = -\hat{\rho}_2\cdot\hat{N}\ . \tag{2.74}$$

Thus the following important results have been derived:

1. The sum of the two surface wave vectors responsible for the scattering (i.e. $\vec{K}_{mn} + \vec{K}_{pq} = \vec{K}_{rs}$) is normal to the scattering ellipse at the scattering patch, and

2. $\vec{K}_{rs}$ bisects the angle, (2ϕ), between the transmitter (T) and receiver (R) as viewed from the scattering patch. These results are effectively illustrated in Figure 2.6, a depiction which corresponds to Figure 2.3 for the first-order scatter. Again, ϕ is referred to as the bistatic angle, and ρ_2'' has exactly the same form as given for ρ_1'' in equation (A.15).

The δ-integral of equation (2.70) is obtained similarly as equation (A.14) and may therefore be written down directly as

$$I_\delta \approx \sqrt{2\pi}(-k\gamma_{E12F,1})F(\rho_2)F(\rho_{20}) \cdot \frac{e^{j\frac{\rho K_{rs}}{2}[\cosh\mu\cos\delta\cos(\theta_{mn}-\theta)+\sinh\mu\sin\delta\sin(\theta_{mn}-\theta)]}}{\sqrt{j\frac{\rho K_{rs}}{2}[\cosh\mu\cos\delta\cos(\theta_{mn}-\theta)+\sinh\mu\sin\delta\sin(\theta_{mn}-\theta)]}} \tag{2.75}$$

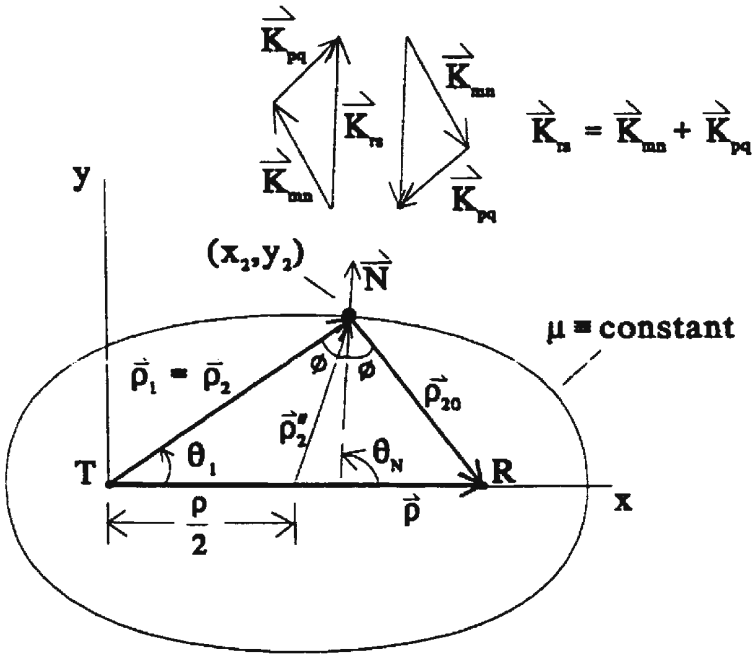

Figure 2.6: Depiction of the geometry associated with the second-order stationary phase condition. R and T are receiver and transmitter, respectively.

which, on converting from (μ, δ) to the natural bistatic geometry parameters ρ_2, ρ_{20} and ϕ, becomes (according to equations (A.22) through (A.26) with $\vec{\rho}_1'' \cdot \vec{K}_{mn}$ replaced by $\vec{\rho}_2'' \cdot \vec{K}_{rs}$)

$$I_\delta \approx \sqrt{2\pi} \cdot \frac{(-k\gamma_{E12F,1})F(\rho_2)F(\rho_{20})}{\sqrt{K_{rs}\rho_{s_{12,1}}\cos\phi}} e^{\pm jK_{rs}\rho_{s_{12,1}}\cos\phi} e^{\mp j\frac{\pi}{4}} . \tag{2.76}$$

By definition,

$$\rho_{s_{12,1}} = \frac{\rho_2 + \rho_{20}}{2} . \tag{2.77}$$

Equation (2.70) for the second-order patch scatter field may now be expressed as a single integral in the form

$$\begin{aligned}(E_{0_n}^+)_{2,F,1} \approx\ & \frac{-kC_0}{(2\pi)^{\frac{3}{2}}} \sum_{m,n} \sum_{p,q} P_{\vec{K}_{mn}} P_{\vec{K}_{pq}} \cdot e^{j\frac{\vec{\rho}}{2}\cdot\vec{K}_{rs}} \\ & \cdot \int_0^\infty \left(\frac{-k\gamma_{E12F,1}}{\sqrt{K_{rs}}}\right) \frac{F(\rho_2)F(\rho_{20})}{\sqrt{\rho_{s_{12,1}}\cos\phi}} \cdot e^{\mp j\frac{\pi}{4}} e^{\pm jK_{rs}\rho_{s_{12,1}}\cos\phi} \\ & \cdot e^{-jk\rho\cosh\mu}\, d\mu .\end{aligned} \tag{2.78}$$

Finally, a change of variable is invoked to write this μ-integral completely in terms of the bistatic parameters. From equations (2.69) and (2.77),

$$\begin{aligned} \rho_{s_{12,1}} &= \tfrac{\varrho}{2}\cosh\mu \\ \text{and} \\ d\rho_{s_{12,1}} &= \sqrt{\rho_{s_{12,1}}^2 - \left(\tfrac{\varrho}{2}\right)^2}\; d\mu\,. \end{aligned} \tag{2.79}$$

Noting also that $\rho_{s_{12,1}}|_{\mu=0} = \dfrac{\mu}{2}$, equation (2.78) is given by

$$(E_{0_n}^{+})_{2,F,1} \approx \frac{-kC_0}{(2\pi)^{\frac{3}{2}}} \sum_{m,n}\sum_{p,q} \frac{P_{\vec{K}_{mn}} P_{\vec{K}_{pq}}}{\sqrt{K_{rs}}} \cdot e^{j\frac{\vec{\varrho}}{2}\cdot\vec{K}_{rs}} \int_{\frac{\varrho}{2}}^{\infty} (-k\gamma_{E12F,1})$$

$$\cdot \left(\frac{F(\rho_2)F(\rho_{20})}{\sqrt{\cos\phi}} \cdot \frac{e^{\mp\frac{j\pi}{4}} e^{j\rho_{s_{12,1}}(\pm K_{rs}\cos\phi - 2k)}}{\sqrt{\rho_{s_{12,1}}(\rho_{s_{12,1}}^2 - \left(\frac{\varrho}{2}\right)^2)}} \right) d\rho_{s_{12,1}}\,. \tag{2.80}$$

Equation (2.80) is the vertical electric field component received from a double scatter on an observed point of the surface. As for the first order, for the moment, the equation is general and this double scattering can occur from any point on the surface. Later (see Section 3.5) radiation observed from an elementary region of the scattering surface is considered – hence the terminology "patch scatter".

2.2.2.4 Scattering at the Transmitting Antenna

Attention is now focussed on the component of the vertical electric field corresponding to the second stationary point $(0,\pi)$ of equation (2.50). Referring to Figures 2.4 and 2.5b, this point has already been interpreted in Section 2.2.2.2 as a single scatter at (in reality, near) the transmitting site, T, followed by a second scatter at a remote "patch" of surface at some arbitrary point, (x_2, y_2), before reception. Considering equations (2.43) and (2.44) and θ_{12} of equation (2.51), for the $(0,\pi)$ stationary point we have, in summary form,

$$\begin{aligned} \rho_1 &= \frac{\rho_2}{2}(\cosh\mu + \cos\delta) = 0\,, \\ \rho_{12} &= \frac{\rho_2}{2}(\cosh\mu - \cos\delta) = \rho_2\,, \end{aligned}$$

$$\begin{aligned}\theta_{12} &= \theta_2\,, \\ \theta_1 &= \tan^{-1}\left[\frac{(1+\cosh\mu\cos\delta)\sin\theta_2+\sinh\mu\sin\delta\cos\theta_2}{1+\cosh\mu\cos\delta)\cos\theta_2-\sinh\mu\sin\delta\sin\theta_2}\right]\,. \end{aligned} \tag{2.81}$$

Equation (2.81) for the $(0,\pi)$ point replaces equation (2.51) for the $(0,0)$ point and the similar format is obvious. However, the values of the various ρ's and θ's are different. Note particularly this time that as $(\mu,\delta)\rightarrow(0,\pi)$, $\theta_{12}\rightarrow\theta_2$ uniquely, while it can be shown that θ_1 is not unique. This last point follows the same argument as for θ_{12} in Section 2.2.2.2. Here, the implication is that radiation may leave the transmitter *in any direction* and scatter nearby before travelling to the second scattering position on a remote patch of surface. Given (2.81), equation (2.46) may be written as

$$\begin{aligned} I_{12F,2} &= -\frac{1}{2}\sum_{m,n}\sum_{p,q} P_{\vec{K}_{mn}} K_{mn} P_{\vec{K}_{pq}} K_{pq} e^{j[\rho_2 K_{pq}\cos(\theta_{pq}-\theta_2)]} \\ &\quad\cdot \cos(\theta_{pq}-\theta_2)\ \cdot\ F(0)F(\rho_2) \\ &\quad\cdot \int_0^{2\pi}\int_0^{\infty} \cos(\theta_{mn}-\theta_1) e^{j\frac{\rho_2}{2}\Phi_{12,2}(\mu,\delta)}\, d\mu d\delta \end{aligned} \tag{2.82}$$

where the last subscript on $I_{12F,2}$ indicates that we are considering the second stationary point. In equation (2.82), which clearly parallels (2.52) for the first stationary point, the following are emphasized:

1. ρ_2 and θ_2 are fixed quantities during the μ, δ integration, as before.

2. $\Phi_{12,2}(\mu\delta)$ is the same general expression as in (2.47), but must now be expanded to second order about the $(0,\pi)$ stationary point.

3. θ_1 is a function of μ and δ.

4. the factor of $\frac{1}{2}$ is required because $(0,\pi)$ is on the boundary of integration.

The function $\Phi_{12}(\mu,\delta)$ expanded in a double Taylor series about $(0,\pi)$ to second order yields (analogous to (2.53)),

$$\Phi_{12,2}(\mu,\delta) \approx -2k+\frac{1}{2}\left\{[-K_{mn}\cos(\theta_{mn}-\theta_2)-2k]\mu^2\right.$$

$$-[2K_{mn}\sin(\theta_{mn}-\theta_2)]\mu(\delta-\pi)$$
$$+[K_{mn}\cos(\theta_{mn}-\theta_2)(\delta-\pi)^2]\Big\}\ . \qquad (2.83)$$

Changing the limits on the δ integral from $(0,2\pi)$ to $(-\pi,\pi)$, noting that $F(0)=1$, $\theta_{12}=\theta_2$ and factoring out the $e^{-j\rho_2 k}$ resulting from the zero order term in Φ_{12}, equation (2.82) has the form

$$I_{12F,2} = -\frac{1}{2}\sum_{m,n}\sum_{p,q} P_{\vec{K}_{mn}} K_{mn} P_{\vec{K}_{pq}} K_{pq} e^{j[\rho_2(K_{pq}\cos(\theta_{pq}-\theta_2)-k)]}$$
$$\cdot\ \cos(\theta_{pq}-\theta_2)F(\rho_2)\ \cdot\ \int_{-\pi}^{\pi}\int_{0}^{\infty}\cos(\theta_{mn}-\theta_1)e^{j\frac{\rho_2}{4}Q_2(\mu,\delta)}\,d\mu d\delta \qquad (2.84)$$

with

$$Q_2(\mu,\delta) = [-K_{mn}\cos(\theta_{mn}-\theta_2)-2k]\mu^2 - 2K_{mn}\sin(\theta_{mn}-\theta_2)\mu\delta$$
$$+K_{mn}\cos(\theta_{mn}-\theta_2)\delta^2\ . \qquad (2.85)$$

Except for the δ-limits (which, incidently, could still be 0 to 2π), we see that the double integral of equation (2.84) along with the stipulation of (2.85) has exactly the same form as equations (2.55) and (2.56). The latter equation, for the first stationary point, was treated extensively in Appendices A.2.1.1 through A.2.1.3 and, while those techniques must be repeated to obtain the appropriate forms, there are no new insights from the analysis being applied to the stationary point now under consideration. Therefore, at this stage we may simply write down the new form of (2.84) as

$$I_{12F,2} \approx -2\pi\sum_{m,n}\sum_{p,q} P_{\vec{K}_{mn}} P_{\vec{K}_{pq}} \frac{F(\rho_2)}{\rho_2}\ \cdot\ \gamma_{E12F,2}\ \cdot\ e^{j\frac{\rho_2}{2}[2K_{pq}\cos(\theta_{pq}-\theta_2)-2k]} \qquad (2.86)$$

where it may be shown on carrying out all of the algebraic detail that the electromagnetic coupling coefficient may be given as

$$\gamma_{E12F,2} = \left\{\frac{[\vec{K}_{pq}\cdot\hat{\rho}_2][\vec{K}_{mn}\ \cdot\ (\vec{K}_{mn}+k\hat{\rho}_2)]}{\sqrt{\vec{K}_{mn}\ \cdot\ [\vec{K}_{mn}+2k\hat{\rho}_2]}}\right\}$$
$$\cdot\left\{\frac{-k-j\sqrt{\vec{K}_{mn}\cdot[\vec{K}_{mn}+2k\hat{\rho}_2]}}{k^2+\vec{K}_{mn}\ \cdot\ [\vec{K}_{mn}+2k\hat{\rho}_2]}\right\}\ . \qquad (2.87)$$

Again, the details of this coupling coefficient will be discussed when the analysis is applied to the ocean in Section 3.6.4, note 4. Comparing the forms of the patch scatter integral of (2.63) with (2.86) we see that the latter has only one exponential factor. This is due to the fact that in (2.86) the first point of scatter is at the transmitter so that the distance parameter associated with it $\rightarrow 0$. The exponential associated with it will therefore be unity. On the other hand, for patch scatter both scattering surface wave vectors are remote from the transmitter and each naturally appears in an exponential factor.

Using exactly the same analysis as was used from equations (2.66) through (2.68) and considering that the form in equation (2.65) is replaced in this current analysis by $e^{j\rho_2[K_{pq}\cos(\theta_{pq}-\theta_2)-k]}$, we may write down directly

$$(E^+_{0_n})_{2,F,2} \approx \frac{-kC_0}{(2\pi)^2}\sum_{m,n}\sum_{p,q} P_{\vec{K}_{mn}} P_{\vec{K}_{pq}} \int_{y_2}\int_{x_2} (-k\gamma_{E12F,1}) \cdot \frac{F(\rho_2)F(\rho_{20})}{\rho_2\rho_{20}} e^{j\rho_2[K_{pq}\cos(\theta_{pq}-\theta_2)]} \cdot e^{-j(\rho_2+\rho_{20})k}\, dx_2 dy_2 \,. \quad (2.88)$$

Clearly, with the exception of (K_{pq}, θ_{pq}) replacing (K_{rs}, θ_{rs}), the form of equation (2.88) is identical to that of (2.68). The last subscript on $(E^+_{0_n})$ has been changed to 2 to indicate that this is the field component due to the second stationary point. We note that all transformations in (2.69) will apply here as will all of the ensuing analysis up to and including (2.80). It is simply required that K_{pq}, θ_{pq} and $\gamma_{E12F,2}$ be substituted into (2.70), (2.71), (2.72), (2.73), (2.75), (2.76) and (2.78) in place of K_{rs}, θ_{rs}, $\gamma_{E12F,1}$, respectively, where appropriate. Then, equation (2.88) may be transformed to get the counterpart to (2.80). That is, for first scatter near the transmitter and a second, before reception, at a remote point on the surface, the vertical electric field component may be written as

$$(E^+_{0_n})_{2,F,2} \approx \frac{-kC_0}{(2\pi)^{\frac{3}{2}}}\sum_{m,n}\sum_{p,q} \frac{P_{\vec{K}_{mn}} P_{\vec{K}_{pq}} \cdot e^{j\frac{\vec{\rho}}{2}\cdot\vec{K}_{pq}}}{\sqrt{K_{pq}}} \cdot \int_{\frac{\rho}{2}}^{\infty} (-k\gamma_{E12F,2}) \cdot \frac{F(\rho_2)F(\rho_{20})}{\sqrt{\cos\phi}} \cdot \frac{e^{\mp\frac{j\pi}{4}} e^{j\rho_{s_{12,1}}(\pm K_{pq}\cos\phi - 2k)}}{\sqrt{\rho_{s_{12,1}}(\rho^2_{s_{12,1}} - \left(\frac{\rho}{2}\right)^2)}}\, d\rho_{s_{12,1}} \,. \quad (2.89)$$

The following important facts incorporated into this component may be summarized as follows:

1. the first scatter may occur in any direction from the transmitter (i.e. θ_1 is not unique);

2. the $\vec{K}_{pq}$ wave vector at the distant scattering point is along the scattering ellipse normal at that point;

3. $\vec{K}_{pq}$ bisects the angle between the receiver and transmitter as viewed from the second scattering point.

These ideas are depicted in Figure 2.7.

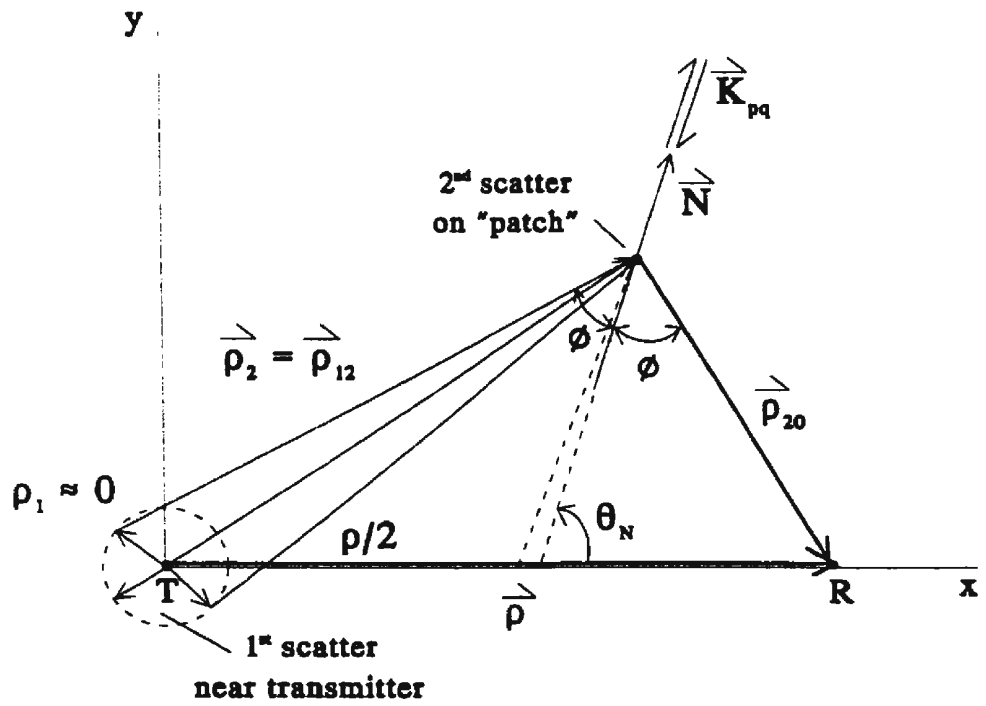

Figure 2.7: Figure 2.5b repeated showing in more detail the geometry of the scatter at the transmitter (T) followed by another on the remote patch.

2.2.3 The Second-order Scatter for a Time Invariant Surface – Backward Analysis

In Section 2.2.2.4, the double scattering consisted of a first scatter near the transmitter and the second at a point remote from both the receiver and transmitter. Intuitively, one might expect that a similar feature should manifest itself by a first scatter on the remote point with the second scatter occurring near the receiver before being received. However, this has not been previously found even in investigations which have presented monostatic cross sections of the ocean surface (eg. Barrick [24], Srivastava [54]). It is also clear that a stationary point corresponding to this situation did not arise from the "forward convolution" approach to equation (2.37) as was undertaken in Section 2.2.2.1. In an attempt to locate this phenomenon, equation (2.37) is revisited here.

Considering property (2.35) for convolutions, equation (2.37) may be grouped as

$$(E_{0_n}^{+})_2 \approx \frac{-k^2 C_0}{(2\pi)^3}\left[\vec{\nabla}_{xy}(\xi)\cdot\hat{\rho}\left(F(\rho)\frac{e^{-jk\rho}}{\rho}\right)\right]_1 \overset{xy}{*} \left\{\left[\vec{\nabla}_{xy}(\xi)\cdot\hat{\rho}\left(\frac{F(\rho)e^{-jk\rho}}{\rho}\right)\right]_2 \overset{xy}{*} \left[\frac{F(\rho)e^{-jk\rho}}{\rho}\right]_3\right\} . \tag{2.90}$$

This equation still pertains to Figure 2.4, but now the last convolution (i.e.$[\cdots]_2 \overset{xy}{*} [\cdots]_3$) will be done first. To distinguish this from the approach found in Section 2.2.2, it has been titled "Backward Analysis".

2.2.3.1 A Stationary Phase Approach to the Second-order Field

Much of the analysis of the previous sections of this chapter along with the respective appendices is applicable here with due attention being paid to the meanings of the various parameters. Of course, in the first member of the second convolution in (2.90), $\vec{\nabla}_{xy} \equiv \vec{\nabla}_{x_2,y_2}$, the required distance parameter is ρ_{12} and its associated direction, θ_{12}. The distance parameter for the second member of this convolution is ρ_{20} with its

corresponding direction θ_{20}. In the left member of this convolution, then,

$$(\vec{\nabla}_{xy}(\xi)\cdot\hat{\rho})_2 = \vec{\nabla}\xi(x_2,y_2)\cdot\hat{\rho}_{12}$$

and this expression is found in equation (2.40). Using the technique of Appendix A.1.1 it is easy to show that

$$\begin{aligned} I_{23B} &= \left[\vec{\nabla}_{xy}(\xi)\cdot\hat{\rho}\frac{F(\rho)e^{-jk\rho}}{\rho}\right]_2 \overset{xy}{*} \left[\frac{F(\rho)e^{-jk\rho}}{\rho}\right]_3 \\ &= j\sum_{p,q} P_{\vec{K}_{pq}} K_{pq} \int_{y_2}\int_{x_2} \cos(\theta_{pq}-\theta_{12}) e^{j\rho_2 K_{pq}\cos(\theta_{pq}-\theta_2)} \\ &\quad \cdot e^{-jk(\rho_{12}+\rho_{20})}\frac{F(\rho_{12})F(\rho_{20})}{\rho_{12}\rho_{20}}\,dx_2dy_2 \end{aligned} \tag{2.91}$$

where the subscript on I_{23B} indicates the order of convolution with the "B" referring to the fact that we are carrying out the convolutions of (2.90) in "backwards" order - i.e. the last convolution is being done first.

Evaluation of equation (2.91) may again be executed by applying a stationary phase method. The concepts are not different than already applied, but the initial elliptic coordinate transformation must be modified.

Referring to Figure 2.8, we introduce a new vector, $\vec{\rho}_4$, given by

$$\vec{\rho}_4 = (x-x_1)\hat{x} + (y-y_1)\hat{y} \tag{2.92}$$

whose direction is

$$\theta_4 = \tan^{-1}\left(\frac{y-y_1}{x-x_1}\right) . \tag{2.93}$$

The first step in effecting the desired transformation is to rotate the coordinate axis *clockwise* by an amount $\theta_4(<0)$ to give in terms of the new (primed) coordinates

$$\begin{aligned} x_2 &= x_2'\cos\theta_4 - y_2'\sin\theta_4 \\ y_2 &= x_2'\sin\theta_4 + y_2'\cos\theta_4 . \end{aligned} \tag{2.94}$$

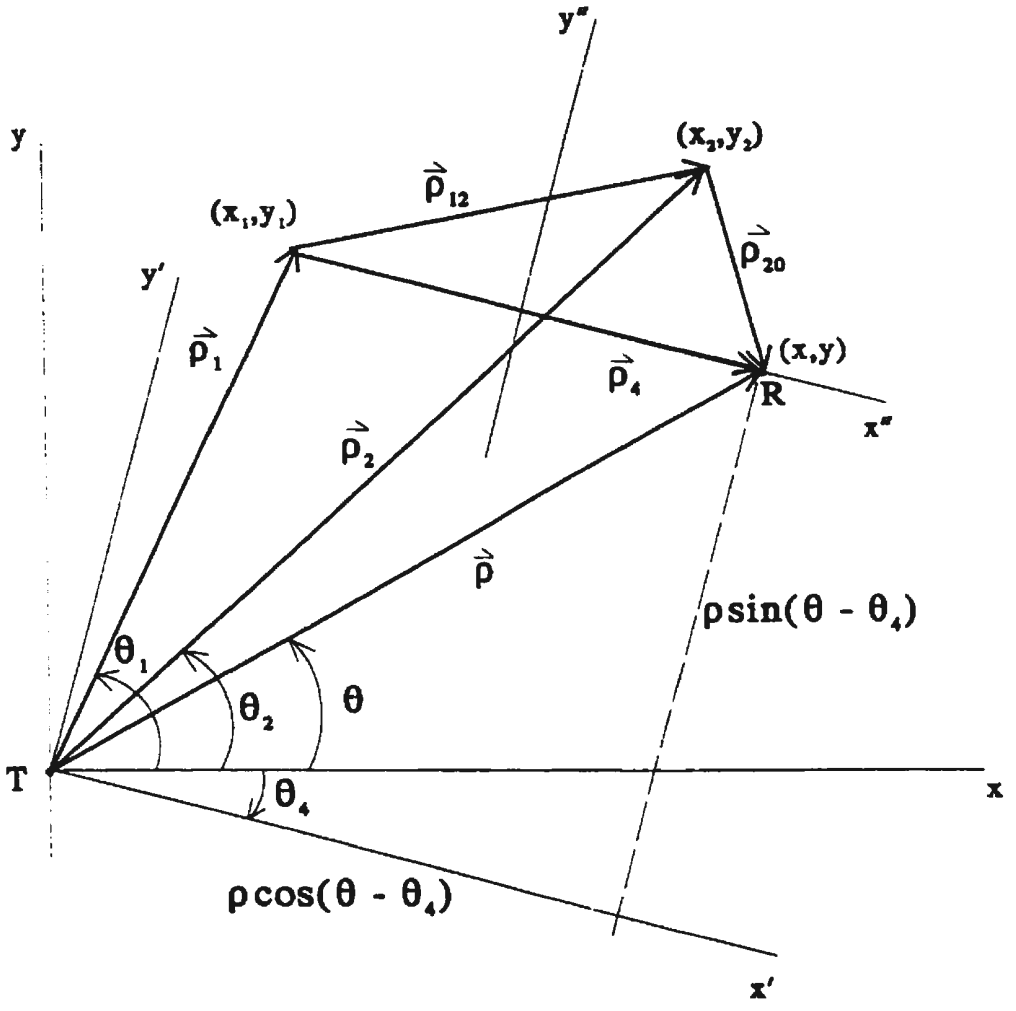

Figure 2.8: The coordinate transformation used in the "backward analysis" referred to in the text.

Next, the (x', y') origin is translated to the midpoint of $\vec{\rho}_4$ so that we may write (in double primed coordinates)

$$\begin{aligned} x_2'' &= x_2' + \frac{\rho_4}{2} - \rho\cos(\theta - \theta_4) \\ y_2'' &= y_2' - \rho\sin(\theta - \theta_4)\ . \end{aligned} \tag{2.95}$$

Finally, the elliptic coordinate transformation

$$\begin{aligned} x_2'' &= \frac{\rho_4}{2}\cosh\mu\cos\delta \\ y_2'' &= \frac{\rho_4}{2}\sinh\mu\sin\delta\ , \end{aligned} \tag{2.96}$$

along with (2.94) and (2.95), leads to the results

$$\left.\begin{aligned}\rho_{12} &= \tfrac{\rho_4}{2}[\cosh\mu + \cos\delta] \\ \rho_{20} &= \tfrac{\rho_4}{2}[\cosh\mu - \cos\delta]\end{aligned}\right\} \Rightarrow \rho_{12} + \rho_{20} = \rho_4 \cosh\mu$$

$$\begin{aligned} x_2 &= \left[\tfrac{\rho_4}{2}(\cosh\mu\cos\delta - 1) + \rho\cos(\theta - \theta_4)\right]\cos\theta_4 \\ &\quad - \left[\tfrac{\rho_4}{2}\sinh\mu\sin\delta + \rho\sin(\theta - \theta_4)\right]\sin\theta_4 \\ y_2 &= \left[\tfrac{\rho_4}{2}(\cosh\mu\cos\delta - 1) + \rho\cos(\theta - \theta_4)\right]\sin\theta_4 \\ &\quad + \left[\tfrac{\rho_4}{2}\sinh\mu\sin\delta + \rho\sin(\theta - \theta_4)\right]\cos\theta_4 \quad . \end{aligned} \tag{2.97}$$

Using these transformations and carrying out the same procedure as in Section 2.2.2.1. gives for equation (2.91)

$$\begin{aligned} I_{23B} &= j\sum_{p,q} P_{\vec{K}_{pq}} K_{pq} \int_0^{2\pi}\int_0^{\infty} \cos(\theta_{pq} - \theta_{12}) F(\rho_{12}) F(\rho_{20}) \\ &\quad \cdot e^{j\frac{\rho_4}{2}\Phi_{23}(\mu,\delta)} \cdot e^{jK_{pq}\rho\cos(\theta_{pq}-\theta)}\, d\mu d\delta \end{aligned} \tag{2.98}$$

with

$$\begin{aligned} \Phi_{23}(\mu,\delta) &= K_{pq}\{[\cosh\mu\cos\delta - 1]\cos(\theta_{pq} - \theta_4) \\ &\quad + (\sinh\mu\sin\delta)\sin(\theta_{pq} - \theta_4)\} - 2k\cosh\mu \\ &\text{and} \\ dx_2 dy_2 &= \rho_{12}\rho_{20} d\mu d\delta \ . \end{aligned} \tag{2.99}$$

The form of $\Phi_{23}(\mu,\delta)$ differs from $\Phi_{12}(\mu,\delta)$ of equation (2.47) only by a constant. Here "-1" replaces the "$+1$" of the $\Phi_{12}(\mu,\delta)$, and the solution of $\dfrac{\partial\Phi_{23}(\mu,\delta)}{\partial\mu} = 0$ and $\dfrac{\partial\Phi_{23}(\mu,\delta)}{\partial\delta} = 0$ leads to exactly the same stationary points as in (2.50). Of course, K_{pq}, θ_{pq} and θ_4 replaces K_{mn}, θ_{mn} and θ_2, respectively, in the third point. For the same reasons as discussed earlier, the first two stationary points, $(0,0)$ and $(0,\pi)$, will be considered here. While these points are numerically the same as in (2.50) their interpretations are now altered:

1. Stationary Point $(\mu, \delta) \equiv (0, 0)$

The first two equations in (2.97) give for this point

$$\begin{aligned} \rho_{12} &= \rho_4 \\ \rho_{20} &= 0 \,. \end{aligned} \tag{2.100}$$

From Figure 2.8, it is obvious that this implies that the second scattering point, (x_2, y_2) has moved to R. Thus, taking equation (2.90) as a whole, it is evident that a component of the scatter at (x_1, y_1), as described by the left member of the first convolution, is scattered again at the receiving antenna before being received. We have therefore developed analytically what was intuitively suspected – that is, in addition to a double scatter on a remote patch of surface and a single scatter at the transmitter followed by a single "patch" scatter, there is also a single "patch" scatter followed by a single scatter near the receiver. The field associated with this stationary point is developed in Section 2.2.3.2.

2. Stationary Point $(\mu, \delta) \equiv (0, \pi)$

The first two equations of (2.97) now yield

$$\begin{aligned} \rho_{12} &= 0 \\ \rho_{20} &= \rho_4 \,. \end{aligned} \tag{2.101}$$

Again, with reference to Figure 2.8, it is evident that the point (x_2, y_2) has moved to (x_1, y_1), the position of the first scatter. Hence, this $(0, \pi)$ point again gives the "patch scatter" condition. In Section 2.2.3.3, with reference to Appendix A.3.2, it is shown that for this point, the backward analysis produces exactly the same result as the forward analysis of Section 2.2.2.2 produced for the $(0, 0)$ point. This is, of course, as it should be.

2.2.3.2 Scattering at the Receiving Antenna

It is not difficult to show that as $(\mu, \delta) \rightarrow (0,0)$, θ_{20} is not unique, $\theta_2 \rightarrow \theta$ and $\theta_{12} \rightarrow \theta_4$ uniquely. This may be done rigorously using $\theta_2 = \tan^{-1}\frac{y_2}{x_2}$ and $\theta_{12} = \tan^{-1}\left(\frac{y_2 - y_1}{x_2 - x_1}\right)$ and using the elliptic coordinate forms of the various x's and y's. However, these angle limits are obvious from Figure 2.8 as (x_2, y_2) moves to R. Even though (x_2, y_2) may approach R from any direction, in the limit the angles must be as stated. Furthermore, during the (μ, δ) integration of equation (2.98), in addition to the pq - subscripted variables, ρ_4, θ_4, ρ and θ are fixed quantities. This means that, for the $(0,0)$ stationary point, θ_{12} is fixed also. Consequently, we may cast equation (2.98) as

$$I_{23B} = j\sum_{p,q} P_{\vec{K}_{pq}} K_{pq} e^{jK_{pq}\rho\cos(\theta_{pq}-\theta)} \cdot \int_0^{2\pi}\int_0^{\infty} \cos(\theta_{pq}-\theta_{12}) F(\rho_{12}) F(\rho_{20}) e^{j\frac{\rho_4}{2}\Phi_{23}(\mu,\delta)}\, d\mu d\delta \,. \qquad (2.102)$$

Now, the double integral portion has exactly the same *form* as the double integrals in either equation (2.52) or (2.82) with one important exception: the cosine factor appearing explicitly in (2.102) is uniquely determined as $(\mu, \delta) \rightarrow (0,0)$, while the corresponding factor in the other two equations depended on the direction of approach toward the stationary point. This uniqueness allows a direct application of a two-dimensional stationary phase solution of the double integral here. For completeness, the procedure is outlined in Appendix A.2.2. The result for equation (2.102) is

$$I_{23B,1} \approx j2\pi\sum_{p,q} P_{\vec{K}_{pq}} K_{pq} \frac{\cos(\theta_{pq}-\theta_{12}) F(\rho_{12})}{\sqrt{K_{pq}^2 - 2kK_{pq}\cos(\theta_{pq}-\theta_{12})}} \cdot \frac{e^{-jk\rho_{12}}}{\rho_{12}} e^{jK_{pq}\rho\cos(\theta_{pq}-\theta)} \qquad (2.103)$$

where the subscript "1" has been used on $I_{23B,1}$ to indicate that this is the result for the first stationary point. At this stage (2.103) represents an approximation of

equation (2.91) so that electric field equation (2.90), for the case under consideration, now takes the form

$$(E_{0_n}^{+})_{2,B,1} \approx \frac{-jk^2C_0}{(2\pi)^2}\left[\vec{\nabla}_{xy}(\xi)\cdot\hat{\rho}\left(F(\rho)\frac{e^{-jk\rho}}{\rho}\right)\right]_1^{xy}_{*}$$

$$\sum_{p,q} P_{\vec{K}_{pq}} K_{pq} \frac{\cos(\theta_{pq}-\theta_{12})F(\rho_{12})}{\sqrt{K_{pq}^2 - 2kK_{pq}\cos(\theta_{pq}-\theta_{12})}}$$

$$\cdot \frac{e^{-jk\rho_{12}}}{\rho_{12}} e^{jK_{pq}\rho\cos(\theta_{pq}-\theta)} \,. \tag{2.104}$$

Comparing this with equation (A.4) for the first order we see that the forms are very similar. Then, regarding $[\cdots]_1$ to be associated with the (x_1, y_1) surface point (see Figure 2.8), following the analysis of Appendix A.1.1 leads immediately to

$$(E_{0_n}^{+})_{2,B,1} \approx \frac{-kC_0}{(2\pi)^2}\sum_{m,n}\sum_{p,q} P_{\vec{K}_{mn}} P_{\vec{K}_{pq}} \int_{x_1}\int_{y_1} (-k\gamma_{E12B,1})$$

$$\cdot e^{jK_{pq}\rho\cos(\theta_{pq}-\theta)} e^{j\rho_1 K_{mn}(\theta_{mn}-\theta_1)}$$

$$\cdot \frac{F(\rho_1)F(\rho_{12})}{\rho_1\rho_{12}} e^{-jk(\rho_1+\rho_{12})}\, dx_1 dy_1 \tag{2.105}$$

where we have defined a coupling coefficient by

$$\gamma_{E12B,1} = \frac{(K_{mn}\cos(\theta_{mn}-\theta_1))(K_{pq}\cos(\theta_{pq}-\theta_{12}))}{\sqrt{K_{pq}^2 - 2kK_{pq}\cos(\theta_{pq}-\theta_{12})}} \,. \tag{2.106}$$

Before proceeding, it is appropriate to compare the result in (2.105) with that for the second-order field when one of the two scatters occurs near the transmitter as described by equation (2.88). We note that, in equation (2.105), the pq wave vectors are associated with that part of the surface near the receiver (i.e. the second scatter position) and *not* on the remote patch. In this sense, they correspond to the mn wave vectors of equation (2.88). It may be further observed that in (2.105) there is a $e^{jK_{pq}\rho\cos(\theta_{pq}-\theta)}$ factor due to the second scatter being a distance ρ from the transmitter. There is no corresponding K_{mn} term in (2.88) because the distance parameter is zero for that case. Additionally, noticing that the numerical subscripts

are different in (2.105) than in (2.88) because the scattering geometry is different, the two equations being referred to still have the same basic form. Because of this, the treatment of equation (2.105) follows directly that for (2.88). That is, referring to Figure 2.8 with (x_2, y_2) having "moved" to (x, y) we effect a coordinate transformation this time by (1) rotating the coordinate axis counterclockwise through angle θ, (2) shifting the origin halfway along ρ and (3) converting to elliptic coordinates. Next, as before, a stationary phase integration is carried out on the δ integral while μ is fixed. To complete the μ - integration, a change of variables similar to that in equation (2.79) is used. None of these details presents new analytical insights so that, for the sake of compactness, we will simply summarize the results. Equation (2.105) becomes, on choosing $\theta = 0$ as before,

$$(E_{0_n}^{+})_{2,B,1} \approx \frac{-kC_0}{(2\pi)^{\frac{3}{2}}} \sum_{m,n} \sum_{p,q} P_{\vec{K}_{mn}} P_{\vec{K}_{pq}} \frac{e^{j\vec{\rho}\cdot\vec{K}_{pq}} e^{j\frac{\vec{\rho}\cdot\vec{K}_{mn}}{2}}}{\sqrt{K_{mn}}} \int_{\frac{\rho}{2}}^{\infty} \frac{(-k\gamma_{E12B,1})}{\sqrt{\cos\phi}}$$

$$\cdot F(\rho_1)F(\rho_{12}) \cdot e^{\mp j\frac{\pi}{4}} \frac{e^{j\rho_{s_{21,1}}(\pm K_{mn}\cos\phi - 2k)}}{\sqrt{\rho_{s_{21,1}}\left(\rho_{s_{21,1}}^2 - \left(\frac{\rho}{2}\right)^2\right)}} d\rho_{s_{21,1}} , \quad (2.107)$$

where

$$\rho_{s_{21,1}} = \frac{\rho_1 + \rho_{12}}{2} .$$

It should be noted, again by analogy with the forward analysis of Section 2.2.2.3, that in deriving equation (2.107) the following outcomes are observed: (1) the $\vec{K}_{mn}$ wave vector on the remote scattering patch is normal to the scattering ellipse there; (2) $\vec{K}_{mn}$ bisects the angle between the transmitter and receiver as viewed from the first scattering point. The field given by (2.107) is due to the scattering depicted in Figure 2.9, which is the same as Figure 2.7 but detailed to reflect the first stationary point of the "backward" analysis; and (3) θ_{20} is not unique - i.e. the second scatter near the receiver can be received from any direction.

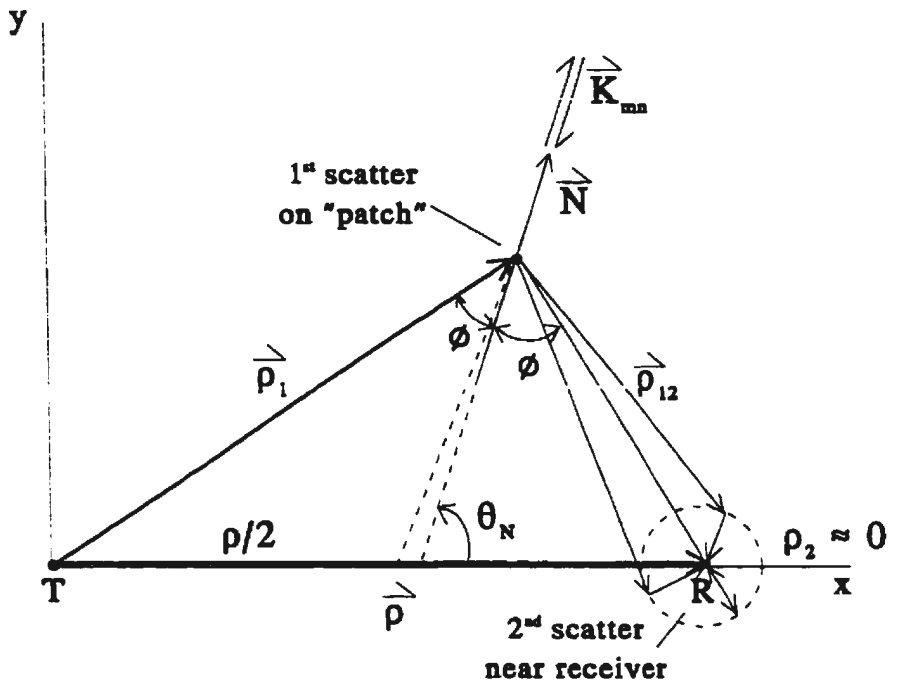

Figure 2.9: The geometry of the scatter at the remote patch followed by another at the receiver (R). Compare with Figure 2.7.

2.2.3.3 Patch Scatter – Backward Analysis

In Section 2.2.3.1, it was shown that the second convolution in equation (2.90) carried out under a stationary phase integration produced a stationary point at $(\mu, \delta) = (0, \pi)$. This was interpreted to mean that a double scattering occurred on a patch of surface remote from both the transmitter and receiver. Calculation of the received electric field component for this case requires that equation (2.104) be revisited. It transpires that as $(\mu, \delta) \rightarrow (0, \pi)$, θ_{12} in the $\cos(\theta_{pq} - \theta_{12})$ factor of that equation is not unique. This necessitates a repetition of the modifications presented in Section 2.2.2.2 for the "forward" analysis of the "patch" scatter. As indicated earlier, the algebra associated with this process is intensive. However, no new insights result from repeating it. Therefore, here we will merely state the result which corresponds to the electric field component given in equation (2.70) and briefly discuss the relationships between them. Using $(E_{0n}^{+})_{2,B,2}$ to indicate the field component associated with the second

stationary point of the backward process we write

$$
\begin{aligned}
(E^{+}_{0_n})_{2,B,2} &= \frac{-kC_0}{(2\pi)^2}\sum_{m,n}\sum_{p,q} P_{\vec{K}_{mn}} P_{\vec{K}_{pq}} \cdot e^{j\frac{\rho}{2}K_{rs}\cos(\theta_{rs}-\theta)} \\
&\quad \cdot \int_0^{\infty} e^{-jk\rho\cosh\mu}\left\{\int_0^{2\pi}(k\gamma_{E12B,2})\right. \\
&\quad \cdot e^{j\frac{\rho K_{rs}}{2}[\cosh\mu\cos\delta\cos(\theta_{rs}-\theta)+\sinh\mu\sin\delta\sin(\theta_{rs}-\theta)]} \\
&\quad \left. \cdot F(\rho_1)F(\rho_{20})\, d\delta\right\}\, d\mu
\end{aligned}
\tag{2.108}
$$

where

$$
\begin{aligned}
k\gamma_{E12B,2} &= k\left\{\frac{j\sqrt{\vec{K}_{pq}\cdot[\vec{K}_{pq}+2k\hat{\rho}_{20}]}+k}{k^2+\vec{K}_{pq}\cdot[\vec{K}_{pq}+2k\hat{\rho}_{20}]}\right\} \\
&\quad \cdot\left\{\frac{\vec{K}_{mn}\cdot\hat{\rho}_2[\vec{K}_{pq}\cdot(\vec{K}_{pq}+k\hat{\rho}_{20}]}{\sqrt{\vec{K}_{pq}\cdot[\vec{K}_{pq}+2k\hat{\rho}_{20}]}}\right\} .
\end{aligned}
\tag{2.109}
$$

All variables here have their usual meanings.

It may be observed from either Figure 2.4 or 2.8 that as $(x_2, y_2) \rightarrow (x_1, y_1)$, $\vec{\rho}_2 \rightarrow \vec{\rho}_1$. This means that $F(\rho_1)$ in equation (2.108) is identical to $F(\rho_2)$ in equation (2.70). Therefore, on comparing the two equations, establishing their total equivalence requires only that it be shown that

$$(k\gamma_{E12B,2}) = (-k\gamma_{E12F,1})$$

where $\gamma_{E12F,1}$ is given in equation (2.64). Final proof of this equivalence between the "forward" and "backward" analysis patch scatter is developed in Appendix A.3.2.

2.2.4 The Monostatic Form of the Second-order Fields

An important, and interesting, special case of the general bistatic received field occurs when the transmitter and receiver of Figures 2.3, 2.6, 2.7 or 2.9 are co-located. That is, the bistatic problem reduces to the monostatic case. Several such investigations have been carried out previously (Barrick [24], Srivastava [54], Walsh *et al.* [8]). However, the analysis here includes the case of a scatter at the receiver which has not been presented before. Furthermore, it will be seen in the next chapter that there are

certain aspects of the fields in this work which better explain some of the features of the Doppler cross sections of the ocean surface derived from them.

2.2.4.1 The Monostatic Form of the First-order Result

With reference to the Figure 2.3, it is seen that the following simplification occurs: the vectors joining the transmitter to the scattering point and vice versa are equal, but opposite, and the vector joining the transmitter to the receiver goes to 0 as does the bistatic angle. Symbolically,

$$\vec{\rho}_2 = -\vec{\rho}_1 \Rightarrow \rho_1 = \rho_2 \Rightarrow \rho_s = \frac{\rho_1 + \rho_2}{2} = \rho_1$$

$$\rho = 0 \ : \ \cos\phi = \cos 0^\circ = 1 \ .$$

Substituting these values into equation (2.30) gives

$$\begin{aligned}(E^+_{0_n})_{1m} \ = \ & \frac{kC_0}{(2\pi)^{\frac{3}{2}}} \sum_{m,n} P_{\vec{K}_{mn}} \sqrt{K_{mn}} \int_0^\infty \frac{F^2(\rho_1)}{\rho_1^{\frac{3}{2}}} (\pm e^{\mp j\frac{\pi}{4}}) \\ & \cdot e^{j\rho_1[\pm K_{mn} - 2k]} \ d\rho_1 \ . \end{aligned} \tag{2.110}$$

The m on $(E^+_{0_n})_{1m}$ represents the monostatic field. This agrees exactly with the monostatic result given by Walsh *et al.* [8].

2.2.4.2 Patch Scatter

Consider equation (2.80) for the case where the receiver and transmitter are co-located. Then, from Figure 2.6 and equation (2.77) we have

$$\begin{aligned} &(1) \quad \rho_{s_{12,1}} = \tfrac{\rho_2 + \rho_2}{2} = \rho_2 \\ &(2) \quad \phi = 0 \Rightarrow \cos\phi = 1 \\ &(3) \quad \rho = 0 \ . \end{aligned}$$

Direct substitution into (2.80) then gives

$$\begin{aligned}(E^+_{0_n})_{2,F,1} \ \approx \ & \frac{-kC_0}{(2\pi)^{\frac{3}{2}}} \sum_{m,n} \sum_{p,q} P_{\vec{K}_{mn}} P_{\vec{K}_{pq}} \\ & \cdot \int_0^\infty \frac{F^2(\rho_2)}{(\rho_2)^{\frac{3}{2}}} (-k\gamma_{E12F,1}) e^{\mp\frac{j\pi}{4}} e^{j\rho_2(\pm K_{rs} - 2k)} \ d\rho_2 \ . \end{aligned} \tag{2.111}$$

When this is compared with the monostatic result given in Walsh *et al.* [8], the form may be seen to be the same. However, in equation (2.111), $(-k\gamma_{E12F,1})$ contains an extra factor when compared to the previous monostatic result. Analytically, this arises because of the modified stationary phase approach which was necessitated by the non-uniqueness of θ_{12} (see Section 2.2.2.2). However, it is verified in Section 3.6.6, where the second-order cross sections of the ocean surface are calculated and illustrated, that this extra factor has no significant effect on the magnitude of the so-called coupling coefficient except at certain discrete (and physically explicable) points.

2.2.4.3 Scatter at Transmitter

Now we wish to consider equation (2.89) for monostatic operation. According to equation (2.77) and Figure 2.7, we again have

$$\begin{array}{lll} (1) & \rho_{s_{12,1}} & = \rho_2 \\ (2) & \phi & = 0 \\ (3) & \rho & = 0\,. \end{array}$$

from which (2.89) becomes

$$\begin{aligned} (E^{+}_{o_m})_{2,F,2} \approx\ & \frac{-kC_0}{(2\pi)^{\frac{3}{2}}} \sum_{m,n} \sum_{p,q} \frac{P_{\vec{K}_{mn}} P_{\vec{K}_{pq}}}{\sqrt{K_{pq}}} \\ & \cdot \int_0^{\infty} (-k\gamma_{E12F,2}) \frac{F^2(\rho_2)}{\rho_2^{\frac{3}{2}}} e^{\mp \frac{j\pi}{4}} \\ & \cdot e^{j\rho_2[\pm K_{pq} - 2k]}\, d\rho_2\,. \end{aligned} \tag{2.112}$$

It will again be verified that the details of the monostatic form of $(-k\gamma_{E12F,2})$ here differ from Srivastava's [54] result, yet on applying equation (2.112) to the ocean surface it reveals the same major points of significance as does Srivastava's formulation (see Section 3.6.4). It should also be pointed out that the techniques applied here because of ambiguities were not addressed by Srivastava. It is, therefore, not surprising that there are some minor discrepancies. In addition, it will be shown that (2.112) better

explains a larger region of the Doppler cross section than does Srivastava's analysis (see Appendix B.8).

2.2.4.4 Scatter at the Receiver

No monostatic form exists with which to compare the field equation when one of the two scatters involved in the second-order return occurs near the receiver. However, for the sake of completeness, the monostatic version of equation (2.107) is given below. Referring to Figures 2.8 and 2.9 and the definition of $\rho_{s_{21,1}}$ following equation (2.107) the appropriate variable changes are

$$\begin{array}{lll} (1) & \rho_{s_{21,1}} = & \frac{\rho_1+\rho_1}{2} = \rho_1 \\ (2) & \phi = & 0 \\ (3) & \rho = & 0\,. \end{array}$$

Immediately, for monostatic operation, equation (2.107) takes the form

$$\begin{aligned} (E^+_{o_n})_{2,B,1} \approx\ & \frac{-kC_0}{(2\pi)^{\frac{3}{2}}} \sum_{m,n} \sum_{p,q} \frac{P_{\vec{K}_{mn}} P_{\vec{K}_{pq}}}{\sqrt{K_{mn}}} \\ & \cdot \int_0^\infty (-k\gamma_{E12B,1}) \frac{F^2(\rho_1)}{\rho_1^{\frac{3}{2}}} e^{\mp j\frac{\pi}{4}} \\ & \cdot e^{j\rho_1[\pm K_{mn}-2k]}\, d\rho_1\,. \end{aligned} \tag{2.113}$$

Recalling that in (2.112) the $\vec{K}_{pq}$ wave vectors are on the remote patch, while in (2.113) the $\vec{K}_{mn}$ wave vectors are on the patch, and that ρ_2 in the former corresponds to exactly the same as ρ_1 in the latter (compare Figures 2.7 and 2.9), we see that the forms of the equations are the same. This is not surprising for monostatic operation since in each case one scatter occurs on the remote patch and the other near the receiver or transmitter. Again, there are small differences in the exact forms of $\gamma_{E12B,1}$ and $\gamma_{E12F,2}$ due to the techniques used in developing them (see Sections 2.2.2.3 and 2.2.3.2). However, on application to the ocean surface it will be seen in Section 3.6.6 that the differences are unimportant – that is, they do not significantly affect the Doppler cross sections depicted there.

2.2.5 The Electric Field Equations for a Pulsed Dipole

At this stage, the vertical electric field components have been derived to second order in scatter. The source is an elementary dipole with arbitrary current distribution – i.e., the waveform of the source radiation is general. Since it is the object of this analysis to develop bistatic cross sections of the ocean surface for a pulsed radar, we shall seek the appropriate field expressions using a pulsed elementary dipole source. As the theory is developed, it will become evident that the cross section expressions will not depend explicitly on the source type. Thus, it is convenient to choose the simple form of the pulsed dipole. In fact, we shall choose a current excitation which is easily extendable to more complicated forms.

The initial approach in seeking the pulsed dipole forms for the field components given in equations (2.30), (2.80), (2.89), and (2.107) is based on the convolution theorem – that is, multiplication in the frequency domain corresponds to convolution in the time domain. In all of the above equations, the parameter, C_0, is a function of radian frequency, ω, by virtue of equation (2.7) and the definition following it. Writing the source current, I, explicitly as a function of frequency, we indeed have

$$kC_0 = \frac{k^3 I(\omega)\Delta\ell}{j\omega\epsilon_0}$$

as a factor in all of the field equations. This is easily seen to be equivalent to

$$kC_0 = -j\frac{\eta_0\Delta\ell}{c^2}\omega^2 I(\omega) \tag{2.114}$$

where, as usual, η_0 is the intrinsic impedance of free space, $c\left(=\frac{\omega}{k}\right)$ is the speed of light in a vacuum, and $\Delta\ell$ is the dipole length. From the Fourier transform property

$$\frac{\partial^n i(t)}{\partial t^n} \underset{\mathcal{F}^{-1}}{\overset{\mathcal{F}}{\rightleftharpoons}} (j\omega)^n I(\omega)\,,$$

the inverse transform of (2.114) may be written as

$$\mathcal{F}^{-1}\left[kC_0\right](t) = j\frac{\eta_0\Delta\ell}{c^2}\frac{\partial^2 i(t)}{\partial t^2} \tag{2.115}$$

where $i(t)$ is the time domain current excitation which determines the waveform.

The choice of $i(t)$ is that of a pulsed sinusoid:

$$i(t) = I_0 e^{j\omega_0 t}[h(t) - h(t - \tau_0)] \tag{2.116}$$

where I_0 is the peak current, ω_0 is the sinusoidal radian frequency, $h(t)$ is the Heaviside function defined as

$$h(t) = \begin{cases} 1, & t \geq 0 \\ 0, & t < 0 \end{cases} \tag{2.117}$$

and τ_0 is the temporal length of the pulse. This complex current is physically realizable by "in-phase" and "quadrature" components. Also, real trigonometric sines and cosines may be given by linear combinations of (2.116) and, since the response equations are linear, superposition allows the generation of more complicated current forms if required.

If we agree to neglect the leading and trailing edge impulse terms in the derivative of (2.116) then we may write

$$\frac{\partial^2 i(t)}{\partial t^2} = -\omega_0^2 I_0 e^{j\omega_0 t}[h(t) - h(t - \tau_0)]$$

so that (2.115) becomes

$$\mathcal{F}^{-1}[kC_0](t) \approx -j\eta_0 \Delta\ell I_0 k_0^2 e^{j\omega_0 t}[h(t) - h(t - \tau_0)] \tag{2.118}$$

where the wavenumber of the excitation current is $k_0 \left(= \frac{\omega_0}{c}\right)$. This approximation is made with a view to simplifications in the subsequent analysis.

Besides the kC_0 factor appearing in field equations (2.30), (2.80), (2.89) and (2.107), the integral portions all have expressions of the form

$$F_i(\rho_i)F_j(\rho_j)e^{-j2k\rho_{ij}} \tag{2.119}$$

where

$$\rho_{ij} = \frac{\rho_i + \rho_j}{2}$$

with the values of the i, j subscripts being obvious from the equations referenced. It should be pointed out that the attenuation functions, F, are really a function of frequency ω, also. Therefore, strictly speaking (2.119) should be cast as

$$F_i(\rho_i,\omega)F_j(\rho_j,\omega)e^{-j2k\rho_{ij}} = F_i(\rho_i,\omega)F_j(\rho_j,\omega)e^{-j\frac{2\omega}{c}\rho_{ij}} \ . \tag{2.120}$$

Furthermore, the exact transform of $i(t)$ in (2.116) is (see, for example, Haykin ([71], Chapter 2))

$$I(\omega) = I_0\tau_0 \mathrm{Sa}\left[(\omega-\omega_0)\frac{\tau_0}{2}\right]$$

where Sa[·] is the sampling function sin[·]/[·]. This means that ω has an infinite number of values (i.e. the finite pulse is not band-limited). However, in the HF band, for any desirable pulse length, the sampling function decays very rapidly and the frequencies within the main lobe are given by $\left(\omega_0 - \frac{2\pi}{\tau_0}\right) \leq \omega \leq \left(\omega_0 + \frac{2\pi}{\tau_0}\right)$. If, for example, $\omega_0 = 20\pi$ M rad/s (i.e. $f_0 = \frac{\omega_0}{2\pi} = 10$ MHz) and the pulse width is 8 μs, then between the first zero crossings of the sampling function, 62.05 Mrad/s $< \omega <$ 63.62 Mrad/s. Using a program developed by Dawe [72] for spherical earth rough surface scatter and a typical wind regime of 15 m/s at 90° to a narrow beam receiver look direction we find that, corresponding to this variation in ω, for $\rho = 50$ km, $0.516 \leq F(\rho,\omega) \leq 0.530$ and for $\rho = 100$ km, $0.263 \leq F(\rho,\omega) \leq 0.276$. These results are representative of what might be expected for operation in the HF band. The largest variation of $F(\rho,\omega)$ occurs when the wind is along the receive beam, but even then for $\rho = 100$ km in the example above, the variation is only $0.121 < F(\rho,\omega) < 0.129$. For this reason we shall approximate the expression in (2.120) as

$$F_i(\rho_i,\omega)F_j(\rho_j,\omega)e^{-j\frac{2\omega}{c}\rho_{ij}} \approx F_i(\rho_i,\omega_0)F_j(\rho_j,\omega_0)e^{-j\frac{2\omega}{c}\rho_{ij}} \tag{2.121}$$

where the ω in the phase term has been left untouched because large changes in the phase will occur for variation of ω within the first lobe of the sampling function.

To complete the introduction to this section, we use (2.121) in approximating the

inverse Fourier transform of (2.119) for use in the subsections which follow:

$$\mathcal{F}^{-1}\left[F(\rho_i,\omega)F(\rho_j,\omega)e^{-j2k\rho_{ij}}\right](t) = \mathcal{F}^{-1}\left[F(\rho_i,\omega)F(\rho_j,\omega)e^{-j\frac{2\rho_{ij}\omega}{c}}\right](t)$$
$$\approx F(\rho_i,\omega_0)F(\rho_j,\omega_0)\delta\left(t-\frac{2\rho_{ij}}{c}\right). \quad (2.122)$$

2.2.5.1 The First-order Electric Field

On the basis of the foregoing, it is clear that $(E^+_{0_n})_1$ for the first-order bistatic electric field in equation (2.30) is a function of ω. To examine the time domain behaviour of this field given the pulsed dipole source whose current distribution is described by equation (2.116), it is logical to take the inverse temporal Fourier transform of (2.30). Thus, using the convolution theorem,

$$\mathcal{F}^{-1}\left[(E^+_{0_n})_1(\omega)\right](t) \approx \frac{1}{(2\pi)^{\frac{3}{2}}}\mathcal{F}^{-1}\left\{-j\frac{\eta_0\Delta\ell}{c^2}\omega^2 I(\omega)\right\} \overset{t}{*} \mathcal{F}^{-1}\left\{\sum_{m,n}P_{\vec{K}_{mn}}\right.$$
$$\cdot\sqrt{K_{mn}}e^{j\frac{\vec{\rho}}{2}\cdot\vec{K}_{mn}}\int_{\frac{\rho}{2}}^{\infty}\frac{F(\rho_1,\omega_0)F(\rho_2,\omega_0)}{\sqrt{\rho_s\left[\rho_s^2-\left(\frac{\rho}{2}\right)^2\right]}}$$
$$\left.\cdot\, e^{\mp\frac{j\pi}{4}}e^{j\rho_s(\pm K_{mn}\cos\phi)}\left(\pm\sqrt{\cos\phi}\right)\cdot e^{\frac{-j2\rho_s\omega}{c}}\,d\rho_s\right\} \quad (2.123)$$

where $\overset{t}{*}$ refers to a time convolution and we have used (2.114), (2.120) and the approximation in (2.121) to write the ω dependence explicitly. Noting that the first inverse transform above has no ρ_s dependence, the order of the convolution and integration may be interchanged. The convolution portion of (2.123) involves

$$\mathcal{F}^{-1}\left\{-j\frac{\eta_0\Delta\ell}{c^2}\omega^2 I(\omega)\right\} \overset{t}{*} \mathcal{F}^{-1}\left\{e^{\frac{-j2\rho_s\omega}{c}}\right\}$$

which from (2.118) is

$$-j\eta_0\Delta\ell I_0 k_0^2 e^{j\omega_0 t}[h(t)-h(t-\tau_0)] \overset{t}{*} \delta\left(t-\frac{2\rho_s}{c}\right) = -j\eta_0\Delta\ell I_0 k_0^2\, e^{j\omega_0\left(t-\frac{2\rho_s}{c}\right)}$$
$$\cdot\left[h\left(t-\frac{2\rho_s}{c}\right)-h\left(t-\frac{2\rho_s}{c}-\tau_0\right)\right]. \quad (2.124)$$

Now

$$\left[h\left(t-\frac{2\rho_s}{c}\right)-h\left(t-\frac{2\rho_s}{c}-\tau_0\right)\right] = \begin{cases} 1, & \frac{c(t-\tau_0)}{2}\le\rho_s\le\frac{ct}{2} \\ 0, & \text{otherwise}\end{cases}, \quad (2.125)$$

so that using (2.124) and replacing $\frac{\omega_0}{c}$ by k_0, the field equation, in time, from (2.123) may be cast as

$$(E_{0_n}^{+})_1(t) \approx \frac{-j\eta_0\Delta\ell I_0 k_0^2}{(2\pi)^{\frac{3}{2}}} \sum_{m,n} P_{\vec{K}_{mn}} \sqrt{K_{mn}} e^{j\frac{\vec{\rho}}{2}\cdot\vec{K}_{mn}} e^{j\omega_0 t} \int_{\frac{c(t-\tau_0)}{2}}^{\frac{ct}{2}} \frac{F(\rho_1,\omega_0)F(\rho_2,\omega_0)}{\sqrt{\rho_s\left[\rho_s^2-\left(\frac{\rho}{2}\right)^2\right]}}$$
$$\cdot\, e^{\mp\frac{j\pi}{4}} \left(\pm\sqrt{\cos\phi}\right) e^{j\rho_s(\pm K_{mn}\cos\phi - 2k_0)}\, d\rho_s \,. \tag{2.126}$$

To facilitate the analysis, the following are defined:

$$\begin{aligned} \rho_{0s} &= \frac{\frac{ct}{2}+\frac{c(t-\tau_0)}{2}}{2} = \frac{c(t-\frac{\tau_0}{2})}{2} \\ \Delta\rho_s &= \frac{c\tau_0}{2} \end{aligned} \tag{2.127}$$

from which

$$\begin{aligned} &\rho_{0s} - \tfrac{\Delta\rho_s}{2} = \tfrac{c(t-\tau_0)}{2} \\ \text{and} \\ &\rho_{0s} + \tfrac{\Delta\rho_s}{2} = \tfrac{ct}{2} \,. \end{aligned} \tag{2.128}$$

For a pulse radar of pulse width τ_0, the quantity $\Delta\rho_s = \frac{c\tau_0}{2}$ is commonly referred to as the *patch width*. That is, it is the smallest distance in range which can be unambiguously interrogated by the radar. Using (2.128) the field equation in (2.126) becomes

$$(E_{0_n}^{+})_1(t) \approx \frac{-j\eta_0\Delta\ell I_0 k_0^2}{(2\pi)^{\frac{3}{2}}} \sum_{m,n} P_{\vec{K}_{mn}} \sqrt{K_{mn}}\, e^{j\frac{\vec{\rho}}{2}\cdot\vec{K}_{mn}} e^{j\omega_0 t}$$
$$\cdot \int_{\rho_{0s}-\frac{\Delta\rho_s}{2}}^{\rho_{0s}+\frac{\Delta\rho_s}{2}} \frac{F(\rho_1,\omega_0)F(\rho_2,\omega_0)}{\sqrt{\rho_s\left[\rho_s^2-\left(\frac{\rho}{2}\right)^2\right]}}$$
$$\cdot\, e^{\mp\frac{j\pi}{4}} \left(\pm\sqrt{\cos\phi}\right) e^{j\rho_s(\pm K_{mn}\cos\phi - 2k_0)}\, d\rho_s \,. \tag{2.129}$$

An asymptotic form of equation (2.129), valid when $\rho_{0s} >> \Delta\rho_s$, is now sought. We want this asymptotic result to give the received field from a particular patch of ocean, and with this in mind an appropriate change of variables is pursued. We note that for a typical HF radar ρ_{0s} is on the order of 10^4 to 10^5 m while $\Delta\rho_s$ is on the order of 10^2 to 10^3 m. Initially, the phase term, $\rho_s(\pm K_{mn}\cos\phi - 2k_0)$ is examined. In Appendix

A.3.1, it is shown that

$$\cos\phi = \sqrt{1 - \left(\frac{\frac{\rho}{2}}{\rho_s}\right)^2 \sin^2\theta_N} \tag{2.130}$$

where θ_N is the direction of the normal to the scattering ellipse discussed in Appendix A.1.2.2. From the interpretation of the stationary result there, the conclusion is reached that for a fixed $\vec{K}_{mn}$ surface wave vector, which is normal to the scattering ellipse, θ_N is constant during the ρ_s integration of equation (2.129). Applying (2.130), the phase term may be expanded as

$$\rho_s(\pm K_{mn}\cos\phi - 2k_0) = \pm K_{mn}\sqrt{\rho_s^2 - \left(\frac{\rho}{2}\right)^2 \sin^2\theta_N} \; - 2k_0\rho_s \; ,$$

which, on defining $\rho'_s = \rho_s - \rho_{0s}$, becomes

$$\begin{aligned}\rho_s(\pm K_{mn}\cos\phi - 2k_0) &= \pm K_{mn}\sqrt{(\rho_{0s}+\rho'_s)^2 - \left(\frac{\rho}{2}\right)^2 \sin^2\theta_N} \; - 2k_0(\rho_{0s}+\rho'_s) \\ &= \pm K_{mn}\sqrt{\rho_{0s}^2 - \left(\frac{\rho}{2}\right)^2 \sin^2\theta_N + \rho_s'^2 + 2\rho'_s\rho_{0s}} - 2k_0(\rho_{0s}+\rho'_s) \; .\end{aligned} \tag{2.131}$$

From the definitions in (2.127) and (2.128) it may be observed that for a particular reception time, t, ρ_{0s} is a fixed quantity *centred* between $\frac{c(t-\tau_0)}{2}$ and $\frac{ct}{2}$. For ordinary, monostatic operation this would correspond to the centre of a scattering patch of radial extent $\frac{c\tau_0}{2}$ at a range determined by t. Similarly, in bistatic operation, it is the central value of $\rho_s \left(= \frac{\rho_1+\rho_2}{2}\right)$ (which is determined by t) over a pulse period, τ_0. In this sense, $\rho'_s(=\rho_s - \rho_{0s})$ is a distance parameter which varies across a particular patch of surface. This assertion emphasizes that, in terms of ρ'_s, the integral limits in equation (2.129) vary from $\frac{-\Delta\rho_s}{2}$ to $\frac{\Delta\rho_s}{2}$; i.e.

$$\frac{-\Delta\rho_s}{2} \le \rho'_s \le \frac{\Delta\rho_s}{2} \; .$$

In view of this discussion, (2.131) may be presented as

$$\begin{aligned}\rho_s(\pm K_{mn}\cos\phi - 2k_0) &= \pm K_{mn}\sqrt{(\rho_{0s}^2(1 - \left(\frac{\frac{\rho}{2}}{\rho_{0s}}\right)^2 \sin^2\theta_N) + \rho_s'^2 + 2\rho'_s\rho_{0s}} \\ &\quad -2k_0(\rho_{0s}+\rho'_s) \\ &= \pm K_{mn}\sqrt{\rho_{0s}^2\cos^2\phi_0 + \rho_s'^2 + 2\rho'_s\rho_{0s}} - 2k_0(\rho_{0s}+\rho'_s)\end{aligned} \tag{2.132}$$

where (2.130) has been used to write

$$\cos\phi_0 = \sqrt{1 - \left(\frac{\frac{\rho}{2}}{\rho_{0s}}\right)^2 \sin^2\theta_N} \tag{2.133}$$

as a representative value of the bistatic angle, ϕ, associated with ρ_{0s}, the "central" value of ρ_s. Invoking the assumption that $\rho_{0s} >> |\rho'_s|$ which, for typical pulse radar operating parameters, will always be the case, and applying a binomial expansion, gives for (2.132)

$$\rho_s(\pm K_{mn}\cos\phi - 2k_0) \approx (\pm K_{mn}\cos\phi_0 - 2k_0)\rho_{0s} + \left(\frac{\pm K_{mn}}{\cos\phi_0} - 2k_0\right)\rho'_s \,. \tag{2.134}$$

Before finally writing equation (2.129) as an integral over the "patch" distance parameter, ρ'_s, the following may be observed:

1. $\rho_s = \rho_{0s} + \rho'_s$ by definition and $\rho_{0s} >> |\rho'_s|$, so $\rho_s \approx \rho_{0s}$

2. ρ_{0s} is a constant so $d\rho_s = d\rho'_s$

3. $\rho_{0s} - \dfrac{\Delta\rho_s}{2} \le \rho_s \le \rho_{0s} + \dfrac{\Delta\rho_s}{2}$ implies $\dfrac{-\Delta\rho_s}{2} \le \rho'_s \le \dfrac{\Delta\rho_s}{2}$

4. Over the limit range given in observation (3), the integrand factors other than the phase term containing ρ'_s will vary very slowly over the integration region and may be safely removed from the integral.

5. Since ρ_1 and ρ_2 vary only slightly over the patch they may be represented by ρ_{01} and ρ_{02} such that $\rho_{0s} = \dfrac{\rho_{01} + \rho_{02}}{2}$.

From equation (2.132) and the considerations above, field equation (2.129) reduces to

$$\begin{aligned}(E^+_{0_n})_1(t) \;\approx\; & \frac{-j\eta_0\Delta\ell I_0 k_0^2}{(2\pi)^{\frac{3}{2}}} \sum_{m,n} P_{\vec{K}_{mn}} \sqrt{K_{mn}}\, e^{j\frac{\vec{\rho}}{2}\cdot\vec{K}_{mn}} e^{j\omega_0 t} \\ & \cdot \frac{F(\rho_{01},\omega_0)F(\rho_{02},\omega_0)}{\sqrt{\rho_{0s}\left[\rho_{0s}^2 - \left(\frac{\rho}{2}\right)^2\right]}} e^{\mp\frac{j\pi}{4}} \left(\pm\sqrt{\cos\phi_0}\right) \\ & \cdot e^{j\rho_{0s}(\pm K_{mn}\cos\phi_0 - 2k_0)} \int_{\frac{-\Delta\rho_s}{2}}^{\frac{\Delta\rho_s}{2}} e^{j\rho'_s\left(\pm\frac{K_{mn}}{\cos\phi_0} - 2k_0\right)}\, d\rho'_s \,. \end{aligned} \tag{2.135}$$

The remaining integral in (2.135) easily reduces to

$$\int_{\frac{-\Delta\rho_s}{2}}^{\frac{\Delta\rho_s}{2}} e^{j\rho_s'\left(\pm\frac{K_{mn}}{\cos\phi_0}-2k_0\right)}\, d\rho_s' = \Delta\rho_s\left[\mathrm{Sa}\left[\frac{\Delta\rho_s}{2}\left(\frac{K_{mn}}{\cos\phi_0}-2k_0\right)\right] + \mathrm{Sa}\left[\frac{\Delta\rho_s}{2}\left(\frac{K_{mn}}{\cos\phi_0}+2k_0\right)\right]\right] \tag{2.136}$$

and the second sampling function is very small relative to the first for any bistatic radar parameters and surface wavenumbers of interest. Retracing the analysis in Appendix A.1.2.2, it is clear that the first sampling function is associated with wave vectors $\vec{K}_{mn} = +K_{mn}\hat{N}$. Thus, it is the outward pointing wave vector of the time invariant surface that is responsible for essentially all of the first-order received field. We note too that the peak occurs at $K_{mn} = 2k_0\cos\phi_0$, a situation discussed in detail when application is made to the ocean (Section 3.6.2). In equation (2.135), $e^{-j\frac{\pi}{4}}$ and $+\sqrt{\cos\phi_0}$ are quantities associated with this vector. Therefore, to a very good approximation, the received field is

$$\begin{aligned}(E_{0_n}^{+})_1(t_0) \approx\ & \frac{-j\eta_0\Delta\ell I_0 k_0^2}{(2\pi)^{\frac{3}{2}}}\sum_{m,n} P_{\vec{K}_{mn}}\sqrt{K_{mn}\cos\phi_0}\, e^{j\frac{\vec{\rho}}{2}\cdot\vec{K}_{mn}} e^{jk_0\Delta\rho_s} \\ & \cdot \frac{F(\rho_{01},\omega_0)F(\rho_{02},\omega_0)}{\sqrt{\rho_{0s}\left[\rho_{0s}^2-\left(\frac{\rho}{2}\right)^2\right]}} e^{\frac{-j\pi}{4}} \\ & \cdot e^{j\rho_{0s}(K_{mn}\cos\phi_0)}\Delta\rho_s\mathrm{Sa}\left[\frac{\Delta\rho_s}{2}\left(\frac{K_{mn}}{\cos\phi_0}-2k_0\right)\right]\end{aligned} \tag{2.137}$$

where the second exponential was derived from

$$\begin{aligned} e^{j\omega_0 t}\cdot e^{j(-2\rho_{0s}k_0)} &= e^{j\omega_0\left(t-\frac{2\rho_{0s}}{c}\right)} \\ &= e^{\frac{j\omega_0}{c}\left(ct-2\left(\frac{c(t-\frac{\tau_0}{2})}{2}\right)\right)} \\ &= e^{jk_0\Delta\rho_s}\ . \end{aligned}$$

While time, t, does not appear explicitly in (2.137), it is there by virtue of the ρ_{0s} parameter. That is, each ρ_{0s} corresponds to a particular scattering ellipse and therefore to a different time for the received field. The fact that the field at any

instant will be of interest as it pertains to a particular scattering ellipse has been emphasized by setting $t = t_0$. This change of variable will also be useful when a time varying surface (Section 3.3) is introduced.

2.2.5.2 The Second-order "Patch" Scatter Electric Field

Following all of the same assumptions and arguments from equations (2.114) to (2.121) we may write (2.80) for the second-order "patch scatter" field in the time domain completely analogously to what was done in equation (2.123) for the first order. Writing the time convolution for the inverse transform of (2.80) explicitly gives

$$\begin{aligned}\mathcal{F}^{-1}\left\{(E^{+}_{0_n})_{2,F,1}(\omega)\right\}(t) \;\approx\; & \frac{1}{(2\pi)^{\frac{3}{2}}}\mathcal{F}^{-1}\left\{-j\frac{\eta_0\Delta\ell}{c^2}\omega^2 I(\omega)\right\} \overset{t}{*} \\ & \cdot\, \mathcal{F}^{-1}\left\{\sum_{m,n}\sum_{p,q}\frac{P_{\vec{K}_{mn}}P_{\vec{K}_{pq}}}{\sqrt{K_{rs}}}\, e^{j\frac{\vec{\rho}}{2}\cdot\vec{K}_{rs}}\int_{\frac{\rho}{2}}^{\infty}(k\gamma_{E12F,1})\right. \\ & \cdot\, \frac{F(\rho_2,\omega_0)F(\rho_{20},\omega_0)}{\sqrt{\cos\phi}}\,\frac{e^{\mp j\frac{\pi}{4}}e^{j\rho_{s12,1}(\pm K_{rs}\cos\phi)}}{\sqrt{\rho_{s12,1}\left[\rho^2_{s12,1}-\left(\frac{\rho}{2}\right)^2\right]}} \\ & \left.\cdot\, e^{-j2\rho_{s12,1}\frac{\omega}{c}}\, d\rho_{s12,1}\right\} \end{aligned} \tag{2.138}$$

where k in $e^{j\rho_{s12,1}(-2k)}$ has been written as $\frac{\omega}{c}$. The convolution, this time, using equation (2.124) with the appropriate change in distance variable from ρ_s to $\rho_{s12,1}$, (defined in (2.77)) is

$$\begin{aligned}\mathcal{F}^{-1}\left\{-j\frac{\eta_0\Delta\ell}{c^2}\omega^2 I(\omega)\right\} \overset{t}{*} \mathcal{F}^{-1}\left\{e^{-j2\rho_{s12,1}\frac{\omega}{c}}\right\} \;=\; & -j\eta_0\Delta\ell I_0 k_0^2 e^{j\omega_0\left(t-\frac{2\rho_{s12,1}}{c}\right)} \\ \cdot\, \left[h\left(t-\frac{2\rho_{s12,1}}{c}\right)-h\left(t-\frac{2\rho_{s12,1}}{c}-\tau_0\right)\right] & \end{aligned} \tag{2.139}$$

so that (2.138) becomes

$$\begin{aligned}(E^{+}_{0_n})_{2,F,1}(t) \;\approx\; & \frac{-j\eta_0\Delta\ell I_0 k_0^2}{(2\pi)^{\frac{3}{2}}}\sum_{m,n}\sum_{p,q}\frac{P_{\vec{K}_{mn}}P_{\vec{K}_{pq}}}{\sqrt{K_{rs}}}\, e^{j\frac{\vec{\rho}}{2}\cdot\vec{K}_{rs}}e^{j\omega_0 t} \\ & \cdot\, \int_{\frac{c(t-\tau_0)}{2}}^{\frac{ct}{2}}(k_0\gamma_{E12F,1})\frac{F(\rho_2,\omega_0)F(\rho_{20},\omega_0)}{\sqrt{\cos\phi}}\,\frac{e^{\mp j\frac{\pi}{4}}}{\sqrt{\rho_{s12,1}\left[\rho^2_{s12,1}-\left(\frac{\rho}{2}\right)^2\right]}} \\ & \cdot\, e^{j\rho_{s12,1}(\pm K_{rs}\cos\phi-2k_0)}\, d\rho_{s12,1}\,. \end{aligned} \tag{2.140}$$

Clearly, equation (2.140) has the same *form* as equation (2.126) for the first order. Now, if in equations (2.127) through (2.136), ρ_{0s}, $\Delta\rho_s$, ρ_s, ρ'_s and K_{mn} are replaced by $\rho_{0s12,1}$, $\Delta\rho_{s12,1}$, $\rho_{s12,1}$, $\rho'_{s12,1}$ and K_{rs}, respectively, then the second-order patch scatter result of (2.140) may be written in the form of (2.137) as

$$\begin{aligned}(E^+_{0_n})_{2,F,1}(t_0) \approx\ & \frac{-j\eta_0\Delta\ell I_0 k_0^2}{(2\pi)^{\frac{3}{2}}}\sum_{m,n}\sum_{p,q}\frac{P_{\vec{K}_{mn}}P_{\vec{K}_{pq}}}{\sqrt{K_{rs}\cos\phi_0}}\,e^{j\frac{\vec{\rho}}{2}\cdot\vec{K}_{rs}}e^{jk_0\Delta\rho_{s12,1}} \\ & \cdot\frac{F(\rho_{02},\omega_0)F(\rho_{020},\omega_0)e^{-j\frac{\pi}{4}}}{\sqrt{\rho_{0s12,1}\left[\rho^2_{0s12,1}-\left(\frac{\rho}{2}\right)^2\right]}}\,(k_0\gamma_{E12F,1})\,e^{j\rho_{0s12,1}(K_{rs}\cos\phi_0)} \\ & \cdot\Delta\rho_{s12,1}\mathrm{Sa}\left[\frac{\Delta\rho_{s12,1}}{2}\left(\frac{K_{rs}}{\cos\phi_0}-2k_0\right)\right]\ . \qquad (2.141)\end{aligned}$$

Before further discussion on this equation, the electromagnetic coupling coefficient for patch scatter, with reference to (2.64), is redefined as

$$_E\Gamma_P = \frac{k_0\gamma_{E12F,1}}{K_{rs}\cos\phi_0}\ . \qquad (2.142)$$

The purpose of this and subsequent redefinitions of the various electromagnetic coupling coefficients is simply that all components of the received field may be cast in the same form. Then, equation (2.141) gives the scatter from an elliptical surface region corresponding to a time $t = t_0$ as

$$\begin{aligned}(E^+_{0_n})_{2,F,1}(t_0) \approx\ & \frac{-j\eta_0\Delta\ell I_0 k_0^2}{(2\pi)^{\frac{3}{2}}}\sum_{m,n}\sum_{p,q}P_{\vec{K}_{mn}}P_{\vec{K}_{pq}}\sqrt{K_{rs}\cos\phi_0}\ {}_E\Gamma_P \\ & \cdot e^{j\frac{\vec{\rho}}{2}\cdot\vec{K}_{rs}}e^{jk_0\Delta\rho_s}\frac{F(\rho_{02},\omega_0)F(\rho_{020},\omega_0)e^{-j\frac{\pi}{4}}}{\sqrt{\rho_{0s12,1}\left[\rho^2_{0s12,1}-\left(\frac{\rho}{2}\right)^2\right]}}e^{j\rho_{0s12,1}K_{rs}\cos\phi_0} \\ & \cdot\Delta\rho_s\mathrm{Sa}\left[\frac{\Delta\rho_s}{2}\left(\frac{K_{rs}}{\cos\phi_0}-2k_0\right)\right]\ . \qquad (2.143)\end{aligned}$$

In (2.143), $\Delta\rho_{s12,1}$ has been set equal to $\Delta\rho_s$ because the same patch of surface is involved here as for the first order. It should also be mentioned that ρ_{02} and ρ_{020} are representative of "central" values of ρ_2 and ρ_{20} with $\rho_{0s12,1} = \frac{\rho_{02}+\rho_{020}}{2}$ analogous to observation (5) following equation (2.134).

The assumptions made on the first-order field integral throughout Section 2.2.5.1 have been used again to obtain equation (2.143) for the second order. Apart from the fact that there are now two wave vectors ($\vec{K}_{mn}$ and $\vec{K}_{pq}$) involved in the scatter, as is evidenced by the presence of $P_{\vec{K}_{pq}}$, $K_{rs}(=|\vec{K}_{pq}+\vec{K}_{mn}|)$ and ${}_E\Gamma_P$, it is obvious that first- and second-order patch scatter have very similar mathematical forms. It is also important to note that the sampling function remaining in (2.143) has its maximum at $K_{rs}=2k_0\cos\phi_0$ and $\vec{K}_{rs}$ is along the outward ellipse normal. The ramifications of this are discussed in Section 3.6.2 and Appendix B.2 in application to the ocean surface.

2.2.5.3 The Second-order Electric Field with One Scatter at the Transmitter

Continuing in the same vein as the previous two subsections, the time domain electric field component associated with a single scatter near the pulsed dipole source followed by another on the remote surface patch is now considered. Again, using the analysis of equations (2.114) through (2.121) the inverse Fourier transform of equation (2.89) when the source is as stated is

$$\begin{aligned}\mathcal{F}^{-1}\left\{(E^{+}_{0_n})_{2,F,2}(\omega)\right\}(t) \approx\ & \frac{1}{(2\pi)^{\frac{1}{2}}}\mathcal{F}^{-1}\left\{-j\frac{\eta_0\Delta\ell}{c^2}\omega^2 I(\omega)\right\}\overset{t}{*} \\ & \mathcal{F}^{-1}\left\{\sum_{m,n}\sum_{p,q}\frac{P_{\vec{K}_{mn}}P_{\vec{K}_{pq}}}{\sqrt{K_{pq}}}\,e^{j\frac{\vec{\rho}}{2}\cdot\vec{K}_{pq}}\int_{\frac{\rho}{2}}^{\infty}(k\gamma_{E12F,2})\right. \\ & \cdot\frac{F(\rho_2,\omega_0)F(\rho_{20},\omega_0)}{\sqrt{\cos\phi}} \\ & \left.\cdot\frac{e^{\mp j\frac{\pi}{4}}e^{j\rho_{s12,1}(\pm K_{pq}\cos\phi)}e^{-j2\rho_{s12,1}\frac{\omega}{c}}}{\sqrt{\rho_{s12,1}\left[\rho^2_{s12,1}-\left(\frac{\rho}{2}\right)^2\right]}}\,d\rho_{s12,1}\right\}. \quad (2.144)\end{aligned}$$

Obviously, equation (2.144) is no different in form than (2.138) for the patch scatter. However, it is important to note that the K_{rs} wavenumbers of the patch scatter are replaced by the K_{pq} wavenumbers here. This is due to the fact that the $\vec{K}_{pq}$ surface wave vectors are the only ones associated with the remote patch here, whereas in

(2.138) both $\vec{K}_{mn}$ and $\vec{K}_{pq}$ wave vectors were associated with that region. Of course $\gamma_{E12F,2}$ for the equation above is not the same as its patch scatter counterpart, but this does not alter the way in which the convolution proceeds. These observations in concert with the first- and second-order patch scatter analysis lead immediately to the final time domain representation of (2.144), analogous to (2.143), as

$$\begin{aligned}(E_{0_n}^{+})_{2,F,2}(t_0) \approx & \frac{-j\eta_0\Delta\ell I_0 k_0^2}{(2\pi)^{\frac{1}{2}}}\sum_{m,n}\sum_{p,q}P_{\vec{K}_{mn}}P_{\vec{K}_{pq}}\sqrt{K_{pq}\cos\phi_0}\;{}_E\Gamma_T \\ & \cdot e^{j\frac{\vec{\rho}}{2}\cdot\vec{K}_{pq}}e^{jk_0\Delta\rho_s}\frac{F(\rho_{02},\omega_0)F(\rho_{020},\omega_0)e^{-j\frac{\pi}{4}}}{\sqrt{\rho_{0s12,1}\left[\rho_{0s12,1}^2-\left(\frac{\rho}{2}\right)^2\right]}}e^{j\rho_{0s12,1}K_{pq}\cos\phi_0} \\ & \cdot \Delta\rho_s \mathrm{Sa}\left[\frac{\Delta\rho_s}{2}\left(\frac{K_{pq}}{\cos\phi_0}-2k_0\right)\right]\;. \end{aligned} \tag{2.145}$$

In (2.145), ${}_E\Gamma_T$ is the electromagnetic coupling coefficient redefined by

$${}_E\Gamma_T = \frac{(k_0\gamma_{E12F,2})}{K_{pq}\cos\phi_0} \tag{2.146}$$

where $\gamma_{E12F,2}$ is given in equation (2.87). The second sampling function is discarded as being small. By virtue of this fact, the $\vec{K}_{pq}$ of significance is that which points along the outward normal of the scattering ellipse (i.e. $\vec{K}_{pq} = K_{pq}\hat{N}$) and the remaining sampling function indicates that most of the contribution comes from $K_{pq} = 2k_0\cos\phi_0$. It should be noticed that the "patch" indicated by the $\Delta\rho_s$ parameter has the same mathematical meaning as before (i.e. $\frac{\tau_0}{2}$). However, for the present case, only one of the two scatters occurs remotely from both transmitter and receiver. In Sections 3.5–3.6 where the ocean cross sections are developed and illustrated, this problem is treated as though all components of the field come from the same place – simply because there is no means of separating the different components in an actual radar. If the surface is homogeneous, again as will be assumed for the ocean, this potential difficulty is not an issue.

2.2.5.4 The Second-order Electric Field with One Scatter at the Receiver

The final component of the second-order electric field we wish to investigate is that when the first scatter on a remote surface patch is followed by another near the receiver, the source being a pulsed dipole as before. To this end, the expression to be investigated is the inverse Fourier transform version of equation (2.107) given, as usual, by

$$\begin{aligned}\mathcal{F}^{-1}\left\{(E^{+}_{0_n})_{2,B,1}(\omega)\right\}(t) \approx\ & \frac{1}{(2\pi)^{\frac{3}{2}}}\mathcal{F}^{-1}\left\{-j\frac{\eta_0\Delta\ell}{c^2}\omega^2 I(\omega)\right\} \overset{t}{*} \\ & \mathcal{F}^{-1}\left\{\sum_{m,n}\sum_{p,q}\frac{P_{\vec{K}_{mn}}P_{\vec{K}_{pq}}}{\sqrt{K_{mn}}}\, e^{j\frac{\vec{\rho}\cdot\vec{K}_{mn}}{2}} e^{j\vec{\rho}\cdot\vec{K}_{pq}} \int_{\frac{\rho}{2}}^{\infty}(k\gamma_{E12B,1})\right. \\ & \cdot \frac{F(\rho_1,\omega_0)F(\rho_{12},\omega_0)}{\sqrt{\cos\phi_0}}\, e^{\mp j\frac{\pi}{4}} \\ & \left.\cdot \frac{e^{j\rho_{s21,1}(\pm K_{mn}\cos\phi)}}{\sqrt{\rho_{s21,1}\left[\rho^2_{s21,1}-\left(\frac{\rho}{2}\right)^2\right]}}\, e^{-j2\rho_{s21,1}\frac{\omega}{c}}\, d\rho_{s21,1}\right\} . \quad (2.147)\end{aligned}$$

Invoking all of the approximations, assumptions and conventions of the previous two subsections, the final time domain result for this component may be written as

$$\begin{aligned}(E^{+}_{0_n})_{2,B,1}(t_0) \approx\ & \frac{-j\eta_0\Delta\ell I_0 k_0^2}{(2\pi)^{\frac{3}{2}}}\sum_{m,n}\sum_{p,q}P_{\vec{K}_{mn}}P_{\vec{K}_{pq}}\sqrt{K_{mn}\cos\phi_0}\ {}_E\Gamma_R \\ & \cdot e^{j\vec{\rho}\vec{K}_{pq}}e^{j\frac{\vec{\rho}}{2}\cdot\vec{K}_{mn}}e^{jk_0\Delta\rho_s}\frac{F(\rho_{01},\omega_0)F(\rho_{012},\omega_0)e^{-j\frac{\pi}{4}}}{\sqrt{\rho_{0s21,1}\left[\rho^2_{0s21,1}-\left(\frac{\rho}{2}\right)^2\right]}} \\ & \cdot e^{j\rho_{0s21,1}K_{mn}\cos\phi_0}\Delta\rho_s \mathrm{Sa}\left[\frac{\Delta\rho_s}{2}\left(\frac{K_{mn}}{\cos\phi_0}-2k_0\right)\right] . \quad (2.148)\end{aligned}$$

Here, the electromagnetic coupling coefficient has been redefined as

$${}_E\Gamma_R = \left(\frac{k_0\gamma_{E12B,1}}{K_{mn}\cos\phi_0}\right) \quad (2.149)$$

with $\gamma_{E12B,1}$ being given by equation (2.106). It should be recalled that the $\vec{K}_{mn}$ wave vector here is associated with the surface which is distant from both transmitter and

receiver. Also, the discarding of the second sampling function arising from the inverse transform means that the remaining $\vec{K}_{mn}$ must point along the outward normal to scattering ellipse. As before, it is clear that the major contribution from this wave vector occurs when $K_{mn} = 2k_0 \cos\phi_0$. Its significance is addressed in Section 3.6.5 where the corresponding ocean cross section is discussed.

2.2.5.5 Summary of Received Field Components for a Pulsed Dipole Source

For reference purposes, the results of the previous three subsections are summarized below.

1. The First-order Field

When a single scatter occurs on an elliptical scattering "patch", equation (2.137) gives the field component as

$$(E^+_{0_n})_1(t_0) \approx \frac{-j\eta_0 \Delta\ell I_0 k_0^2}{(2\pi)^{\frac{3}{2}}} \sum_{m,n} P_{\vec{K}_{mn}} \sqrt{K_{mn}\cos\phi_0}\, e^{j\frac{\vec{\varrho}}{2}\cdot\vec{K}_{mn}} e^{jk_0\Delta\rho_s} \cdot \frac{F(\rho_{01},\omega_0)F(\rho_{02},\omega_0)}{\sqrt{\rho_{0s}\left[\rho_{0s}^2 - \left(\frac{\varrho}{2}\right)^2\right]}} e^{\frac{-j\pi}{4}} e^{j\rho_{0s}(K_{mn}\cos\phi_0)} \Delta\rho_s \mathrm{Sa}\left[\frac{\Delta\rho_s}{2}\left(\frac{K_{mn}}{\cos\phi_0} - 2k_0\right)\right] \quad (2.150)$$

2. Second-order Field – Two Scatters at Same Position

Equation (2.143) gives the field component when two scatters occur near each other on the scattering ellipse as

$$(E^+_{0_n})_{2,F,1}(t_0) \approx \frac{-j\eta_0 \Delta\ell I_0 k_0^2}{(2\pi)^{\frac{3}{2}}} \sum_{m,n}\sum_{p,q} P_{\vec{K}_{mn}} P_{\vec{K}_{pq}} \sqrt{K_{rs}\cos\phi_0}\; {}_E\Gamma_P \cdot e^{j\frac{\vec{\varrho}}{2}\cdot\vec{K}_{rs}} e^{jk_0\Delta\rho_s} \frac{F(\rho_{02},\omega_0)F(\rho_{020},\omega_0)e^{-j\frac{\pi}{4}}}{\sqrt{\rho_{0s12,1}\left[\rho_{0s12,1}^2 - \left(\frac{\varrho}{2}\right)^2\right]}} e^{j\rho_{0s12,1}K_{rs}\cos\phi_0} \cdot \Delta\rho_s \mathrm{Sa}\left[\frac{\Delta\rho_s}{2}\left(\frac{K_{rs}}{\cos\phi_0} - 2k_0\right)\right] . \quad (2.151)$$

3. Second-order Field – One Scatter Near the Transmitter

When one of the two scatters occurs near the transmitter, the other occurring on

the scattering ellipse, the field component is obtained from equation (2.145). It is

$$(E_{0_n}^{+})_{2,F,2}(t_0) \approx \frac{-j\eta_0 \Delta\ell I_0 k_0^2}{(2\pi)^{\frac{3}{2}}} \sum_{m,n} \sum_{p,q} P_{\vec{K}_{mn}} P_{\vec{K}_{pq}} \sqrt{K_{pq} \cos\phi_0}\ {}_E\Gamma_T \cdot e^{j\frac{\vec{\rho}}{2}\cdot\vec{K}_{pq}} e^{jk_0\Delta\rho_s} \frac{F(\rho_{02},\omega_0)F(\rho_{020},\omega_0)e^{-j\frac{\pi}{4}}}{\sqrt{\rho_{0s12,1}\left[\rho_{0s12,1}^2 - \left(\frac{\rho}{2}\right)^2\right]}} e^{j\rho_{0s12,1}K_{pq}\cos\phi_0} \cdot \Delta\rho_s \mathrm{Sa}\left[\frac{\Delta\rho_s}{2}\left(\frac{K_{pq}}{\cos\phi_0} - 2k_0\right)\right] . \quad (2.152)$$

4. Second-order Field – One Scatter Near the Receiver

When one of the two scatters occurs near the receiver, equation (2.148) gives the appropriate field component as

$$(E_{0_n}^{+})_{2,B,1}(t_0) \approx \frac{-j\eta_0 \Delta\ell I_0 k_0^2}{(2\pi)^{\frac{3}{2}}} \sum_{m,n} \sum_{p,q} P_{\vec{K}_{mn}} P_{\vec{K}_{pq}} \sqrt{K_{mn} \cos\phi_0}\ {}_E\Gamma_R \cdot e^{j\vec{\rho}\cdot\vec{K}_{pq}} e^{j\frac{\vec{\rho}}{2}\cdot\vec{K}_{mn}} e^{jk_0\Delta\rho_s} \frac{F(\rho_{01},\omega_0)F(\rho_{012},\omega_0)e^{-j\frac{\pi}{4}}}{\sqrt{\rho_{0s21,1}\left[\rho_{0s21,1}^2 - \left(\frac{\rho}{2}\right)^2\right]}} \cdot e^{j\rho_{0s21,1}K_{mn}\cos\phi_0} \Delta\rho_s \mathrm{Sa}\left[\frac{\Delta\rho_s}{2}\left(\frac{K_{mn}}{\cos\phi_0} - 2k_0\right)\right] . \quad (2.153)$$

Again, for easy reference, the general meanings of the various parameters may be summarized as follows:

t_0	$\equiv$	a fixed time corresponding to a particular scattering ellipse
k_0	$\equiv$	transmitted signal wavenumber
η_0	$\equiv$	intrinsic impedance of free space
$\Delta\ell$	$\equiv$	dipole length
I_0	$\equiv$	dipole current magnitude
$P_{\vec{K}}$'s	$\equiv$	the Fourier surfaces coefficients
$\vec{K}$'s	$\equiv$	the surface wave vectors (and $\vec{K}_{rs} = \vec{K}_{mn} + \vec{K}_{pq}$)
${}_E\Gamma$'s	$\equiv$	the electromagnetic coupling coefficients
ρ's	$\equiv$	various distance parameters associated with the scattering geometry
$\Delta\rho_s$	$\equiv$	radial "patch" width $\left(= \frac{cT_0}{2}\right)$
$\mathrm{Sa}(\cdot)$	$\equiv$	sampling function $\left(\equiv \sin\frac{(\cdot)}{(\cdot)}\right)$

Thus, to second order in scatter, the received field from a pulsed elementary vertical

dipole source may be written as

$$(E_{0_n}^+)(t_0) \approx (E_{0_n}^+)_1(t_0) + (E_{0_n}^+)_{2,F,1}(t_0) + (E_{0_n}^+)_{2,F,2}(t_0) + (E_{0_n}^+)_{2,B,1}(t_0) \qquad (2.154)$$

where all of the terms on the right are given in this summary. The similarities in structure of equations (2.150) to (2.153) are evident and will be utilized in the subsequent analysis.

2.3 General Chapter Summary

In this chapter, the basis has been laid for the analysis throughout the remainder of the work. Starting with a vertical dipole source, while maintaining a general current excitation, the received electric field components for the case of bistatic HF radar operation were derived. The surface was taken to be time invariant and representable by a two-dimensional Fourier series.

It was determined that there are four components of the electric field which appear to be worthy of more investigation. These components are (1) the field received from a single scatter which occurs remotely from both the transmitter and receiver - this is the so-called first-order component; (2) the second-order "patch" scatter in which a double scatter occurs far from both transmitter and receiver; (3) a second-order scatter in which one scatter occurs very near the transmitter and the second is at the remote point referred to in (1) and (2) ; and (4) a second-order scatter in which the first scatter occurs at the remote point and the second occurs very near the receiver.

It was found that for the first-order scatter and the remote scatters involved in each of components (3) and (4) of the second order, the surface wave vector associated with the surface component responsible for the scatter is perpendicular to the scattering ellipse. By "scattering ellipse" is meant that region of surface, corresponding to a fixed total path length from transmitter to remote patch to receiver, of which the transmitter and receiver are foci. Additionally, the surface wave vector was found

to bisect the angle between the transmitter and receiver as viewed from the distant scattering point.

Having carried out the preliminary analysis, attention was turned to the case of a pulsed sinusoidal excitation of the dipole. One of the important outcomes of this revealed that in the first-order interaction and components (3) and (4) of the second order, the surface wave vector on the remote patch associated with the scatter was not only perpendicular to the ellipse but had a magnitude of essentially $2k_0 \cos\phi_0$. That is, the surface wavenumber was twice the product of the transmitted radiation wavenumber (k_0) and the cosine of the bistatic angle, ϕ_0. It was found that for the "patch" scatter, the sum of the two surface wave vectors responsible for the scatter was perpendicular to the scattering ellipse and also had a magnitude of $2k_0 \cos\phi_0$. These results will prove to be of paramount importance as attention is turned, in the next chapter, to applying the analysis to a time varying surface, of which the ocean is an example.

Chapter 3

The Bistatic HF Radar Cross Sections of the Ocean Surface

3.1 Introduction

Having developed the expressions for the important received electric field from a pulsed dipole source, attention will now be focussed on applying these results to a time varying surface. The goal is to develop the bistatic HF radar cross sections of the ocean surface. The initial step in this endeavour is to characterize a random time varying surface as a three dimensional entity – two-dimensional in space and one in time. This will be accomplished by introducing a randomness into the Fourier coefficients of the surface along with an $e^{j\omega t}$ time dependency (ω now being the angular frequency of a *surface wave* component). The fact that a real surface is being considered will have certain ramifications for the statistical treatment which ensues.

Before recasting the field equations to account for the random surface, some relevant ocean features, such as wave-wave interaction, will also be addressed briefly. The assumptions on the surface characteristics which affect the way in which the analysis proceeds are delineated in Sections 3.2.1 and 3.2.2.

Upon determining the proper form of the field equations given the time varying random surface, power spectral densities for the received signal are calculated. Appealing to the bistatic geometry, the various portions of the cross section, normalized

to patch area, are then determined.

The important features of the cross sections are discussed in Section 3.6. These bistatic cross sections will be shown to contain the features of their monostatic counterparts as a special, less general, case (where such results are available). That the cross sections do indeed contain the monostatic results, which have been extensively verified, lends credibility to the new analysis. Also, unlike any previous investigations, the analysis here produces a cross section associated with a scatter at the receiving antenna, which intuitively, should be as important as scattering at the transmitter as developed by Srivastava [54] for monostatic operation.

3.2 Specification of a Real Random Time Varying Surface

3.2.1 General Properties of the Surface

It will be assumed that the surface is representable by a three dimensional Fourier series in (x, y, t), where x and y are spatial variables and t is a temporal quantity. Referencing equation (2.17), we reformulate it to include this time variation as

$$\xi(x,y,t) = \sum_{m,n,\ell} P_{m,n,\ell}\, e^{jN(mx+ny)} e^{j\ell Wt} \tag{3.1}$$

where $N = \dfrac{2\pi}{L}$, L being the fundamental wavelength of the surface and $W = \dfrac{2\pi}{T}$, T being the fundamental period. From the definitions of $\vec{K}_{mn}$ and the planar distance vector, $\vec{\rho}$, following equation (2.17), equation (3.1) may be written more compactly as

$$\xi(\vec{\rho},t) = \sum_{\vec{K},\omega} P_{\vec{K},\omega}\, e^{j\vec{K}\cdot\vec{\rho}}\, e^{j\omega t}\ , \tag{3.2}$$

it being understood that $\omega = \ell W$ and $\vec{K} \equiv \vec{K}_{mn}$. The Fourier coefficients, $P_{\vec{K},\omega}$, of the time varying surface are given by

$$P_{\vec{K},\omega} = \frac{1}{L^2 T} \int_{\frac{-L}{2}}^{\frac{L}{2}} \int_{\frac{-L}{2}}^{\frac{L}{2}} \int_{\frac{-T}{2}}^{\frac{T}{2}} \xi(\vec{\rho},t) e^{-j(\vec{K}\cdot\vec{\rho}+\omega t)}\, dx dy dt\ . \tag{3.3}$$

The random roughness of the surface is established by considering the $P_{\vec{K},\omega}$'s to be zero-mean Gaussian random variables. Noticing only the summation over ω in (3.2), it is obvious that replacing $P_{\vec{K}_{mn}}$ and/or $P_{\vec{K}_{pq}}$ in the earlier electric field equations (Section 2.2.5.4) with the form $\sum_{\omega} P_{\vec{K},\omega}\, e^{j\omega t}$ will produce the field components as they are received from the time varying random surface.

Since we shall be investigating a real, zero-mean surface, a requirement on the Fourier coefficients can readily be seen to be, in our notation, (Rice, [11])

$$P_{-\vec{K},-\omega} = P^{*}_{\vec{K},\omega} \tag{3.4}$$

where $*$ denotes the complex conjugate and, in particular, $P_{\vec{0},0} = 0$. Additionally, as is common in oceanographical treatments, (e.g. Phillips, [64]) the surface $\xi(\vec{\rho}, t)$, shall be taken to be homogeneous in space and stationary in time. This condition, by definition, means that the surface statistics are invariant to (1) the addition of a constant vector, $\Delta\vec{\rho}$, to all space points and (2) the addition of a constant time, τ, to all time points. It is easy to verify that the autocorrelation, R, of the surface function, denoted as

$$R(\Delta\vec{\rho}, \tau) = < \xi(\vec{\rho} + \Delta\vec{\rho}, t + \tau)\xi^{*}(\vec{\rho}, t) > \tag{3.5}$$

where $< \cdot >$ indicates an ensemble average, (see, for example, Papoulis [73], Chapter 9), is dependent only on the shifts $\Delta\vec{\rho}$ and τ as indicated.

As a consequence of this fact it may be readily shown that the different Fourier coefficients in equation (3.2) are *uncorrelated*. That is to say, their ensemble average is

$$< P_{\vec{K},\omega} P^{*}_{\vec{K}',\omega'} > = \begin{cases} < |P_{\vec{K},\omega}|^2 >, & \vec{K} = \vec{K}',\ \omega = \omega' \\ 0, & \text{otherwise} \end{cases} \tag{3.6}$$

where $|P_{\vec{K},\omega}|$ indicates the magnitude of the generally complex coefficient. For completeness, it may be noted that, since the $P_{\vec{K},\omega}$'s are Gaussian random variables, uncorrelatedness implies independence. These statements can be made in view of

the fact that while L and T are not strictly infinite, they may be treated as though they were as long as they are much greater than the dominant spatial and temporal periods of the surface.

Using equations (3.3) and (3.6), the definition of N and W, and the Fourier transform of $\xi(\vec{\rho}, t)$ it is straightforward to show that a power spectral density, $S(\vec{K}, \omega)$, for the surface may be defined according to

$$< P_{\vec{K},\omega} P^*_{\vec{K}',\omega'} >= \begin{cases} N^2 W S(\vec{K}, \omega)\,, & \vec{K} = \vec{K}',\ \omega = \omega' \\ 0\,, & \text{otherwise} \end{cases} \tag{3.7}$$

Thus, equation (3.7) presents the relationship between the ensemble average of the zero-mean Gaussian random Fourier surface coefficients and the power spectral density when the surface is real, stationary and homogeneous. This equation, or some variation of it, has been used by several investigators of radar operation in an ocean environment (i.e. Barrick [24], Srivastava [54], Walsh *et al.* [8]). A modification of it, discussed in Section 3.2.2 below, will be used extensively in applying the analysis of Chapter 2 to the ocean surface.

3.2.2 Relevant Ocean Surface Characteristics

Several excellent texts, including Phillips [64] and Kinsman [20], have detailed the physics of ocean surface waves. The rudiments of such presentations, as are pertinent to the work at hand, will be addressed briefly in this section.

The whole spectrum of ocean surface waves may contain components ranging in length from many kilometres to a few millimetres with such diverse restoring forces as the Coriolis "force" for the very long waves and surface tension for the very short ones. The waves which are the subject of this research are the so-called *gravity waves*, their primary generator being the wind and the chief restoring force being gravity. In general, it is this wave class which contributes most significantly to the overall surface wave energy. Their wavelengths vary from a few centimetres, these waves being termed ultragravity waves, to several hundreds of metres, the uppermost of

which belong to the infragravity region. Typically, an HF radar spectrum, depending on the operating frequency, may be significantly affected by waves ranging from a few metres to as much as a kilometre in length. Thus, our attention is focussed here on the properties of gravity waves as they are related to HF radar in a marine environment.

3.2.2.1 The Linear Dispersion Relationship for First-order Gravity Waves

Kinsman [20] (Chapters 2 and 3) provides an excellent overview of the hydrodynamics of water waves. The underlying assumptions that the supporting medium, i.e. the water, is incompressible, inviscid and irrotational are used to simplify the hydrodynamical equations. The latter include a statement of conservation of mass (referred to in the treatment of fluids as the *equation of continuity*), an *equation of motion* describing the various forcing function relationships, and expressions for the behaviour at the fluid boundaries – i.e. the *boundary conditions*. From equations of continuity and motion, a wave equation may be developed and solved subject to the boundary conditions. In general, the equations as a whole are nonlinear, but the first-order or linear approximation to their solution for the gravity wave region may be effected without undue difficulty.

It transpires that from the analysis for first-order (in slope) gravity waves, a relationship between the frequency and wavelength (λ_w) of individual wave components becomes apparent. This is commonly referred to as the *linear dispersion relation* for gravity waves and is written as

$$\omega = \sqrt{gK \tanh Kd} \tag{3.8}$$

where ω is the angular frequency of a water wave whose wave number is $K = \left(\frac{2\pi}{\lambda_w}\right)$ when it travels in water of depth, d. The quantity, g, is the gravitational acceleration and tanh is the hyperbolic tangent. Since the phase speed of the wave is $\left(\frac{\omega}{K}\right)$, equation (3.8) clearly indicates that waves of different lengths, λ_w, will have different speeds. When several such waves are travelling on the ocean surface, even though

they may be generated in the same region in the same time frame, the surface profile will change as the longer waves outrun the shorter. That is, water wave *dispersion* occurs and hence the name for equation (3.8).

If the water is of sufficient depth so that a component wave is not significantly affected by the ocean bottom, a "deep water" approximation to the dispersion relationship may be given as

$$\omega = \sqrt{gK} \; . \tag{3.9}$$

That is, for deep water, defined theoretically as $\frac{d}{\lambda_w} \geq \frac{1}{2}$ and, more realistically, in oceanographical measurements as $\frac{d}{\lambda_w} \geq \frac{1}{4}$ (see [20]), $\tanh(K\,d) \approx 1$ in equation (3.8). Since the deep water approximation is usually valid for HF radar operation, and since, if desired, (3.9) may be used in the final cross section results directly (see Section 3.5) there is no analytical advantage in implementing the general form for the dispersion relation at this stage. Therefore, throughout the remainder of this work, equation (3.9) will be employed as required.

Given the linear dispersion relationship, it will prove convenient to express the power spectral density spectrum for first-order gravity waves in generalized form as

$$S_1(\vec{K},\omega) = \frac{1}{2} \sum_{m=\pm 1} S_1(m\vec{K}) \delta \left(\omega + m\sqrt{gK} \right) \tag{3.10}$$

where $S_1(\vec{K},\omega)$ is the first-order component of $S(\vec{K},\omega)$ in equation (3.7) and $\delta(\cdot)$ is the Dirac delta function. This form of $S_1(\vec{K},\omega)$ will be very helpful in our examination of the positive and negative portions of the HF Doppler power spectral density of the e–m echo from the ocean found in Section 3.4 and has been similarly used by Barrick [21].

3.2.2.2 The Problem of Wave-Wave Interactions

As mentioned in the previous section, the hydrodynamic equations of the surface under consideration are nonlinear. Several investigators, among the most notable in

recent decades Hasselmann [59] and Weber and Barrick [74], have addressed this problem of nonlinearity in the ocean wave spectrum. Their approach has been, essentially to expand the velocity potential and surface displacement into a perturbational series for substitution into the governing equations. In Hasselmann's formulation, wave slope was used as the perturbational parameter. In addition to the velocity potential and displacement expansions, Weber and Barrick also included a perturbation on the angular frequency, ω, but, as they note, their results reduce to those of Hasselmann to second order.

Noting that equation (3.2) for the surface is really the sum of all orders of surface displacement, we may write it to second order as

$$\xi(\vec{\rho},t) = {}_1\xi(\vec{\rho},t) + {}_2\xi(\vec{\rho},t) \tag{3.11}$$

where ${}_1\xi(\vec{\rho},t)$ is the contribution from first-order surface features (i.e. first-order gravity waves here) and ${}_2\xi(\vec{\rho},t)$ accounts for second-order waves. This may be emphasized in the Fourier series sense by using ${}_1P_{\vec{K},\omega}$ and ${}_2P_{\vec{K},\omega}$ as the coefficients for first- and second-order components, respectively. Then, taking (3.11) and (3.2) together we write

$$\begin{aligned} {}_1\xi(\vec{\rho},t) &= \sum_{\vec{K},\omega} {}_1P_{\vec{K},\omega}\, e^{j\vec{K}\cdot\vec{\rho}} e^{j\omega t} \\ &\text{and} \\ {}_2\xi(\vec{\rho},t) &= \sum_{\vec{K},\omega} {}_2P_{\vec{K},\omega}\, e^{j\vec{K}\cdot\vec{\rho}} e^{j\omega t} \ . \end{aligned} \tag{3.12}$$

$\vec{K}$ in the second equation is the wave vector of a second-order gravity wave. The perturbational analyses lead to the very important and convenient result that ${}_2P_{\vec{K},\omega}$ may be written in terms of products of first-order waves and a *hydrodynamic coupling coefficient*, ${}_H\Gamma$, as

$${}_2P_{\vec{K},\omega} = \sum_{\substack{\vec{K}_1+\vec{K}_2=\vec{K} \\ \omega=\omega_1+\omega_2}} {}_H\Gamma\, {}_1P_{\vec{K}_1,\omega_1}\, {}_1P_{\vec{K}_2,\omega_2} \tag{3.13}$$

This form emphasizes that the wavenumber of the second-order gravity wave arises from the sum of the wavenumbers of the two first-order components, i.e.

$$\vec{K} = \vec{K}_1 + \vec{K}_2 \,. \tag{3.14}$$

However, as pointed out in both investigations referred to above, $\vec{K}$ does not follow the linear dispersion relationship (i.e. $\omega \neq \sqrt{gK}$). In keeping with the notational change between equations (3.1) and (3.2), it is understood that in (3.13) and (3.14), $\vec{K}_1 \equiv \vec{K}_{mn}$, $\vec{K}_2 \equiv \vec{K}_{pq}$, and the respective angular frequencies associated with $\vec{K}_{mn}$ and $\vec{K}_{pq}$ are ω_1 and ω_2.

The factor ${}_H\Gamma$ in equation (3.13) accounts for the manner in which the first-order waves couple to give the second-order wave – hence the name *hydrodynamic coupling coefficient.* Except for some notational variation, essentially equivalent forms of this quantity, useful for HF radar analyses, have been derived by Weber and Barrick [74] and Johnstone [33]. Also, Barrick and Lipa [27] have derived ${}_H\Gamma$ for the case of shallow water, and, more recently, Walsh *et al.* [8], using Hasselmann [59], have presented both second- and third-order coupling coefficients for shallow water. While the forms appear slightly differently in the last two works, it is easy to show that for deep water the two are identical. The Walsh *et al.* [8] form for second-order interactions will be used here and is given, in general, by

$${}_H\Gamma = \frac{-g^2}{\omega_1\omega_2}\left\{\frac{j(\omega_1+\omega_2)}{g\left[gK\tanh(Kd)-(\omega_1+\omega_2)^2\right]}D^{\omega_1,\omega_2}_{\vec{K}_1,\vec{K}_2} + E^{\omega_1,\omega_2}_{\vec{K}_1,\vec{K}_2}\right\} \tag{3.15}$$

where

$$\begin{aligned} D^{\omega_1,\omega_2}_{\vec{K}_1,\vec{K}_2} &= j(\omega_1+\omega_2)(K_1K_2\tanh(K_1d)\tanh(K_2d) - \vec{K}_1\cdot\vec{K}_2) \\ &\quad - \frac{j}{2}\left(\frac{\omega_1K_2^2}{\cosh^2(K_2d)} + \frac{\omega_2K_1^2}{\cosh^2(K_1d)}\right) \end{aligned} \tag{3.16}$$

and

$$E^{\omega_1,\omega_2}_{\vec{K}_1,\vec{K}_2} = \frac{1}{2g}\left\{(\vec{K}_1\cdot\vec{K}_2) - g^{-2}\omega_1\omega_2(\omega_1^2+\omega_2^2+\omega_1\omega_2)\right\} \,. \tag{3.17}$$

While it was not given explicitly in Walsh *et al.* [8], it is easily shown that, for the case of deep water,

$$_H\Gamma = \frac{1}{2}\left\{K_1 + K_2 + \frac{g}{\omega_1\omega_2}(K_1K_2 - \vec{K}_1 \cdot \vec{K}_2)\left(\frac{gK + (\omega_1+\omega_2)^2}{gK - (\omega_1+\omega_2)^2}\right)\right\} . \qquad (3.18)$$

It is worthy of note that $_H\Gamma$ contains no singularities. This is due to the fact that since the angular frequency, $\omega(=\omega_1+\omega_2)$, of the second-order wave is *not* related to the corresponding wavenumber, K, via the linear dispersion relationship, in the denominator of the last factor, gK is never equal to $(\omega_1+\omega_2)^2$.

This discussion concludes what is immediately necessary for analyzing scattering from a random time varying surface, namely the ocean, on which nonlinear interactions of the surface wave components occur.

3.3 The Electric Field Equations for Scatter from a Time Varying Surface

In Section 2.2.5.5, the received electric field components due to radiation from a vertical pulsed dipole source being scattered from a rough time invariant surface were summarized. Having specified a model for a time varying random surface in Section 3.2, we are now in a position to revisit these field equations and to cast them in a more general form which includes this time variation. In order to accomplish this without having to rederive a completely new set of equations from first principles, appropriate assumptions may be made. It has already been discussed in Section 2.2.5.1 that the time argument, t_0, in the electric field equations fixes an elliptical patch of ocean from which the scatter due to a particular pulse is received. It is legitimately assumed that the variation in the ocean surface profile is negligible during a single interrogation of such a patch. That is, even though the surface has a temporal variation, as indicated by the variable, t, in equation (3.2), the time necessary for a significant change in the ocean surface is much greater than that required to make a single measurement. Thus, the surface may be considered *time invariant* for each individual measurement.

The implications of these considerations are discussed further in Section 3.4.

1. The Time Varying First-order Field

Before addressing the first-order field expression, we note from equations (3.2), (3.11) and (3.12) that to second order the Fourier coefficients, $P_{\vec{K},\omega}$, may be written as

$$P_{\vec{K},\omega} = {}_1P_{\vec{K},\omega} + {}_2P_{\vec{K},\omega} \tag{3.19}$$

where the terms on the right are defined in the previous section. Now, equation (2.150) for the first-order field (i.e. for a single scatter), using the new Fourier surface coefficient notation, becomes

$$\begin{aligned}
\left(E^+_{0_n}\right)_1(t_0,t) \;\approx\; & \frac{-j\eta_0\Delta\ell I_0 k_0^2}{(2\pi)^{\frac{3}{2}}} \\
& \cdot \left\{ \left[\sum_{\vec{K},\omega} {}_1P_{\vec{K},\omega}\, e^{j\omega t}\sqrt{K\cos\phi_0}\, e^{j\frac{\vec{\rho}}{2}\cdot\vec{K}} e^{j\rho_{0_s}K\cos\phi_0}\Delta\rho_s \mathrm{Sa}\left[\frac{\Delta\rho_s}{2}\left(\frac{K}{\cos\phi_0}-2k_0\right)\right]\right] \right. \\
& + \left[\sum_{\vec{K}_1,\omega_1}\sum_{\vec{K}_2,\omega_2} {}_H\Gamma\, {}_1P_{\vec{K}_1,\omega_1}\, {}_1P_{\vec{K}_2,\omega_2}\, e^{j(\omega_1+\omega_2)t}\sqrt{K\cos\phi_0}\, e^{j\frac{\vec{\rho}}{2}\cdot\vec{K}} e^{j\rho_{0_s}K\cos\phi_0}\Delta\rho_s \right. \\
& \left. \left. \cdot\, \mathrm{Sa}\left[\frac{\Delta\rho_s}{2}\left(\frac{K}{\cos\phi_0}-2k_0\right)\right]\right]\right\} \cdot \left\{ \frac{F(\rho_{01},\omega_0)F(\rho_{02},\omega_0)e^{-j\frac{\pi}{4}}}{\sqrt{\rho_{0_s}\left[\rho_{0_s}^2-\left(\frac{\rho}{2}\right)^2\right]}} e^{jk_0\Delta\rho_s} \right\} .
\end{aligned} \tag{3.20}$$

Since equation (3.20) is really a prototype of all the other electric field components, it will now be discussed in detail. The first summation in (3.20) accounts for a single scatter of incident radiation from first-order surface waves. The double summation term indicates the field due to a single scatter from a second-order surface component. The decision to write the double summation notation of (3.13) as an explicit double sum in (3.20) (i.e. $\sum_{\substack{\vec{K}_1+\vec{K}_2=\vec{K}\\ \omega_1+\omega_2=\omega}} \equiv \sum_{K_1,\omega_1}\sum_{K_2,\omega_2}$) has been made with a view to being consistent with that which appears in equation (3.24) for double scatter from two first-order surface waves. It is important to realize, however, that for this term the constraints, $\vec{K}_1 + \vec{K}_2 = \vec{K}$ and $\omega_1 + \omega_2 = \omega$, still apply. To this point in the

analysis, the term "first-order field" must thus be interpreted to mean the component associated with a single electromagnetic scatter, but now it is seen that even this order of scatter contains a higher (i.e. second) order term as indicated by the double sum. Strictly, then, only the first summation in (3.20) will be referred to as the first-order received electromagnetic field, and the second double sum will be appropriately addressed in conjunction with the second-order terms arising from double scattering. To later differentiate between the causes for higher-order field components, the portion of (3.20) associated with the double sum will be referred to as the second-order *hydrodynamic* term.

To underscore the two distinct portions of equation (3.20), we write

$$\left(E_{0_n}^{+}\right)_1(t_0,t) = \left(E_{0_n}^{+}\right)_{11}(t_0,t) + \left(E_{0_n}^{+}\right)_{12}(t_0,t)$$

where

$$\begin{aligned}\left(E_{0_n}^{+}\right)_{11}(t_0,t) &= \frac{-j\eta_0\Delta\ell I_0 k_0^2}{(2\pi)^{\frac{3}{2}}}\cdot\sum_{\vec{K},\omega}{}_1P_{\vec{K},\omega}e^{j\omega t}\sqrt{K\cos\phi_0} \\ &\quad\cdot e^{j\frac{\vec{\rho}}{2}\cdot\vec{K}}e^{j\rho_{0_s}K\cos\phi_0}\Delta\rho_s\mathrm{Sa}\left[\frac{\Delta\rho_s}{2}\left(\frac{K}{\cos\phi_0}-2k_0\right)\right] \\ &\quad\cdot\frac{F(\rho_{01},\omega_0)F(\rho_{02},\omega_0)e^{-j\frac{\pi}{4}}}{\sqrt{\rho_{0_s}\left[\rho_{0_s}^2-\left(\frac{\rho}{2}\right)^2\right]}}e^{jk_0\Delta\rho_s}\end{aligned} \tag{3.21}$$

and

$$\begin{aligned}\left(E_{0_n}^{+}\right)_{12}(t_0,t) &= \frac{-j\eta_0\Delta\ell I_0 k_0^2}{(2\pi)^{\frac{3}{2}}}\sum_{\vec{K}_1,\omega_1}\sum_{\vec{K}_2,\omega_2}{}_H\Gamma\,{}_1P_{\vec{K}_1,\omega_1}\,{}_1P_{\vec{K}_2,\omega_2}e^{j(\omega_1+\omega_2)t}\sqrt{K\cos\phi_0} \\ &\quad\cdot e^{j\frac{\vec{\rho}}{2}\cdot\vec{K}}e^{j\rho_{0_s}K\cos\phi_0}\Delta\rho_s\mathrm{Sa}\left[\frac{\Delta\rho_s}{2}\left(\frac{K}{\cos\phi_0}-2k_0\right)\right] \\ &\quad\cdot\frac{F(\rho_{01},\omega_0)F(\rho_{02},\omega_0)e^{-j\frac{\pi}{4}}}{\sqrt{\rho_{0_s}\left[\rho_{0_s}^2-\left(\frac{\rho}{2}\right)^2\right]}}e^{jk_0\Delta\rho_s}\,.\end{aligned} \tag{3.22}$$

The wave vector $\vec{K}$ in equation (3.21) is that of a first-order surface wave and is exactly the same as $\vec{K}_{mn}$ $(= mN\hat{x} + nN\hat{y})$ of equation (2.150). Meanwhile, $\vec{K}$ in equation

(3.22) is associated with a second-order surface wave and is given by (3.14). Furthermore, $\vec{K}_1$ and $\vec{K}_2$ are completely analogous to $\vec{K}_{mn}$ and $\vec{K}_{pq}$ of equation (2.151). For reference, the following are summarized:

$$\begin{aligned} \vec{K}_1 &= \vec{K}_{mn} = mN\hat{x} + nN\hat{y} \\ \vec{K}_2 &= \vec{K}_{pq} = pN\hat{x} + qN\hat{y} \\ \vec{K} &= (m+p)N\hat{x} + (n+q)N\hat{y} = K_x\hat{x} + K_y\hat{y} \\ \text{and} \quad \theta_{\vec{K}} &= \tan^{-1}\left(\frac{K_y}{K_x}\right) , \end{aligned} \tag{3.23}$$

$\theta_{\vec{K}}$ being the direction of $\vec{K}$. Again, it is to be emphasized that in equations (3.20)–(3.22), t_0 fixes a particular scattering ellipse, while time, t, indicates that the received field is fluctuating because the scattering surface is time varying.

2. The Time Varying Second-order Patch Scatter Field

Attention is now focussed on equation (2.151) which describes the received field when two scatters occur at essentially the same position remote from both the transmitter and receiver. Introducing the time variation as for equation (3.20) above, we may immediately write

$$\begin{aligned} \left(E^+_{0_n}\right)_{2,F,1}(t_0,t) \approx & \frac{-j\eta_0\Delta\ell I_0 k_0^2}{(2\pi)^{\frac{3}{2}}} \sum_{\vec{K}_1,\omega_1} \sum_{\vec{K}_2,\omega_2} {}_E\Gamma_P \, {}_1P_{\vec{K}_1,\omega_1} \, {}_1P_{\vec{K}_2,\omega_2} \, e^{j(\omega_1+\omega_2)t} \sqrt{K\cos\phi_0} \\ & \cdot e^{j\frac{\vec{\rho}}{2}\cdot\vec{K}} e^{j\rho_{0s12,1}K\cos\phi_0} \Delta\rho_s \mathrm{Sa}\left[\frac{\Delta\rho_s}{2}\left(\frac{K}{\cos\phi_0} - 2k_0\right)\right] \\ & \cdot \frac{F(\rho_{02},\omega_0)F(\rho_{020},\omega_0)e^{-j\frac{\pi}{4}}}{\sqrt{\rho_{0s12,1}\left[\rho^2_{0s12,1} - \left(\frac{\rho}{2}\right)^2\right]}} e^{jk_0\Delta\rho_s} . \end{aligned} \tag{3.24}$$

It may be recalled from Section 2.2.5.2 that in (2.151), $\vec{K}_{rs} = \vec{K}_{mn} + \vec{K}_{pq}$. Thus, using the notation of (3.23) above, $\vec{K}$, $\vec{K}_1$ and $\vec{K}_2$ have been substituted for $\vec{K}_{rs}$, $\vec{K}_{mn}$ and $\vec{K}_{pq}$, respectively, in equation (3.24).

Since this analysis is being carried only to second order, equation (3.24) represents a double scatter from first-order surface waves. The ${}_2P_{\vec{K},\omega}$ surface coefficients are not included here as (1) a double scatter from the second-order waves associated with

them would constitute an overall fourth-order effect (in a way completely comparable to a single scatter from a second-order wave producing a second-order effect in equation (3.22)) or (2) a scatter from a first-order wave followed by another from a second-order wave, or vice versa, would lead to third-order effects.

Next, it is appropriate to compare the second-order received field arising because of the hydrodynamic coupling of first-order surface waves in equation (3.22) with that resulting from double scattering from two distinct (i.e. uncoupled, first order) waves on the time varying surface in equation (3.24). In order to do this, it is useful to consider Figures 2.3 and 2.6 for the first- and second-order patch scatter geometry, respectively. Replacing the various ρ's in these diagrams with their representative ρ_{0j}'s as discussed for a pulsed source in Sections 2.2.5.1 and 2.2.5.2, it becomes immediately evident that ρ_{01}, ρ_{02} and ρ_{0s} for the first order corresponds exactly to ρ_{02} ρ_{020} and $\rho_{0s12,1}$ for the second-order component. This leads to the important conclusion that the only difference between (3.22), which represents a single scatter from a wave arising due to hydrodynamic coupling, and (3.24), which describes the effect of two scatters from first-order surface waves, lies in the coupling coefficients, ${}_H\Gamma$ and ${}_E\Gamma_P$. Therefore, equations (3.22) and (3.24) may be grouped to give the total second-order effect arising due to scattering occurring remotely from both the transmitter and receiver. The result, labelled as $\left(E_{0_n}^+\right)_{2P}$ to indicate the association with the remote "patch", is

$$\begin{aligned}
\left(E_{0_n}^+\right)_{2P}(t_0,t) &\approx \left(E_{0_n}^+\right)_{12}(t_0,t) + \left(E_{0_n}^+\right)_{2,F,1}(t_0,t) \\
&\approx \frac{-j\eta_0\Delta\ell I_0 k_0^2}{(2\pi)^{\frac{3}{2}}} \sum_{\vec{K}_1,\omega_1}\sum_{\vec{K}_2,\omega_2} \Gamma_P\, {}_1P_{\vec{K}_1,\omega_1}\, {}_1P_{\vec{K}_2,\omega_2}\, e^{j(\omega_1+\omega_2)t}\sqrt{K\cos\phi_0} \\
&\quad \cdot e^{j\frac{\vec{\rho}}{2}\cdot\vec{K}} e^{j\rho_{0s}K\cos\phi_0} e^{jk_0\Delta\rho_s} \\
&\quad \cdot \frac{F(\rho_{01},\omega_0)F(\rho_{02},\omega_0)e^{-j\frac{\pi}{4}}}{\sqrt{\rho_{0s}\left[\rho_{0s}^2-\left(\frac{\rho}{2}\right)^2\right]}}\Delta\rho_s \mathrm{Sa}\left[\frac{\Delta\rho_s}{2}\left(\frac{K}{\cos\phi_0}-2k_0\right)\right] \quad (3.25)
\end{aligned}$$

where

$$\Gamma_P = {}_H\Gamma + {}_E\Gamma_P \ . \tag{3.26}$$

Here, the ρ_{02} and ρ_{020} of equation (2.152) have been replaced by ρ_{01} and ρ_{02}, respectively, where the latter retain the same meaning as the former – i.e. they are the distances from the transmitter to the remote patch and from the remote patch to the receiver, respectively. This change is made so that similar features of the various field components may be readily observed. The former notation of Chapter 2 was useful in determining the various stationary points, but having done so the only distances for which $F(\cdot) \neq 1$ are those being discussed here. In terms of this notation,

$$\rho_{0s} = \frac{\rho_{01} + \rho_{02}}{2} \ . \tag{3.27}$$

The relative importance of the hydrodynamic and electromagnetic effects incorporated into equation (3.25) are addressed in Section 3.6.6 where the second-order patch cross section is discussed.

3. The Time Varying Second-order Field – One Scatter at the Transmitter

Implementing exactly the same ideas as were used to write equations (3.22), (3.24), and (3.25), equation (2.152) representing a single scatter at the transmitter followed by another on the remote scattering patch may be written to second order in time varying form as

$$\begin{aligned}\left(E^+_{0_n}\right)_{2T}(t_0,t) \approx\ & \frac{-j\eta_0\Delta\ell I_0 k_0^2}{(2\pi)^{\frac{3}{2}}} \sum_{\vec{K}_1,\omega_1} \sum_{\vec{K}_2,\omega_2} {}_E\Gamma_T\, {}_1P_{\vec{K}_1,\omega_1}\, {}_1P_{\vec{K}_2,\omega_2}\, e^{j(\omega_1+\omega_2)t} \sqrt{K_2\cos\phi_0} \\ & \cdot e^{j\frac{\vec{\rho}}{2}\cdot\vec{K}_2} e^{j\rho_{0s}K_2\cos\phi_0} e^{jk_0\Delta\rho_s} \\ & \cdot \frac{F(\rho_{01},\omega_0)F(\rho_{02},\omega_0)e^{-j\frac{\pi}{4}}}{\sqrt{\rho_{0s}\left[\rho_{0s}^2 - \left(\frac{\rho}{2}\right)^2\right]}} \Delta\rho_s \mathrm{Sa}\left[\frac{\Delta\rho_s}{2}\left(\frac{K_2}{\cos\phi_0} - 2k_0\right)\right] \ . \end{aligned} \tag{3.28}$$

Here, the subscript on $E^+_{0_n}$ has been changed to $_{2T}$ from $_{2,F,2}$ to emphasize that one of the scatters involved in this second-order component occurs at the transmitter, T.

The $\vec{K}_1$ and $\vec{K}_2$ wave vectors are associated with surface waves at the transmitter and remote patch, respectively. The ρ subscripts have been adjusted as discussed following equation (3.26).

Again, as the analysis is to second order, the ${}_2P_{\vec{K},\omega}$ coefficients are not included here. As before, if this double scatter did indeed involve a second-order surface wave, it would lead to a third- or higher- order received field.

4. The Time Varying Second-order Field – One Scatter at the Receiver

The final portion of the electric field which must be adjusted to include the time varying surface features is found in equation (2.153). Taking the $\vec{K}_1$ surface wave vector to be associated with a scatter on the remote patch and the $\vec{K}_2$ vector to be associated with a scatter near the receiver, equation (2.153) may be written in time varying form as

$$\begin{aligned}\left(E_{0_n}^{+}\right)_{2R}(t_0,t) \approx\ & \frac{-j\eta_0\Delta\ell I_0 k_0^2}{(2\pi)^{\frac{3}{2}}} \sum_{\vec{K}_1,\omega_1} \sum_{\vec{K}_2,\omega_2} E\Gamma_R\, {}_1P_{\vec{K}_1,\omega_1}\, {}_1P_{\vec{K}_2,\omega_2}\, e^{j(\omega_1+\omega_2)t} \sqrt{K_1\cos\phi_0} \\ & \cdot e^{j\frac{\vec{\rho}}{2}\cdot\vec{K}_1} e^{j\vec{\rho}\cdot\vec{K}_2} e^{j\rho_{0s}K_1\cos\phi_0} e^{jk_0\Delta\rho_s} \\ & \cdot \frac{F(\rho_{01},\omega_0)F(\rho_{02},\omega_0)}{\sqrt{\rho_{0s}\left[\rho_{0s}^2-\left(\frac{\rho}{2}\right)^2\right]}} \Delta\rho_s \mathrm{Sa}\left[\frac{\Delta\rho_s}{2}\left(\frac{K_1}{\cos\phi_0}-2k_0\right)\right] . \end{aligned} \tag{3.29}$$

Once more, ρ_{0s}, ρ_{01}, and ρ_{02} must be interpreted as previously in this section. Also, to emphasize second-order scattering involving a scatter near the *receiver*, the subscript on $E_{0_n}^{+}$ has been changed from $_{2,F,2}$ to $_{2R}$. For reasons discussed following equation (3.28), the ${}_2P_{\vec{K},\omega}$ coefficients are not considered here. The $\vec{K}_1$ and $\vec{K}_2$ are the wave vectors of two first-order surface wave components.

By virtue of equations (3.21), (3.25), (3.28), and (3.29), the total received electric field, $\left(E_{0_n}^{+}\right)(t_0,t)$, to second order, including hydrodynamic effects, is given by

$$\left(E_{0_n}^{+}\right)(t_0,t) \approx \left(E_{0_n}^{+}\right)_{11}(t_0,t) + \left(E_{0_n}^{+}\right)_{2P}(t_0,t) + \left(E_{0_n}^{+}\right)_{2T}(t_0,t) + \left(E_{0_n}^{+}\right)_{2R}(t_0,t) . \tag{3.30}$$

To this point in the analysis, $\left(E_{0_n}^{+}\right)(t_0, t)$ represents the vertical electric field component from a pulsed dipole source as it is received bistatically after scattering from a random time varying slightly rough surface. The condition of "slightly rough" was imposed and discussed in Section 2.2 and entered the analysis following equation (2.12). The nature of the time variation mentioned briefly at the start of this section is used in the following section in order to develop a power spectral density for the received electric field.

3.4 The Power Spectral Density of the Received Electric Field

3.4.1 The General Approach

It has already been mentioned that even though the surface has a temporal variation as indicated by the time variable, t, in equation (3.30), the time necessary for a significant change in the ocean surface is much greater than that required for a single measurement. For this reason, the surface is considered to be "fixed" during a single measurement. Then, as time progresses, a series of measurements, corresponding to a train of transmitted pulses, for a region corresponding to a particular t_0 may be developed. As there will, in general, be a change in the ocean surface from one measurement to the next, the time variable, t, will account for the generation of a Doppler spectrum when the appropriate statistical analysis is carried out on equation (3.30).

We have made the assumption that the ocean surface is statistically stationary and that its first-order Fourier coefficients (i.e. ${}_1P_{\vec{K},\omega}$) are normally distributed. As a result, the received electric field from such a surface is stationary and, as verified experimentally by Barrick and Snider [75], the first- and second-order received field is indeed described by a Gaussian process. Bearing in mind that the power spectral density of a random process may be determined as the Fourier transform of its auto-

correlation, we seek the latter for the received electric field. Given stationarity, then at a particular, t_0, (i.e. for a given elliptical scattering patch), the autocorrelation will be a function only of the time shift, τ. It is convenient to express the autocorrelation, $\mathcal{R}$, of the field in (3.30) in normalized form as

$$\mathcal{R}(\tau) = \frac{A_r}{2\eta_0} < E^+_{0_n}(t_0, t+\tau) E^{+^*}_{0_n}(t_0, t) > \tag{3.31}$$

where $*$ denotes the complex conjugate, $< \cdot >$ indicates the statistical or ensemble average, η_0 is the intrinsic impedance of free space and A_r is referred to as the effective free space aperture of the receiving antenna. A_r is given by Collin [63], for example, as

$$A_r = \frac{\lambda_0^2}{4\pi} G_r \tag{3.32}$$

where λ_0 is the free space wavelength of the transmitted signal and G_r is the free space gain of the receiving antenna. The $\frac{1}{2}$ in equation (3.31) indicates that rms values of the E-field are being used. It is easy to see that the normalization of $\mathcal{R}(\tau)$ by $\frac{A_r}{2\eta_0}$ conveniently makes $\mathcal{R}(0)$ the average power, P_r^0, received from the particular patch of ocean for which $E^+_{0_n}(t_0, t)$ is being considered, i.e.

$$\mathcal{R}(0) = P_r^0 = \frac{A_r}{2\eta_0} < |E^+_{0_n}(t_0, t)|^2 > \ . \tag{3.33}$$

It should also be noted that at this point in the analysis, t_0 has been suppressed in the argument of $\mathcal{R}(\cdot)$. Still, of course, the autocorrelation and, subsequently, the power spectral density derived from it will strictly correspond to a definite region of the scattering surface as dictated by the parameter t_0. Now, applying equation (3.31) to (3.30) clearly gives formally

$$\begin{aligned} \mathcal{R}(\tau) \ = \ & \frac{A_r}{2\eta_0} < \Big[(E^+_{0_n})_{11}(t_0, t+\tau) + (E^+_{0_n})_{2P}(t_0, t+\tau) \\ & + (E^+_{0_n})_{2T}(t_0, t+\tau) + (E^+_{0_n})_{2R}(t_0, t+\tau) \Big] \\ \cdot & \Big[(E^+_{0_n})^*_{11}(t_0, t) + (E^+_{0_n})^*_{2P}(t_0, t) + (E^+_{0_n})^*_{2T}(t_0, t) + (E^+_{0_n})^*_{2R}(t_0, t) \Big] > \ . \end{aligned} \tag{3.34}$$

Since the average of the sums is the same as the sum of the averages, equation (3.34) may be written as the sum of sixteen terms i.e.

$$\begin{aligned}
\mathcal{R}(\tau) \;=\; & \frac{A_r}{2\eta_0}\Big\{ < (E^+_{0_n})_{11}(t_0, t+\tau)(E^+_{0_n})^*_{11}(t_0, t) > \\
& + < (E^+_{0_n})_{11}(t_0, t+\tau)(E^+_{0_n})^*_{2P}(t_0, t) > + \ldots \\
& + < (E^+_{0_n})_{2P}(t_0, t+\tau)(E^+_{0_n})^*_{11}(t_0, t) > + < (E^+_{0_n})_{2P}(t_0, t+\tau)(E^+_{0_n})^*_{2P}(t_0, t) > + \ldots \\
& + < (E^+_{0_n})_{2T}(t_0, t+\tau)(E^+_{0_n})^*_{11}(t_0, t) > + < (E^+_{0_n})_{2T}(t_0, t+\tau)(E^+_{0_n})^*_{2P}(t_0, t) > + \ldots \\
& + < (E^+_{0_n})_{2R}(t_0, t+\tau)(E^+_{0_n})^*_{11}(t_0, t) > + < (E^+_{0_n})_{2R}(t_0, t+\tau)(E^+_{0_n})^*_{2P}(t_0, t) > + \ldots \Big\}
\end{aligned} \tag{3.35}$$

where ... represent the remaining obvious averages. It is clear that the overall autocorrelation, $\mathcal{R}(\tau)$, contains both auto- and cross-correlations of the individual E-field components. It transpires (see Appendix B.1) that products containing $(E^+_{0_n})_{11}(t_0, t+\tau)$ and a second-order field component will have as factors an odd number of the first-order Fourier surface coefficients, $({}_1P_{K,\omega})$, which have been stated to be zero-mean Gaussian random variables. Thomas [76], for example, has shown that the ensemble average of a product of odd numbers of such variables is zero. This immediately eliminates six terms from (3.35). Another useful result from Thomas is that for four random variables, V_1, V_2, V_3, V_4, which are Gaussian and zero-mean,

$$< V_1V_2V_3V_4 > = < V_1V_2 >< V_3V_4 > + < V_1V_3 >< V_2V_4 > + < V_1V_4 >< V_2V_3 > \; . \tag{3.36}$$

Using the ideas in this section, the various portions of the power spectral density may now be determined via the Fourier transform of $\mathcal{R}(\tau)$ in (3.35). Since this is a linear operation, the transform of the sum of the components of (3.35) is the same as the sum of the individual transforms. Thus, the concept of determining a power spectral density, $\mathcal{P}(\omega_d)$, using (3.35) is, in principle, straightforward and may be simply stated as

$$\mathcal{P}(\omega_d) = \mathcal{F}[\mathcal{R}(\tau)] \; . \tag{3.37}$$

$\mathcal{P}(\omega_d)$ is the *Doppler* power spectral density for reasons discussed in the first paragraph of this section. The quantity, ω_d, which is the transform variable for τ is the angular Doppler frequency (i.e. $\omega_d = 2\pi f_d$, f_d being the Doppler frequency in hertz).

In the following section, equation (3.37) is examined in detail for each component appearing in equation (3.35).

3.4.2 The Doppler Power Density Spectrum

Since the calculation of all components of the Doppler power spectral density from equation (3.35) follows essentially the same path, we shall detail only the first-order case in the body of the thesis. The other components are derived in Appendix B with the results appearing in Section 3.4.2.2. Certain characteristics of the surface and the scattering constraints used in simplifying some of the more complicated second-order effects are also discussed in the appendix.

3.4.2.1 The First-order Doppler Spectrum

The first term of equation (3.35), by virtue of equation (3.21), is the autocorrelation of the first-order field as received after a single scatter from first-order ocean waves. Thus, we define

$$\mathcal{R}_{11}(\tau) = \frac{A_r}{2\eta_0} < \left(E^+_{0_n}\right)_{11}(t_0, t+\tau)\left(E^+_{0_n}\right)^*_{11}(t_0, t) > \tag{3.38}$$

from which, using equation (3.37), a Doppler power spectral density, $\mathcal{P}_{11}(\omega_d)$, may be found. Applying this expression to equation (3.21) gives

$$\begin{aligned}\mathcal{R}_{11}(\tau) \;=\; & \frac{A_r}{2\eta_0}\left\{\frac{\eta_0^2 k_0^4 \left|I_0 \Delta\ell\right|^2 (\Delta\rho_s)^2}{(2\pi)^3 \rho_{0s}\left[\rho_{0s}^2 - \left(\frac{\rho}{2}\right)^2\right]} \sum_{\vec{K},\omega}\sum_{\vec{K}',\omega'}\left\{< {}_1P_{\vec{K},\omega}\,{}_1P^*_{\vec{K}',\omega'} > \right.\right. \\ & \cdot e^{j\omega(t+\tau)}e^{-j\omega' t}\sqrt{K\cos\phi_0}\sqrt{K'\cos\phi_0'} \\ & \cdot F(\rho_{01},\omega_0)F(\rho_{02},\omega_0)F^*(\rho_{01}',\omega_0)F^*(\rho_{02}',\omega_0) \\ & \left.\left. \cdot \;\mathrm{Sa}\left[\frac{\Delta\rho_s}{2}\left(\frac{K}{\cos\phi_0} - 2k_0\right)\right]\mathrm{Sa}\left[\frac{\Delta\rho_s}{2}\left(\frac{K'}{\cos\phi_0'} - 2k_0\right)\right]\right\}\right\}\end{aligned} \tag{3.39}$$

where $< \cdot >$ and the summation have been interchanged and, as indicated, the only randomness is found in the first-order Fourier surface coefficients, ${}_1P_{\vec{K},\omega}$ and ${}_1P_{\vec{K}',\omega'}$. From the stipulations on the ${}_1P$'s for a real surface given in equation (3.4) and then using the first-order portion of (3.7) for the *surface* power spectral density, equation (3.39) becomes

$$\begin{aligned}\mathcal{R}_{11}(\tau) &= \frac{A_r}{2\eta_0}\left\{\frac{\eta_0^2 k_0^4 \left|I_0 \Delta\ell\right|^2 (\Delta\rho_s)^2}{(2\pi)^3 \rho_{0s}\left[\rho_{0s}^2 - \left(\frac{\varrho}{2}\right)^2\right]} N^2 W \sum_{\vec{K},\omega}\left\{S_1(\vec{K},\omega)\right.\right. \\ &\quad \cdot e^{j\omega\tau}(K\cos\phi_0)|F(\rho_{01},\omega_0)F(\rho_{02},\omega_0)|^2 \\ &\quad \left.\left. \cdot\ \mathrm{Sa}^2\left[\frac{\Delta\rho_s}{2}\left(\frac{K}{\cos\phi_0} - 2k_0\right)\right]\right\}\right\} . \end{aligned} \tag{3.40}$$

If it is agreed to let the fundamental wavelength, L, and period, T, of the surface become very large so that $N\left(=\frac{2\pi}{L}\right)$ and $W\left(=\frac{2\pi}{T}\right)$ become very small, then

$$N^2 \to d^2\vec{K} \text{ and } W \to d\omega \text{ where } d^2\vec{K} \equiv dK_x dK_y \equiv K dK d\theta_{\vec{K}} .$$

The summation in (3.40) may now be written as an integral. Using this idea, which has been similarly used by Rice [11] and others, along with the formulation of $S_1(\vec{K},\omega)$ found in equation (3.10), equation (3.40) becomes

$$\begin{aligned}\mathcal{R}_{11}(\tau) &= \frac{A_r}{2\eta_0}\left\{\frac{1}{2}\cdot\frac{\eta_0^2 k_0^4 \left|I_0 \Delta\ell\right|^2 (\Delta\rho_s)^2}{(2\pi)^3 \rho_{0s}\left[\rho_{0s}^2 - \left(\frac{\varrho}{2}\right)^2\right]}\right\} \sum_{m=\pm 1}\int_{-\infty}^{\infty}\int_{-\pi}^{\pi}\int_0^{\infty} S_1(m\vec{K}) \\ &\quad \cdot \delta\left(\omega + m\sqrt{gK}\right) e^{j\omega\tau} K^2 \cos\phi_0 |F(\rho_{01},\omega_0)F(\rho_{02},\omega_0)|^2 \\ &\quad \cdot \mathrm{Sa}^2\left[\frac{\Delta\rho_s}{2}\left(\frac{K}{\cos\phi_0} - 2k_0\right)\right] dK d\theta_{\vec{K}} d\omega . \end{aligned} \tag{3.41}$$

The ω integral in (3.41) yields immediately to the δ-function so that

$$\begin{aligned}\mathcal{R}_{11}(\tau) &= \frac{A_r}{2\eta_0}\left\{\frac{1}{2}\cdot\frac{\eta_0^2 k_0^4 \left|I_0 \Delta\ell\right|^2 (\Delta\rho_s)^2}{(2\pi)^3 \rho_{0s}\left[\rho_{0s}^2 - \left(\frac{\varrho}{2}\right)^2\right]}\right\} \sum_{m=\pm 1}\int_{-\pi}^{\pi}\int_0^{\infty} S_1(m\vec{K}) \\ &\quad \cdot e^{j\omega\tau} K^2 \cos\phi_0 |F(\rho_{01},\omega_0)F(\rho_{02},\omega_0)|^2 \\ &\quad \cdot \mathrm{Sa}^2\left[\frac{\Delta\rho_s}{2}\left(\frac{K}{\cos\phi_0} - 2k_0\right)\right] dK d\theta_{\vec{K}} , \end{aligned} \tag{3.42}$$

it now being understood that

$$\omega = -m\sqrt{gK} \tag{3.43}$$

Now, from Lathi [77], Chapter 1, for example, we have

$$\mathcal{F}\left[e^{j\omega\tau}\right] = \mathcal{F}\left[e^{j(-m\sqrt{gK})\tau}\right] = 2\pi\delta\left(\omega_d + m\sqrt{gK}\right)$$

where as mentioned previously, ω_d is the transform variable for τ. Therefore, from equations (3.37) and (3.42) we may write the Doppler power spectral density, $\mathcal{P}_{11}(\omega_d)$, for the first-order electric field as

$$\begin{aligned}\mathcal{P}_{11}(\omega_d) = \mathcal{F}\left[\mathcal{R}_{11}(\tau)\right] \;=\; & \frac{A_r\eta_0 k_0^4 \left|I_0\Delta\ell\right|^2 (\Delta\rho_s)^2}{4\,(2\pi)^2\,\rho_{0s}\left[\rho_{0s}^2 - \left(\frac{\rho}{2}\right)^2\right]} \sum_{m=\pm 1}\int_{-\pi}^{\pi}\int_{0}^{\infty} S_1(m\vec{K}) \\ & \cdot K^2\cos\phi_0 |F(\rho_{01},\omega_0)F(\rho_{02},\omega_0)|^2 \mathrm{Sa}^2\left[\frac{\Delta\rho_s}{2}\left(\frac{K}{\cos\phi_0} - 2k_0\right)\right] \\ & \cdot \delta\left(\omega_d + m\sqrt{gK}\right) dK\, d\theta_{\vec{K}}\ . \end{aligned} \tag{3.44}$$

Noting, then, that the Dirac delta function constrains K to

$$K = \frac{\omega_d^2}{g}\ , \tag{3.45}$$

so that

$$dK = \frac{2\omega_d d\omega_d}{g} = \frac{2\sqrt{K}}{\sqrt{g}}\, d\omega_d\ ,$$

(3.44) may be written as

$$\begin{aligned}\mathcal{P}_{11}(\omega_d) \;=\; & \frac{A_r\eta_0 k_0^4 \left|I_0\Delta\ell\right|^2 (\Delta\rho_s)^2}{2\sqrt{g}\,(2\pi)^2\,\rho_{0s}\left[\rho_{0s}^2 - \left(\frac{\rho}{2}\right)^2\right]} \\ & \cdot \sum_{m=\pm 1}\int_{-\pi}^{\pi} S_1(m\vec{K}) K^{\frac{5}{2}} \cos\phi_0 |F(\rho_{01},\omega_0)F(\rho_{02},\omega_0)|^2 \\ & \cdot \mathrm{Sa}^2\left[\frac{\Delta\rho_s}{2}\left(\frac{K}{\cos\phi_0} - 2k_0\right)\right] d\theta_{\vec{K}}\ . \end{aligned} \tag{3.46}$$

At the moment, equation (3.46) is the power spectral density of the first-order field being received from an elliptical surface region of width $\Delta\rho_s(=\frac{c\tau_0}{2})$. The locus of this region is specified via the parameter ρ_{0s} of equation (3.27). In Section 3.5 it is shown how this may be used to determine a first-order radar cross section of an elementary area or patch of the ocean surface.

3.4.2.2 The Higher-order Correlations and Doppler Spectra

All of the results given in this section are deduced in Appendix B.

1. The Cross Correlations and Spectra of the First- and Second-order Fields

On the basis of equation (3.35), there are six correlations involving the first- and second-order fields. They may be labelled

$$\begin{aligned}
\mathcal{R}_{11,2P}(\tau) &= <(E^+_{0_n})_{11}(t_0,t+\tau)(E^+_{0_n})^*_{2P}(t_0,t)> \\
\mathcal{R}_{11,2T}(\tau) &= <(E^+_{0_n})_{11}(t_0,t+\tau)(E^+_{0_n})^*_{2T}(t_0,t)> \\
&\vdots \quad \vdots \quad \vdots \\
\mathcal{R}_{2R,11}(\tau) &= <(E^+_{0_n})_{2R}(t_0,t+\tau)(E^+_{0_n})^*_{11}(t_0,t)> \ . \qquad (3.47)
\end{aligned}$$

It transpires from Appendix B.1 that

$$\mathcal{R}_{11,2P}(\tau) = \mathcal{R}_{11,2T}(\tau) = \mathcal{R}_{11,2R}(\tau) = \mathcal{R}_{2P,11}(\tau) = \mathcal{R}_{2T,11}(\tau) = \mathcal{R}_{2R,11}(\tau) = 0 \ . \qquad (3.48)$$

Therefore, the corresponding power spectral densities are also zero, i.e.

$$\mathcal{P}_{11,2P}(\omega_d) = \cdots = \mathcal{P}_{2R,11}(\omega_d) = 0 \ . \qquad (3.49)$$

2. The Patch Scatter Autocorrelation and Doppler Spectrum

The autocorrelation of the field involving both electromagnetic and hydrodynamic second-order effects, associated strictly with the remote scattering region is, from (3.35),

$$\mathcal{R}_{2P}(\tau) = \frac{A_r}{2\eta_0} <(E^+_{0_n})_{2P}(t_0,t+\tau)(E^+_{0_n})^*_{2P}(t_0,t)> \ . \qquad (3.50)$$

In Appendix B.2, this is shown to be

$$\begin{aligned}
\mathcal{R}_{2P}(\tau) &= \frac{A_r}{2\eta_0}\left\{\frac{\eta_0^2 k_0^4 \left|I_0 \Delta\ell\right|^2 (\Delta\rho_s)^2}{2(2\pi)^3 \rho_{0s}\left[\rho_{0s}^2 - \left(\frac{\varrho}{2}\right)^2\right]}\right\} \sum_{m_1=\pm1}\sum_{m_2=\pm1}\int_{-\pi}^{\pi}\int_0^{\infty}\int_{-\pi}^{\pi}\int_0^{\infty} \\
&\cdot \left\{S_1(m_1\vec{K}_1)S_1(m_2\vec{K}_2)e^{j\omega\tau}\left|{}_s\Gamma_P\right|^2 (K^2\cos\phi_0)\right. \\
&\cdot \left|F(\rho_{01},\omega_0)F(\rho_{02},\omega_0)\right|^2 \\
&\cdot \left.\mathrm{Sa}^2\left[\frac{\Delta\rho_s}{2}\left(\frac{K}{\cos\phi_0} - 2k_0\right)\right]K_1\right\} dK_1 d\theta_1 dK d\theta_{\vec{K}} \ . \qquad (3.51)
\end{aligned}$$

Of course the very important stipulations that (1) $\vec{K} = \vec{K}_1 + \vec{K}_2$ and (2) $\omega = \omega_1 + \omega_2$ still apply. It is understood that the wave vectors $\vec{K}_1$ and $\vec{K}_2$ are associated with the surface components which are essentially coincident on the remote scattering patch. It has already been discussed that $\vec{K}$ lies along the outward ellipse normal at all scattering positions, but $\vec{K}_1$ and $\vec{K}_2$ have no such restrictions. Also ${}_s\Gamma_P$ is a symmetric form of the coupling coefficient as described by equations (B.10) and (B.11). It has the feature that ${}_s\Gamma_P(\vec{K}_1, \vec{K}_2) = {}_s\Gamma_P(\vec{K}_2, \vec{K}_1)$. The resemblance of equation (3.51) to (3.42) for the first-order return is striking and the power spectral density, $\mathcal{P}_{2P}(\omega_d)$, may be written analogously to $\mathcal{P}_{11}(\omega_d)$ in (3.44) as

$$\begin{aligned}\mathcal{P}_{2P}(\omega_d) \;=\; & \frac{A_r \eta_0 k_0^4 \left|I_0 \Delta\ell\right|^2 (\Delta\rho_s)^2}{4(2\pi)^2 \rho_{0s}\left[\rho_{0s}^2 - \left(\frac{\rho}{2}\right)^2\right]} \sum_{m_1=\pm 1} \sum_{m_2=\pm 1} \int_{-\pi}^{\pi}\int_{0}^{\infty}\int_{-\pi}^{\pi}\int_{0}^{\infty} \\ & \cdot \left\{S_1(m_1\vec{K}_1) S_1(m_2\vec{K}_2) \left|{}_s\Gamma_P\right|^2 (K^2 \cos\phi_0)\right. \\ & \cdot \left|F(\rho_{01}, \omega_0) F(\rho_{02}, \omega_0)\right|^2 \mathrm{Sa}^2\left[\frac{\Delta\rho_s}{2}\left(\frac{K}{\cos\phi_0} - 2k_0\right)\right] \\ & \left. \cdot \delta\left(\omega_d + m_1\sqrt{gK_1} + m_2\sqrt{gK_2}\right) K_1\right\} dK_1 d\theta_{\vec{K}_1} dK d\theta_{\vec{K}} \,. \end{aligned} \tag{3.52}$$

Thus, the Doppler power spectral density for an essentially coincident double scattering on the (elliptical) surface patch is seen to depend on the product of the spectra, $S_1(\cdot)S_1(\cdot\cdot)$, of the surface components involved in the process. Several other important features of (3.52) are addressed in Section 3.6 where the associated cross section of an elementary region or "patch" of surface is discussed.

3. The Autocorrelation and Doppler Spectrum when One of Two Scatters Occurs Near the Transmitting Antenna

In the general autocorrelation expression of equation (3.35), there is a component which addresses the correlation of $(E_{0_n}^+)_{2T}$ with itself. This may be written as

$$\mathcal{R}_{2T}(\tau) = \frac{A_r}{2\eta_0} < (E_{0_n}^+)_{2T}(t_0, t+\tau)(E_{0_n}^+)_{2T}^*(t_0, t) > \,. \tag{3.53}$$

It is shown in detail in Appendix B.3 that while (3.53) consists of three separate averages, only one of these contributes significantly to the corresponding Doppler

power spectral density, $\mathcal{P}_{2T}(\omega_d)$. This important piece is given by equation (B.21) so that we may write

$$\begin{aligned}
\mathcal{R}_{2T}(\tau) &\approx \mathcal{R}_{2T,2}(\tau) \\
&= \frac{A_r}{2\eta_0}\left\{\frac{\eta_0^2 k_0^4 \left|I_0 \Delta\ell\right|^2 (\Delta\rho_s)^2}{4(2\pi)^3 \rho_{0s}\left[\rho_{0s}^2 - \left(\frac{\varrho}{2}\right)^2\right]}\right\} \sum_{m_1=\pm 1}\sum_{m_2=\pm 1}\int_{-\pi}^{\pi}\int_0^{\infty}\int_{-\pi}^{\pi}\int_0^{\infty} \\
&\quad \left\{S_1(m_1\vec{K}_1)S_1(m_2\vec{K}_2)\left|_E\Gamma_T\right|^2 e^{j(\omega_1+\omega_2)\tau}(K_2^2\cos\phi_0)\right. \\
&\quad \cdot \left|F(\rho_{01},\omega_0)F(\rho_{02},\omega_0)\right|^2 \\
&\quad \left.\cdot \,\mathrm{Sa}^2\left[\frac{\Delta\rho_s}{2}\left(\frac{K_2}{\cos\phi_0} - 2k_0\right)\right]K_1\right\} dK_1 d\theta_{\vec{K}_1} dK_2 d\theta_{\vec{K}_2}\,. \qquad (3.54)
\end{aligned}$$

Here, as usual, the wave vector $\vec{K}_1$ is associated with a scatter near the transmitter and $\vec{K}_2$ with a scatter on the remote elliptical scattering patch. It may be recalled that $\vec{K}_2$ is along the outward normal at all positions on the scattering ellipse. No such condition is placed explicitly on $\vec{K}_1$, although it will be seen in Section 3.6.4 that there is a direction of maximum contribution for this vector. As indicated by the limits on the $\theta_{\vec{K}_2}$ integral, $\mathcal{R}_{2T}(\tau)$ involves, for a particular ρ_{0s}, scattering from a complete elliptical surface patch.

Fourier transforming (3.54) gives the Doppler power spectral density for this component (see equations (B.22) and (B.32)) as

$$\begin{aligned}
\mathcal{P}_{2T}(\omega_d) &\approx \mathcal{P}_{2T,2}(\omega_d) \\
&= \frac{A_r \eta_0 k_0^4 \left|I_0 \Delta\ell\right|^2 (\Delta\rho_s)^2}{8(2\pi)^2 \rho_{0s}\left[\rho_{0s}^2 - \left(\frac{\varrho}{2}\right)^2\right]} \sum_{m_1=\pm 1}\sum_{m_2=\pm 1}\int_{-\pi}^{\pi}\int_0^{\infty}\int_{-\pi}^{\pi}\int_0^{\infty} \\
&\quad \cdot \left\{S_1(m_1\vec{K}_1)S_1(m_2\vec{K}_2)\left|_E\Gamma_T\right|^2 (K_2^2\cos\phi_0)\right. \\
&\quad \cdot \left|F(\rho_{01},\omega_0)F(\rho_{02},\omega_0)\right|^2 \cdot \mathrm{Sa}^2\left[\frac{\Delta\rho_s}{2}\left(\frac{K_2}{\cos\phi_0} - 2k_0\right)\right] \\
&\quad \left.\cdot\, \delta\left(\omega_d + m_1\sqrt{gK_1} + m_2\sqrt{gK_2}\right)K_1\right\} dK_1 d\theta_{\vec{K}_1} dK_2 d\theta_{\vec{K}_2}\,. \qquad (3.55)
\end{aligned}$$

Equation (3.55) represents the contribution to the Doppler power spectral density due to a single scatter at the transmitting antenna followed by another on a remote

elliptical patch whose locus is determined by the ρ_{0s} parameter (see equation (3.27)) and whose width is determined by $\Delta\rho_s$. While in its present form (3.55) determines the power density component, $\mathcal{P}_{2T}(\omega_d)$, for a full elliptical region of fixed ρ_{0s} and $\Delta\rho_s$, it is used in Section 3.5 to determine part of the cross section of an *elemental* area of the scattering surface.

4. The Auto Correlation and Doppler Spectrum when One of Two Scatters Occurs Near the Receiving Antenna

Equation (3.35) also contains a correlation of $(E^+_{0_n})_{2R}$ with itself. This component, in which the second of two scatters occurs near the receiving antenna, is given by

$$\mathcal{R}_{2R}(\tau) = \frac{A_r}{2\eta_0} < (E^+_{0_n})_{2R}(t_0, t+\tau)(E^+_{0_n})^*_{2R}(t_0, t) > \ . \tag{3.56}$$

It is argued in Appendix B.4, that of the three averages arising from (3.56) only one is important, that being given by equation (B.35). Therefore,

$$\begin{aligned}
\mathcal{R}_{2R}(\tau) \ &\approx \ \mathcal{R}_{2R,2}(\tau) \\
&= \ \frac{A_r}{2\eta_0}\left\{\frac{\eta_0^2 k_0^4 \left|I_0 \Delta\ell\right|^2 (\Delta\rho_s)^2}{4\,(2\pi)^3\,\rho_{0s}\left[\rho_{0s}^2 - \left(\frac{\rho}{2}\right)^2\right]}\right\} \sum_{m_1=\pm 1}\sum_{m_2=\pm 1}\int_{-\pi}^{\pi}\int_{0}^{\infty}\int_{-\pi}^{\pi}\int_{0}^{\infty} \\
&\quad \cdot \left\{S_1(m_1\vec{K}_1)S_1(m_2\vec{K}_2)\left|_E\Gamma_R\right|^2 e^{j(\omega_1+\omega_2)\tau}\right. \\
&\quad \cdot (K_1^2\cos\phi_0)\left|F(\rho_{01},\omega_0)F(\rho_{02},\omega_0)\right|^2 \\
&\quad \cdot \left.\mathrm{Sa}^2\left[\frac{\Delta\rho_s}{2}\left(\frac{K_1}{\cos\phi_0} - 2k_0\right)\right] K_2\right\} dK_1 d\theta_{\vec{K}_1} dK_2 d\theta_{\vec{K}_2} \ .
\end{aligned} \tag{3.57}$$

Correspondingly, the Doppler power spectral density component is, from equations (B.35) and (B.41),

$$\begin{aligned}
\mathcal{P}_{2R}(\omega_d) \ &\approx \ \mathcal{P}_{2R,2}(\omega_d) \\
&= \ \frac{A_r \eta_0 k_0^4 \left|I_0 \Delta\ell\right|^2 (\Delta\rho_s)^2}{8\,(2\pi)^2\,\rho_{0s}\left[\rho_{0s}^2 - \left(\frac{\rho}{2}\right)^2\right]} \sum_{m_1=\pm 1}\sum_{m_2=\pm 1}\int_{-\pi}^{\pi}\int_{0}^{\infty}\int_{-\pi}^{\pi}\int_{0}^{\infty} \\
&\quad \cdot \left\{S_1(m_1\vec{K}_1)S_1(m_2\vec{K}_2)\left|_E\Gamma_R\right|^2\right. \\
&\quad \cdot (K_1^2\cos\phi_0)\left|F(\rho_{01},\omega_0)F(\rho_{02},\omega_0)\right|^2 \cdot \mathrm{Sa}^2\left[\frac{\Delta\rho_s}{2}\left(\frac{K_1}{\cos\phi_0} - 2k_0\right)\right] \\
&\quad \cdot \left.\delta\left(\omega_d + m_1\sqrt{gK_1} + m_2\sqrt{gK_2}\right) K_2\right\} dK_1 d\theta_{\vec{K}_1} dK_2 d\theta_{\vec{K}_2} \ .
\end{aligned} \tag{3.58}$$

Equation (3.58) is the Doppler power spectral density due to a single scatter on the remote elliptical surface patch followed by another near the receiver. The similarities between it and equation (3.55), which involves a scatter at the transmitter, are striking. This time, however, the direction of $\vec{K}_1$ must be along the outward normal to the scattering ellipse while $\vec{K}_2$ is, in general, not so constrained. In Section 3.5 equation (3.58) is used to determine a corresponding part of the cross section of an elemental surface area.

5. The Remaining Terms of Equation (3.35)

Besides the previous components (equations (3.47), (3.50), (3.53) and (3.56)) of equation (3.35), there remain the following: (1) the cross correlation of $(E^+_{0_n})_{2P}$ and $(E^+_{0_n})_{2T}$, (2) the cross correlation of $(E^+_{0_n})_{2P}$ and $(E^+_{0_n})_{2R}$ and, finally, (3) the cross correlation of $(E^+_{0_n})_{2T}$ and $(E^+_{0_n})_{2R}$.

It is shown in Appendices (B.5) and (B.6) that these terms may be neglected because they are either identically zero, or are small in comparison to those already discussed. This means that, essentially, the two second-order components, arising when one of two scatters occurs near the transmitter or near the receiver, are uncorrelated with the field from a double scatter on a remote surface region and are also uncorrelated with each other. Furthermore, it may be deduced from the derivations of Appendix B that the only non-negligible results occur when the factors arising from the ensemble average of the Fourier surface coefficients (i.e. expressions of the form $< {}_1P_{\vec{K}_i,\omega_i}\, {}_1P_{\vec{K}_j,\omega_j} >$) contain wave vectors which are coincident on the scattering surface. That is, $\vec{K}_i$ and $\vec{K}_j$ are in the same scattering neighbourhood. This, in turn, means that the condition of a fully homogeneous surface could have been relaxed to one of *local* homogeneity. Thus, the same results would have been derived had we assumed surface homogeneity near the transmitter, a (perhaps) different yet homogeneous surface near the receiver, and again similarly so for the remote region responsible for double scatter. In practice, the size of these regions would be dic-

tated by the beam widths of the transmitter and receiver and the pulse width of the transmitted radiation.

On the basis of the results in this section, the overall bistatic Doppler power spectral density, $\mathcal{P}(\omega_d)$, may be written simply as

$$\mathcal{P}(\omega_d) \approx \mathcal{P}_{11}(\omega_d) + \mathcal{P}_{2P}(\omega_d) + \mathcal{P}_{2T}(\omega_d) + \mathcal{P}_{2R}(\omega_d) \tag{3.59}$$

where the four terms on the right are given by equations (3.46), (3.52), (3.55) and (3.58), respectively. These expressions will next be used to determine first and second orders of the bistatic HF radar cross section of an elementary patch of the ocean surface.

3.5 Derivation of the HF Bistatic Cross Sections of the Ocean Surface

Because the only surviving terms of the Doppler power spectral density for electromagnetic returns from the ocean surface are those given in equation (3.59), the general development of all portions of the HF bistatic cross section conveniently follows closely that of the first order given by Walsh and Dawe [9]. To facilitate the presentation of the second-order effects, which contain significantly more intricacies than the first order, their approach is presented here. Additionally, for readability, some of the detail omitted in that work is included here.

3.5.1 An Elementary Scattering Region

It is convenient to develop an expression for an elementary area, dA, of the scattering surface in terms of the bistatic scattering geometry. To this end, the following discussion may be referenced to Figure 3.1. From elementary analytic geometry (eg., Trim [78]) it is known that for a smooth curve in the $x-y$ plane, the curvature, $\mathcal{K}$, defined by

$$\mathcal{K}(s) = \left| \frac{d\hat{T}}{ds} \right|$$

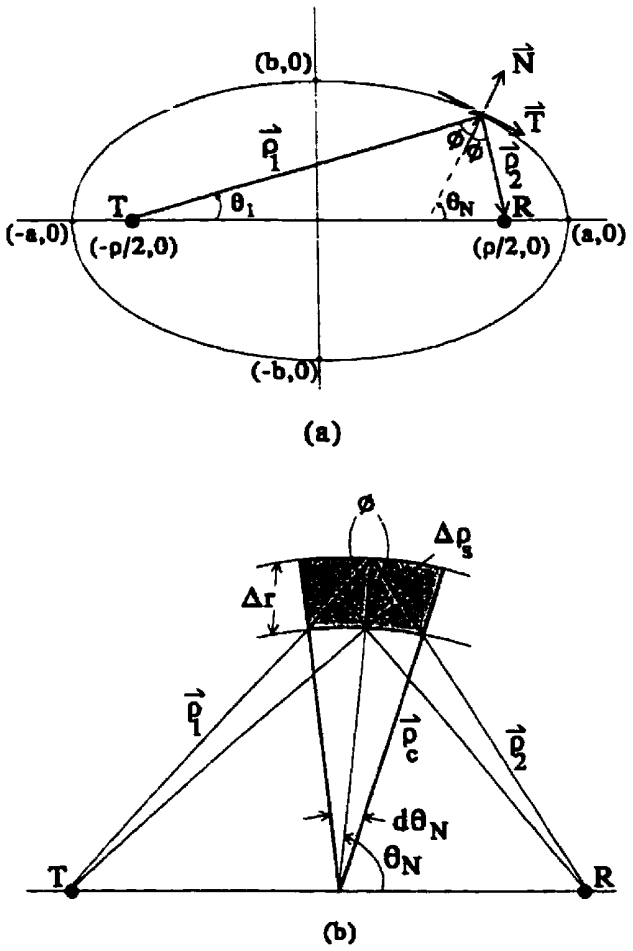

Figure 3.1: (a) The general geometry of the first-order scatter and (b) an expanded view showing an elemental scattering region.

where $\hat{T}$ is the unit tangent at a particular point and s is the distance along the curve, reduces to

$$\mathcal{K}(x) = \frac{\left|\frac{d^2y}{dx^2}\right|}{\left[1+\left(\frac{dy}{dx}\right)^2\right]^{\frac{3}{2}}} . \tag{3.60}$$

Applying this to the ellipse of Figure 3.1a gives

$$\mathcal{K} = \frac{ab}{(\rho_1\rho_2)^{\frac{3}{2}}} . \tag{3.61}$$

Given that the radius of curvature, ρ_c, in Figure 3.1b is the reciprocal of $\mathcal{K}$, it is easily concluded from the relationships between the major and minor axes and foci,

$\left(\frac{\pm\rho}{2},0\right)$, of the ellipse that

$$\begin{aligned}\rho_c &= \frac{(\rho_1\rho_2)^{\frac{3}{2}}}{ab} \\ &= \frac{(\rho_1\rho_2)^{\frac{3}{2}}}{\rho_s\sqrt{\rho_s^2-\left(\frac{\rho}{2}\right)^2}}\,. \end{aligned} \tag{3.62}$$

From Section 2.2.5.1, the representative values ρ_{01}, ρ_{02}, ρ_{03} and ϕ_0 for the various distance parameters and bistatic angle may be introduced here. It is easily shown that

$$\cos\phi_0 = \sqrt{\frac{\rho_{0s}^2-\left(\frac{\rho}{2}\right)^2}{\rho_{01}\rho_{02}}}$$

so that using equation (3.62), the shaded region of Figure 3.1b may be approximated as

$$\begin{aligned} dA \approx \rho_c d\theta_N \Delta r &= \rho_c d\theta_N \frac{\Delta\rho_s}{\cos\phi_0} \\ &= \frac{(\rho_{01}\rho_{02})^{\frac{3}{2}}}{\rho_{0s}\sqrt{\rho_{0s}^2-\left(\frac{\rho}{2}\right)^2}}\cdot\frac{1}{\cos\phi_0}d\theta_N\Delta\rho_s \\ &= \frac{(\rho_{01}\rho_{02})^2}{\rho_{0s}\left[\rho_{0s}^2-\left(\frac{\rho}{2}\right)^2\right]}d\theta_N\Delta\rho_s\,. \end{aligned} \tag{3.63}$$

The remarks regarding the distance parameters of (3.63) which are found throughout Section 3.3 permit the above form to be used for all parts of the first- and second-order fields. It is important to recall and summarize the significance of the angle, θ_N :

1. for the first order and the "double patch scatter" second order, θ_N is precisely the direction, $\theta_{\vec{K}}$, of the wave vector $\vec{K}$ appearing in equations (3.46) and (3.52) for the respective power spectral densities;

2. for the second order involving one scatter near the transmitter and another on the remote patch, θ_N is the direction, $\theta_{\vec{K}_2}$, of the remote $\vec{K}_2$ wave vector as discussed in conjunction with equations (3.54) and (3.55); and

3. for the remaining second-order effect in which one scatter occurs on the remote patch before another near the receiver, θ_N corresponds to $\theta_{\vec{K}_1}$ which is the direction of the patch wave vector, $\vec{K}_1$, as found in equation (3.58).

In consequence of equation (3.63) and the nature of θ_N, each of the Doppler power spectral densities referenced above may be observed to contain a form

$$\frac{\Delta\rho_s \, d\theta_N}{\rho_{0s}\left[\rho_{0s}^2 - \left(\frac{\rho}{2}\right)^2\right]} = \frac{dA}{(\rho_{01}\rho_{02})^2} \, . \tag{3.64}$$

This fact conveniently permits all components of the bistatic HF cross section per unit area to be developed in a single manner.

3.5.2 The Bistatic Radar Range Equation

Before implementing (3.64) in the relevant Doppler power spectral density equations, it is useful to consider the standard bistatic radar range equation. Using received power spectral density, $\mathcal{P}(\omega_d)$, in place of received power and cross section per unit area ($\sigma(\omega_d)$) instead of strictly cross section, the standard bistatic radar range equation (see, for example, Barton [79], Chapter 1) may be appropriately modified in incremental form as

$$\frac{d\mathcal{P}(\omega_d)}{dA} = \frac{\lambda_0^2 P_t G_t G_r \left|F(\rho_{01},\omega_0)F(\rho_{02},\omega_0)\right|^2}{(4\pi)^3\rho_{01}^2\rho_{02}^2}\sigma(\omega_d) \, . \tag{3.65}$$

The new parameters, P_t and G_t, are the transmitted power and free space gain of the transmitting antenna, respectively. For the elementary vertical dipole source assumed in this analysis, the product P_tG_t may be ascertained from any elementary electromagnetics reference (eg. Collin [63]) as

$$P_tG_t = \frac{\eta_0 k_0^2 \left|I_0\Delta\ell\right|^2}{8\pi} \, . \tag{3.66}$$

Also, from equation (3.32), the relationship between the receiver gain, G_r, and the freespace wavelength, λ_0, of the transmitted signal may be written as

$$G_r = \frac{4\pi A_r}{\lambda_0^2} \tag{3.67}$$

where it will be recalled that A_r is the effective free space aperture of the receiving antenna. Combining equations (3.65), (3.66) and (3.67),

$$\frac{d\mathcal{P}(\omega_d)}{dA} = \frac{A_r \eta_0 k_0^2 \left|I_0 \Delta\ell\right|^2 \left|F(\rho_{01},\omega_0)F(\rho_{02},\omega_0)\right|^2}{16(2\pi)^3 \left(\rho_{01}\rho_{02}\right)^2}\sigma(\omega_d) \; . \tag{3.68}$$

Given equation (3.59) for the various parts of $\mathcal{P}(\omega_d)$, it is understood here that

$$\sigma(\omega_d) = \sigma_{11}(\omega_d) + \sigma_{2P}(\omega_d) + \sigma_{2T}(\omega_d) + \sigma_{2R}(\omega_d) \tag{3.69}$$

where $\sigma_j(\cdot)$ is the component of the cross section corresponding to the appropriate portion of the Doppler power spectral density.

3.5.3 The Cross Sections

Having developed the power spectral densities and presented the radar range equation for bistatic radar operation, the analysis leads logically to expressions for the radar cross section components presented in this section. Discussion of the extensive detail associated with the numerical calculation of the resulting expressions is reserved for Section 3.6. In that section, important features of the results are also interpreted.

1. The First-order Bistatic Cross Section, $\sigma_{11}(\omega_d)$

Given equation (3.64) and the fact that $d\theta_N \equiv d\theta_{\vec{K}}$, equation (3.46) for the first-order power spectral density expression may be written as

$$\begin{aligned}\frac{d\mathcal{P}_{11}(\omega_d)}{dA} &= \frac{A_r \eta_0 k_0^4 \left|I_0 \Delta\ell\right|^2 (\Delta\rho_s)}{2\sqrt{g}\,(2\pi)^2 (\rho_{01}\rho_{02})^2} \\ &\quad \cdot \sum_{m=\pm 1} S_1(m\vec{K}) K^{\frac{5}{2}} \cos\phi_0 \left|F(\rho_{01},\omega_0)F(\rho_{02},\omega_0)\right|^2 \\ &\quad \cdot \mathrm{Sa}^2\left[\frac{\Delta\rho_s}{2}\left(\frac{K}{\cos\phi_0} - 2k_0\right)\right] \\ &= \frac{A_r \eta_0 k_0^2 \left|I_0 \Delta\ell\right|^2 \left|F(\rho_{01},\omega_0)F(\rho_{02},\omega_0)\right|^2}{16(2\pi)^3 \left(\rho_{01}\rho_{02}\right)^2}\sigma_{11}(\omega_d) \; . \end{aligned} \tag{3.70}$$

where the last equality follows from the radar range equation, (3.68). It immediately follows that

$$\sigma_{11}(\omega_d) = 2^4 \pi k_0^2 \sum_{m=\pm 1} S_1(m\vec{K}) \frac{K^{\frac{5}{2}} \cos\phi_0}{\sqrt{g}} \, \Delta\rho_s \mathrm{Sa}^2\left[\frac{\Delta\rho_s}{2}\left(\frac{K}{\cos\phi_0} - 2k_0\right)\right] \; . \tag{3.71}$$

This is the first-order component of the HF bistatic radar cross section of the ocean surface normalized to the scattering area. Its unit is $\frac{\mathrm{m}^2}{\mathrm{m}^2}$ (radian/second)$^{-1}$ or simply (radian/second)$^{-1}$. It should be observed, for the purpose of distinguishing $\sigma_{11}(\omega_d)$ from the higher-order cross section components, that $\vec{K}$ is associated with a first-order ocean wave in the sense discussed in Sections 3.2.2.1 and 3.2.2.2. It may be pointed out that here, as in all other components of the cross section, $\sigma(\cdot)$ is technically a function not only of ω_d, but also of ϕ_0. In keeping with the literature, it has been chosen to suppress this explicit dependence on the bistatic angle.

2. The Second-order Cross Section – Double Scatter on Remote Patch

Again, in equation (3.52), which characterizes the Doppler power spectral density when two scatters occur near each other on the remote elliptical scattering patch, $d\theta_{\vec{K}} \equiv d\theta_N$. Using equation (3.64), equations (3.52) and (3.68) lead to

$$\begin{aligned}\frac{d\mathcal{P}_{2P}(\omega_d)}{dA} &= \frac{A_r \eta_0 k_0^4 \left|I_0 \Delta\ell\right|^2 \Delta\rho_s}{4\left(2\pi\right)^2 \left(\rho_{01}\rho_{02}\right)^2} \sum_{m_1=\pm1} \sum_{m_2=\pm1} \int_0^{\infty} \int_{-\pi}^{\pi} \int_0^{\infty} \left\{ S_1(m_1\vec{K}_1) S_1(m_2\vec{K}_2) \right. \\ &\quad \cdot \left|{}_s\Gamma_P\right|^2 \left(K^2 \cos\phi_0\right) \left|F(\rho_{01},\omega_0) F(\rho_{02},\omega_0)\right|^2 \mathrm{Sa}^2 \left[\frac{\Delta\rho_s}{2}\left(\frac{K}{\cos\phi_0} - 2k_0\right)\right] \\ &\quad \left. \cdot\, \delta\left(\omega_d + m_1\sqrt{gK_1} + m_2\sqrt{gK_2}\right)\right\} dK_1 d\theta_{\vec{K}_1} dK \\ &= \frac{A_r \eta_0 k_0^2 \left|I_0 \Delta\ell\right|^2 \left|F(\rho_{01},\omega_0) F(\rho_{02},\omega_0)\right|^2}{16(2\pi)^3 (\rho_{01}\rho_{02})^2}\, \sigma_{2P}(\omega_d) \,. \end{aligned} \tag{3.72}$$

From this, the second-order "patch scatter" cross section becomes

$$\begin{aligned}\sigma_{2P}(\omega_d) &= 2^3 \pi k_0^2 \Delta\rho_s \sum_{m_1=\pm1} \sum_{m_2=\pm1} \int_0^{\infty} \int_{-\pi}^{\pi} \int_0^{\infty} \left\{ S_1(m_1\vec{K}_1) S_1(m_2\vec{K}_2) \right. \\ &\quad \cdot \left|{}_s\Gamma_P\right|^2 K^2 \cos\phi_0 \mathrm{Sa}^2 \left[\frac{\Delta\rho_s}{2}\left(\frac{K}{\cos\phi_0} - 2k_0\right)\right] \\ &\quad \left. \cdot\, \delta\left(\omega_d + m_1\sqrt{gK_1} + m_2\sqrt{gK_2}\right) K_1 \right\} dK_1 d\theta_{\vec{K}_1} dK \,. \end{aligned} \tag{3.73}$$

Here, $\vec{K}_1$ and $\vec{K}_2$ are the wave vectors of first-order ocean waves while $\vec{K}$ their sum (i.e. $\vec{K}_2 = \vec{K} - \vec{K}_1$). In Section 3.6.3, $\sigma_{2P}(\omega_d)$ is further simplified and discussed in detail.

3. The Second-order Cross Section – One of Two Scatters Near the Transmitter

Comparison of equation (3.55) for the Doppler power spectral density involving a

scatter at the transmitter followed by another, remote scatter, with equation (3.52) for double patch scatter reveals only the following differences: (1) in (3.55) there is an extra factor of 2 in the denominator preceding the summations, (2) the coupling coefficient, ${}_s\Gamma_P$, in (3.52) is replaced by ${}_E\Gamma_T$ in (3.55), and (3) the $\vec{K}$ wave vector of (3.52) is replaced by $\vec{K}_2$ in (3.55) so that $dKd\theta_{\vec{K}}$ is replaced by $dK_2d\theta_{\vec{K}_2}$. Here, $\vec{K}_2$ is along the outward normal to the scattering patch just as $\vec{K}$ was in (3.52).

Considering the minor differences in detail, but not in form, a cross section component, $\sigma_{2T}(\omega_d)$, may be written from (3.55) analogously to σ_{2P} of equation (3.73) as

$$\begin{aligned}\sigma_{2T}(\omega_d) &= 2^2\pi k_0^2\Delta\rho_s \sum_{m_1=\pm1}\sum_{m_2=\pm1}\int_0^\infty\int_{-\pi}^{\pi}\int_0^\infty \Big\{S_1(m_1\vec{K}_1)S_1(m_2\vec{K}_2) \\ &\quad\cdot |{}_E\Gamma_T|^2\, K_2^2\cos\phi_0 \mathrm{Sa}^2\left[\frac{\Delta\rho_s}{2}\left(\frac{K_2}{\cos\phi_0}-2k_0\right)\right] \\ &\quad\cdot \delta\left(\omega_d + m_1\sqrt{gK_1} + m_2\sqrt{gK_2}\right)K_1\Big\}\, dK_1d\theta_{\vec{K}_1}dK_2\,. \qquad (3.74)\end{aligned}$$

As is discussed further in Section 3.6.4, the major contribution from wavenumber K_2 in (3.74) is, due to the sampling function, confined to a small range about $2k_0\cos\phi_0$. This, in conjunction with the forms of the coupling coefficients, is what provides the major difference between equations (3.74) and (3.73). In Section 3.6, where the cross section components are calculated, it is seen that for most of the ω_d range of interest, $\sigma_{2P}(\omega_d) >> \sigma_{2T}(\omega_d)$. Points where this inequality is not valid are examined closely.

4. The Second-order Cross Section - One of Two Scatters Near the Receiver

From equations (3.58), (3.64) and (3.68), the Doppler cross section per unit area, $\sigma_{2R}(\omega_d)$, associated with a scatter at the remote patch followed by another near the receiver may be written similarly as equation (3.74) with K_1 and K_2 being interchanged and ${}_E\Gamma_T$ being replaced by ${}_E\Gamma_R$. The result is

$$\begin{aligned}\sigma_{2R}(\omega_d) &= 2^2\pi k_0^2\Delta\rho_s \sum_{m_1=\pm1}\sum_{m_2=\pm1}\int_0^\infty\int_{-\pi}^{\pi}\int_0^\infty \Big\{S_1(m_1\vec{K}_1)S_1(m_2\vec{K}_2) \\ &\quad\cdot |{}_E\Gamma_R|^2\, K_1^2\cos\phi_0 \mathrm{Sa}^2\left[\frac{\Delta\rho_s}{2}\left(\frac{K_1}{\cos\phi_0}-2k_0\right)\right] \\ &\quad\cdot \delta\left(\omega_d + m_1\sqrt{gK_1} + m_2\sqrt{gK_2}\right)K_2\Big\}\, dK_2d\theta_{\vec{K}_2}dK_1\,. \qquad (3.75)\end{aligned}$$

Here, it may be seen that it is now the K_1 wavenumber which is constrained to lie near $2k_0 \cos\phi_0$. For an homogeneous ocean surface, it is not surprising that $\sigma_{2T}(\omega_d)$ and $\sigma_{2R}(\omega_d)$ are of comparable magnitudes. Small differences are noted in Section 3.6.

3.6 Calculation and Interpretation of the Cross Sections

3.6.1 The Choice of an Ocean Spectral Model

To this point in the analysis, we have discussed only those features of the ocean surface that were immediately necessary to develop the electric field equations for scattering from a time varying surface. However, to carry out calculations of the cross sections derived in Section 3.5, it is necessary to specify a *particular* model for the ocean surface.

Tucker [1] (Chapters 2, 7 and 10), discusses from an engineering perspective, several of the ocean spectral models in current use. All of these consist of a product of an omnidirectional spectrum, $S_1(K)$, and a normalized directional distribution, $G(\theta_{\vec{K}})$, such that in our notation,

$$\text{with} \quad \begin{array}{l} S_1(\vec{K}) = S_1(K, \theta_{\vec{K}}) = S_1(K) G(\theta_{\vec{K}}) \\ \int_{-\pi}^{\pi} G(\theta_{\vec{K}}) d\theta_{\vec{K}} = 1 \ . \end{array} \tag{3.76}$$

One version of $S_1(K)$, whose experimental basis and formula derivation is condensed by Ewing [80], is the so-called JONSWAP (Joint North Sea Wave Project) spectrum, $S_J(\vec{K})$. There is an abundance of literature on the generation of wind waves which deals extensively with this spectrum. The JONSWAP model addresses the aspect of fetch-limited spectra, *fetch* being the term used to describe the distance over which a steady wave-generating wind blows. Its general form in terms of wavenumber, K, is

$$S_J(K) = S_F(K) \cdot S_{PM}(K) \tag{3.77}$$

where $S_F(K)$ contains parameters which are functions of fetch and duration, and $S_{PM}(K)$ is the still widely used Pierson-Moskowitz [60] spectrum. It has been common for illustrative purposes to ignore the fetch limitation factor and use only $S_{PM}(K)$ which assumes a long fetch and a fully developed sea – i.e. there is no more growth or decay in the spectrum. So that results presented here may be compared to those of other investigators, $S_{PM}(K)$ will be used as the non-directional part of $S_1(\vec{K})$ found throughout the cross section expressions. Its form is

$$S_{PM}(K) = \frac{\alpha_{PM}}{2K^4} e^{\left(\frac{-0.74g^2}{K^2U^4}\right)} \tag{3.78}$$

where g is the acceleration due to gravity, U is wind speed in m/s as measured at a level of 19.5 m above the mean ocean surface, and α_{PM} is a non-dimensional parameter whose value is 0.0081. U is the sole variable parameter describing the spectrum and there is clearly no fetch or *duration* – i.e. time over which wind blows – dependence.

A detail worthy of note is that Pierson's [61] definition of the surface expansion differs from that in (3.12) of this analysis. On the basis of a derivation by Walsh [81], it is shown in Appendix B.7 that the difference leads to our definition of $S_1(K)$ being related to that of Pierson by the expression

$$S_1(K) = \frac{1}{2} S_{PM}(K) \; . \tag{3.79}$$

This results in a 3 dB decrease in the first-order power spectral density, and associated cross section, from that which appears in the literature. Correspondingly, because the second-order densities contain a product of $S_1(K)$'s, the magnitude of these quantities is 6 dB below what has been heretofore reported for monostatic operation.

Historically, just as several forms of $S_1(K)$ have evolved, so has a variety of directional models, $G(\theta_{\vec{K}})$.

The form which has become standard (Tucker, [1]) is, strictly speaking, a function of frequency, or equivalently wavenumber, K, as well as $\theta_{\vec{K}}$ and is given by

$$G(\theta_{\vec{K}}, K) = F(s(K)) \cos^{2(s(K))}\left[\frac{\theta_{\vec{K}} - \bar{\theta}(K)}{2}\right]$$

where $\bar{\theta}(K)$ is the dominant direction of the waves whose wavenumber is K and $s(K)$ is referred to as the spread function. In simulating HF radar ocean surface cross sections, it has been customary to replace $\bar{\theta}(K)$ with $\bar{\theta}$, an overall mean direction, typically chosen to be that of the wind responsible for spectral growth. Also, as Tucker [1] notes, for practical purposes it is not possible to take account of $s(K)$ across the entire spectrum so a representative value, s, is employed. An excellent discussion of s, as it pertains to wave directional spectra obtained from radar scatter is presented by Tyler *et al.* [82]. From [1], using fixed s and $\bar{\theta}$ for simulation purposes, we may simply write the cardioid directional distribution in the form

$$G(\theta_{\vec{K}}) = F(s)\cos^{2s}\left[\frac{\theta_{\vec{K}} - \bar{\theta}}{2}\right] . \tag{3.80}$$

In order to satisfy the normalization in equation (3.76), $F(s)$ is written as

$$F(s) = \frac{2^{(2s-1)}\Gamma^2(s+1)}{\pi\Gamma(2s+1)} \tag{3.81}$$

where Γ is the usual gamma function. For integer values of s, (3.81) becomes

$$F(s) = F(s-1)\frac{s}{s-0.5}$$

with $F(1) = \frac{1}{\pi}$. A value of $s = 2$ has been used extensively in monostatic HF radar simulations (see, for example, Lipa and Barrick [28], Howell [58], Gill and Walsh [30]). This value will be used as required in the calculations to follow so that equation (3.81) reduces to

$$F(s) = F(2) = \frac{4}{3\pi} .$$

Throughout the cross section expressions of Section 3.5.3 the ocean surface wave vector spectrum appears in the form $S_1(m\vec{K})$ with $m = \pm 1$. From equations (3.76), (3.78), (3.79), (3.80) and (3.81), this quantity now becomes, when $s = 2$,

$$S_1(m\vec{K}) = \left[\frac{\alpha_{PM}}{4K^2}e^{\left(\frac{-0.74g^2}{K^2U^4}\right)}\right] \cdot \left[\frac{4}{3\pi}\cos^4\left(\frac{\theta_{\vec{K}} + \frac{(1-m)\pi}{2} - \bar{\theta}}{2}\right)\right] . \tag{3.82}$$

This model for the ocean gravity wave spectrum is used as necessary throughout the cross section calculations.

3.6.2 The First-order Bistatic Cross Section

For discussion purposes, the first-order cross section per unit area found in equation (3.71) is repeated here as

$$\sigma_{11}(\omega_d) = 2^4\pi k_0^2 \sum_{m=\pm 1} S_1(m\vec{K}) \frac{K^{\frac{5}{2}} \cos\phi_0}{\sqrt{g}} \Delta\rho_s \mathrm{Sa}^2 \left[\frac{\Delta\rho_s}{2}\left(\frac{K}{\cos\phi_0} - 2k_0\right)\right] \qquad (3.83)$$

where $S_1(m\vec{K})$ is now given by (3.82). The following properties and specifications lead to a straightforward numerical calculation:

1. From equation (3.44),

$$\omega_d = -m\sqrt{gK}\,.$$

   This indicates that

$$m = 1 \text{ when } \omega_d < 0$$

   and

$$m = -1 \text{ when } \omega_d > 0\,.$$

2. From Figure 3.1, specification of a representative bistatic angle, ϕ_0, fixes the position on a particular elliptical patch from which the scatter is received.

3. Identifying $\vec{K}$ as the $\vec{K}_{mn}$ of equation (A.19) and referring to the discussion following equation (2.136) it has been seen already that

$$\vec{K} = K\hat{N}$$

   with $\hat{N}$ being the unit vector along the *outward* ellipse normal. That is

$$\theta_{\vec{K}} = \theta_N\,,$$

   which means that $\theta_{\vec{K}}$ may be found from equation (2.133) when the distance, ρ, between transmitter and receiver and the distance $\rho_{0s} = \dfrac{\rho_{01} + \rho_{02}}{2}$ are fixed (see Figure 3.1 with ρ_1 and ρ_2 replaced by their representative values, ρ_{01} and ρ_{02}, respectively.)

4. Finally, a radar operating frequency, ω_0, and a pulse duration, τ_0, must be specified. These two quantities, respectively, determine operating wavenumber k_0 ($= \frac{\omega_0}{c}$ where c is the speed of light in a vacuum) and the scattering patch width $\Delta\rho_s$ ($= \frac{c\tau_0}{2}$).

By virtue of the $\mathrm{Sa}^2(\cdot)$ function in equation (3.71) the major peaks of the cross section are located at

$$\omega_d = \pm\sqrt{2gk_0\cos\phi_0} = \pm\omega_B \ . \tag{3.84}$$

Classically, these values of ω_d have been referred to as the Bragg frequencies, ω_B, Barrick [24]. They are indicative of scatter from two ocean waves, one travelling inward and the other outward along a scattering ellipse normal, and their wavelength is $\left(\frac{\lambda_0}{2\cos\phi_0}\right)$ where λ_0 is the operating wavelength. For monostatic operation, the bistatic angle, ϕ_0, is zero, and these waves have a length of $\frac{\lambda_0}{2}$. As noted in Chapter 1, this phenomenon led Crombie [22] to deduce that the primary mechanism responsible for HF scatter from the ocean surface is Bragg scattering. In the more general bistatic case, it is now obvious that the position of the first-order Bragg spectral peaks is dependent on the position on the scattering ellipse from which the radiation is observed to come – i.e. the peak positions are governed by the bistatic angle, ϕ_0.

In addition to establishing sharp primary peaks, the $\mathrm{Sa}^2(\cdot)$ factor introduces a rapidly oscillating first-order continuum. System timing effects as well as surface fluctuations and noise will, in practice, provide a smoothing effect of this periodic behaviour. In Figures 3.2–3.3 this has been simulated by convolving the cross section with a Hamming window (Harris, [83]).

From equation (3.83) it is clear that the smaller the radial scattering patch width, $\Delta\rho_s$, the broader will be the spectral peaks. Conversely, a large $\Delta\rho_s$ produces narrower but slightly higher Bragg peaks. This is depicted in Figure 3.2 for a 10 MHz operating frequency, patch widths of 400, 1200 and 2000 m, a bistatic angle of 30°,

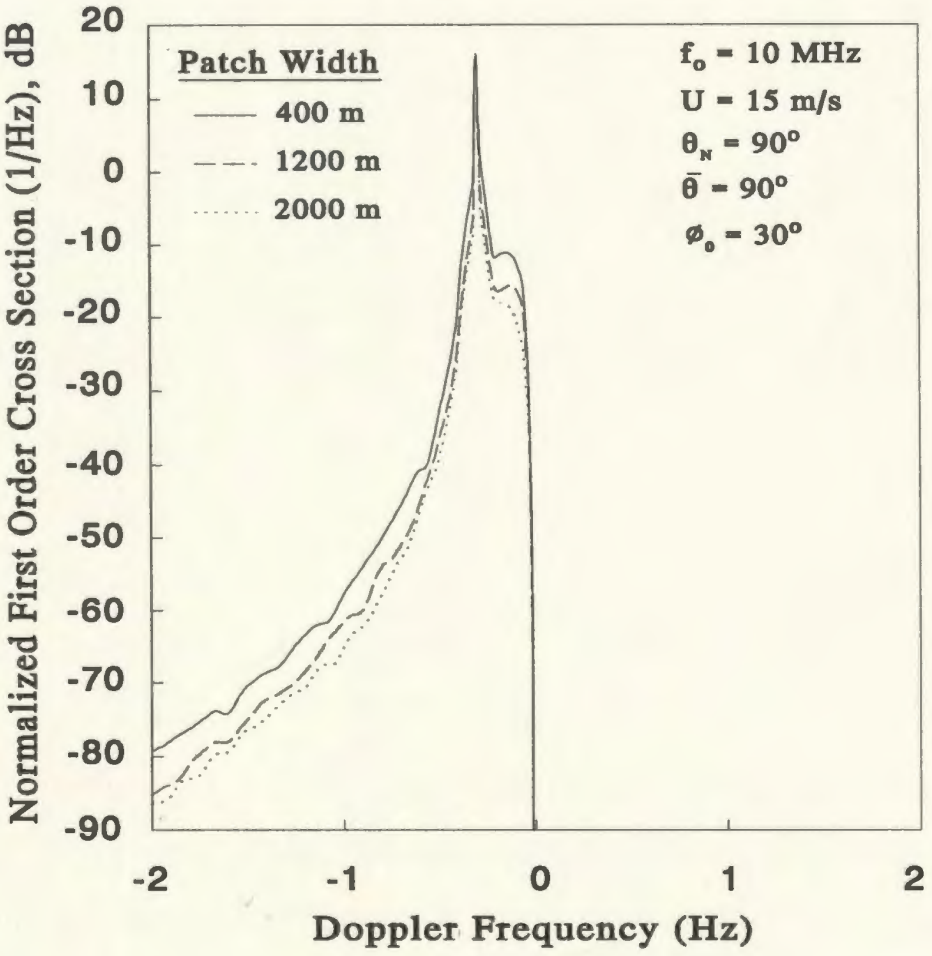

Figure 3.2: The effect of increasing radial patch width on the first-order cross section. The wind is outward along the ellipse normal resulting in non-zero results for the negative Doppler region only.

an ellipse normal of 90°, and wind speed and direction of 15 m/s and 90°, respectively.

Relative maxima just below the near-zero first-order cut off region of the cross section may be explained by the fact that since $\omega_d = \pm\sqrt{gK}$, small ω_d implies small K and thus large wavelength, λ, for the scattering waves. In the Pierson-Moskowitz model of equation (3.78), the maximum occurs well away from the Bragg wave region. For example, for a 10 MHz operating frequency and a wind speed of 15 m/s, the bistatic Bragg wave for $\phi_0 = 30°$ has a wavelength of $\frac{\lambda_0}{2\cos\phi_0} \approx 17.3$ m. However, the Pierson-Moskowitz spectral peak is at a wavelength of ≈ 190 m, which corresponds to an angular Doppler frequency of ≈ 0.573 rad/s or a frequency of ≈ 0.09 Hz. The large spectral energy of this long surface wave mitigates the rapid decrease in

the $\mathrm{Sa}^2(\cdot)$ function in the near-zero Doppler cross section. As expected, no such phenomenon occurs in the high Doppler tails which are a result of scatter from short, low energy waves. Of course, the absolute maxima at the Bragg peaks are resonance phenomena which are very strong in spite of the relatively low energy of the ocean waves responsible for them.

Figure 3.3 illustrates the effect of increasing the bistatic angle until the condition of forward scatter ($\phi_0 = 90°$) is approached. Not surprisingly, in view of equation (3.83), the spectral peaks rapidly reduce in power as ϕ_0 becomes large, implying that essentially no forward scattering takes place. The lateral shifts of the maxima are required by equation (3.84). It should be observed that in Figures 3.2–3.3, it has been chosen to use Doppler frequency (f_d) in hertz rather than angular Doppler frequency ($\omega_d = 2\pi f_d$). This is customary in the literature on scattering cross sections.

Other important features of the bistatic cross section, which are not unique to the first-order analysis, are depicted and discussed throughout Section 3.6.6. There, the effects of such factors as wind speed and direction and operating frequency are considered in detail.

3.6.3 The $\sigma_{2P}(\omega_d)$ Component of the Second-order Bistatic Cross Section

Attention is now focussed on that part of the second-order bistatic HF radar cross section of the ocean surface which results from (1) a single scatter from a second-order ocean wave and (2) a double scatter from two first-order ocean waves. These first-order waves are near each other on the elliptical scattering patch. The required cross section, $\sigma_{2P}(\omega_d)$, which must be simplified for calculation purposes is found in equation (3.73) and is repeated here for reference:

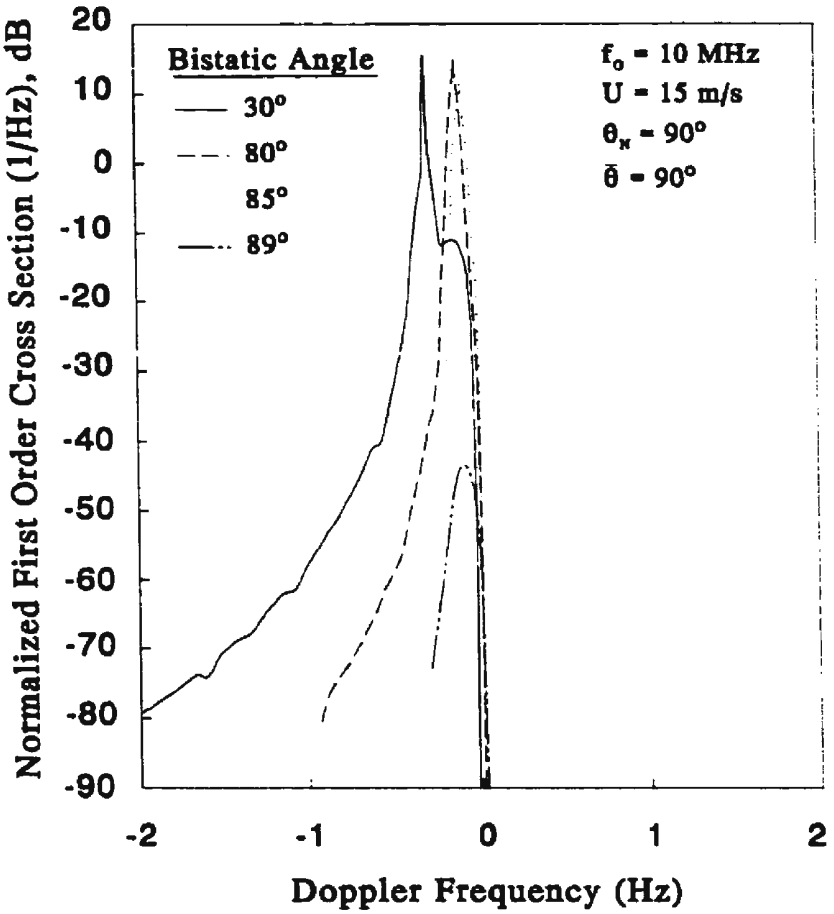

Figure 3.3: The effect of increasing bistatic angle for the first-order cross section. The radial patch width is fixed at 400 m.

$$\begin{aligned}\sigma_{2P}(\omega_d) &= 2^3\pi k_0^2 \Delta\rho_s \sum_{m_1=\pm1}\sum_{m_2=\pm1}\int_0^\infty\int_{-\pi}^{\pi}\int_0^\infty \Big\{S_1(m_1\vec{K}_1)S_1(m_2\vec{K}_2) \\ &\quad \cdot |{}_s\Gamma_P|^2 K^2 \cos\phi_0 \mathrm{Sa}^2\left[\frac{\Delta\rho_s}{2}\left(\frac{K}{\cos\phi_0}-2k_0\right)\right] \\ &\quad \cdot \delta\left(\omega_d + m_1\sqrt{gK_1} + m_2\sqrt{gK_2}\right)K_1\Big\} dK_1 d\theta_{\vec{K}_1} dK \ . \end{aligned} \tag{3.85}$$

A typical approach in monostatic calculations, for example in Walsh *et al* [8], has been to invoke a large radial width, $\Delta\rho_s$, of the scattering region. In the strict mathematical sense, we may write using Lathi ([77], Chapter 1)

$$\lim_{M\to\infty} M\mathrm{Sa}^2[Mx] = \pi\delta(x) \tag{3.86}$$

where $\delta(x)$ is the Dirac delta function. Applying this to the $\mathrm{Sa}^2[\cdot]$ function of equation (3.85), we may write

$$\begin{aligned}
&\lim_{\frac{\Delta\rho_s}{2\cos\phi_0}\to\infty} \mathrm{Sa}^2\left[\frac{\Delta\rho_s}{2\cos\phi_0}(K-2k_0\cos\phi_0)\right] \\
&= \frac{2\cos\phi_0}{\Delta\rho_s}\lim_{\frac{\Delta\rho_s}{2\cos\phi_0}\to\infty}\frac{\Delta\rho_0}{2\cos\phi_0}\mathrm{Sa}^2\left[\frac{\Delta\rho_s}{2\cos\phi_0}(K-2k_0\cos\phi_0)\right] \\
&= \frac{2\pi\cos\phi_0}{\Delta\rho_s}\delta(K-2k_0\cos\phi_0)\,. \qquad (3.87)
\end{aligned}$$

Using (3.87), equation (3.85) may now be represented as

$$\begin{aligned}
\sigma_{2P}(\omega_d) \approx\ & 2^4\pi^2k_0^2\cos^2\phi_0\sum_{m_1=\pm1}\sum_{m_2=\pm1}\int_0^\infty\int_{-\pi}^{\pi}\int_0^\infty\Big\{S_1(m_1\vec{K}_1)S_1(m_2\vec{K}_2) \\
&\cdot\ |{}_s\Gamma_P|^2\,K^2\delta(K-2k_0\cos\phi_0) \\
&\cdot\ \delta\left(\omega_d+m_1\sqrt{gK_1}+m_2\sqrt{gK_2}\right)K_1\Big\}\,dK_1d\theta_{\vec{K}_1}dK \qquad (3.88)
\end{aligned}$$

which, invoking the first delta function to do the dK integral, gives

$$\begin{aligned}
\sigma_{2P}(\omega_d) \approx\ & 2^6\pi^2k_0^4\cos^4\phi_0\sum_{m_1=\pm1}\sum_{m_2=\pm1}\int_{-\pi}^{\pi}\int_0^\infty\Big\{S_1(m_1\vec{K}_1)S_1(m_2\vec{K}_2) \\
&|{}_s\Gamma_P|^2\,\delta\left(\omega_d+m_1\sqrt{gK_1}+m_2\sqrt{gK_2}\right)K_1\Big\}\,dK_1d\theta_{\vec{K}_1}\,. \qquad (3.89)
\end{aligned}$$

It is now understood that $K = 2k_0\cos\phi_0$. The object, then, is to calculate $\sigma_{2P}(\omega_d)$. There are several intricate details which are enumerated in the following paragraphs.

1. The Relationship Between K_1 and K_2

It has been previously emphasized that $\vec{K} = \vec{K}_1 + \vec{K}_2$. Given the approach used to develop (3.89), not only is $\vec{K}$ perpendicular to the scattering ellipse, but it is also of magnitude $\approx 2k_0\cos\phi_0$. The magnitude of $\vec{K}_2$ is easily found, from the law of cosines, to be

$$K_2 = K_1^2 + 4k_0^2\cos^2\phi_0 - 4K_1k_0\cos\phi_0\cos(\theta_{\vec{K}_1}-\theta_N) \qquad (3.90)$$

and from the bistatic geometry (see Figure 3.1, and use representative parameter values)

$$\phi_0 = \frac{1}{2}\cos^{-1}\left[\frac{\rho_{01}^2+\rho_{02}^2-\rho^2}{2\rho_{01}\rho_{02}}\right] \qquad (3.91)$$

Then, angle, θ_N, of the ellipse normal is easily shown to be, using equation (2.133) and referring to Figure 3.1,

$$\theta_N = \begin{cases} \pm \sin^{-1}\left[\frac{\rho_{01}+\rho_{02}}{\rho} \sin\phi_0\right], & \rho_{01} > \rho_{02} \\ \pi \mp \sin^{-1}\left[\frac{\rho_{01}+\rho_{02}}{\rho} \sin\phi_0\right], & \rho_{01} < \rho_{02} \end{cases} \tag{3.92}$$

where $+\sin^{-1}(\cdot)$ or $\pi - \sin^{-1}(\cdot)$ should be used when the scatter position is in the $y > 0$ half-plane and $-\sin^{-1}(\cdot)$ and $\pi + \sin^{-1}(\cdot)$ when $y < 0$ at the place of scatter. Equation (3.92) is general, but if it is agreed to use a narrow beam receiver, ϕ_0 and θ_N are fixed by the bistatic geometry and it is obvious from Figure 3.1a that

$$\theta_N = \theta_1 + \phi_0 \, . \tag{3.93}$$

2. Disjoint Doppler Regions Dictated by m_1 and m_2

It will now be shown that the four possible combinations of m_1 and m_2 represent distinct Doppler regions. For non-zero results, it is required from the argument of the delta function in (3.89) that

$$\omega_d = -m_1\sqrt{gK_1} - m_2\sqrt{gK_2} \, . \tag{3.94}$$

Case 1: $m_1 = m_2$

When $m_1 = m_2$,

$$\omega_d^2 = gK_1 + gK_2 + 2g\sqrt{K_1K_2} \, .$$

From the triangle inequality $K_1 + K_2 \geq K = 2k_0\cos\phi_0$ and since $\sqrt{K_1K_2} > 0$, referring to equation (3.84),

$$\omega_d^2 > 2gk_0\cos\phi_0 = \omega_B \, .$$

That is, $\omega_d > \omega_B$ or $\omega_d < -\omega_B$.

Clearly, then,

$$\left.\begin{array}{ll} \omega_d < -\omega_B, & m_1 = m_2 = 1 \\ \omega_d > \omega_B, & m_1 = m_2 = -1 \end{array}\right\} \, . \tag{3.95}$$

Case 2: $m_1 \neq m_2$

From (3.94), when $m_1 \neq m_2$

$$\begin{aligned} \omega_d^2 &= gK_1 + gK_2 - 2g\sqrt{K_1K_2} \\ \Rightarrow \quad \omega_d^2 &< 2gk_0\cos\phi_0 - 2g\sqrt{K_1K_2} \\ \Rightarrow \quad \omega_d^2 &< 2gk_0\cos\phi_0 = \omega_B^2 \,. \end{aligned}$$

Therefore, $-\omega_B < \omega_d < \omega_B$ when $m_1 \neq m_2$.

Additionally, from (3.94)

$$\left.\begin{array}{rll} & m_1 = -1, \quad m_2 = +1 \quad \text{and} \quad K_1 > K_2 \ \text{or} \\ 0 < \omega_d < \omega_b, & m_1 = +1, \quad m_2 = -1 \quad \text{and} \quad K_1 < K_2 \\ \text{and} & \\ & m_1 = -1, \quad m_2 = +1 \quad \text{and} \quad K_1 < K_2 \ \text{or} \\ -\omega_B < \omega_B < 0, & m_1 = +1, \quad m_2 = -1 \quad \text{and} \quad K_1 > K_2 \end{array}\right\} . \qquad (3.96)$$

The sign of ω_d in the cross section argument thus dictates whether $m_1 = m_2 = 1$ or $m_1 = m_2 = -1$ outside the Bragg peaks. Similarly, the sign of ω_d in conjunction with knowledge of the relative magnitudes of $\vec{K}_1$ and $\vec{K}_2$ dictates the values of m_1 and m_2 between the Bragg peaks. A procedure similar to this was invoked by Lipa and Barrick [84] for monostatic cross sections. However, symmetry conditions in their analysis reduced the complexity of the calculation between the Bragg peaks.

3. Solution of the Delta Function Constraint and Related Results

Next, a form for $\delta(\cdot)$ in equation (3.89) is sought such that its arguments are in terms of the integration variables $\vec{K}_1$ and $\theta_{\vec{K}_1}$. Adapting a technique presented by Lipa and Barrick [84] for monostatic cross sections, we define

$$Y = \sqrt{K_1} \,, \qquad (3.97)$$

implying

$$K_1 dK_1 = 2Y^3 dY \qquad (3.98)$$

and the delta function takes the form

$$\delta(\cdot) = \delta(\omega_d - D_P(Y, \theta_{\vec{K}_1}))$$

where, using equation (3.90), it is readily verified that

$$Y = \frac{-D_P(Y,\theta_{\vec{K}_1}) - m_2\left[g^2\left(Y^4 + 4k_0^2\cos^2\phi_0 - 4Y^2k_0\cos\phi_0\cos(\theta_{\vec{K}_1} - \theta_N)\right)\right]^{\frac{1}{4}}}{m_1\sqrt{g}} . \tag{3.99}$$

Then, for a given $\theta_{\vec{K}_1}$,

$$dY = \left|\frac{\partial Y}{\partial D_P}\right|_{\theta_{\vec{K}_1}} dD_P \tag{3.100}$$

with the Jacobian of the transformation, using $L = m_1m_2$, given as

$$\left|\frac{\partial Y}{\partial D_P}\right|_{\theta_{\vec{K}_1}} = \frac{1}{\sqrt{g}\left|1 + \frac{L(Y^3 - 2Yk_0\cos\phi_0\cos(\theta_{\vec{K}_1} - \theta_N))}{\left[Y^4 + 4k_0^2\cos^2\phi_0 - 4Y^2k_0\cos\phi_0\cos(\theta_{\vec{K}_1} - \theta_N)\right]^{\frac{3}{4}}}\right|} . \tag{3.101}$$

Applying these transformations, allows equation (3.89) to be written as

$$\begin{aligned}\sigma_{2P}(\omega_d) \approx\ & 2^7\pi^2k_0^4\cos^4\phi_0 \sum_{m_1=\pm1}\sum_{m_2=\pm1}\int_{-\pi}^{\pi}\int_{D_P} S_1(m_1\vec{K}_1)S_1(m_2\vec{K}_2) \\ & |{}_s\Gamma_P|^2\,\delta(\omega_d - D_P(Y,\theta_{\vec{K}_1}))Y^3\left|\frac{\partial Y}{\partial D_P}\right|_{\theta_{\vec{K}_1}} dD_P\, d\theta_{\vec{K}_1} .\end{aligned} \tag{3.102}$$

It should be recognized from equation (3.99) that the limits on the D_P integral will depend on the values of m_1 and m_2 under consideration. To illustrate, when $m_1 = m_2 = 1$, $-\infty < D_P < -\omega_B$ where ω_B is given by equation (3.84). Clearly, this case corresponds, as it should from (3.95), to $\omega_d < -\omega_B$. The other cases for the D_P limits similarly follow.

In general, the delta function constraint of equation (3.102) must be "solved" numerically. That is, for

$$G(Y) = \omega_d - D_P(Y,\theta_{\vec{K}_1}) \tag{3.103}$$

we seek a $Y = Y^*$ such that

$$G(Y^*) = 0 . \tag{3.104}$$

Any suitable scheme may be used, and here the Newton-Raphson method (eg., Jeffrey [67]) is employed. The technique requires a Taylor series expansion of $G(Y)$ about

$Y = Y^*$ so that, to first order,

$$Y^* = Y - \left[\frac{G(Y)}{\left(\frac{\partial G}{\partial Y}\right)_{Y=Y^*}}\right] . \tag{3.105}$$

An initial guess, Y_i^*, say, is made and a better approximation, Y_{i+1}^*, is calculated from equation (3.105) with the process repeated until (3.104) is satisfied within a specified tolerance. It is not difficult to show that when ω_d is close to ω_B,

$$Y^* \approx \frac{-m_1}{\sqrt{g}}(\omega_d + m_2\omega_B) . \tag{3.106}$$

It is found, numerically, that this value of Y^* is a suitable initial guess for all regions of the integral.

There are several features of $G(Y) = 0$ in equation (3.103) which are significant aids in establishing an approach to numerically integrating the cross section of equation (3.102). Verification of these properties is not difficult and, in general, only the end results are presented here. A basic consideration which affects all the other factors associated with

$$\omega_d - D_P(Y, \theta_{\vec{K}_1}) = 0 \tag{3.107}$$

is that the contours of ω_d as given in the $K_{1x} - K_{1y}$ plane (where $\vec{K}_1 = K_{1x}\hat{x} + K_{1y}\hat{y}$ or $K_1 = \sqrt{K_{1x}^2 + K_{1y}^2}$ and $\theta_{\vec{K}_1} = \tan^{-1}\left(\frac{K_{1y}}{K_{1x}}\right)$) are symmetric about the lines

$$K_{1y} = K_{1x}\tan\theta_N \tag{3.108}$$

and

$$K_{1y} = -(K_{1x} - k_0\cos\phi_0\cos\theta_N)\cot\theta_N + k_0\cos\phi_0\sin\theta_N . \tag{3.109}$$

The ω_d surfaces of equation (3.107) are shown in Figure 3.4a and a detailed version of their $K_{1x} - K_{1y}$ contours for $m_1 = m_2 = -1$ in Figure 3.4b. It should be noted that in Figure 3.4b, $\vec{K} = \vec{K}_1 + \vec{K}_2 \approx 2k_0\cos\phi_0\hat{N}$ as usual. The symmetry dictated by (3.109) ensures that if the delta function constraint is solved for $K_1 < K_2$ it is also solved for the half plane where $K_2 > K_1$ by simply interchanging the vector magni-

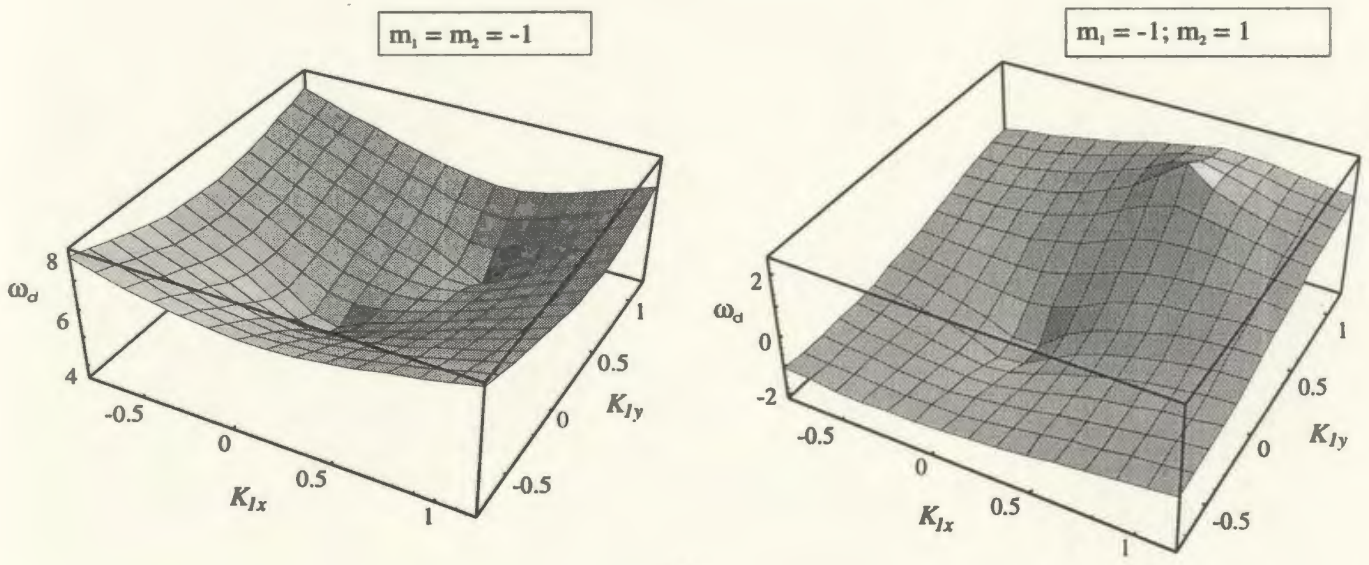

(a)

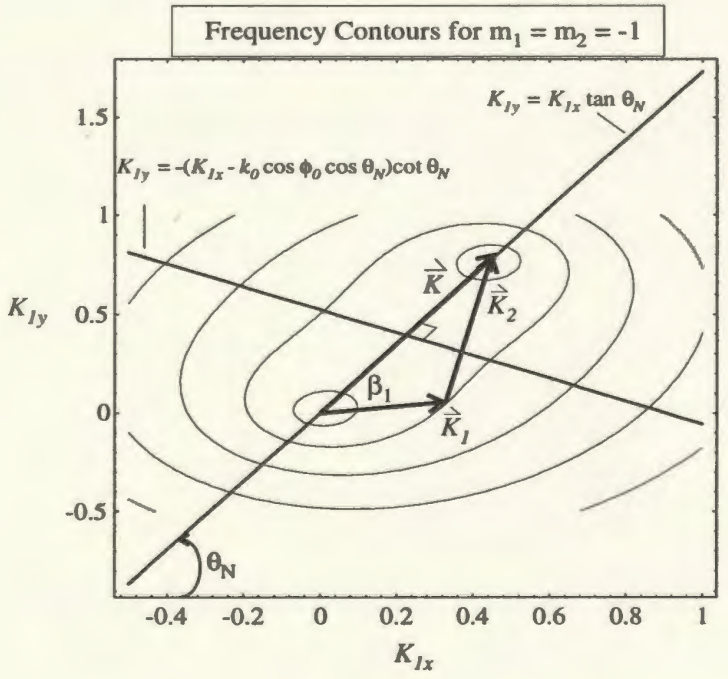

(b)

Figure 3.4: (a) The Doppler frequency surfaces for the patch scatter cross section. The cases of $m_1 = m_2 = -1$ and $m_1 = -1$, $m_2 = 1$ are shown. The $m_1 = m_2 = 1$ and $m_1 = 1$, $m_2 = -1$ are mirror images of these (i.e. reflection in the K_{1x}–K_{1y} plane). (b) The contours corresponding to the $m_1 = m_2$ case with enhancements as used for derivations in the text.

tudes. Furthermore, equations (3.108)–(3.109) are a help in establishing the proper way of partitioning the $\theta_{\vec{K}_1}$ integral of (3.102). It is possible to show that the frequency contours for $m_1 = m_2$ split apart when $\omega_B < \omega_d < \sqrt{2}\omega_B$ (or $-\sqrt{2}\omega_B < \omega_d < -\omega_B$). It may be verified that, when $K_1 < K_2$,

$$\left.\begin{array}{l} \theta_N - \pi \leq \theta_{\vec{K}_1} < \theta_N - \beta_1 \ \text{ for } \ K_{1y} < K_{1x}\tan\theta_N \\ \text{and} \\ \theta_N + \beta_1 \leq \theta_{\vec{K}_1} < \theta_N + \pi \ \text{ for } \ K_{1y} > K_{1x}\tan\theta_N \end{array}\right\} \tag{3.110}$$

where

$$\beta_1 = \begin{cases} \cos^{-1}\left(2\left(\frac{\omega_B}{\omega_d}\right)^2\right) \ ; & |\omega_d| > \sqrt{2}\,\omega_B \\ 0\ ; & |\omega_d| < \sqrt{2}\,\omega_B\ . \end{cases} \tag{3.111}$$

Now, for every $\vec{K}_1, \vec{K}_2$ pair in the region $K_1 < K_2$, there is a matching $\vec{K}_1', \vec{K}_2'$ pair in the region $K_1 > K_2$ such that

$$\left.\begin{array}{l} K_1' = K_2\ , \ \ \theta_{\vec{K}_1'} = 2\theta_N - \theta_{\vec{K}_2} \\ K_2' = K_1\ , \ \ \theta_{\vec{K}_2'} = 2\theta_N - \theta_{\vec{K}_1} \end{array}\right\}\ . \tag{3.112}$$

The significance of equations (3.110 - 3.112) is that (1) the delta function constraint needs only be "solved" for the region in which $K_1 < K_2$ and (2) given a single $(K_1, \theta_{\vec{K}_1})$, not only is K_2 established (see equation (3.90)) but

$$\theta_{\vec{K}_2} = \begin{cases} \theta_N + \cos^{-1}\beta_2\ , & \theta_N - \pi \leq \theta_{\vec{K}_1} \leq \theta_N - \beta_1 \\ \theta_N - \cos^{-1}\beta_2\ , & \text{otherwise} \end{cases} \tag{3.113}$$

where

$$\beta_2 = \frac{[4k_0^2\cos^2\phi_0 + K_2^2 - K_1^2]}{4k_0K_2\cos\phi_0}\ . \tag{3.114}$$

4. Singularities in the Integrand

The fourth, and final, major consideration in calculating the cross section of equation (3.102) is the singularities which may arise in the integrand. Firstly, consideration is given to the Jacobian of the transformation in equation (3.101), and, subsequently, the coupling coefficient, ${}_s\Gamma_P$, is addressed. In each case, the physical significance is addressed.

It may be observed that, when $\theta_{\vec{K}_1} = \theta_N$, $Y = \sqrt{K_1} = \sqrt{k_0\cos\phi_0}$, and $L = 1$ in $\left|\frac{\partial Y}{\partial D_P}\right|_{\theta_{\vec{K}_1}}$ of equation (3.101), the denominator of that expression vanishes. Hence,

there is a singularity at $\vec{K}_1 = (k_0 \cos\phi_0, \theta_N)$. Since $\vec{K}_1 + \vec{K}_2 = \vec{K} = 2k_0 \cos\phi_0 \hat{N}$, at the singular point, $\vec{K}_2 = (k_0 \cos\phi_0, \theta_N)$ also. Then, from equation (3.94),

$$\begin{aligned} \omega_d &= -m_1\sqrt{gk_0\cos\phi_0} - m_2\sqrt{gk_0\cos\phi_0} \\ &= \mp\sqrt{2}\,\sqrt{2gk_0\cos\phi_0} \\ &= \mp\sqrt{2}\,\omega_B\ . \end{aligned}$$

This means that there is a singularity when the Doppler frequency is $\mp\sqrt{2}$ times the first-order Bragg frequency with $K_1 = K_2 = k_0 \cos\phi_0$ and $\theta_{\vec{K}_1} = \theta_{\vec{K}_2} = \theta_N$. Thus, in bistatic operation where, in general, $\phi_0 \neq 0$, the waves responsible for the scattering at the singular point have a wavenumber $k_0 \cos\phi_0$ which is half that of the bistatic Bragg wave. Equivalently, the wavelength, λ, of this scatterer is twice that of the Bragg wave, λ_B, and since the wave phase speed of first-order deep water waves is proportional to $\sqrt{\lambda}(= \sqrt{2\lambda_B}$ here), the Doppler shift it produces is $\sqrt{2}\omega_B$. Additionally, the same Jacobian applies to that part of the integral arising from a single scattering from a second-order wave. In the singular case being discussed, this wave has its wave vector given by $\vec{K} = \vec{K}_1 + \vec{K}_2 = (2k_0 \cos\phi_0, \theta_N)$ and its wavelength is therefore equivalent to λ_B. However, from the Hasselmann [59] second-order theory the speed of this wave is $\sqrt{2}$ that of a first-order wave of the same length. Thus, the $\sqrt{2}\omega_B$ peak in the second-order cross section may be explained as a combination of two first-order scatters from waves of length $2\lambda_B$ and a single scatter from a second-order surface component of length λ_B. It is obvious that for monostatic operation, where $\phi_0 = 0$, this observation reduces to that discussed by Barrick [24] and Srivastava [54].

The second source of singularities is the coupling coefficient, ${}_s\Gamma_P$. It may be recalled that this symmetricized coupling coefficient given by equations (2.64), (2.142), (3.18), (3.26), and (B.11) consists of the sum of electromagnetic and hydrodynamic terms, ${}_E\Gamma_P$ and ${}_H\Gamma$, respectively. For reference it may be written in full as

$${}_s\Gamma_P(\vec{K}_1, \vec{K}_2) = \frac{1}{2}\left\{\left[\frac{j\sqrt{\vec{K}_1 \cdot [\vec{K}_1 - 2k_0\hat{\rho}_2]} + k_0}{k_0^2 + \vec{K}_1 \cdot [\vec{K}_1 - 2k_0\hat{\rho}_2]}\right] \cdot \left[\frac{(\vec{K}_1 \cdot \hat{\rho}_2)[\vec{K}_2 \cdot (\vec{K}_1 - k_0\hat{\rho}_2)]}{\sqrt{\vec{K}_1 \cdot [\vec{K}_1 - 2k_0\hat{\rho}_2]}}\right]\right.$$

$$+\left[\frac{j\sqrt{\vec{K}_2\cdot[\vec{K}_2-2k_0\hat{\rho}_2]}+k_0}{k_0^2+\vec{K}_2\cdot[\vec{K}_2-2k_0\hat{\rho}_0]}\right]\cdot\left[\frac{(\vec{K}_2\cdot\hat{\rho}_2)[\vec{K}_1\cdot(\vec{K}_2-k_0\hat{\rho}_2)]}{\sqrt{\vec{K}_2\cdot[\vec{K}_2-2k_0\hat{\rho}_2]}}\right]$$
$$+\left[K_1+K_2+\frac{g}{\omega_1\omega_2}(K_1K_2-\vec{K}_1\cdot\vec{K}_2)\left(\frac{gK+(\omega_1+\omega_2)}{gK-(\omega_1+\omega_2}\right)\right]\Bigg\}\ . \qquad (3.115)$$

It must be emphasized here that unit vector $\hat{\rho}_2$ is associated with the $\vec{\rho}_2$ of Figure 2.5 and for the present discussion is better understood as $\hat{\rho}_1$ of Figure 3.1.

It was discussed following equation (3.18) that ${}_H\Gamma$, represented by the last term in (3.115), has no singularities. However it is evident that the electromagnetic portion will be singular whenever

$$\vec{K}_1\cdot\left[\vec{K}_1-2k_0\hat{\rho}_2\right]=0 \qquad (3.116)$$

(or equivalently, $\vec{K}_2\cdot\left[\vec{K}_2-2k_0\hat{\rho}_2\right]=0$). It may be readily shown from the conditions that $\vec{K}_1+\vec{K}_2=\vec{K}\approx 2k_0\cos\phi_0\hat{N}$ and $\theta_N=\theta_2+\phi_0$ (see Figure 2.6), that (3.116) is a circle of singularity of radius k_0 and centred at $(k_0\cos(\theta_N-\phi_0), k_0\sin(\theta_N-\phi_0))$ in the $K_{1x}-K_{1y}$ plane. To determine the effect of these singularities, the condition giving the positions where this circle is tangent to the ω_d contours, and thus contributory to the cross section integral, was sought. It is tedious, but not difficult, to show that the greatest effect of the singularities occurs for

$$\begin{aligned} &K_1=K_2 \\ &\text{and} \\ &\omega_d=\pm 2^{\frac{3}{4}}\sqrt{\frac{|1\pm\sin\phi_0|^{\frac{1}{2}}}{\cos\phi_0}}\,\omega_B\ . \end{aligned} \qquad (3.117)$$

The $\pm$ in the radicand is independent of that outside. We note, importantly, that for monostatic operation, in which $\phi_0=0$, (3.117) reduces to

$$(\omega_d)_{\text{monostatic}}=\pm 2^{\frac{3}{4}}(\omega_B)_{\text{monostatic}} \qquad (3.118)$$

which is the well known "corner reflector" condition discussed by Barrick [24] and Srivastava [54]. Mathematically, (3.117) produces *four* values of ω_d of interest because the centre of the circle of singularity is not, in general, on the axes of symmetry of the $\pm\omega_d$ contours. Physically, these singularities correspond to double specular reflections

from the $(\vec{K}_1, \vec{K}_2)$ pairs of scattering wave vectors involved. For completeness, we note that directions of these wave vectors are

$$\begin{aligned} \theta_{\vec{K}_1} &= \theta_N - \left(\tfrac{2\phi_0 \pm \pi}{4}\right) \\ \text{and} \\ \theta_{\vec{K}_2} &= \theta_N + \left(\tfrac{2\phi_0 \pm \pi}{4}\right) \end{aligned} \tag{3.119}$$

where the $\pm$ corresponds to that in the radicand of (3.117). Further comments on the relative importance of these singularities is found in Section 3.6.6 as well as in Section 4.5.3.

All of the features of the integrand in equation (3.102) which are important in calculating the second-order "patch" cross section have now been addressed. Since the only singularities which contribute significantly to the integral are at the ω_d values discussed above, at all other Doppler frequencies, they may be effectively removed from the integration process. Based on the considerations presented here, a FORTRAN 77 routine was developed to calculate $\sigma_{2P}(\omega_d)$. Plots of the outcomes are presented and discussed in Section 3.6.6 in conjunction with other components of the cross section.

3.6.4 The $\sigma_{2T}(\omega_d)$ Component of the Second-order Bistatic Cross Section

The initial treatment of equation (3.74), which gives the Doppler cross section component involving a first scatter near the transmitter followed by another on the remote patch, follows that of (3.85). That is, the $\mathrm{Sa}^2[\cdot]$ function appearing in the $\sigma_{2T}(\omega_d)$ formulation is converted to a delta function via the transformation effected through equations (3.86) and (3.87). The result, on using the delta function to evaluate the K_2 integral, is

$$\sigma_{2T}(\omega_d) \approx 2^5\pi^2 k_0^4 \cos^4\phi_0 \sum_{m_1=\pm1}\sum_{m_2=\pm1}\int_{-\pi}^{\pi}\int_0^{\infty}\left\{S_1(m_1\vec{K}_1)S_1(m_2\vec{K}_2)\right.$$
$$\left.|E_T|^2\,\delta\left(\omega_d + m_1\sqrt{gK_1} + m_2\sqrt{gK_2}\right)K_1\right\}dK_1 d\theta_{\vec{K}_1}\,. \qquad (3.120)$$

The fact that $\vec{K}_2 \approx 2k_0\cos\phi_0\hat{N}$ is now implicit so that $S_1(m\vec{K}_2)$ is really the spectral content of only two waves of length $2k_0\cos\phi_0$ and travelling, one inward and one outward, along the ellipse normal. For HF operating frequencies, ocean waves of length $2k_0\cos\phi_0$ are usually in the high frequency (or wavenumber) end of the energy spectrum, far removed from the spectral peak. This, in general, makes $\sigma_{2T}(\omega_d)$ of secondary importance as compared to $\sigma_{2P}(\omega_d)$, and more discussion on this issue is found in Section 3.6.6.

Following the approach of the previous section, several observations, as listed below, aid in the calculation of $\sigma_{2T}(\omega_d)$.

1. The Wave Vector $\vec{K}_1$

While $\vec{K}_2$ is restricted as stated above, $\vec{K}_1$ may take any magnitude imposed by the remaining delta function, $\delta\left(\omega_d + m_1\sqrt{gK_1} + m_2\sqrt{gk_0\cos\phi_0}\right)$, and its direction, $\theta_{\vec{K}_1}$, may assume any value between $-\pi$ and π.

2. Doppler Regions Dictated by m_1 and m_2

The argument of disjoint Doppler regions formed by the four combinations of m_1 and m_2 in the $\sigma_{2P}(\omega_d)$ equation cannot be made here. From the argument of the delta function in (3.120) it is required that

$$\omega_d = -m_1\sqrt{gK_1} - m_2\sqrt{2gk_0\cos\phi_0}\,. \qquad (3.121)$$

Again, setting $\omega_B = \sqrt{2gk_0\cos\phi_0}$, it becomes obvious that

$$\left.\begin{array}{lll} m_1 = m_2 = -1 & \Rightarrow & \omega_d > +\omega_B \\ m_1 = m_2 = +1 & \Rightarrow & \omega_d < -\omega_B \\ m_1 = -1,\ m_2 = +1 & \Rightarrow & \omega_d > -\omega_B \\ m_1 = +1,\ m_2 = -1 & \Rightarrow & \omega_d < +\omega_B \end{array}\right\}\,. \qquad (3.122)$$

Clearly, then the Doppler regions dictated by m_1 and m_2 overlap and care must be taken to consider all possible combinations of m's for a particular ω_d when calculating $\sigma_{2T}(\omega_d)$.

3. Solution of the Delta Function Constraint and Variable Transformation

Letting $Y = \sqrt{K_1}$, as before, implies equation (3.98) and

$$\delta(\cdot) = \delta(\omega_d - D_T(Y))$$

where

$$Y = \frac{-(D_T(Y) + m_2\omega_B)}{m_1\sqrt{g}} \tag{3.123}$$

with the Jacobian being

$$\left|\frac{\partial Y}{\partial D_T}\right| = \frac{1}{\sqrt{g}} \, . \tag{3.124}$$

This permits us to write (3.120) as

$$\begin{aligned}\sigma_{2T}(\omega_d) \approx\ & 2^6\pi^2 k_0^4 \cos^4\phi_0 \sum_{m_1=\pm1}\sum_{m_2=\pm1}\int_{-\pi}^{\pi}\int_{D_T}\Big\{S_1(m_1\vec{K}_1) \\ & \cdot S_1\left(2k_0\cos\phi_0, \theta_N + \left(\frac{1-m_2}{2}\right)\pi\right)|_E\Gamma_T|^2\,\delta(\omega_d - D_T(Y)) \\ & \cdot \frac{1}{\sqrt{g}}\cdot Y^3\Big\}\,dD_T\,d\theta_{\vec{K}_1} \, .\end{aligned} \tag{3.125}$$

The solution, Y^*, to the delta function is trivial because of *a priori* knowledge of K_2 and the result may be written simply as

$$Y^* = \frac{-(\omega_d + m_2\omega_B)}{m_1\sqrt{g}} \, . \tag{3.126}$$

4. Singularities in the Integrand

The only factor in need of consideration when examining the possibility of singularities in (3.125) is the coupling coefficient, $_E\Gamma_T$. From equations (2.87) and (2.146) and carrying out the notation change for the $\vec{K}$'s as discussed following equations (3.2) and (3.14),

$$_E\Gamma_T = \left\{\frac{\vec{K}_1\cdot(\vec{K}_1 + k_0\hat{\rho}_2)}{\sqrt{\vec{K}_1\cdot[\vec{K}_1 + 2k_0\hat{\rho}_2]}}\right\}\cdot\left\{\frac{-k_0^2 - jk_0\sqrt{\vec{K}_1\cdot[\vec{K}_1 + 2k_0\hat{\rho}_2]}}{k_0^2 + \vec{K}_1\cdot[\vec{K}_1 + 2k_0\hat{\rho}_2]}\right\} \, . \tag{3.127}$$

Here $\hat{\rho}_2$ is the unit vector associated with $\vec{\rho}_2$ of Figure 2.7, and, as in ${}_s\Gamma_P$, it is identical to a $\hat{\rho}_1$ vector which would be identified with $\vec{\rho}_1$ of Figure 3.1. Singularities occur in ${}_E\Gamma_T$ when

$$\vec{K}_1 \cdot [\vec{K}_1 + 2k_0\hat{\rho}_2] = 0 \, .$$

Thus, there is again a circle of singularity and, in this case, it is easily shown to be of radius k_0 and to be centred at $(-k_0\cos(\theta_N - \phi_0), -k_0\sin(\theta_N - \phi_0))$ in the $K_{1x} - K_{1y}$ plane.

An investigation of where this circle is tangent to the ω_d contours, which are themselves circles, leads to the important result that at such points

$$K_1 = 2k_0 \text{ and } \theta_{\vec{K}_1} = (\theta_1 + \pi) \ \text{(in Figure 3.1)} \, . \tag{3.128}$$

This means that the Doppler frequencies where the singularities will have a non-zero contribution to the $\sigma_{2T}(\omega_d)$ integral are given from equation (3.121) as

$$\begin{aligned} \omega_d &= -m_1\sqrt{2gk_0} - m_2\omega_B \\ &= \omega_B\left(-m_2 - \frac{m_1}{\cos\phi_0}\right) \, . \end{aligned} \tag{3.129}$$

When $m_1 = m_2 = \pm 1$, these Doppler frequencies are located at $\mp\omega_B\left(1 + \frac{1}{\sqrt{\cos\phi_0}}\right)$, respectively. When $m_1 \neq m_2$ there are two peaks removed from zero Doppler by an amount governed by $\cos\phi_0$. The physical cause of these singularities, which may manifest themselves as peaks in the Doppler spectrum, may be deduced from (3.128). The $\vec{K}_1$ wave vector in these cases evidently lies along the direction from the patch to the transmitter. Such a wave, from which the first scatter occurs, can provide a strong backscatter toward the patch where the second scatter occurs from the "bistatic" Bragg wave whose wavenumber is $2k_0\cos\phi_0$. Practically, then, if there is ocean behind the transmitter, this phenomenon could be expected to manifest itself. Further, for monostatic operation, the Doppler frequencies in equation (3.129) reduce

to

$$(\omega_d)_{\text{monostatic}} = \begin{cases} \pm(2\omega_B)_{\text{monostatic}}\,, & m_1 = m_2 = \pm 1 \\ 0, & m_1 \neq m_2 \end{cases} \tag{3.130}$$

where $(\omega_d)_{\text{monostatic}} = \sqrt{2gk_0}$. This is precisely the result obtained by Srivastava [54], so that the more general result of (3.129) reduces to the proper monostatic form (i.e. when $\phi_0 = 0$).

The above items contain the basic features which must be incorporated into a calculation of the $\sigma_{2T}(\omega_d)$ component of the cross section. As with the $\sigma_{2P}(\omega_d)$ portion, $\sigma_{2T}(\omega_d)$ was implemented via a FORTRAN 77 routine. Plots of the results for a variety of operating parameters appear in Section 3.6.6. Further comparison with the existing monostatic counterpart is also carried out there.

3.6.5 The $\sigma_{2R}(\omega_d)$ Component of the Second-order Bistatic Cross Section

Consideration of the $\sigma_{2R}(\omega_d)$ cross section for a single scatter on the remote scattering patch followed by another at the receiver closely parallels that for $\sigma_{2T}(\omega_d)$ above. However, because this portion of the cross section does not appear in any form in the literature, the important parts of the integral will be summarized.

Treating the $\text{Sa}^2[\cdot]$ function in the usual fashion by assuming large $\dfrac{\Delta\rho_s}{2\cos\phi_0}$, equation (3.75) may be approximated as

$$\begin{aligned} \sigma_{2R}(\omega_d) \;\approx\; & 2^5\pi^2 k_0^4 \cos^4\phi_0 \sum_{m_1=\pm1} \sum_{m_2=\pm1} \int_{-\pi}^{\pi} \int_0^{\infty} \Big\{ S_1(m_1\vec{K}_1) S_1(m_2\vec{K}_2) \\ & \cdot\; |_E\Gamma_R|^2\, \delta\left(\omega_d + m_1\sqrt{gK_1} + m_2\sqrt{gK_2}\right) K_2 \Big\}\, dK_2 d\theta_{\vec{K}_2}\,. \end{aligned} \tag{3.131}$$

The delta function resulting from the $\text{Sa}^2[\cdot]$ of equation (3.75) has been utilized to solve the K_1 integration so it must be understood that $K_1 \approx 2k_0\cos\phi_0$ in (3.131). From previous considerations, $\theta_{\vec{K}_1} \approx \theta_N$, implying $\vec{K}_1 \approx 2k_0\cos\phi_0\hat{N}$.

The following notes will be seen to be analogous to those of the previous section.

1. The Wave Vector $\vec{K}_2$

While $\vec{K}_1$ associated with the scatter on the remote scattering ellipse, is fixed in

magnitude and direction, $\vec{K}_2$, which is linked to a surface wave at the receiver, may assume any direction from $-\pi$ to π and any magnitude which complies with the remaining delta function, $\delta\left(\omega_d + m_1\sqrt{2gk_0\cos\phi_0} + m_2\sqrt{gK_2}\right)$.

2. Doppler Regions Dictated by m_1 and m_2

The delta function of (3.131) requires that

$$\omega_d = -m_1\sqrt{2gk_0\cos\phi_0} - m_2\sqrt{gK_2} \tag{3.132}$$

which is clearly analogous to (3.121) with m_1 and m_2 reversed and K_1 replaced by K_2 here. Therefore, the Doppler regions are not disjoint for the various combinations of m's and, in particular,

$$\left.\begin{array}{lll} m_1 = m_2 = -1 & \Rightarrow & \omega_d > +\omega_B \\ m_1 = m_2 = +1 & \Rightarrow & \omega_d < -\omega_B \\ m_1 = -1,\ m_2 = +1 & \Rightarrow & \omega_d < +\omega_B \\ m_1 = +1,\ m_2 = -1 & \Rightarrow & \omega_d > -\omega_B \end{array}\right\} . \tag{3.133}$$

This is similar to (3.122) but with the m_1 and m_2 interchanged, and, as before, care must be taken to ensure that for a given ω_d, (3.131) is calculated using all relevant combinations of m_1 and m_2.

3. Solution of the Delta Function Constraint and Variable Transformation

Using a comparable analysis to that in equations (3.123–3.126), equation (3.131) may be written immediately as

$$\begin{aligned} \sigma_{2R}(\omega_d) \approx\ & 2^6\pi^2 k_0^4 \cos^4\phi_0 \sum_{m_1=\pm1}\sum_{m_2=\pm1}\int_{-\pi}^{\pi}\int_0^{\infty}\Big\{S_1(m_2\vec{K}_2) \\ & \cdot S_1\left(2k_0\cos\phi_0, \theta_N + \left(\frac{1-m_1}{2}\right)\pi\right)|_E\Gamma_R|^2\,\delta(\omega_d - D_R(Y)) \\ & \cdot \frac{1}{\sqrt{g}}\cdot Y^3\Big\}\,dD_R\,d\theta_{\vec{K}_2} \end{aligned} \tag{3.134}$$

where

$$\begin{aligned} Y &= \sqrt{K_2} \\ &= \frac{-(D_R(Y) + m_1\omega_B)}{m_2\sqrt{g}} \end{aligned} \tag{3.135}$$

and the delta function solution is

$$Y^* = \frac{-(\omega_d + m_1\omega_B)}{m_2\sqrt{g}} \,. \tag{3.136}$$

4. Singularities in the Integrand

The source of singularities in (3.134) is the coupling coefficient ${}_E\Gamma_R$. From equations (2.106) and (2.149) and Figures 2.9 and 3.1, this may be written as

$${}_E\Gamma_R = \frac{k_0\vec{K}_2 \cdot \hat{\rho}_2}{\sqrt{\vec{K}_2 \cdot [\vec{K}_2 - 2k_0\hat{\rho}_2]}} \tag{3.137}$$

where $\hat{\rho}_2$ is in the direction of $\vec{\rho}_2$ of Figure 3.1. The circle of singularity,

$$\vec{K}_2 \cdot [\vec{K}_2 - 2k_0\hat{\rho}_2] = 0 \tag{3.138}$$

has radius k_0 and is centred at $(-k_0\cos(\theta_N + \phi_0), -k_0\sin(\theta_N + \phi_0))$ in the $K_{2x} - K_{2y}$ plane. Here, too, the ω_d contours are circles in this plane and the locus of (3.138) is tangent to these at

$$\begin{aligned} \omega_d &= -m_1\omega_B - m_2\sqrt{2gk_0} \\ &= \omega_B\left(-m_1 - \frac{m_2}{\sqrt{\cos\phi_0}}\right) \end{aligned} \tag{3.139}$$

with

$$\vec{K}_2 = (2k_0, \theta_{12}) \tag{3.140}$$

Therefore, when $m_1 = m_2 = \pm 1$, there may be additional spectral peaks which are located at $\mp\omega_B\left(1 + \frac{1}{\sqrt{\cos\phi_0}}\right)$, respectively. For $m_1 \neq m_2$, there are two more peaks removed from zero Doppler by an amount dependent on $\cos\phi_0$. What has been deduced at this stage is that $\sigma_{2T}(\omega_d)$ and $\sigma_{2R}(\omega_d)$ have theoretical peaks in the same places.

The physical significance of (3.140) is that the major contribution from the second scatter at the receiver for the singular points is a backscatter. That is, the four peaks at the ω_d's given by (3.139) are produced by a combination of a first-order bistatic

scatter on the remote patch followed by a backscatter at the receiver. Again, for the peaks to be in evidence, there must be ocean behind the receiver. Finally, it may be immediately seen from (3.139) that for monostatic operation the spectral peaks associated with $\sigma_{2R}(\omega_d)$ will occur at

$$(\omega_d)_{\text{monostatic}} = \begin{cases} \pm(2\omega_B)_{\text{monostatic}}, & m_1 = m_2 = \pm 1 \\ 0, & m_1 \neq m_2 \end{cases} \tag{3.141}$$

which, from (3.130), are identical to those for $\sigma_{2T}(\omega_d)$.

The actual manifestation of the phenomena discussed above will depend on such factors as the bistatic geometry parameters, the wind conditions and the operating frequency. Such considerations are the topics of investigation in the next section.

3.6.6 Depiction and Description of the Cross Section Results

This section is used to illustrate the calculations described in Sections 3.6.2–3.6.5. Initially, the general features of the bistatic cross section will be compared to the monostatic case by setting $\phi_0 = 0$. Then, for a fixed operating frequency, the effect of wind speed (or, equivalently, sea state) will be examined. Subsequently, wind direction is considered. The ramifications of changing operating frequency are then investigated. Finally, a range of bistatic angles is surveyed to determine the influence this parameter has on the overall cross section. There are, of course, many permutations of these parameters which could arise in practice, but here we seek to illustrate only the basic response of the Doppler cross sections by changing the variables in a simple way, one by one.

It may be noted that, strictly speaking, the cross sections were developed without explicit specification of the receiving antenna beamwidth. That is, they exist as Doppler cross section per unit area. It is implicit in what follows, that for a particular bistatic angle, the receiver beamwidth is narrow enough so that there is very little deviation from this specific angle over the patch of surface being interrogated by the radar.

The directional ocean spectrum given by equation (3.82), which is the product of a Pierson-Moskowitz non-directional factor and a cardioid directional distribution, is used in all of the figures of this section. The wind directions, $\bar{\theta}$, are given with respect to the positive x axis.

For the first order, a radial patch width, $\Delta\rho_s$, of 2000 m corresponding to a transmitted pulse width, τ_0, of $\approx 13\ \mu$s ($\tau_0 = \frac{2\Delta\rho_s}{c}$) is used. This value has been used by Walsh *et al.* [8] in monostatic simulations. As for the first order, the cross section plots are given in terms of Doppler frequency, f_d, in hertz and are plotted on a decibel scale.

1. Typical Comparison of Bistatic and Monostatic Cross Section

Figure 3.5 shows cross sections produced assuming an operating frequency, f_0, of 25 MHz, a wind speed of 15 m/s and a wind direction, $\bar{\theta}$, as referenced above, of 90° to the ellipse normal direction, θ_N. The bistatic angle is chosen to be 30°. The monostatic cross section is similarly calculated with the wind 90° to the look direction, θ_L. Figures 3.5a and 3.5b show the individual components of each cross section and Figure 3.5c depicts a comparison of the combined effects.

The monostatic Bragg frequencies indicated by peaks $F_{N,M}$ and $F_{P,M}$ in Figure 3.5b are located at ± 0.5099 Hz while their bistatic counterparts, $F_{N,B}$, $F_{P,B}$ in Figure 3.5a, are at ± 0.5099 Hz $\times\sqrt{\cos 30°} = \pm 0.4745$ Hz. Of course, the bistatic Bragg frequencies will always be nearer zero Doppler that those of the corresponding monostatic case. Implicit in these values is the assumption that there is no net surface transport due to ocean currents. The latter would cause additional shifts in the Bragg frequencies, and, in monostatic operation, these deviations from the theoretical values are an indicator of the current regime (see, for example, Hickey *et al.* [32]). The a_B and a_M in Figures 3.5a and 3.5b are the $\left(\sqrt{2}\frac{\omega_B}{2\pi}\right)$ peaks discussed in Section 3.6.3. For the parameters above, they occur at $\approx \pm 0.6710$ Hz and ± 0.7210 Hz, respectively.

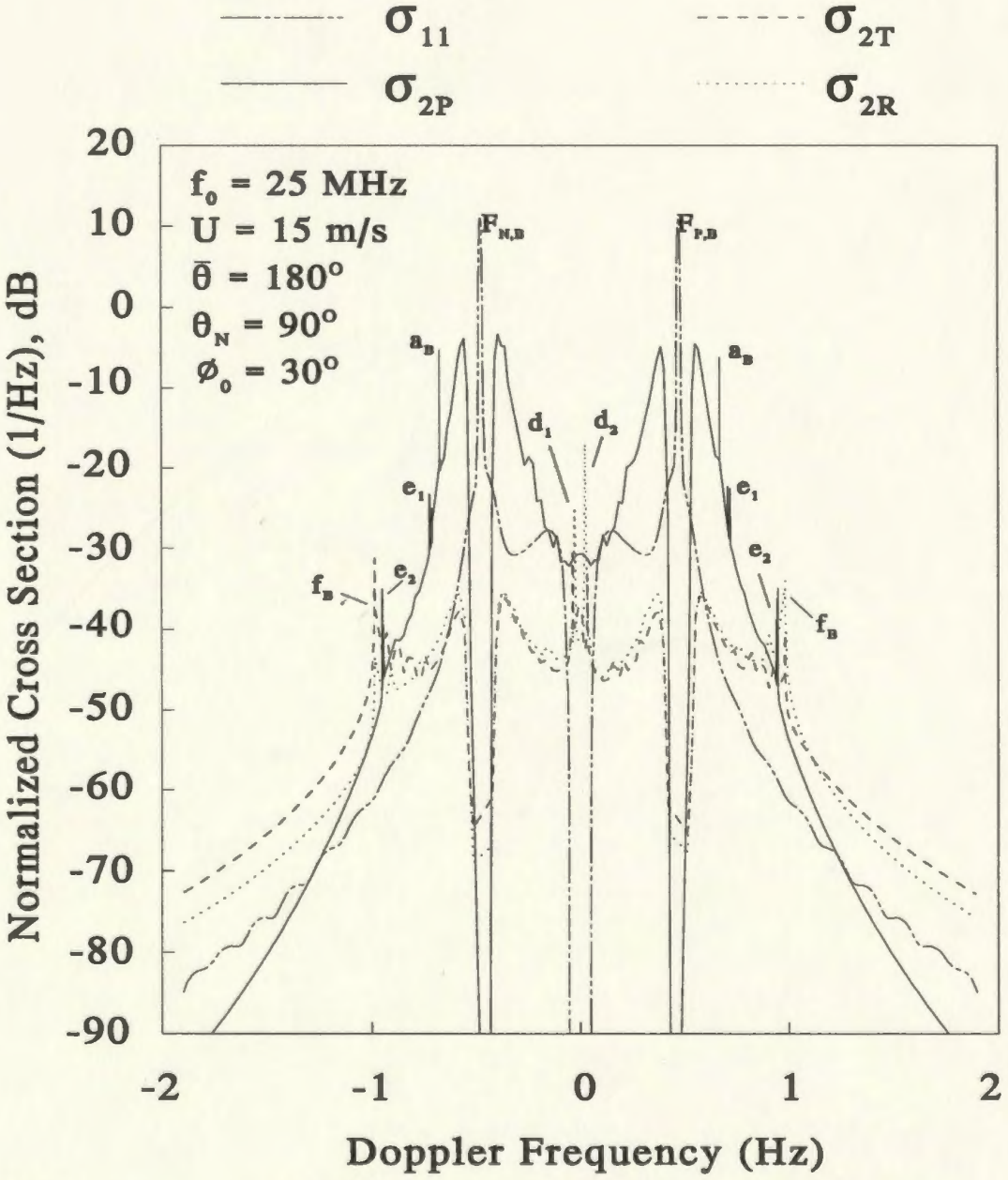

Figure 3.5a: An example of the components of the bistatic cross section. The various parameters and the labelled spectral peaks are discussed throughout Section 3.6.6.

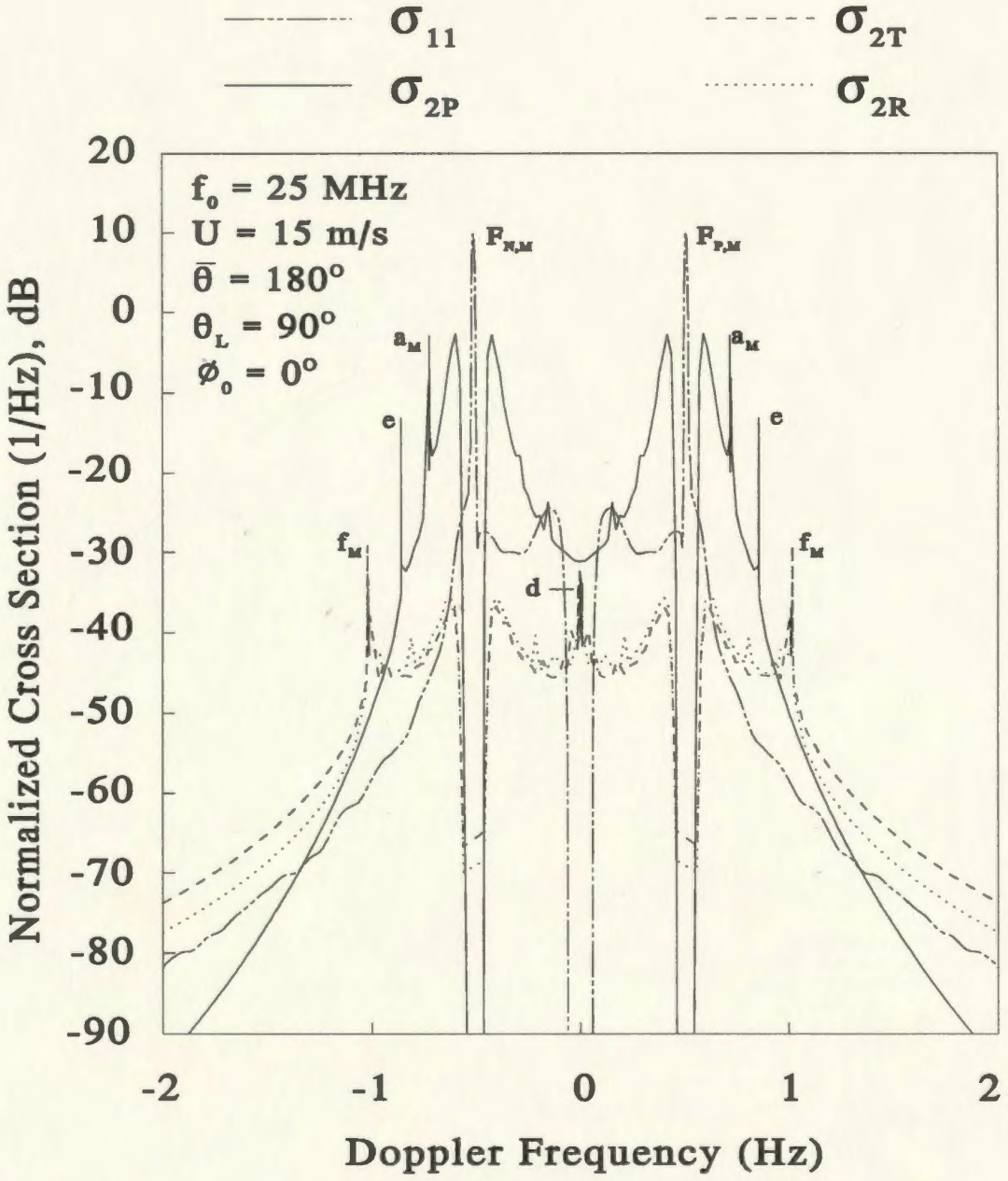

Figure 3.5b: An example of the components of the monostatic cross section. The various parameters and the labelled spectral peaks are discussed throughout Section 3.6.6.

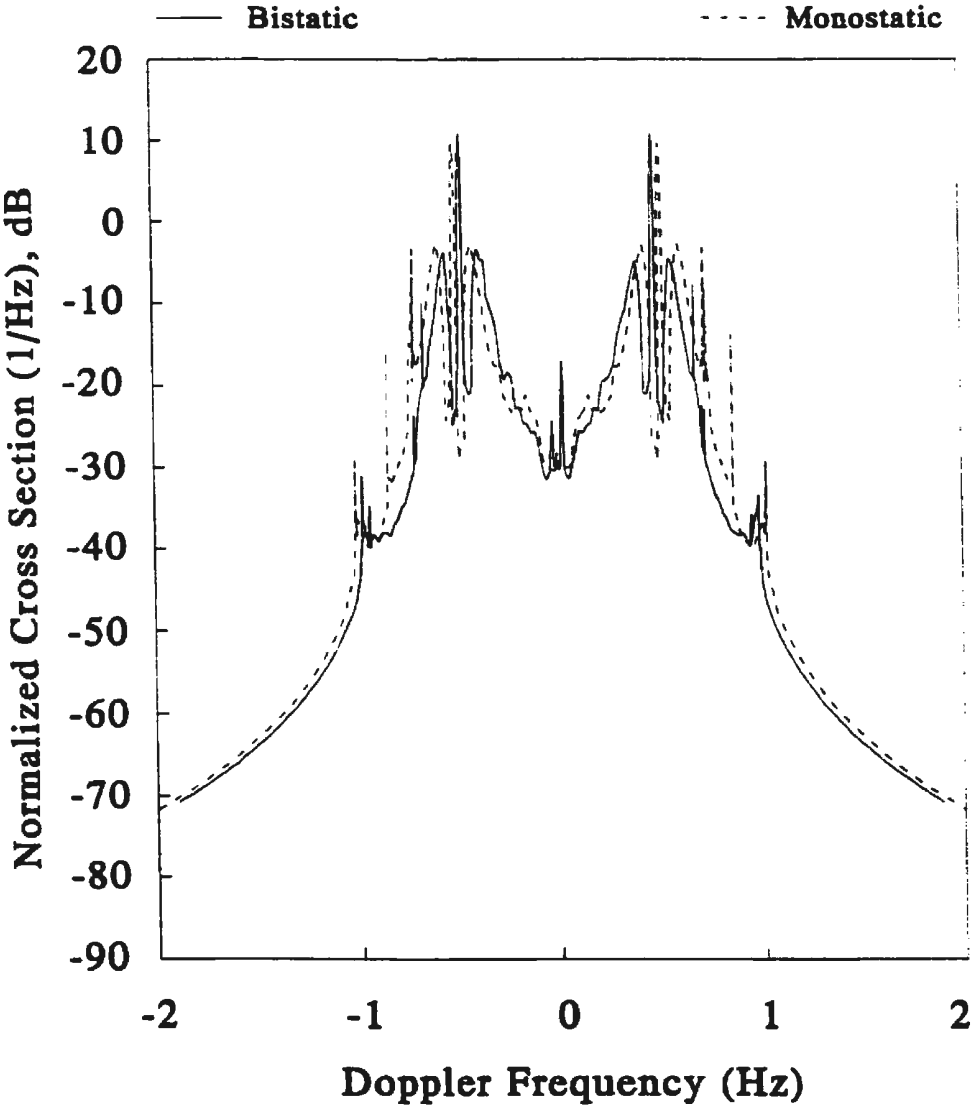

Figure 3.5c: The combined components of Figures 5a and 5b.

The electromagnetic "corner reflector" peaks $e_1(\approx \pm 0.9489$ Hz) and $e_2(\approx \pm 0.7210$ Hz) for bistatic operation are seen to collapse to a single $2^{\frac{3}{4}}\frac{\omega_B}{2\pi}(\approx \pm 0.8575$Hz) at e for the monostatic configuration. In both cases, there are two contributions to peaks at f_B and f_M due to scattering occurring at the transmitting and receiving antennas. For the illustration here, as dictated by equations (3.129) or (3.139) and (3.130), $f_B \approx \pm 0.9843$ Hz and $f_M \approx \pm 1.020$ Hz. Finally, from the same equations, the split singularities near zero Doppler at d_1 and d_2 ($\approx \pm 0.0354$ Hz) for bistatic operation are seen to degenerate to a single peak, d, (at 0 Hz) in Figure 5.3b.

Figure 5.3c is simply a repetition of 5.3a and 5.3b in which all portions of the cross section have been combined. The relative positions of the bistatic and monostatic features discussed above are evident. Apart from these singularities, however, the cross section when the wind is perpendicular to the ellipse normal at the scattering patch in the bistatic model is clearly very similar to when the wind is normal to the look direction in monostatic operation. In each case the ocean wave energy is mapped to the cross section in an essentially symmetric fashion. A small deviation in this for the bistatic case is discussed in note 3 below.

Implicit in the considerations above is that the monostatic radar may interrogate a surface region independently of the bistatic radar. Otherwise, in general, the comparison of a wind direction relative to boresight in the former case could not have been compared to the same relative direction to the ellipse normal in the latter. What is more practical, however, is to have a transmitter (T) and receiver (R) at one radar site and a receiver (R) at another (see inset of Figures 3.6a and 3.6b). These figures illustrate the following important observation: due to symmetry, two winds of equal magnitude but different direction which have identical components along the bistatic normal provide essentially the same bistatic cross section. However, this wind will, in general, have an inward component along the boresight of the monostatic radar (whose scatter geometry is indicated by the double-headed arrow) in one instance

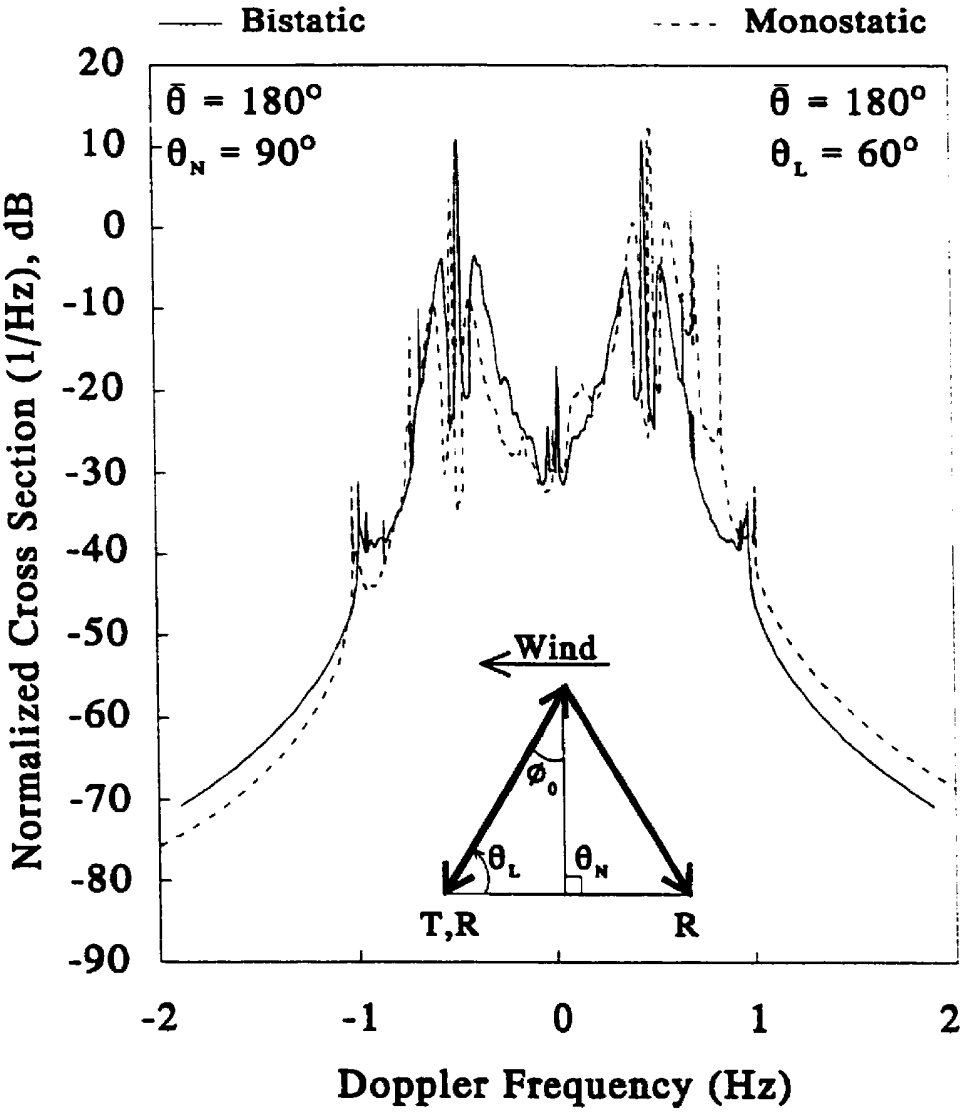

Figure 3.6a: Monostatic and bistatic cross sections for a wind direction of 180° when the transmitter (T) and receiver (R) geometry is as shown.

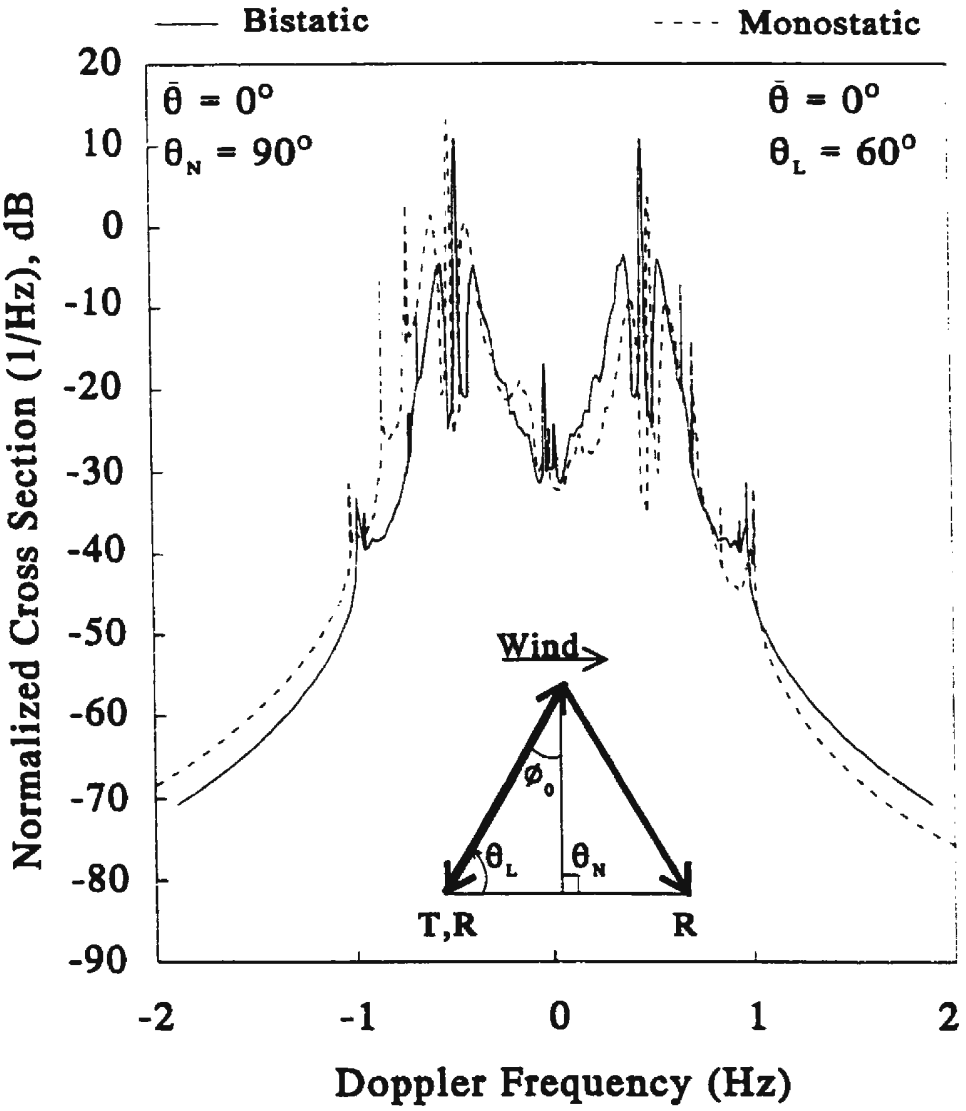

Figure 3.6b: Monostatic and bistatic cross sections for a wind direction of 0° when the transmitter (T) and receiver (R) geometry is, as shown, the same as in Figure 3.6a.

and an outward component, which may be different in magnitude, in the other. This latter fact is indicated by an increase in the positive monostatic Doppler cross section (Figure 3.6a) when a wind component lies inward along the boresight and a similar enhancement in the negative Doppler region (Figure 3.6b) when the wind has a component outward along the boresight. Thus, simultaneous bistatic and monostatic operation, which involves one transmitter but two receivers, provides a method of removing the directional ambiguities inherent in single-site observations of the ocean surface.

2. The Effects of Wind Speed on the Bistatic Cross Section

Since wind speed is the chief factor determining the gravity wave spectral energy, it is not surprising, as has been extensively investigated for monostatic radars, that it will significantly affect the magnitude of the bistatic cross sections. Figure 3.7 indicates this effect for wind speeds of 5, 10 and 15 m/s.

An initial observation is that the strength of the bistatic Bragg frequencies and the tails of the spectra are nearly identical for the three cases shown. For a 25 MHz signal and a bistatic angle of 30° the Bragg wavelength $\left(= \frac{2\pi}{2k_0 \cos\phi_0}\right)$ is about 6.93 m. In the Pierson-Moskowitz spectrum, this wave appears in the high frequency end which is saturated for any wind speed greater than a few metres per second. Thus, increasing the wind speed beyond that which produces saturation in the relevant portion of the ocean spectrum will cause no change in the radar cross section of the surface. Similarly, as indicated by the delta function arguments in equations (3.94), (3.121) and (3.132), as the absolute Doppler frequency increases so do the wavenumbers of the scattering waves. Again, this dictates that the scatterers responsible for the high-Doppler tails will lie in the saturated region of the ocean spectrum and their effects on the Doppler spectrum will be largely independent of wind speed. Of course as the radar operating frequency decreases towards the lower end of the HF region, the Bragg waves increase in length (eg. for $f_0 = 5.75$ MHz and $\phi_0 = 30°$, the Bragg

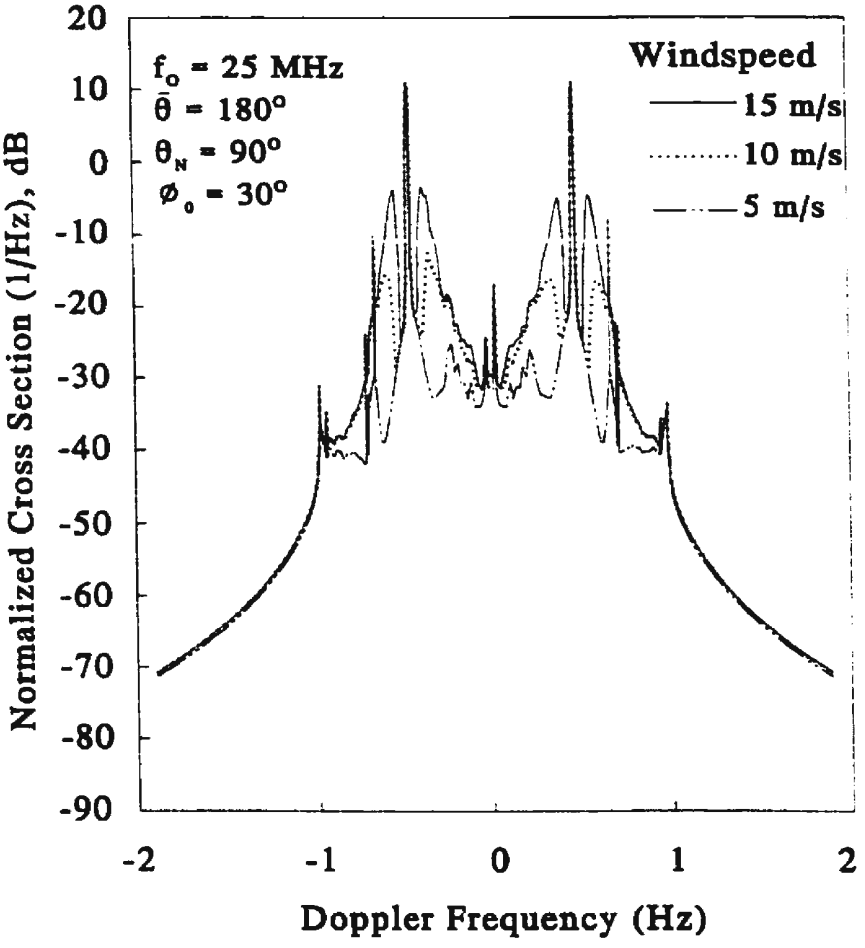

Figure 3.7: Bistatic cross sections for various wind speeds when the transmitter (T) and receiver (R) geometry is as shown in Figure 3.6a.

wavelength is 30.1 m). Still, the first-order Doppler maxima are largely unaffected by changing wind speed, again due to the saturation as discussed above.

It might also be noted, that the spectral tails, while being enhanced by the σ_{2T} and σ_{2R} portion of the cross section (see Figures 3.5a and 3.5b), fall off much more rapidly than the comparable σ_{2T} monostatic cross section developed by Srivastava [54]. In fact, beyond $\pm 2\omega_B$, the tails of Srivastava's cross sections are nearly flat, unlike what is commonly observed in the portions of the monostatic radar spectra where the

power scattered by the ocean exceeds the noise thresholds. A brief comparison of Srivastava's result and that presented here is considered in Appendix B.8.

The Doppler region of greatest importance, in an oceanographic sense, lies adjacent to the Bragg peaks for upper HF. It may be deduced from the Doppler contours of Figure 3.4, that in this near-Bragg portion, at least one of the ocean waves responsible for the second-order patch cross section, σ_{2P}, is a long wave. At higher wind speeds, these waves carry a significant amount of the spectral energy. At $U = 10$ m/s in Figure 3.7 it is seen that the peak of the region is already ≈ 10 dB below its value for 15 m/s winds, and at $U = 5$ m/s no significant amount of energy is mapped into this part of the radar spectrum (or cross section). Similar observations have been made by others (Lipa and Barrick [84], Gill [85]). At the corner reflector and other peaks discussed earlier, the wind speed is not a significant factor in determining the cross section content for the operating frequency shown. The effect which changing the operating frequency has on these regions is examined in relation to Figure 3.9 below.

3. The Effect of Wind Direction on the Bistatic Cross Section

Figure 3.8 portrays how the wind direction influences the cross section. In each graph shown, the operating frequency is 25 MHz, the bistatic angle is 30° and the normal to the scattering ellipse is 90°. The wind direction, $\bar{\theta}$, is measured counterclockwise from the positive x–axis.

One obvious feature in Figure 3.8 is the antisymmetry produced by changing the wind direction from $\bar{\theta}$ to $\bar{\theta} + 180°$ (vertical pairs of graphs). Of course, such a change is also equivalent to 180° change with respect to the ellipse normal. Then, what has been previously observed for wind direction relative to a narrow beam for a monostatic configuration (eg., see Lipa and Barrick [84]) translates to the effect of wind direction relative to the ellipse normal for bistatic operation. For example, since $\theta_N = 90°$, here, $\bar{\theta} = 90°$ means that the wind is *outward* along the normal, and, as can be seen,

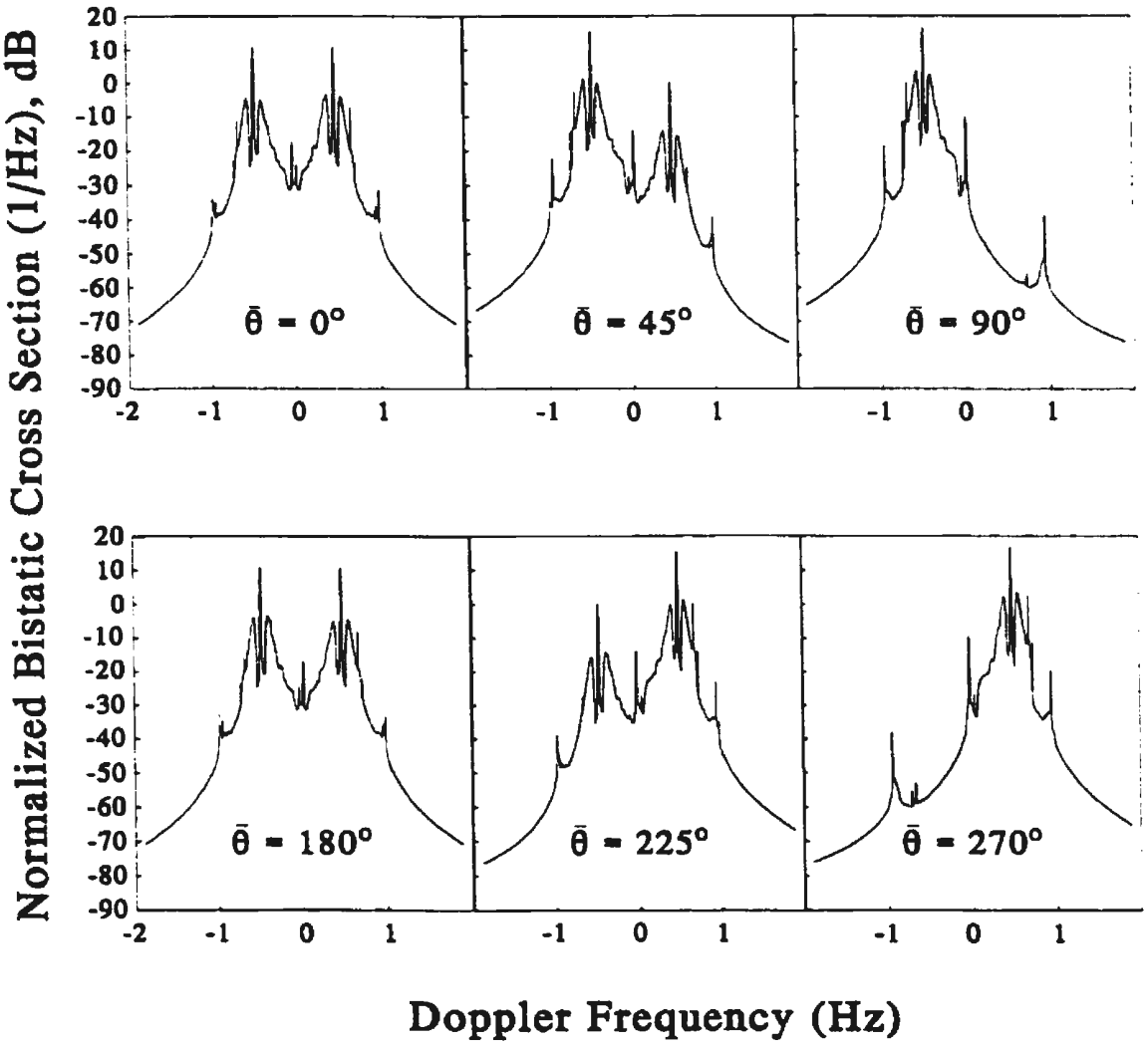

Figure 3.8: The effect on the bistatic cross sections of changing wind direction, $\bar{\theta}$. The operating frequency is 25 MHz, the bistatic angle is 30°, the ellipse normal is 90° and the wind speed is 15 m/s.

almost all of the spectral energy is in the negative Doppler region. Then, for $\bar{\theta} = 270°$, the wind, and, thus the wave direction maximum, is *inward* along the normal and the positive Doppler section is enhanced.

As well, it is clear that the relative importance of the spectral peaks depends on the wind direction. For example, when $\bar{\theta} = 270°$, the wind is directly inward along the ellipse normal and also has a substantial component along the direction from the "patch" to the receiver. The backscatter at the receiver can therefore occur from an relatively energetic Bragg wave and produce a substantial spectral peak near zero Doppler. On the other hand, when $\bar{\theta} = 0°$, the wind is 90° to the ellipse normal and also makes a larger angle with the line from the patch to the receiver. Thus, the peak near zero Doppler produced by scatter at the receiver will not be as large as for $\bar{\theta} = 270°$. Discussion of the other second-order peaks could similarly follow.

At this point, it might also be observed that the spectral peaks produced near zero Doppler in the σ_{2T} cross section do not appear to be the same size as their counterparts in σ_{2R}. This difference will be accentuated for some wind directions. In general, the direction which the wind makes with the line joining the transmitter to the patch will not be same as it is relative to the direction from the patch to the receiver. This would manifest itself in the radar spectrum as peaks of differing heights. It should also be observed, however, that the coupling coefficient in the σ_{2T} expression was not derived in exactly the same way as that for σ_{2R} (see Sections 2.2.2.3 and 2.2.3.2 and related appendices), and, while the important features are very similar (eg. location of peaks and overall contribution to the cross section) slight differences are to be expected.

4. Comparison of Cross Sections for Differing Operating Frequency

Figure 3.9 displays the cross sections for three values of operating frequency. The bistatic angle, wind speed, and the wind direction relative to the scattering ellipse normal are fixed at 30°, 15 m/s and −90° respectively. It is clear that the first-order

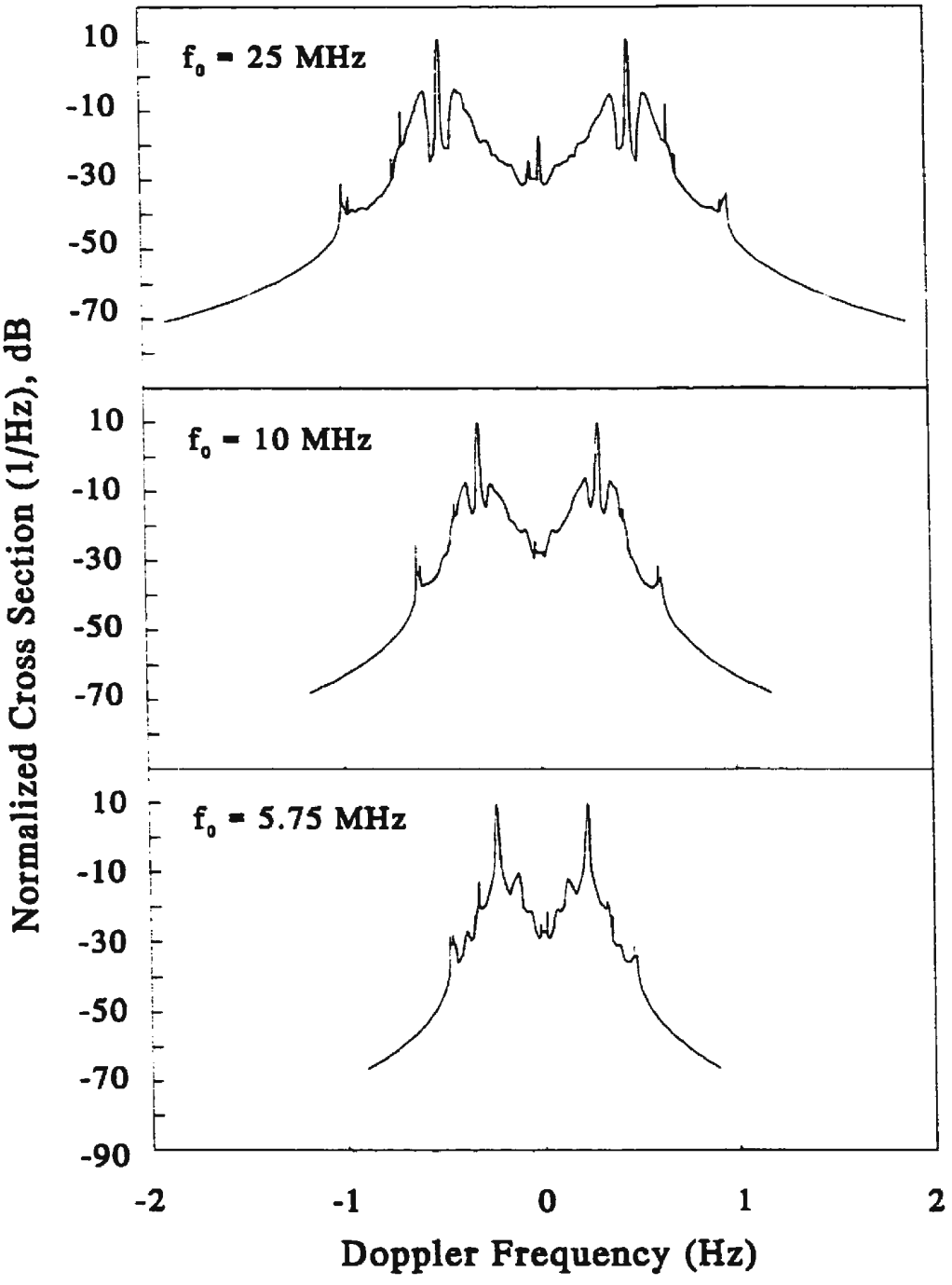

Figure 3.9: The effect on the bistatic cross sections of changing the operating frequency, f_0. The wind direction is 180°, the bistatic angle is 30°, the ellipse normal is 90° and the wind speed is 15 m/s.

maxima, while shifted in Doppler, are of comparable magnitudes. Again, this is due to the fact, that for moderate bistatic angles, the ocean waves producing these peaks are generally in the high frequency, saturated region of the ocean spectrum across the entire HF band (3–30 MHz).

Obvious and important differences occur in the second-order region of the cross sections. At the high end of the HF band, as illustrated by the 25 MHz result, much of the ocean spectral energy is mapped to the near Bragg regions. However, as the operating frequency drops so does the energy content of these regions if the other parameters are unchanged. Thus, for example, in the 5.75 MHz cross section, for the wind speed given, much of the ocean spectral energy is mapped to Doppler outside the $\sqrt{2}$ singularities. It may be noted that, in the extended Doppler regions, the cross section integrands are highly nonlinear in wavenumber and for this reason the lower HF frequencies are not as practical as the higher ones for ocean wave parameter estimation (see Gill *et al.*, [2]).

While, in general, the cross section is smaller at the lower HF frequencies, there are clearly regions where this is not the case. Notably, near zero Doppler where, according to the delta function constraints discussed earlier, long energetic ocean waves are involved in the scatter, the cross sections for each frequency are of comparable values. Also, near the singularities examined in relation to Figure 3.5a and b, the cross sections are similarly affected.

It has been noted that the actual spikes due to scatter near the receiver or transmitter require ocean behind these radar components. Where this is not true, there can still be a "levelling off" effect in the cross section as the scatter occurs in directions other than that required for backscatter (see discussion in Sections 3.6.4 and 3.6.5). Figure 3.10 provides a depiction of this for actual monostatic radar measurements of the ocean surface. Figure 3.10a is taken from Gill *et al.* [2] where the operational

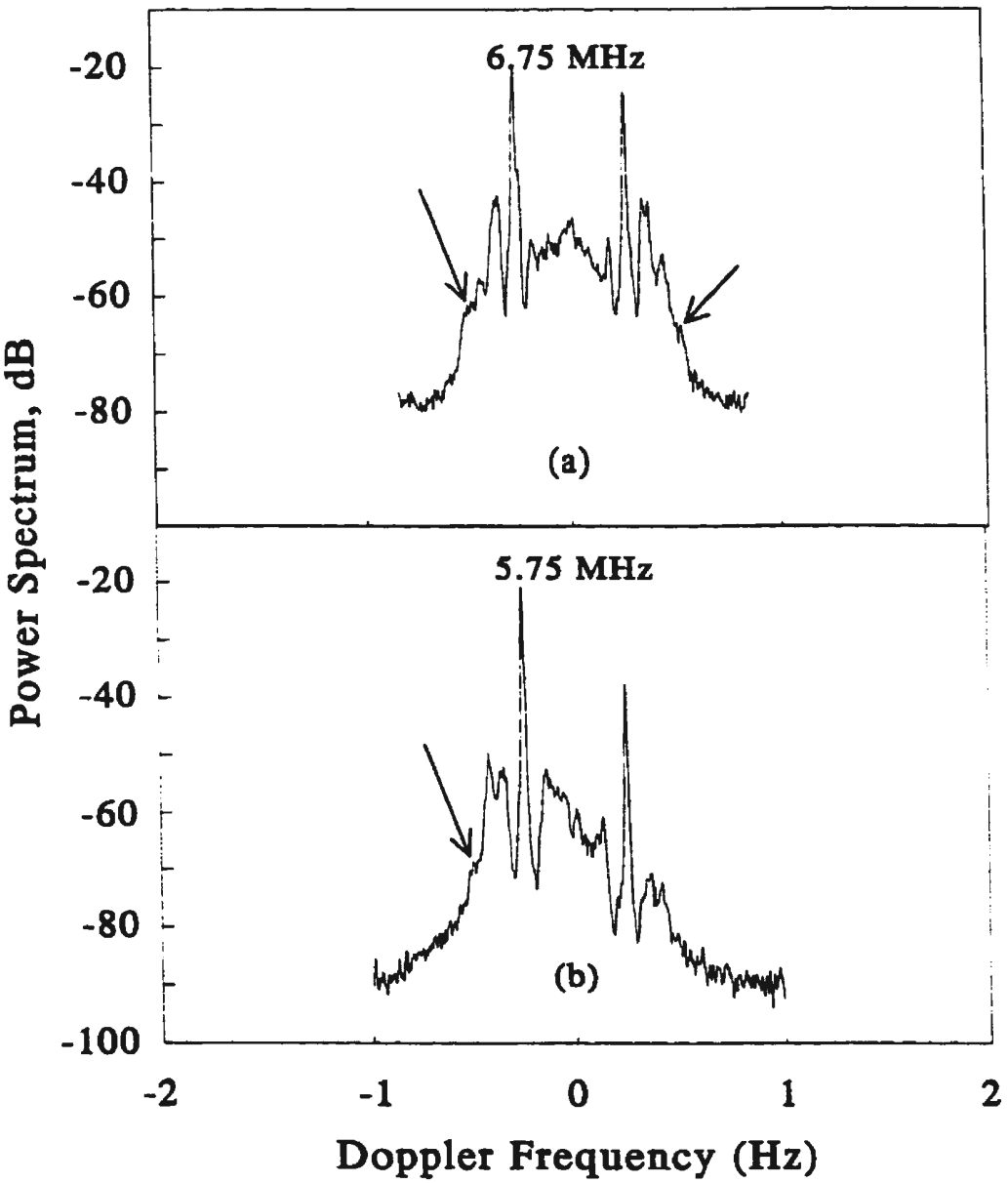

Figure 3.10: Real monostatic spectra with the (2×Bragg Frequency) regions indicated by bold arrows.

frequency was 6.75 MHz, while 3.10b, for a frequency of 5.75 MHz, was gathered by Northern Radar Systems Limited at Cape Race, Newfoundland during a November, 1995 ship trial experiment under contract from Defense Research Establishment, Ottawa. There is, therefore, evidence that even in monostatic operation with land based equipment, the σ_{2T} and σ_{2R} cross section components prevent the cross section tails from decreasing as rapidly as dictated by the patch scatter alone, especially in the regions of expected singularity at $\pm 2\omega_B$. As with the simulations, the effects are more noticeable in that half of the Doppler cross sections favoured by the directional characteristics of the ocean wave spectrum. The increase in energy at zero Doppler appears evident in Figure 3.10a but not in 3.10b. Further experimentation dedicated to examining the effects theorized here are required in order that some conclusive statement may be made regarding the relative importance of the scatter at the transmitter or receiver under a variety of operating conditions.

5. The Consideration of Large Bistatic Angles

We have seen from the theory, the radian Bragg frequency $\omega_B = \sqrt{2gk_0 \cos\phi_0}$ so that as $\phi_0 \rightarrow 90°$, $\omega_B \rightarrow 0$. Furthermore, as $\phi_0 \rightarrow 90°$, the Bragg wavelength, $\lambda_B \rightarrow \infty$. From these observations it is not surprising that for large ϕ_0 (but $< 90°$) the entire cross section (and not simply the first-order component) should be substantially reduced when compared to the monostatic ($\phi_0 = 0°$) case or to the case of more moderate bistatic angles. Figure 3.11 depicts this for an operating frequency of 25 MHz, wind speed of 15 m/s, an ellipse normal of 90° and a wind direction of 0° (i.e. $-90°$ to normal). Under these stipulations each bistatic angle corresponds to scatter from a different position on the scattering surface which is still assumed to be homogeneous.

At $\phi_0 = 80°$, in Figure 3.11, there is a small contribution from σ_{2P} as is evidenced by the peaks in the continuum adjacent to the Bragg regions. These have virtually disappeared when $\phi_0 = 85°$. However, there is not a significant reduction in the σ_{2T}

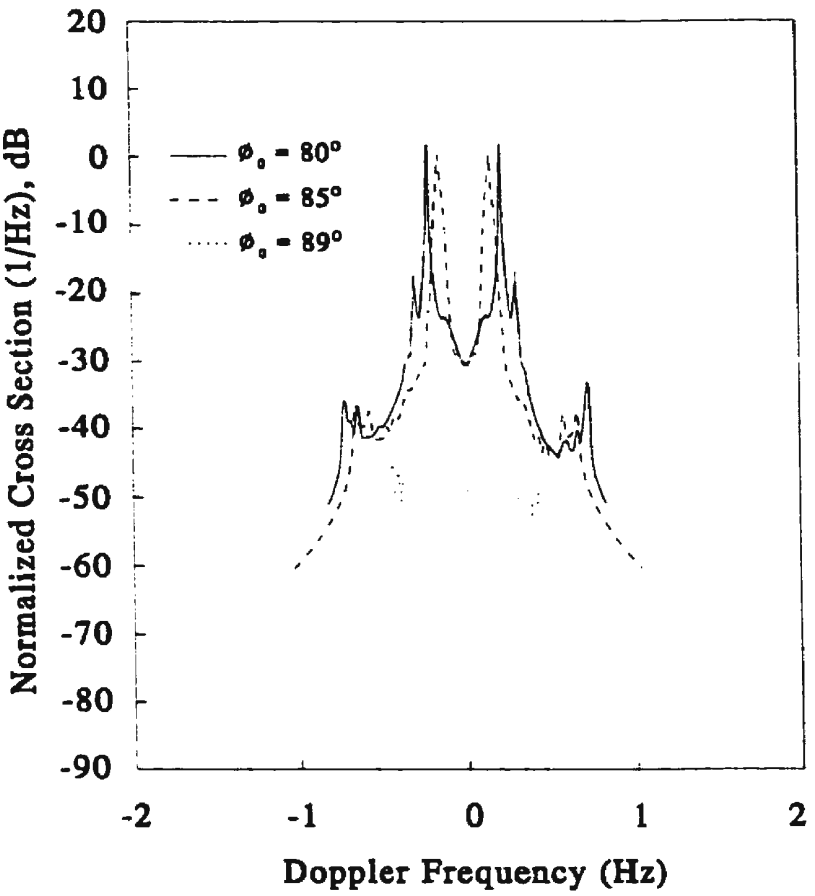

Figure 3.11: The effect on the total bistatic cross sections of increasing the bistatic angle, ϕ_0. The wind direction is $-90°$ to the ellipse normal in each instance. The operating frequency is 25 MHz and the wind speed is 15 m/s.

and σ_{2R} levels at $\phi_0 = 80°$, 85° as compared to those for $\phi_0 = 30°$ (see Figure 3.7, for example). It should be remembered that in these components there is a strong backscatter possible at either the transmitter or receiver, but even this is overpowered by the $\cos\phi_0$ factor when ϕ_0 approaches 90° (see the $\phi_0 = 89°$ curve).

It may be easily verified that the σ_{2P}, which is the largest portion of the second-order continuum adjacent to the first-order peaks, is dominated by a single scatter from second-order waves as discussed in Section 3.3. This is depicted in Figure 3.12, where the combined electromagnetic and hydrodynamic terms of σ_{2P} (included in the ${}_s\Gamma_P$ coupling coefficient) are compared with the σ_{2P} when only the hydrodynamic coupling coefficient, ${}_H\Gamma$, of equation (3.18) is used. However, it is shown in Appendix

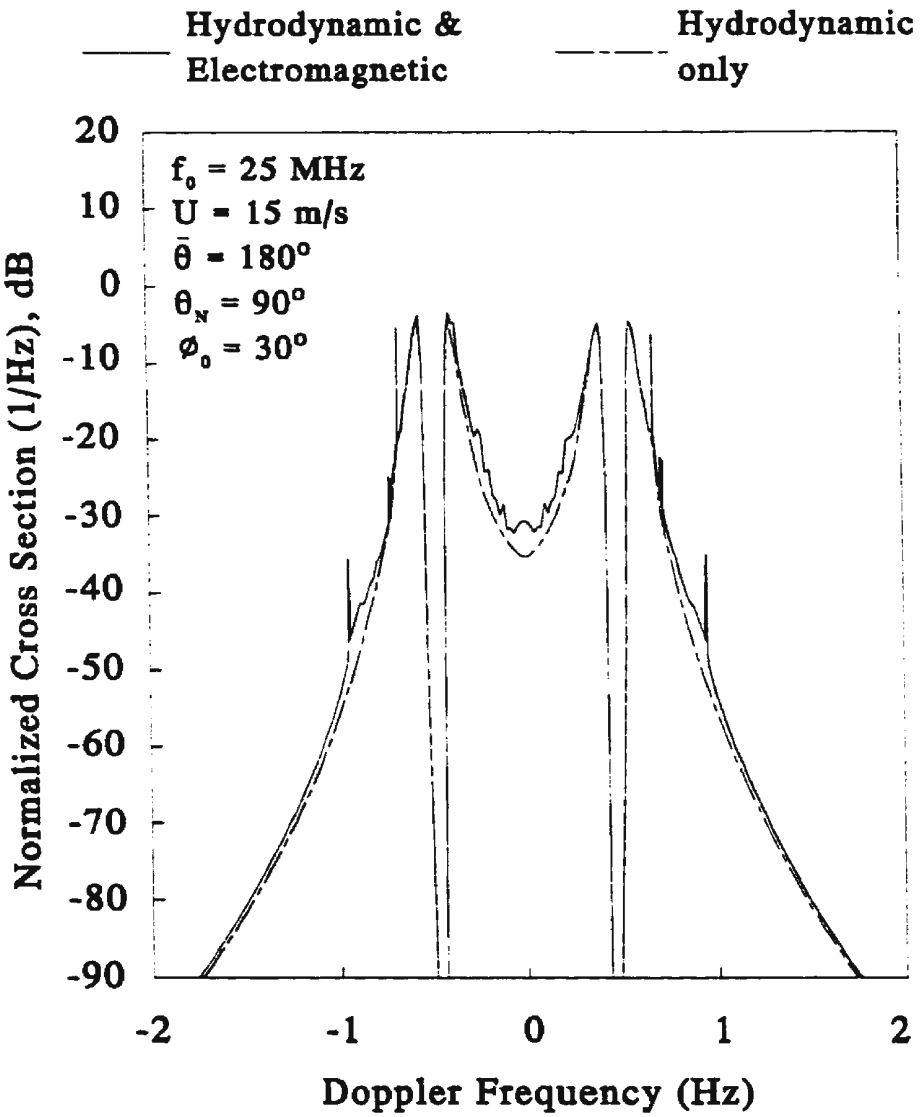

Figure 3.12: A comparison of the sum of the electromagnetic and hydrodynamic effects with the hydrodynamic contribution only for the bistatic patch scatter cross section, σ_{2P}.

B.9, that ${}_H\Gamma \rightarrow 0$ as $\phi_0 \rightarrow 90°$. This, therefore, explains why even σ_{2P} becomes very small as the condition of forward scatter (i.e. large bistatic angle) is approached.

3.7 General Chapter Summary

This chapter has been devoted to applying the theory developed in Chapter 2 to the ocean surface. After a brief discussion of the relevant ocean gravity wave characteristics, the pulsed radar field equations were adjusted to account for a time varying

random scattering surface. Without appealing to a particular beam form for the transmitting antenna, the received power spectral density and, subsequently, the cross sections of the ocean per unit surface area were developed to second order. By virtue of the field equations, the total cross section contains four components consisting of: (1) a first-order portion arising from a single scatter from first-order surface waves; (2) a second-order component which itself consisted of a single scatter from second-order surface features and two first-order scatters; (3) a second-order term due to a scatter near the transmitting antenna followed by another at a remote patch of ocean; and (4) a final second-order expression as a consequence of a scatter at a remote patch followed by another near the receiving antenna. Of course these components, while being mathematically separate entities, can be obtained only as a combined sum at the receiving antenna.

Finally, the interesting features of the bistatic cross section were explored. A variety of parameters impinging on the nature of the cross section were examined. These include operating frequency, wind speed and direction, and the bistatic angle. While many combinations of these parameters are possible, this chapter sought to delineate a representative sample of the effects which their values have upon the cross section. Also, comparisons verifying that the bistatic cross sections here essentially reduce, with the appropriate geometry, to their monostatic counterparts, where the latter exist, were carried out. A cursory comparison with real (monostatic) data (see Figure 3.10) indicates that the major spectral properties suggested by the analysis manifest themselves in measured radar spectra. Also, from [8] it may be noted that the continuum beyond the Bragg peaks in the monostatic case appears to be well described by the second-order theory. Consequently, third and higher order effects were not addressed here.

In the following chapter, an attempt is made to quantify the effect which ambient noise has upon the cross section attributes discussed previously.

Chapter 4

A Model for the Signal to Noise Ratio for Scattering from the Ocean Surface Assuming a Pulsed Radar

4.1 Introduction

Using the basic theory in Chapter 2, the first- and second-order cross sections of the ocean surface were derived and illustrated in Chapter 3. However, to this point in the analysis, no indication of the actual received power due to scatter from a remote surface patch has been given. Based on the radar range equation (3.65), it is clear that this quantity will depend upon the distances of the patch from the radar components, the frequency (or wavelength) of transmission, the gains of the antennas, the transmitted power, the attenuation functions and the scattering cross section. Still, even if these quantities are known, there is no assurance that all of the features described in the previous chapter will always be visible in the radar power spectrum. One of the major reasons for this is the fact that any received signal is contaminated, to some extent, by noise.

The purpose of this chapter is to present a suitable model for the ocean clutter signal to noise ratio ($(\mathrm{SNR})_c$) for a pulsed radar. By "ocean clutter" is meant the HF radiation scattered from the sea surface. This will involve characterizing first

the noise signal and, subsequently, its spectral density as observed in a pulsed radar system. The analysis proceeds on the assumption of an ideal, externally noise limited, system. The aliasing due to noise undersampling will flow naturally from the analysis.

In the body of this chapter, the noise spectral density is first calculated on the basis of a finite number of pulses and the noise is assumed to be statistically stationary. The analysis is then extended to an infinite number of pulses. An alternative analysis for the latter, which may be used to verify the initial result, is shown in Appendix C.1. Secondly, a non-stationary noise model for both finite and infinite numbers of pulses is considered.

In addition to a noise spectral density, it is necessary to derive the proper analogous form of the clutter power spectral density received from the ocean surface. The ratio of the two spectral densities so determined will then constitute a useful SNR model for pulsed HF radar interrogation of an ocean environment. The noise spectral density will be shown to be a constant for the characterization considered and, rather than explicitly calculating the SNR at every Doppler frequency, it is more convenient to graphically illustrate the simultaneous noise and clutter power spectral densities.

Finally, to reflect what generally occurs in practice, a time domain representation of the combined clutter and noise is considered. The standard procedure of Fourier transforming this result to obtain an estimate of the total Doppler power spectral density due to scatter from the ocean, in the presence of external noise, is then conducted. The details of this are outlined in Appendix C.2 with illustrations and further discussions occurring in Section 4.5.3.

4.2 Characterization of the Noise Voltage and Spectral Density – Stationary Noise

In the HF band, the external noise power may arise from a combination of atmospheric, galactic and man-made sources [86]. It shall be assumed, as in [86], that the

noise is a stationary Gaussian white process and is understood to have zero mean. From Pierson's model [61] for a stationary Gaussian process in one variable, the ambient noise voltage, $n_a(t)$, may be cast, using the complex exponential, as

$$n_a(t) = \int_{\omega'} \left[h\left(\omega' + \frac{B}{2}\right) - h\left(\omega' - \frac{B}{2}\right) \right] e^{j\omega' t} e^{j\epsilon(\omega')} \sqrt{S_N(\omega') \frac{d\omega'}{2\pi}} \qquad (4.1)$$

where t is time, ω' is radian frequency ($= 2\pi f'$), $S_N(\omega')$ is the power spectral density of the noise, $\epsilon(\omega')$ is the random phase uniformly distributed on the interval 0 to 2π, and $h[\cdot]$ is the Heaviside function introduced to account for the fact that any receiving system will have a limited noise bandwidth, B. The integral limits may be understood to be over the entire set of real numbers, but only $-\frac{B}{2} < \omega' < \frac{B}{2}$ actually contribute to a non-zero integrand.

4.2.1 The Noise Power Spectral Density for a Finite Pulse Train

In this section, a finite pulse train is considered. Initially, we construct a series of $(2q + 1)$ pulses by gating an infinite sequence of pulses as illustrated in Figure 4.1. With the assumptions on the nature of the noise as given in equation (4.1), this truncated version may be characterized as

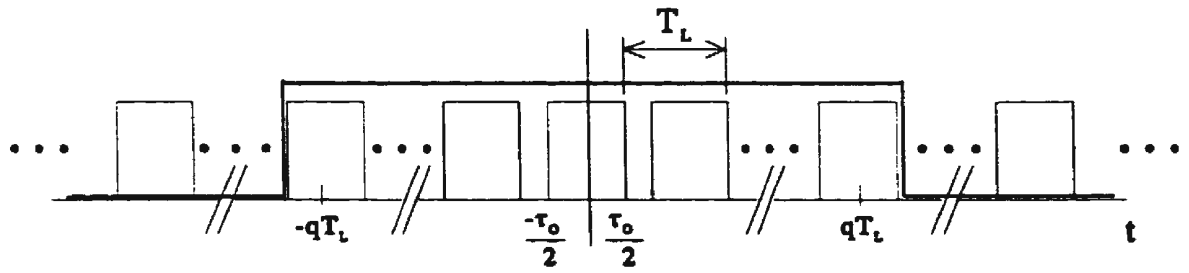

Figure 4.1: A finite pulse train containing $2q + 1$ pulses. The pulse width is τ_0 and the pulse repetition period is T_L.

$$
\begin{aligned}
n(t)) \;=\; & \left[h\left(t+qT_L+\frac{\tau_0}{2}\right)-h\left(t-qT_L-\frac{\tau_0}{2}\right)\right] \\
& \cdot \sum_{m=-\infty}^{\infty}\left[h\left(t-mT_L+\frac{\tau_0}{2}\right)-h\left(t-mT_L-\frac{\tau_0}{2}\right)\right] \\
& \cdot \int_{\omega'}\left[h\left(\omega'+\frac{B}{2}\right)-h\left(\omega'-\frac{B}{2}\right)\right] e^{j\omega' t}e^{j\epsilon(\omega')}\sqrt{S_N(\omega')\frac{d\omega'}{2\pi}} \,. \qquad (4.2)
\end{aligned}
$$

From here, an autocorrelation of $n(t)$ is sought so that, on Fourier transforming the result, a power spectral density may be obtained. The randomness in (4.2) appears only in the phase exponential, and given that the ensemble average,

$$
< e^{j\epsilon(\omega_1')}e^{-j\epsilon(\omega_2')} >= \begin{cases} 1, & \omega_1'=\omega_2'=\omega' \\ 0, & \text{otherwise}, \end{cases}
$$

the autocorrelation, $\mathcal{R}_{N_f}(t_1,t_2)$, for a finite number of pulses is given by

$$
\begin{aligned}
\mathcal{R}_{N_f}(t_1,t_2) \;=\; & < n(t_1)n^*(t_2) >= \left[h\left(t_1+qT_L+\frac{\tau_0}{2}\right)-h\left(t_1-qT_L-\frac{\tau_0}{2}\right)\right] \\
& \cdot \left[h\left(t_2+qT_L+\frac{\tau_0}{2}\right)-h\left(t_2-qT_L-\frac{\tau_0}{2}\right)\right] \\
& \cdot \sum_{m=-\infty}^{\infty}\sum_{n=-\infty}^{\infty}\left[h\left(t_1-mT_L+\frac{\tau_0}{2}\right)-h\left(t_1-mT_L-\frac{\tau_0}{2}\right)\right] \\
& \cdot \left[h\left(t_2-nT_L+\frac{\tau_0}{2}\right)-h\left(t_2-nT_L-\frac{\tau_0}{2}\right)\right] \\
& \cdot \int_{-\frac{B}{2}}^{\frac{B}{2}} e^{j\omega'(t_1-t_2)}S_N(\omega')\frac{d\omega'}{2\pi} \,. \qquad (4.3)
\end{aligned}
$$

Putting $\tau = t_1 - t_2$ and $t_2 = t$ and Fourier transforming with respect to τ gives, after some algebra, the noise power spectral density expression, $\mathcal{P}_{N_f}(\omega,t)$, as

$$
\begin{aligned}
\mathcal{P}_{N_f}(\omega,t) \;=\; & \left[h\left(t+qT_L+\frac{\tau_0}{2}\right)-h\left(t-qT_L-\frac{\tau_0}{2}\right)\right] \\
& \cdot \sum_{n=-\infty}^{\infty}\left[h\left(t-nT_L+\frac{\tau_0}{2}\right)-h\left(t-nT_L-\frac{\tau_0}{2}\right)\right] \\
& \cdot \int_{-\frac{B}{2}}^{\frac{B}{2}}\sum_{m=-q}^{q}\int_{-\infty}^{\infty}\left[h\left(\tau+t-mT_L+\frac{\tau_0}{2}\right)-h\left(\tau+t-mT_L-\frac{\tau_0}{2}\right)\right] \\
& \cdot e^{j(\omega'-\omega)\tau}S_N(\omega')d\tau\frac{d\omega'}{2\pi} \,. \qquad (4.4)
\end{aligned}
$$

Here, ω is the transform variable and is, physically, the radian Doppler noise frequency and is completely analogous to ω_d as discussed in Section 3.4.1. A further change of variables using $\tau_1 = \tau + t$ produces

$$\begin{aligned}\mathcal{P}_{N_f}(\omega,t) &= \left[h\left(t+qT_L+\frac{\tau_0}{2}\right)-h\left(t-qT_L-\frac{\tau_0}{2}\right)\right] \\ &\cdot \sum_{n=-\infty}^{\infty}\left[h\left(t-nT_L+\frac{\tau_0}{2}\right)-h\left(t-nT_L-\frac{\tau_0}{2}\right)\right] \\ &\cdot \int_{-\frac{B}{2}}^{\frac{B}{2}} \sum_{m=-q}^{q}\left\{\int_{-\infty}^{\infty}\left[h\left(\tau_1-mT_L+\frac{\tau_0}{2}\right)\right.\right. \\ &\left.\left.-h\left(\tau_1-mT_L-\frac{\tau_0}{2}\right)\right]e^{j(\omega'-\omega)\tau_1}d\tau_1\right\}e^{-j(\omega'-\omega)t}S_N(\omega')\frac{d\omega'}{2\pi} \quad (4.5)\end{aligned}$$

The τ_1 integral in equation (4.5) may be easily shown to evaluate to

$$\left\{\int_{-\infty}^{\infty}\ldots d\tau_1\right\} = \tau_0 e^{j(\omega'-\omega)mT_L}\mathrm{Sa}\left[(\omega'-\omega)\frac{\tau_0}{2}\right] . \quad (4.6)$$

Now, $\sum_{m=-q}^{q} e^{jmT_L(\omega'-\omega)}$ is a geometric progression whose first term is $e^{-jqT_L(\omega'-\omega)}$, whose constant ratio is $e^{jT_L(\omega'-\omega)}$, and which contains $(2q+1)$ terms. This summation over m may therefore be reduced to

$$\frac{\sin\left[\frac{(\omega'-\omega)(2q+1)T_L}{2}\right]}{\sin\left[\frac{(\omega'-\omega)T_L}{2}\right]} . \quad (4.7)$$

Applying (4.6) and (4.7) to equation (4.5), the power spectral density is

$$\begin{aligned}\mathcal{P}_{N_f}(\omega,t) &= \left[h\left(t+qT_L+\frac{\tau_0}{2}\right)-h\left(t-qT_L-\frac{\tau_0}{2}\right)\right] \\ &\cdot \sum_{n=-\infty}^{\infty}\left[h\left(t-nT_L+\frac{\tau_0}{2}\right)-h\left(t-nT_L-\frac{\tau_0}{2}\right)\right] \\ &\cdot \tau_0\int_{-\frac{B}{2}}^{\frac{B}{2}} S_N(\omega')e^{-j(\omega'-\omega)t}\,\mathrm{Sa}\left[(\omega'-\omega)\frac{\tau_0}{2}\right] \\ &\cdot \frac{\sin\left[\frac{(\omega'-\omega)(2q+1)T_L}{2}\right]}{\sin\left[\frac{(\omega'-\omega)T_L}{2}\right]}\frac{d\omega'}{2\pi} . \quad (4.8)\end{aligned}$$

Equation (4.8) is, formally, the Doppler noise power spectral density when a finite number (i.e. $2q+1$) of pulses is sampled. It is clearly time dependent. This time dependency will now be considered in two ways: (1) the pulses are sampled at their centres and (2) the pulses are sampled in the same places relative to their leading (or

lagging) edges but not necessarily at the pulse centres.

1. Sampling at the Pulse Centre

If the sampling time occurs in the centre of a pulse at $t = pT_L$, say, where p is an integer and $|p| \leq q$ (see Figure 4.1), the first Heaviside expression reduces to unity. Furthermore, it may be noted that since $\frac{\tau_0}{2} < T_L$,

$$h\left((p-n)T_L + \frac{\tau_0}{2}\right) - h\left((p-n)T_L - \frac{\tau_0}{2}\right) = \begin{cases} 1, & p = n \\ 0, & \text{otherwise.} \end{cases} \tag{4.9}$$

This immediately implies

$$\sum_{n=-\infty}^{\infty} \left[h\left((p-n)T_L + \frac{\tau_0}{2}\right) - h\left((p-n)T_L - \frac{\tau_0}{2}\right)\right] = 1\,. \tag{4.10}$$

When sampling occurs at the pulse centre, equation (4.8) thus becomes

$$\begin{aligned} \mathcal{P}_{N_f}(\omega, pT_L) \;=\; & \tau_0 \int_{-\frac{B}{2}}^{\frac{B}{2}} S_N(\omega') e^{-j(\omega'-\omega)pT_L} \,\mathrm{Sa}\left[(\omega'-\omega)\frac{\tau_0}{2}\right] \\ & \cdot \frac{\sin\left[\frac{(\omega'-\omega)(2q+1)T_L}{2}\right]}{\sin\left[\frac{(\omega'-\omega)T_L}{2}\right]} \frac{d\omega'}{2\pi}\,. \end{aligned} \tag{4.11}$$

If matched filter conditions (eg. Barton, [79]) are assumed to exist, $B = \frac{2\pi}{\tau_0}$. Then, by defining $\alpha = \frac{(\omega'-\omega)\tau_0}{2}$ and assuming $S_N(\omega')$ to be flat (i.e. white noise), it is easy to show that

$$\mathcal{P}_{N_f}(\omega, pT_L) \approx \frac{2}{\pi} S_N(\omega') \int_0^{\frac{\pi}{2}} \cos\left[\left(\frac{2p}{d}\right)\alpha\right] \mathrm{Sa}\,[\alpha] \frac{\sin\left[\frac{(2q+1)}{d}\alpha\right]}{\sin\left[\frac{\alpha}{d}\right]} d\alpha \tag{4.12}$$

where $d = \frac{\tau_0}{T_L}$ is, by definition, the duty cycle of the radar. The fact that $B \gg \omega$ (i.e. the radar receiver bandwidth is very much greater than the Doppler bandwidth of the echo from the ocean) has been used to write the integral in this form. It may be verified numerically that (4.12) is essentially independent of p even for a small number of pulses. It will be seen in Section 4.2.2 that as the number of pulses becomes unbounded (i.e. $q \to \infty$), no explicit p-dependence remains. The chief determining factor on the overall multiplier on the ambient noise spectral density,

$S_N(\omega')$, is the duty cycle, d. Figure 4.2 gives one example of this for $q = 10$, that is a pulse train consisting of 21 pulses. The similarity with the $S_N(\omega')$ multiplier for $q \to \infty$ is depicted in Figure 4.4 of Section 4.2.2.

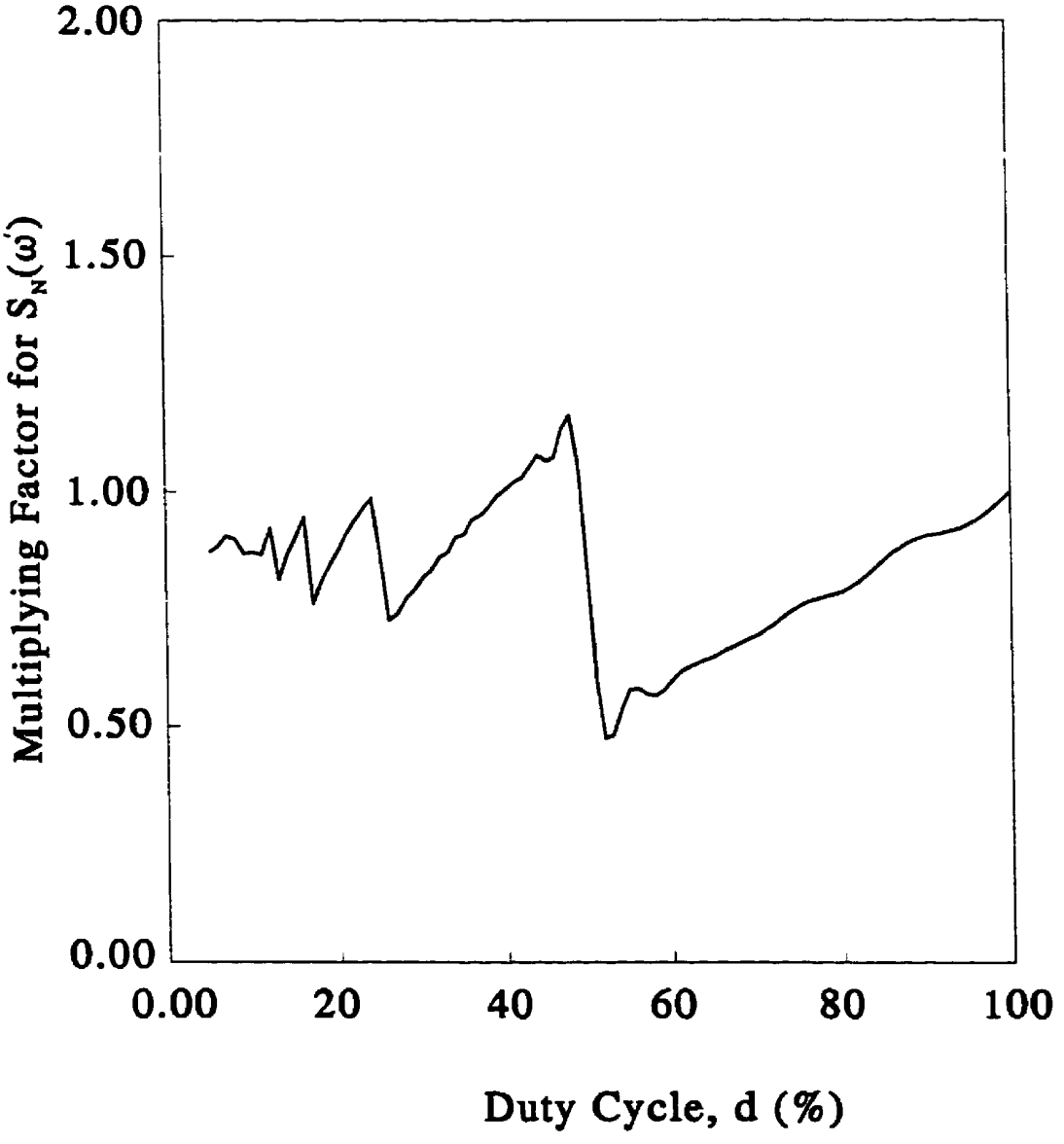

Figure 4.2: The multiplier on the ambient noise power spectral density, $S_N(\omega')$, as a function of duty cycle, d, when a sampling of 21 pulses is made.

2. Sampling the Pulse Off-centre

Suppose in Figure 4.1, the pulses are sampled at a time, t, given by

$$t = pT_L + x \text{ where } \frac{-\tau_0}{2} < x < \frac{\tau_0}{2} . \tag{4.13}$$

That is, the points of sampling are displaced by $|x|$ from the pulse centres. Equation (4.8), on including the subscript "*oc*" for "off-centre", then takes the form

$$\begin{aligned} \mathcal{P}_{N_{foc}}(\omega, t) \quad &= \left[h\left((p+q)T_L + x + \frac{\tau_0}{2}\right) - h\left((p-q)T_L + x - \frac{\tau_0}{2}\right)\right] \\ &\cdot \sum_{n=-\infty}^{\infty} \left[h\left((p-n)T_L + x + \frac{\tau_0}{2}\right) - h\left((p-n)T_L + x - \frac{\tau_0}{2}\right)\right] \\ &\cdot \tau_0 \int_{-\frac{B}{2}}^{\frac{B}{2}} S_N(\omega') e^{-j(\omega'-\omega)(pT_L+x)} \operatorname{Sa}\left[(\omega'-\omega)\frac{\tau_0}{2}\right] \\ &\cdot \frac{\sin\left[\frac{(\omega'-\omega)(2q+1)T_L}{2}\right]}{\sin\left[\frac{(\omega'-\omega)T_L}{2}\right]} \frac{d\omega'}{2\pi} . \end{aligned} \tag{4.14}$$

Now, $\frac{\tau_0}{2} < T_L$ and, in general, for a pulse radar $T_L \gg |x|$ so that

$$h\left((p-n)T_L + x + \frac{\tau_0}{2}\right) - h\left((p-n)T_L + x - \frac{\tau_0}{2}\right) = \begin{cases} 1, & p = n \\ 0, & \text{otherwise.} \end{cases} \tag{4.15}$$

Therefore, in equation (4.14), the summation may be removed since for a given p only one n gives a non-zero sum. Also, $|p| \leq q$ and $|x| < \frac{\tau_0}{2}$ so that

$$h\left((p+q)T_L + x + \frac{\tau_0}{2}\right) - h\left((p-q)T_L + x - \frac{\tau_0}{2}\right) = 1 . \tag{4.16}$$

Again, letting $\alpha = \frac{(\omega'-\omega)\tau_0}{2}$ while noting $B \gg \omega$, equation (4.14) may be written as

$$\mathcal{P}_{N_{foc}}(\omega, pT_L + x) = \frac{2}{\pi} S_N(\omega') \int_0^{\frac{\pi}{2}} \cos\left[\left(\frac{2p}{d} + \frac{2x}{\tau_0}\right)\alpha\right] \operatorname{Sa}[\alpha] \frac{\sin\left[\frac{(2q+1)}{d}\alpha\right]}{\sin\left[\frac{\alpha}{d}\right]} d\alpha . \tag{4.17}$$

When $x = 0$, i.e. when sampling occurs in the pulse centres, equation (4.17) obviously reduces to (4.12). Before further discussion on these Doppler noise power spectral densities, the case of a large number of pulses, typical of HF radar operation, is considered. In fact, it shall be considered that the number of pulses is unbounded. This proves useful in facilitating the analysis and leads to simple, valid results.

4.2.2 The Noise Power Spectral Density Assuming Infinitely Many Pulses

Here, an expression for the power spectral density, $\mathcal{P}_N(\omega, t)$, given that the number of pulses is unbounded, is sought. To this end, we let the $(2q+1)$ pulses of equation (4.8) be represented by M and seek a simplification of

$$\begin{aligned}\mathcal{P}_N(\omega,t) &= \lim_{M\to\infty}\left[h\left(t+\left(\frac{M-1}{2}\right)T_L+\frac{\tau_0}{2}\right)-h\left(t-\left(\frac{M-1}{2}\right)T_L-\frac{\tau_0}{2}\right)\right]\\ &\cdot\sum_{n=-\infty}^{\infty}\left[h\left(t-nT_L+\frac{\tau_0}{2}\right)-h\left(t-nT_L-\frac{\tau_0}{2}\right)\right]\\ &\cdot\tau_0\int_{-\frac{B}{2}}^{\frac{B}{2}}S_N(\omega')e^{-j(\omega'-\omega)t}\,\mathrm{Sa}\left[(\omega'-\omega)\frac{\tau_0}{2}\right]\\ &\cdot\frac{\sin\left[\frac{(\omega'-\omega)MT_L}{2}\right]}{\sin\left[\frac{(\omega'-\omega)T_L}{2}\right]}\frac{d\omega'}{2\pi}\,. \end{aligned} \tag{4.18}$$

We note, initially, that

$$\lim_{M\to\infty}\left[h\left(t+\left(\frac{M-1}{2}\right)T_L+\frac{\tau_0}{2}\right)-h\left(t-\left(\frac{M-1}{2}\right)T_L-\frac{\tau_0}{2}\right)\right]=1\,. \tag{4.19}$$

Next, it is appropriate to consider

$$\lim_{M\to\infty}\left\{\frac{\sin\left[\frac{(\omega'-\omega)MT_L}{2}\right]}{\sin\left[\frac{(\omega'-\omega)T_L}{2}\right]}\right\}\,. \tag{4.20}$$

It may be argued that the maximum contribution from this factor in the integrand of (4.18), for large M, will occur as

$$\sin\left[\frac{(\omega'-\omega)T_L}{2}\right]\longrightarrow 0;$$

i.e. when $\dfrac{(\omega'-\omega)T_L}{2}\to m\pi$ where m is an integer. As $M\to\infty$, the numerator in (4.20) oscillates rapidly, but the denominator varies slowly in the neighbourhood of $m\pi$. With this in view, we define

$$x_1=(\omega'-\omega)\tfrac{T_L}{2}$$

and

$$\mu=m\pi-x_1\Longrightarrow x_1=-\mu+m\pi\,.$$

Thus, as $x_1 \to m\pi$, $\mu \to 0$ and, for the region of major contribution, (4.20) may be cast as

$$\lim_{M\to\infty}\left\{\frac{\sin\left[\frac{(\omega'-\omega)MT_L}{2}\right]}{\sin\left[\frac{(\omega'-\omega)T_L}{2}\right]}\right\} \approx \lim_{\mu\to 0}\lim_{M\to\infty}\sum_{m=-\infty}^{\infty}\left\{\frac{\sin\left[M(\mu-m\pi)\right]}{\sin\left[\mu-m\pi\right]}\right\} . \tag{4.21}$$

Here, the summation accounts for the fact that over the ω' integral in (4.18) there is a major contribution from the factor under consideration each time x_1 approaches an integer multiple of π. It might be noted that the integral limits in (4.18) may be extended from $-\infty$ to ∞ by introducing a Heaviside function as is done in equation (4.24) below. Now, by virtue of its definition, M is odd so that

$$mM = \begin{cases} \text{odd integer}, & m \text{ odd}, \\ \text{even integer}, & m \text{ even} . \end{cases}$$

The right hand side of (4.21) may therefore be written as

$$\sum_{m=-\infty}^{\infty}\lim_{M\to\infty}\lim_{\mu\to 0}\left\{\frac{M\sin(M\mu)\cos(m\pi)}{M\sin\mu\cos(m\pi)}\right\} . \tag{4.22}$$

Arguing μ in the denominator to be small, we have

$$\begin{aligned}\sum_{m=-\infty}^{\infty}\lim_{M\to\infty}\lim_{\mu\to 0}\left\{\frac{M\sin(M\mu)\cos(m\pi)}{M\sin\mu\cos(m\pi)}\right\} &\approx \sum_{m=-\infty}^{\infty}\lim_{M\to\infty}\left\{\frac{M\sin(M\mu)}{M\mu}\right\} \\ &= \sum_{m=-\infty}^{\infty}\lim_{M\to\infty} M\mathrm{Sa}\left[M\mu\right)] .\end{aligned}$$

From Lathi [77], Chapter 1, we have the identity

$$\lim_{M\to\infty} M\mathrm{Sa}\left[M\mu\right)] = \pi\delta(\mu)$$

where $\delta(\cdot)$ is the Dirac delta function. Using this identity, and the definitions of μ and x_1, to a good approximation, (4.22) becomes

$$\begin{aligned}\sum_{m=-\infty}^{\infty}\lim_{M\to\infty}\lim_{\mu\to 0}\left\{\frac{M\sin(M\mu)\cos(m\pi)}{M\sin\mu\cos(m\pi)}\right\} &= \pi\sum_{-\infty}^{\infty}\delta(m\pi - x_1) \\ &= \pi\sum_{-\infty}^{\infty}\delta(x_1 - m\pi) \\ &= \pi\sum_{-\infty}^{\infty}\delta\left[(\omega'-\omega)\frac{T_L}{2} - m\pi\right] \\ &= \frac{2\pi}{T_L}\sum_{-\infty}^{\infty}\delta\left(\omega'-\omega-\frac{m2\pi}{T_L}\right) . \end{aligned} \tag{4.23}$$

The final form in (4.23) arises from the identity

$$\delta(ax) = \frac{1}{|a|}\delta(x) \, .$$

From (4.19) and (4.23), equation (4.18) may be written as

$$\begin{aligned}
\mathcal{P}_N(\omega,t) &= \lim_{M\to\infty} \mathcal{P}_{N_f}(\omega,t) \\
&= \sum_{n=-\infty}^{\infty} \left[h\left(t - nT_L + \frac{\tau_0}{2}\right) - h\left(t - nT_L - \frac{\tau_0}{2}\right)\right] \\
&\quad \cdot \frac{\tau_0}{T_L} \int_{-\infty}^{\infty} \left[h\left(\omega' + \frac{B}{2}\right) - h\left(\omega' - \frac{B}{2}\right)\right] S_N(\omega') \\
&\quad \cdot e^{-j(\omega'-\omega)t} \, \mathrm{Sa}\left[(\omega'-\omega)\frac{\tau_0}{2}\right] \delta\left(\omega' - \omega - \frac{m2\pi}{T_L}\right) d\omega'
\end{aligned}$$

or

$$\begin{aligned}
\mathcal{P}_N(\omega,t) &= \frac{\tau_0}{T_L} \sum_{m=-\infty}^{\infty} \left\{ \left[h\left(\omega + \frac{m2\pi}{T_L} + \frac{B}{2}\right) - h\left(\omega + \frac{m2\pi}{T_L} - \frac{B}{2}\right)\right] \right. \\
&\quad \left. \cdot \, \mathrm{Sa}\left[m\pi\frac{\tau_0}{T_L}\right] S_N\left(\omega + \frac{m2\pi}{T_L}\right) e^{-j\left(\frac{m2\pi}{T_L}\right)t} \right\} \\
&\quad \cdot \sum_{n=-\infty}^{\infty} \left[h\left(t + nT_L + \frac{\tau_0}{2}\right) - h\left(t + nT_L - \frac{\tau_0}{2}\right)\right] \, . \qquad (4.24)
\end{aligned}$$

In the last sum, $-n$ has been changed to $+n$, which is acceptable since n varies across the entire set of integers. Equation (4.24) represents the general form of a time dependent Doppler noise power spectral density for a pulsed radar assuming an external noise which is a stationary zero-mean Gaussian process. The number of pulses sampled is infinite. In Appendix C, equation (4.24) is derived in an alternate fashion, starting with infinitely many pulses rather than extending the finite case. The result is recorded in equation (C.15) and is seen to be identical to that above.

The time dependency will again be considered in two ways: (1) each pulse is sampled at its centre and (2) each pulse is sampled in the same place relative to the leading (or lagging) edge but not necessarily at the pulse centre.

1. Sampling at the Pulse Centre

To impose sampling at the pulse centres, it is again required that $t = pT_L$ where p belongs to the integers. Of course, m is also an integer so that the exponential in equation (4.24) becomes

$$e^{-j\left(\frac{m2\pi}{T_L}\right)t} = e^{-j2\pi mp} = 1 \,. \tag{4.25}$$

It has been assumed at the outset that the ambient noise spectrum is flat (i.e. white noise) so that $S_N\left(\omega + \frac{m2\pi}{T_L}\right)$ may be removed from the summations and designated as $S_N(\omega')$. The noise spectral density for the pulsed radar then becomes, from equations (4.24) and (4.25),

$$\begin{aligned} \mathcal{P}_N(\omega, pT_L) &= \frac{\tau_0}{T_L} S_N(\omega') \sum_{m=-\infty}^{\infty} \left[h\left(\omega + \frac{m2\pi}{T_L} + \frac{B}{2}\right) - h\left(\omega + \frac{m2\pi}{T_L} - \frac{B}{2}\right)\right] \\ &\quad \cdot \mathrm{Sa}\left[m\pi\frac{\tau_0}{T_L}\right] \sum_{n=-\infty}^{\infty} \left[h\left((p+n)T_L + \frac{\tau_0}{2}\right) - h\left((p+n)T_L - \frac{\tau_0}{2}\right)\right] \,, \end{aligned} \tag{4.26}$$

it being understood that $t = pT_L$. Next, it may be noted that since $\frac{\tau_0}{2} < T_L$

$$\left[h\left((p+n)T_L + \frac{\tau_0}{2}\right) - h\left((p+n)T_L - \frac{\tau_0}{2}\right)\right] = \begin{cases} 1, & p = -n \\ 0, & \text{otherwise,} \end{cases}$$

which immediately implies

$$\sum_{n=-\infty}^{\infty} \left[h\left((p+n)T_L + \frac{\tau_0}{2}\right) - h\left((p+n)T_L - \frac{\tau_0}{2}\right)\right] = 1 \,.$$

Equation (4.26) further reduces to

$$\begin{aligned} \mathcal{P}_N(\omega, pT_L) &= \frac{\tau_0}{T_L} S_N(\omega') \sum_{m=-\infty}^{\infty} \left[h\left(\omega + \frac{m2\pi}{T_L} + \frac{B}{2}\right) - h\left(\omega + \frac{m2\pi}{T_L} - \frac{B}{2}\right)\right] \\ &\quad \cdot \mathrm{Sa}\left[m\pi\frac{\tau_0}{T_L}\right] \,. \end{aligned} \tag{4.27}$$

The remaining Heaviside functions ensure that for non-zero results,

$$-\frac{BT_L}{4\pi} - \omega T_L \leq m \leq \frac{BT_L}{4\pi} - \omega T_L \tag{4.28}$$

where ω is the Doppler radian frequency of the noise, which is again completely analogous to the ω_d of the previous chapter. In a typical pulse radar, the receiver

bandwidth, B, is on the order of kilohertz (or krad/s in terms of radian frequency) while ω is on the order of rad/s (or Doppler frequency is on the order of hertz). Therefore, to a very good approximation, (4.28) becomes

$$-\frac{BT_L}{4\pi} \leq m \leq \frac{BT_L}{4\pi}\,, \tag{4.29}$$

and the asymmetry in the summation of (4.27) is removed. Furthermore, if match filter conditions [79] are imposed as before, $B = \frac{2\pi}{\tau_0}$. The limits on m in (4.29) are then given by

$$-\frac{T_L}{2\tau_0} \leq m \leq \frac{T_L}{2\tau_0}\,. \tag{4.30}$$

With these stipulations, for sampling at the pulse centres, the Doppler noise power spectral density in (4.27) simplifies to

$$\mathcal{P}_N(\omega, pT_L) = dS_N(\omega') \sum_{m=L\left(-\frac{1}{2d}\right)}^{G\left(\frac{1}{2d}\right)} \mathrm{Sa}\left[m\pi d\right] \tag{4.31}$$

where the radar duty cycle, d, has replaced $\frac{\tau_0}{T_L}$. The quantity $L\left(-\frac{1}{2d}\right)$ is the smallest integer $\geq -\frac{1}{2d}$, and $G\left(\frac{1}{2d}\right)$ is the greatest integer $\leq \frac{1}{2d}$. The argument pT_L has been explicitly retained only to emphasize sampling at the pulse centre. Since $S_N(\omega')$ is assumed constant, $\mathcal{P}_N(\omega, pT_L)$ is also constant for all ω. Equation (4.31) illustrates the very important property that the aliasing appearing by virtue of the summation is "buffered" by the duty cycle multiplier. That is, a low duty cycle, d, will increase aliasing as it increases the range of m, but at the same time this small d also multiplies the sum to mitigate the aliasing effect. Conversely, a higher duty cycle will reduce the aliasing since there will be fewer m's in the sum, but this reduction is subject to multiplication by a larger external factor. It may be verified numerically that for typical duty cycles in a pulse radar, $\mathcal{P}_N(\omega, pT_L)$ does not vary significantly from the ambient noise power spectral density, $S_N(\omega')$. The result is illustrated in Figure 4.3.

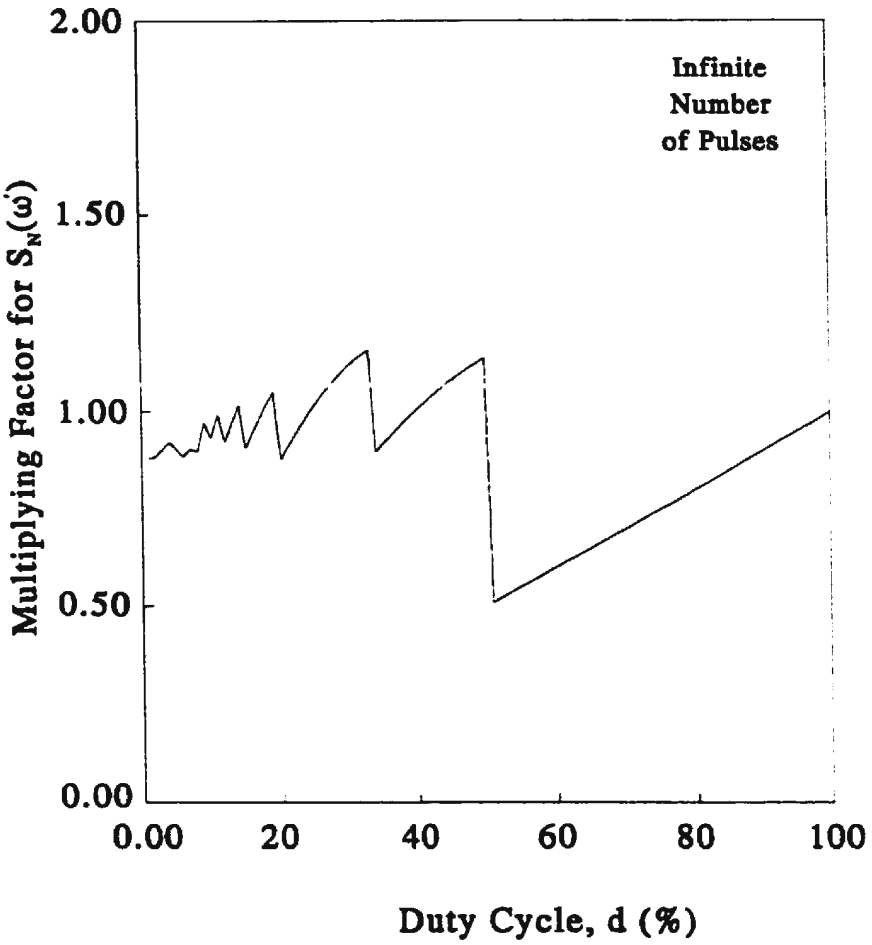

Figure 4.3: The multiplier on the ambient noise power spectral density, $S_N(\omega')$, for infinitely many pulses.

When $d > 0.5$, there is, logically, only the $m = 0$ pulse in the summation of equation (4.31). For these cases, the total multiplier on $S_N(\omega')$ is simply d and the slope of the curve is unity. Finally, the effect of using only a few pulses is not significantly different from the case given here. To illustrate this fact, Figure 4.4 combines the results of Figures 4.2 (for a finite number of pulses) and 4.3 (for infinitely many pulses). The discrepancy between the two results is always less than 3 dB for all duty cycles.

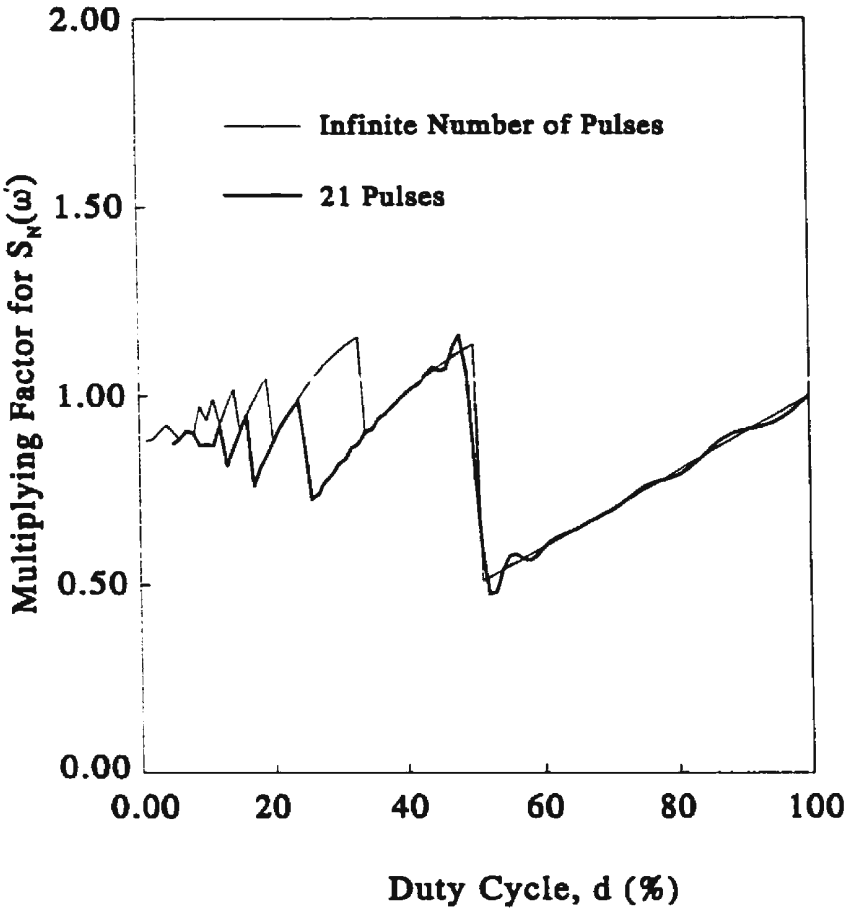

Figure 4.4: The multiplier on the ambient noise power spectral density, $S_N(\omega')$, compared for a finite and infinite number of pulses.

2. Sampling the Pulse Off-centre

Suppose, next, that the pulses are sampled at a time given by equation (4.13). Equation (4.24), on using the subscript "*oc*" (for off-centre) as before, takes the form

$$\begin{aligned}\mathcal{P}_{N_{oc}}(\omega,t) &= \frac{\tau_0}{T_L}\sum_{m=-\infty}^{\infty}\left\{\left[h\left(\omega+\frac{m2\pi}{T_L}+\frac{B}{2}\right)-h\left(\omega+\frac{m2\pi}{T_L}-\frac{B}{2}\right)\right]\right. \\ &\quad \left.\cdot\,\mathrm{Sa}\left[m\pi\frac{\tau_0}{T_L}\right]S_N\left(\omega+\frac{m2\pi}{T_L}\right)e^{-j\left(\frac{m2\pi}{T_L}\right)(pT_L+x)}\right\} \\ &\quad \cdot\sum_{n=-\infty}^{\infty}\left[h\left((n+p)T_L+x+\frac{\tau_0}{2}\right)-h\left((n+p)T_L+x-\frac{\tau_0}{2}\right)\right] \quad (4.32)\end{aligned}$$

Again, using the fact that $\frac{\tau_0}{2} < T_L$ and $T_L \gg |x|$,

$$\left[h\left((p+n)T_L+x+\frac{\tau_0}{2}\right)-h\left((p+n)T_L+x-\frac{\tau_0}{2}\right)\right]=\begin{cases}1, & p=-n\\ 0, & \text{otherwise.}\end{cases} \quad (4.33)$$

Therefore,

$$\sum_{n=-\infty}^{\infty}\left[h\left((n+p)T_L+x+\frac{\tau_0}{2}\right)-h\left((n+p)T_L+x-\frac{\tau_0}{2}\right)\right]=1\,.$$

Additionally, all that transpired in connection with $\sum_m$ between equations (4.27) and (4.31) still holds for (4.32). The latter thus reduces to

$$\mathcal{P}_{N_{oc}}(\omega,pT_L+x)=d\,S_N(\omega')\sum_{m=L(-\frac{1}{2d})}^{G(\frac{1}{2d})}\mathrm{Sa}\left[m\pi d\right]\cdot e^{-j\left(\frac{m2\pi(pT_L+x)}{T_L}\right)}\,. \tag{4.34}$$

Since the sampling function in (4.34) is an even function of m, terms containing $j\sin(m2\pi(pT_L+x))$ as a factor will vanish over the summation. Because $\cos(2\pi mp)=1$ and $\sin(2\pi mp)=0$, there remains for the power spectral density

$$\mathcal{P}_{N_{oc}}(\omega,pT_L+x)=d\,S_N(\omega')\sum_{m=L(-\frac{1}{2d})}^{G(\frac{1}{2d})}\mathrm{Sa}\left[m\pi d\right]\cos\left(\frac{2\pi mx}{T_L}\right)\,. \tag{4.35}$$

It may be observed that, given the limits on m and x as discussed previously, the argument in the cosine in equation (4.35) has the property

$$\left|\frac{2\pi mx}{T_L}\right|\le\left|\frac{2\pi\frac{x}{2d}}{T_L}\right|\,.$$

Then, since $d=\frac{\tau_0}{T_L}$ and $|x|<\frac{\tau_0}{2}$, $\left|\frac{2\pi mx}{T_L}\right|<\frac{\pi}{2}$, which means that

$$0<\cos\left(\frac{2\pi mx}{T_L}\right)<1\,,$$

and the noise power spectral density for sampling off-centre is indeed positive as required. Equation (4.35) indicates that the maximum noise power spectral density occurs for sampling at the pulse centre and falls off according to the cosine function as the sampling point in time approaches the pulse edge. Finally, if $|x|\ll\frac{\tau_0}{2}$, the expression in (4.35) clearly reduces to that in equation (4.31) where sampling occurred at the pulse centre.

4.3 Non-stationary White Noise

For the sake of completeness, it is appropriate to consider the Doppler noise power spectral density from the pulsed radar if the ambient noise is non-stationary, but is still a white Gaussian process. The analysis begins with a finite number of pulses. It will be seen that the Doppler noise power spectral density is, in fact, independent of the number of pulses for this particular specification of the noise regime – i.e. white. Gaussian, non-stationary noise.

Supposing that the noise voltage, $n(t)$, is non–stationary, the phase ϵ appearing in equation (4.1) is a function not only of the radian frequency, ω', but also of time. This latter fact may be accounted for, in the case of a pulse radar, by introducing the pulse number, m, in the argument of the phase. Thus, equation (4.2) for the stationary case may be altered to give for q pulses

$$\begin{aligned} n(t) &= \left[h\left(t+qT_L+\frac{\tau_0}{2}\right)-h\left(t-qT_L-\frac{\tau_0}{2}\right)\right] \\ &\cdot \sum_{m=-\infty}^{\infty}\left[h\left(t-mT_L+\frac{\tau_0}{2}\right)-h\left(t-mT_L-\frac{\tau_0}{2}\right)\right] \\ &\cdot \int_{\omega'}\left[h\left(\omega'+\frac{B}{2}\right)-h\left(\omega'-\frac{B}{2}\right)\right]e^{j\omega' t}e^{j\epsilon(\omega',m)}\sqrt{S_N(\omega')\frac{d\omega'}{2\pi}} \quad (4.36) \end{aligned}$$

An autocorrelation of this noise voltage gives

$$\begin{aligned} \mathcal{R}_{N_n}(t_1,t_2) &= < n(t_1)n^*(t_2) >= \left[h\left(t_1+qT_L+\frac{\tau_0}{2}\right)-h\left(t_1-qT_L-\frac{\tau_0}{2}\right)\right] \\ &\cdot \left[h\left(t_2+qT_L+\frac{\tau_0}{2}\right)-h\left(t_2-qT_L-\frac{\tau_0}{2}\right)\right] \\ &\cdot \sum_{m=-\infty}^{\infty}\sum_{n=-\infty}^{\infty}\left[h\left(t_1-mT_L+\frac{\tau_0}{2}\right)-h\left(t_1-mT_L-\frac{\tau_0}{2}\right)\right] \\ &\cdot \left[h\left(t_2-nT_L+\frac{\tau_0}{2}\right)-h\left(t_2-nT_L-\frac{\tau_0}{2}\right)\right] \\ &\cdot \int_{-\frac{B}{2}}^{\frac{B}{2}} e^{j(\omega_1' t_1-\omega_2' t_2)} < e^{j(\epsilon(\omega_1',m)-\epsilon(\omega_2',n))} > \\ &\cdot \sqrt{S_N(\omega_1')S_N(\omega_2')\frac{d\omega_1'}{2\pi}\frac{d\omega_2'}{2\pi}} \quad (4.37) \end{aligned}$$

Given that, for the random phase, the ensemble average may be specified as usual by

$$< e^{j(\epsilon(\omega_1',m)-\epsilon(\omega_2',n))} >= \begin{cases} 1, & \omega_1' = \omega_2' = \omega', \text{ say} \\ & m = n \\ 0, & \text{otherwise} \end{cases} \tag{4.38}$$

equation (4.37) becomes

$$\begin{aligned} \mathcal{R}_{N_{ns}}(t_1, t_2) &= \left[h\left(t_1 + qT_L + \frac{\tau_0}{2}\right) - h\left(t_1 - qT_L - \frac{\tau_0}{2}\right)\right] \\ &\cdot \left[h\left(t_2 + qT_L + \frac{\tau_0}{2}\right) - h\left(t_2 - qT_L - \frac{\tau_0}{2}\right)\right] \\ &\cdot \sum_{m=-\infty}^{\infty}\left[h\left(t_1 - mT_L + \frac{\tau_0}{2}\right) - h\left(t_1 - mT_L - \frac{\tau_0}{2}\right)\right] \\ &\cdot \left[h\left(t_2 - mT_L + \frac{\tau_0}{2}\right) - h\left(t_2 - mT_L - \frac{\tau_0}{2}\right)\right] \\ &\cdot \int_{-\frac{B}{2}}^{\frac{B}{2}} e^{j\omega'(t_1-t_2)} S_N(\omega')\frac{d\omega'}{2\pi} . \end{aligned} \tag{4.39}$$

Putting, $\tau = t_1 - t_2$ and $t_2 = t$ so that $t_1 = \tau + t$, equation (4.39) may be written in the form

$$\begin{aligned} \mathcal{R}_{N_{ns}}(\tau + t, t) &= \left[h\left(\tau + t + qT_L + \frac{\tau_0}{2}\right) - h\left(\tau + t - qT_L - \frac{\tau_0}{2}\right)\right] \\ &\cdot \left[h\left(t + qT_L + \frac{\tau_0}{2}\right) - h\left(t - qT_L - \frac{\tau_0}{2}\right)\right] \\ &\cdot \sum_{m=-\infty}^{\infty}\left[h\left(\tau + t - mT_L + \frac{\tau_0}{2}\right) - h\left(\tau + t - mT_L - \frac{\tau_0}{2}\right)\right] \\ &\cdot \left[h\left(t - mT_L + \frac{\tau_0}{2}\right) - h\left(t - mT_L - \frac{\tau_0}{2}\right)\right] \\ &\cdot \int_{-\frac{B}{2}}^{\frac{B}{2}} e^{j\omega'\tau} S_N(\omega')\frac{d\omega'}{2\pi} . \end{aligned} \tag{4.40}$$

Taking the Fourier transform of $\mathcal{R}_{N_{ns}}$ with respect to τ, using ω as the transform variable, yields

$$\begin{aligned} \mathcal{F}\left\{\mathcal{R}_{N_{ns}}(\tau + t, t)\right\}(\omega, t) &= \mathcal{P}_{N_{ns}}(\omega, t) \\ &= \left[h\left(t + qT_L + \frac{\tau_0}{2}\right) - h\left(t - qT_L - \frac{\tau_0}{2}\right)\right] \\ &\cdot \sum_{m=-\infty}^{\infty}\left[h\left(t - mT_L + \frac{\tau_0}{2}\right) - h\left(t - mT_L - \frac{\tau_0}{2}\right)\right] \\ &\cdot \int_{-\infty}^{\infty}\int_{-\frac{B}{2}}^{\frac{B}{2}}\left[h\left(\tau + t + qT_L + \frac{\tau_0}{2}\right) - h\left(\tau + t - qT_L - \frac{\tau_0}{2}\right)\right] \\ &\cdot \left[h\left(\tau + t - mT_L + \frac{\tau_0}{2}\right) - h\left(\tau + t - mT_L - \frac{\tau_0}{2}\right)\right] \\ &\cdot e^{j(\omega'-\omega)\tau} S_N(\omega')\frac{d\omega'}{2\pi}d\tau . \end{aligned} \tag{4.41}$$

From the Heaviside functions in the integrand of (4.41), it becomes immediately apparent that their product is non-zero only in the range $-q \leq m \leq q$. This means that the summation index becomes finite, and defining $\tau_1 = \tau + t$, we have the time dependent power spectral density as

$$\begin{aligned}\mathcal{P}_{N_{ns}}(\omega, t) &= \left[h\left(t + qT_L + \frac{\tau_0}{2}\right) - h\left(t - qT_L - \frac{\tau_0}{2}\right)\right] \\ &\cdot \sum_{m=-q}^{q}\left[h\left(t - mT_L + \frac{\tau_0}{2}\right) - h\left(t - mT_L - \frac{\tau_0}{2}\right)\right] \\ &\cdot \int_{-\infty}^{\infty}\int_{-\frac{B}{2}}^{\frac{B}{2}}\left[h\left(\tau_1 - mT_L + \frac{\tau_0}{2}\right) - h\left(\tau_1 - mT_L - \frac{\tau_0}{2}\right)\right] \\ &\cdot e^{j(\omega'-\omega)\tau_1}e^{-j(\omega'-\omega)t}S_N(\omega')\frac{d\omega'}{2\pi}d\tau_1 \ . \end{aligned} \tag{4.42}$$

The τ_1 integral is identical to that in equation (4.5) and it therefore evaluates to

$$\tau_0 e^{j(\omega'-\omega)mT_L}\mathrm{Sa}\left[(\omega'-\omega)\frac{\tau_0}{2}\right] \ .$$

Thus, the Doppler noise power spectral density becomes

$$\begin{aligned}\mathcal{P}_{N_{ns}}(\omega, t) &= \tau_0\left[h\left(t + qT_L + \frac{\tau_0}{2}\right) - h\left(t - qT_L - \frac{\tau_0}{2}\right)\right] \\ &\cdot \sum_{m=-q}^{q}\left[h\left(t - mT_L + \frac{\tau_0}{2}\right) - h\left(t - mT_L - \frac{\tau_0}{2}\right)\right] \\ &\cdot \int_{-\frac{B}{2}}^{\frac{B}{2}}\mathrm{Sa}\left[(\omega'-\omega)\frac{\tau_0}{2}\right]e^{j(\omega'-\omega)mT_L}e^{-j(\omega'-\omega)t}S_N(\omega')\frac{d\omega'}{2\pi} \ . \end{aligned} \tag{4.43}$$

1. Sampling at the Pulse Centres

Next, suppose that the sampling occurs at $t = pT_L$ where p is an integer. Clearly,

$$\begin{aligned}\left[h\left((p+q)T_L + \frac{\tau_0}{2}\right) - h\left((p-q)T_L - \frac{\tau_0}{2}\right)\right] &= \begin{cases} 1, & |p| \leq q \\ 0, & \text{otherwise} \end{cases} \\ \text{and} \\ \left[h\left((p-m)T_L + \frac{\tau_0}{2}\right) - h\left((p-m)T_L - \frac{\tau_0}{2}\right)\right] &= \begin{cases} 1, & p = m \\ 0, & \text{otherwise.} \end{cases} \end{aligned} \tag{4.44}$$

The last fact in (4.44) removes the phase terms in the integrand of (4.43). Therefore, for sampling at the pulse centres, the Doppler power spectral density for a non-stationary white Gaussian noise reduces simply to

$$\mathcal{P}_{N_{ns}}(\omega) = \frac{\tau_0}{2\pi}S_N(\omega')\int_{-\frac{B}{2}}^{\frac{B}{2}}\mathrm{Sa}\left[(\omega'-\omega)\frac{\tau_0}{2}\right]d\omega' \tag{4.45}$$

where the ambient noise spectral density, $S_N(\omega')$, is removed from the integral since, by definition, it is constant across the entire bandwidth. An interesting feature of (4.45) is that $\mathcal{P}_{N_{ns}}(\omega)$ is independent of the number of pulses. Thus, for sampling time $t = pT_L$, a finite or infinite number of pulses will have the same power spectral density when the process is white Gaussian but non–stationary. Suppose, next, that to aid in evaluating (4.45) we let

$$\alpha = (\omega' - \omega)\frac{\tau_0}{2} = (\omega' - \omega)\frac{\pi}{B} \approx \frac{\omega'\pi}{B} \tag{4.46}$$

by using the arguments similar to those surrounding equation (4.12). This gives

$$\begin{aligned} \mathcal{P}_{N_{ns}}(\omega) &\approx \frac{2}{\pi} S_N(\omega') \int_0^{\frac{\pi}{2}} \mathrm{Sa}[\alpha] d\alpha \\ &\approx 0.873\, S_N(\omega') \end{aligned} \tag{4.47}$$

so that the noise power spectral density is a constant for all radian Doppler frequencies, ω. Again, the argument of $S_N(\cdot)$ has not been altered because of its constancy over bandwidth.

2. Sampling Off-centre

As was done for stationary noise, it is next assumed that the pulses may be sampled at times given by

$$t = pT_L + x \text{ where } -\frac{\tau_0}{2} < x < \frac{\tau_0}{2}\,. \tag{4.48}$$

Since $T_L > \tau_0$ and $|x| < \frac{\tau_0}{2}$, the relationships in equation (4.44) are still valid. Consequently, equation (4.43) becomes, on using (4.48),

$$\begin{aligned} \mathcal{P}_{N_{ns}}(\omega, x) &= \tau_0 \int_{-\frac{B}{2}}^{\frac{B}{2}} \mathrm{Sa}\left[(\omega' - \omega)\frac{\tau_0}{2}\right] e^{-j(\omega' - \omega)x} \\ &\quad \cdot S_N(\omega')\frac{d\omega'}{2\pi}\,. \end{aligned} \tag{4.49}$$

Using the change of variables as in (4.47),

$$\mathcal{P}_{N_{ns}}(\omega, x) \approx \frac{2}{\pi} S_N(\omega') \int_0^{\frac{\pi}{2}} \mathrm{Sa}[\alpha] \cos\left(\frac{2\alpha x}{\tau_0}\right) d\alpha\,. \tag{4.50}$$

It may be noted that since $|x| < \frac{\tau_0}{2}$ and $0 \leq \alpha \leq \frac{\pi}{2}$,

$$0 < \cos\left(\frac{2\alpha x}{\tau_0}\right) \leq 1\,,$$

and the integral is everywhere positive. The result is analogous to that in equation (4.35) where the outcome for sampling at the pulse centres is modified by the cosine factor when off-centre sampling is used. However, in (4.50) there is no dependence on the number of pulses. Figure 4.5 depicts this variation in the multiplier on $S_N(\omega')$ for the case of off-centre sampling of pulses of non-stationary noise.

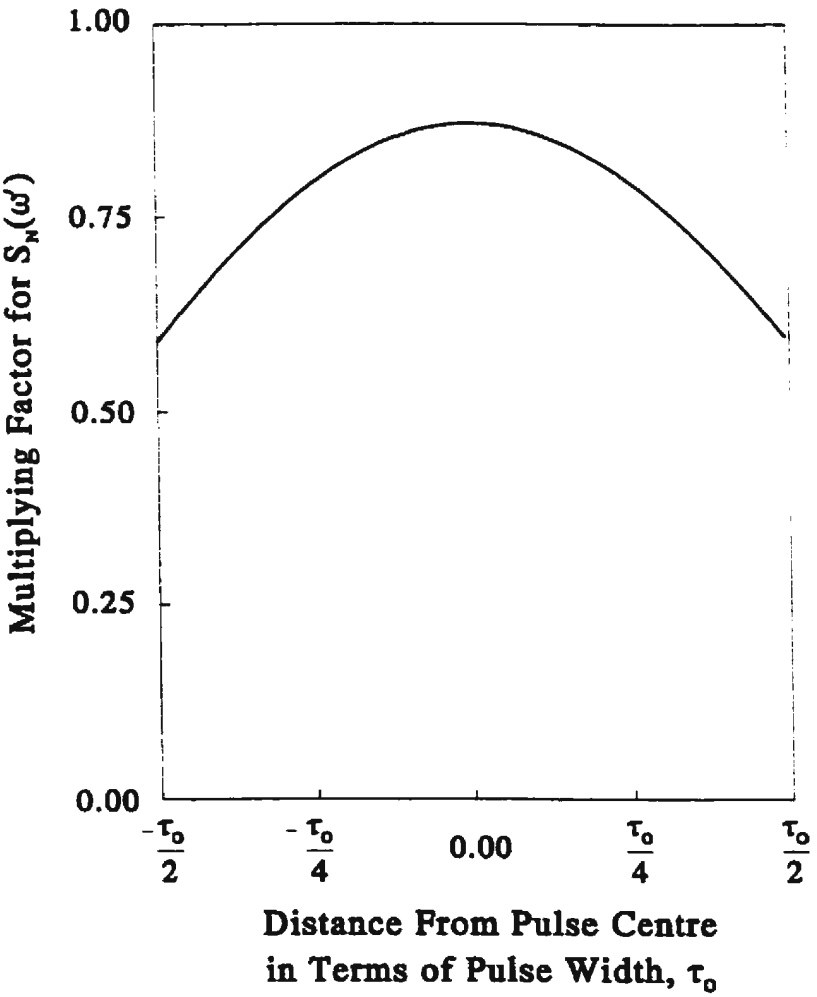

Figure 4.5: The variation of the multiplier on the ambient non-stationary noise power spectral density as a function of distance from the pulse centre at which the sampling occurs.

4.4 A Form for the Ocean Clutter Power Spectral Density

Implicit in the bistatic radar range equation (3.65) is the fact that the transmitter power P_t is the *peak pulse power*. This, by definition, is not the maximum instantaneous power of a single sinusoid. Rather, it is the power averaged over the pulse length, τ_0. For the simple pulsed sinusoid assumed here, this translated into the peak pulse power being one half the peak instantaneous power. The question to be addressed now is "What is the proper form of the Doppler power spectral density for the ocean clutter which is obtained for a particular patch of ocean by gating the received signal on and off?" This query has already been discussed for the Doppler *noise* power spectral density in Section 4.2 with the result for a large number of pulses being given by equations (4.31) or (4.38), depending on the sampling positions relative to the pulse centres. A similar analysis for the ocean clutter ensues.

For the temporal periods, typically several minutes, used in examining HF sea echo, Barrick and Snider [75] have argued that the ocean surface wave field may be modelled as a stationary Gaussian process. This results in the echo signal being likewise approximately stationary and Gaussian for the same time frames. Certainly, in our deliberations of the previous chapter we have already imposed these conditions, as well as homogeneity. This means that with these assumptions the ocean clutter signal, $c_a(t)$, may be cast analogously to the noise voltage of equation (4.1). Thus,

$$\begin{aligned} c_a(t) &= \int_{\omega_c'} \left[h\left(\omega_c' + \frac{B_c}{2}\right) - h\left(\omega_c' - \frac{B_c}{2}\right) \right] e^{j\omega_c' t} \\ &\quad \cdot e^{j\epsilon(\omega_c')} \cdot \sqrt{S_c(\omega_c') \frac{d\omega_c'}{2\pi}} \, . \end{aligned} \tag{4.51}$$

Here, B_c is the clutter bandwidth, ω_c' the radian frequency, $\epsilon(\cdot)$ is the random phase and $S_c(\cdot)$ is the peak power spectral density of the continuous clutter signal. Gating this signal, under the assumption of infinitely many pulses (in reality, a large number

of pulses) (4.51) may be modified to give

$$\begin{aligned} c(t) &= \sum_{m=-\infty}^{\infty} \left[h\left(t - mT_L + \frac{\tau_0}{2}\right) - h\left(t - mT_L - \frac{\tau_0}{2}\right) \right] c_a(t) \\ &= \sum_{m=-\infty}^{\infty} \left[h\left(t - mT_L + \frac{\tau_0}{2}\right) - h\left(t - mT_L - \frac{\tau_0}{2}\right) \right] \\ &\quad \cdot \int_{\omega_c'} \left[h\left(\omega_c' + \frac{B_c}{2}\right) - h\left(\omega_c' - \frac{B_c}{2}\right) \right] e^{j\omega_c' t} e^{j\epsilon(\omega_c')} \\ &\quad \cdot \sqrt{S_c(\omega_c') \frac{d\omega_c'}{2\pi}} \,. \end{aligned} \tag{4.52}$$

The form of the gated clutter, $c(t)$, is obviously identical to that for the gated noise in equation (C.1) of Appendix C. Therefore, the spectral density for $c(t)$ may be written down immediately from that given for the noise in equation (C.15). Using subscript c to indicate "clutter" quantities, the Doppler power spectral density of the gated signal is

$$\begin{aligned} \mathcal{P}_c(\omega, t) &= \frac{\tau_0}{T_L} \sum_{m=-\infty}^{\infty} \left\{ \left[h\left(\omega + \frac{m2\pi}{T_L} + \frac{B_c}{2}\right) - h\left(\omega + \frac{m2\pi}{T_L} - \frac{B_c}{2}\right) \right] \right. \\ &\quad \cdot \mathrm{Sa}\left[\frac{m\pi\tau_0}{T_L}\right] S_c\left(\omega + \frac{m2\pi}{T_L}\right) e^{-j\frac{m2\pi t}{T_L}} \\ &\quad \left. \cdot \sum_{n=-\infty}^{\infty} \left[h\left(t + nT_L + \frac{\tau_0}{2}\right) - h\left(t + nT_L - \frac{\tau_0}{2}\right) \right] \right\} \,. \end{aligned} \tag{4.53}$$

If, next, it is assumed that the sampling occurs at the pulse centres – i.e. $t = pT_L$ with p integer - equation (4.53) may be shown, as before, to reduce to

$$\mathcal{P}_c(\omega, pT) = \frac{\tau_0}{T_L} \sum_{m=\frac{-B_c T_L}{4\pi} - \omega T_L}^{\frac{B_c T_L}{4\pi} - \omega T_L} S_c\left(\omega + \frac{m2\pi}{T_L}\right) \mathrm{Sa}\left[\frac{m\pi\tau_0}{T_L}\right] \,. \tag{4.54}$$

Typically, the Doppler clutter bandwidth is on the order of hertz while the pulse repetition period, T_L, is in the microsecond range. This means that

$$B_c << \left(\frac{1}{T_L}\right) \Rightarrow \frac{B_c T_L}{4\pi} << 1 \,,$$

and since $|\omega| \leq \frac{B_c}{2}$,

$$\omega T_L << 1$$

as well. This means that the limits on the sum in equation (4.54) which trivially may be written as

$$\frac{-B_c T_L}{4\pi} - \omega T_L \leq m \leq \frac{B_c T_L}{4\pi} - \omega T_L$$

indicate that $m = 0$ is the only surviving term. Therefore, from equation (4.54), and using the fact that $\mathcal{P}_c(\cdot)$ is clearly independent of p, we may write

$$\mathcal{P}_c(\omega) = \frac{\tau_0}{T_L} S_c(\omega) \; . \tag{4.55}$$

Unlike the Doppler noise power spectral density, $\mathcal{P}_N(\omega)$, there is no aliasing apparent in $\mathcal{P}_c(\omega)$. Of course, this is not surprising as adequate sampling of the clutter signal was implicitly imposed by the assumptions on the summation indices following equation (4.54). That is, while the noise is a broadband signal and is folded into the narrow Doppler bandwidth, the ocean clutter is already narrowband and is therefore not affected in this way. The other important feature in equation (4.55) is the factor $\left(\frac{\tau_0}{T_L}\right)$ multiplying the peak spectral density. It is easily shown that this combination is, in fact, the *average* power spectral density. This means that, when considering the *gated* clutter signal, the average power, rather than the peak power, should be used in the radar range equation.

This analysis in conjunction with Section 4.2 provides a basis for defining the ocean clutter signal to noise ratio for a pulse Doppler radar as

$$(SNR)_c = \frac{\mathcal{P}_c(\omega)}{\mathcal{P}_N(\omega)} \; . \tag{4.56}$$

It should be noted that $\mathcal{P}_c(\omega)$ may be identified with $\mathcal{P}(\omega_d)$ of equation (3.65) (the radar range equation) as long as *average* transmitted power is used in place of *peak* power.

The results of this and the preceding sections may now be used to examine the relative importance of the various portions of the HF cross sections of the ocean surface when the radar system is externally noise limited.

4.5 Calculation and Illustration of Typical Noise and Clutter Power Spectral Densities

4.5.1 The Ambient Noise

As already noted, when radio operation is carried out in the HF band, the external noise of significance falls into three categories: (1) atmospheric; (2) galactic and (3) man-made [86] . The first includes radiation from lightning discharges and emissions from atmospheric gases. Galactic noise is the term used to describe radiation from celestial radio sources, while man-made noise may originate from such things as electrical machinery and power transmission lines. The relative importance of each type of noise depends on location, the frequency of operation, the time of day and even the season of the year, the latter dependencies arising due to variable solar activity. While significant fluctuations may occur as these parameters vary, median noise values will suffice for illustrative purposes.

In [86], the external noise factor, f_a, is defined as

$$f_a = \frac{\mathcal{P}_n}{kT_0B_n} \tag{4.57}$$

where $\mathcal{P}_n$ is the available noise power from an equivalent lossless antenna, $k = 1.38 \times 10^{-23}$ J/K is Boltzmann's constant, T_0 is the reference temperature which is taken as 290 K and B_n is the noise power bandwidth of the receiving system. For a matched filter system, B_n may be taken as the reciprocal of the transmit pulse width, τ_0. It is common to define an external noise *figure*, F_a, as

$$F_a = 10 \log f_a \ , \tag{4.58}$$

a median value of which may be designated as F_{am}. This is the quantity which is readily available in [86]. For a white noise process, as is assumed in Section 4.2, the power spectral density, $S_N(\omega')$, in equation (4.31) is

$$S_N(\omega') = \frac{\mathcal{P}_n}{2\pi B_n} \ . \tag{4.59}$$

Therefore, from equations (4.57)–(4.59),

$$S_N(\omega') = \frac{kT_0}{2\pi} 10^{\frac{F_{am}}{10}} \quad . \tag{4.60}$$

Then, equation (4.31) for the external Doppler noise power spectral density, $\mathcal{P}_N(\omega)$, becomes

$$\mathcal{P}_N(\omega) = \frac{dkT_0}{2\pi} 10^{\left(\frac{F_{am}}{10}\right)} \sum_{m=L\left(\frac{-1}{2d}\right)}^{G\left(\frac{1}{2d}\right)} \mathrm{Sa}[m\pi d] \; . \tag{4.61}$$

Here, the pT_L argument has been dropped from the power spectral density as it does not enter the calculation for infinitely many pulses. It was discussed following equation (4.12) that this is also true for even a small number of pulses.

Before carrying out an actual calculation of (4.61), the relevant operating parameters of a typical HF radar system will be considered so that representative clutter spectral densities may be determined also.

4.5.2 Ocean Clutter Power Spectral Density

If it is assumed that observations of the pulsed HF radiation scatter from the ocean surface are made via a narrow beam receiving system, the radar range equation (3.65) may be written as

$$\mathcal{P}_c(\omega_d) = \frac{\lambda_0^2 \left(\frac{\tau_0}{T_L}\right) P_t G_t G_r |F(\rho_{01}, \omega_0) F(\rho_{02}, \omega_0)|^2 A\sigma(\omega_d)}{(4\pi)^3 \rho_{01}^2 \rho_{02}^2} \; . \tag{4.62}$$

It should be remarked that $\left(\frac{\tau_0}{T_L} P_t\right)$ is the average transmitted power as dictated by equation (4.55). $\mathcal{P}_c(\omega_d)$ is the same as $\mathcal{P}_c(\omega)$ and is so subscripted as to emphasize that it is a *Doppler clutter* power spectral density. The differentials of equation (3.65) have been removed under the assumption that the receiver beamwidth is narrow enough to ensure constancy of the various parameters over the area (A) being interrogated.

For the purpose of illustration, the following radar parameters are considered initially:

- operating frequency: $f_o = 25$ MHz (i.e. $\lambda_0 = 12$ m)

- pulse width: $\tau_0 = 13.3\ \mu s$ (chosen so that $\frac{c\tau_0}{2}$ as used in simulation of the first-order cross section = 2000 m)

- pulse repetition frequency: prf = 3 kHz $\Rightarrow T_L = 333\,\mu s$

- peak power: $P_t = 16$ kW

- transmitter gain: $G_t = 2\,\mathrm{dBi}$ (i.e. $2\,\mathrm{d}B$ above isotropic) $\rightarrow G_t \approx 1.585$

- receive array: 24 element linear array with element spacing, d_s, of $\frac{\lambda_0}{2}$, operating in broadside mode

- receive array beamwidth: from Collin [63], the half-power beamwidth of an $(N+1)$ element broadside array is

$$BW_{\frac{1}{2}} = \frac{2.65\lambda_0}{(N+1)\pi d_s} = 0.07029\,\mathrm{rad}\,(4.03°)\,(\frac{\lambda_0}{2}\ \text{spacing})$$

- receive array gain: assuming 100% efficiency, [63] gives

$$G_r = \frac{5.48(N+1)d_s}{\lambda_0} = 65.76$$

- patch area: $A = \frac{c\tau_0 \rho_{02} BW_{\frac{1}{2}}}{2}$ where $\frac{c\tau_0}{2}$ and $\rho_{02} BW_{\frac{1}{2}}$ are the radial and azimuthal extents of the patch, respectively

- normalized patch cross section: $\sigma(\omega_d)$ as calculated in Chapter 3

- rough spherical earth attenuation functions: $F(\cdot)$'s are calculated from a FORTRAN routine devised by Dawe [72]. In monostatic operation, the angle of the wind with respect to the radar beam is an important parameter. In bistatic operation the wind directions with respect to the transmit beam and the receive beam are used in determining $F(\rho_{01})$ and $F(\rho_{02})$, respectively. The surface roughness is a function of wind speed. Antenna heights are chosen to be zero. The relative permittivity of seawater is taken as 80, and an average conductivity of $4\mho/\mathrm{m}$ is used.

The assumption of the system being externally noise limited is still in view and, consequently, the noise analysis in the receiving system as a whole will not be an issue here. Extension to that case is a well understood process and is given in detail by Collin [63].

4.5.3 Illustrations and Discussion

The cross sections depicted in Figures 3.6a, 3.8 and 3.9 will be used for $\sigma(\omega_d)$ in equation (4.62). It should be recalled that the bistatic cross sections in those figures assumed a bistatic angle of 30°. For calculation purposes here, we set $\rho_{01} = \rho_{02} = 50$ km and the distance between receiver and transmitter as 100 km which indeed ensures that $\phi_0 = 30°$.

For the 4% duty cycle, $\left(\frac{\tau_0}{T_L}\right)$, suggested above, the summation index in the noise equation (4.61) ranges from -12 to 12. From [86], the noise figure F_{am} may be determined as 22 dB, 36 dB and 42 dB, for operating frequencies of 25 MHz, 10 MHz and 5.75 MHz, respectively. It may be noted that the "quiet receiving site" category was used for the man-made noise. Also, in the case of 25 MHz, the man-made and atmospheric noise is negligible, while galactic contributions are relevant for all three frequencies. The atmospheric noise figure was chosen halfway between that which is exceeded 0.5% and 99.5% of the time. From Figure 4.3, the multiplier on $S_N(\omega')$ of equation (4.60) is not significantly different from unity for a 4% duty cycle. Therefore, in the decibel sense, the noise power spectral density of equation (4.61), to an extremely good approximation, may be given on using frequency, f, in hertz rather than ω in radians/second as

$$(\mathcal{P}_N(f))_{\text{dB}} = 10\log \mathcal{P}_N(f) = 10\log kT_0 + 10\log 10^{\frac{F_{am}}{10}} = -204\,\text{dB} + F_{am} \qquad (4.63)$$

in the simulations here.

Figure 4.6 shows that the bistatic and monostatic results are very similar. In conjunction with Figure 4.7, it is clear that the observation of various spectral singu-

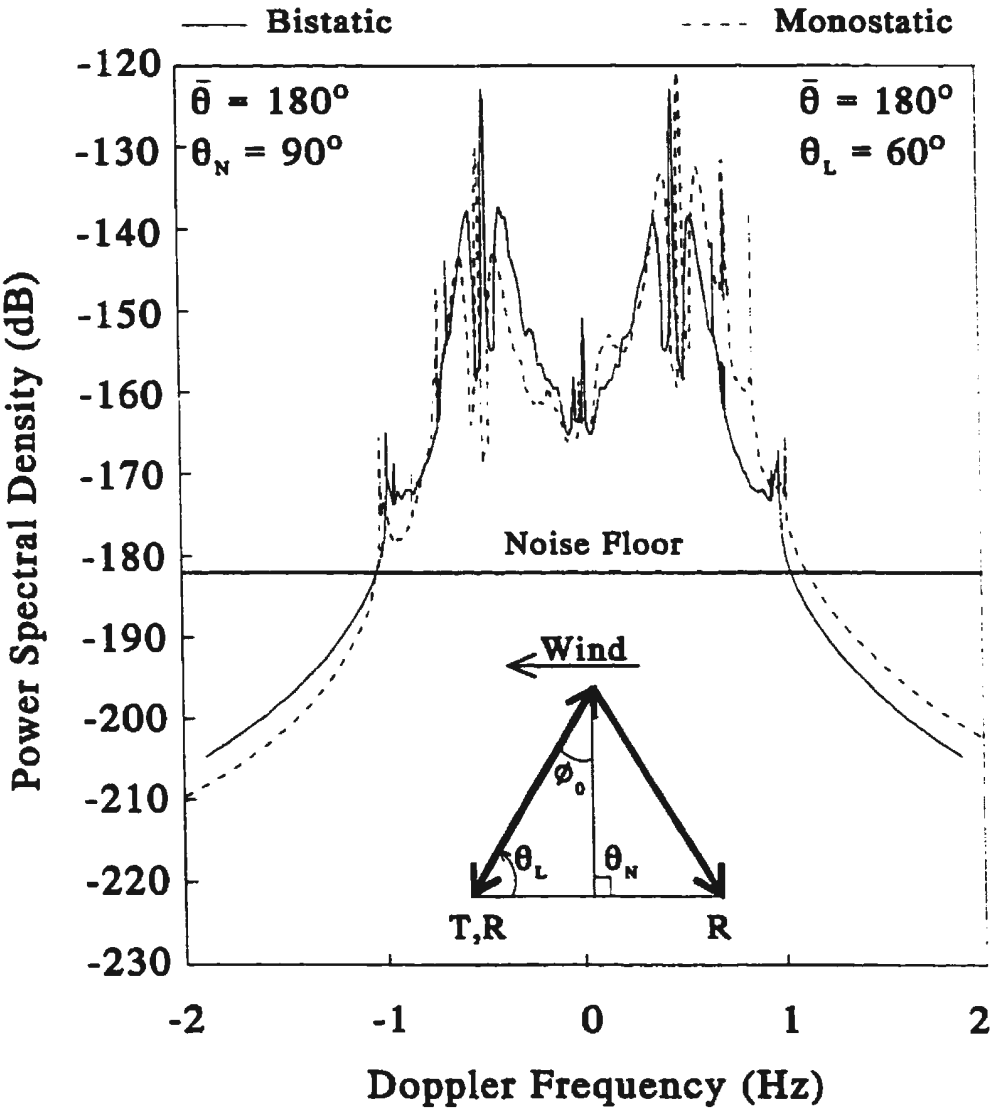

Figure 4.6: The relationship of the noise floor to the clutter power spectral density for the cross sections of Figure 3.6a. The radar range is 50 km.

larities is dependent on the directional nature of the wind-driven sea. In fact, at 25 MHz, if there is a 15 dB increase in the noise floor from sources not included here, at a range of 50 km the increase in the spectral tails due to scatter at the transmitter or receiver will not be visible. However, the peaks near zero Doppler at 25 MHz may still exceed the noise floor and may be visible provided there is no dc contribution from other sources.

Figure 4.8 clearly shows the improvement in SNR as the operating frequency is

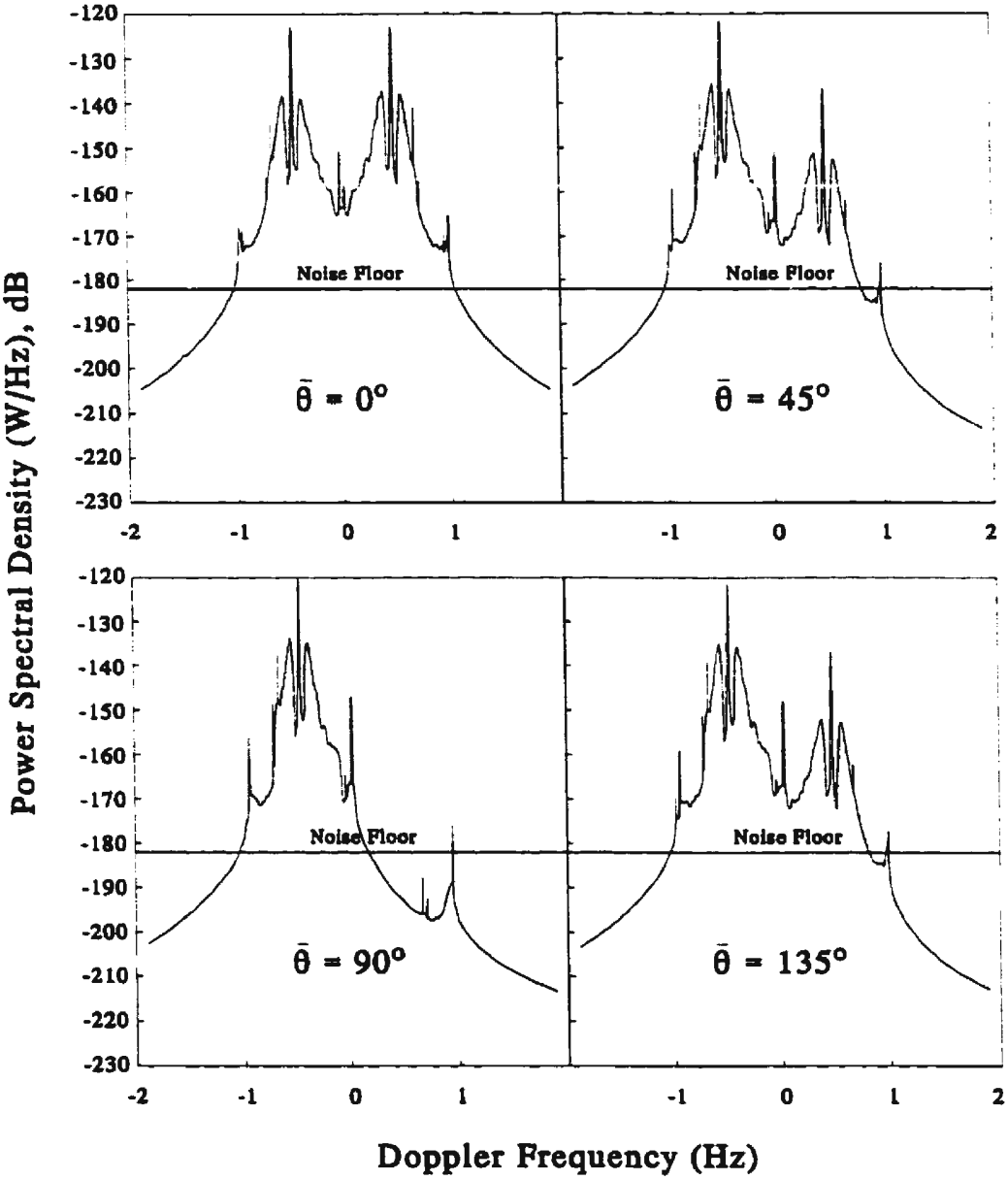

Figure 4.7: The effect of wind direction on the relationship between the clutter and noise power spectral densities. The cross sections are obtained from Figure 3.8 and the radar range is 50 km.

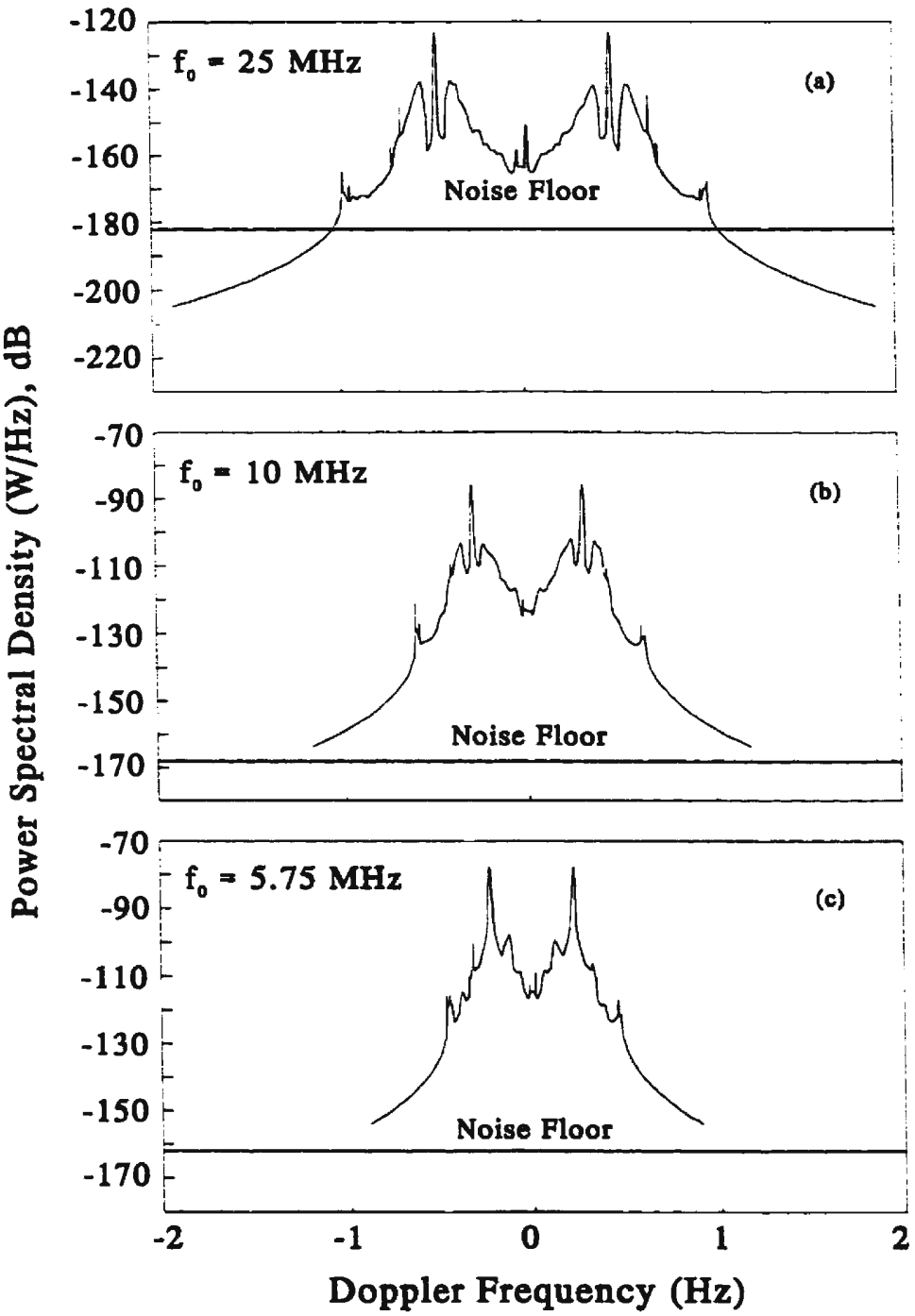

Figure 4.8: The relationship between the clutter and noise power spectral densities for different operating frequencies, f_0. The cross sections are obtained from Figure 3.9 and the radar range is 50 km.

lowered. This is largely due to the fact that increasing noise levels are mitigated by a large increase in the spherical earth attenuation functions $F(\cdot)$ appearing in the radar range equation. In relation to the overall spectrum, the peaks near zero Doppler for 10 MHz and 5.75 MHz contain very little power and may be easily masked by system effects. For example, even small amounts of spectral smearing due to finite system timing could obliterate this phenomenon. However, at these lower frequencies the increase in the spectral tails due to scatter near the transmitting and receiving sites is well above the noise floor.

It must be realized that the results presented in Figures 4.6–4.8 are for an idealized system. Such factors as ground losses and receiver noise, for example, are not included. Furthermore, and perhaps more importantly, the results all find their basis in the ensemble averaging of the received electric field. By definition, this presumes that infinitely many, statistically similar oceans are available for interrogation. Thus, the results discussed to this point represent an *idealized* scenario and no adjustment of system parameters may be effected to improve the $(\mathrm{SNR})_c$ beyond that depicted. A technique better reflecting reality ensues.

In practice, the power spectral density is often *estimated* using the squared magnitude of the Fourier transform of a finite time series. Pierson's model for a stationary Gaussian time process provides a means of simulating such a time series from the ideal power spectral densities obtained by ensemble averaging. From equation (4.1), it is seen that this model accounts for a random phase at each frequency point of the spectral density. Appendix C.2 contains an outline of the steps which may be used to model a practical estimate of the power spectral density with this "magnitude-squared" of the Fourier transformed time series approach. A typical result is found in Figure 4.9. The ideal power spectral density used as input to Pierson's time model was calculated in exactly the same fashion as that for 5.75 MHz in Figure 4.8c. To simulate an approximation of the directional features of Figure 3.10b, a wind direction

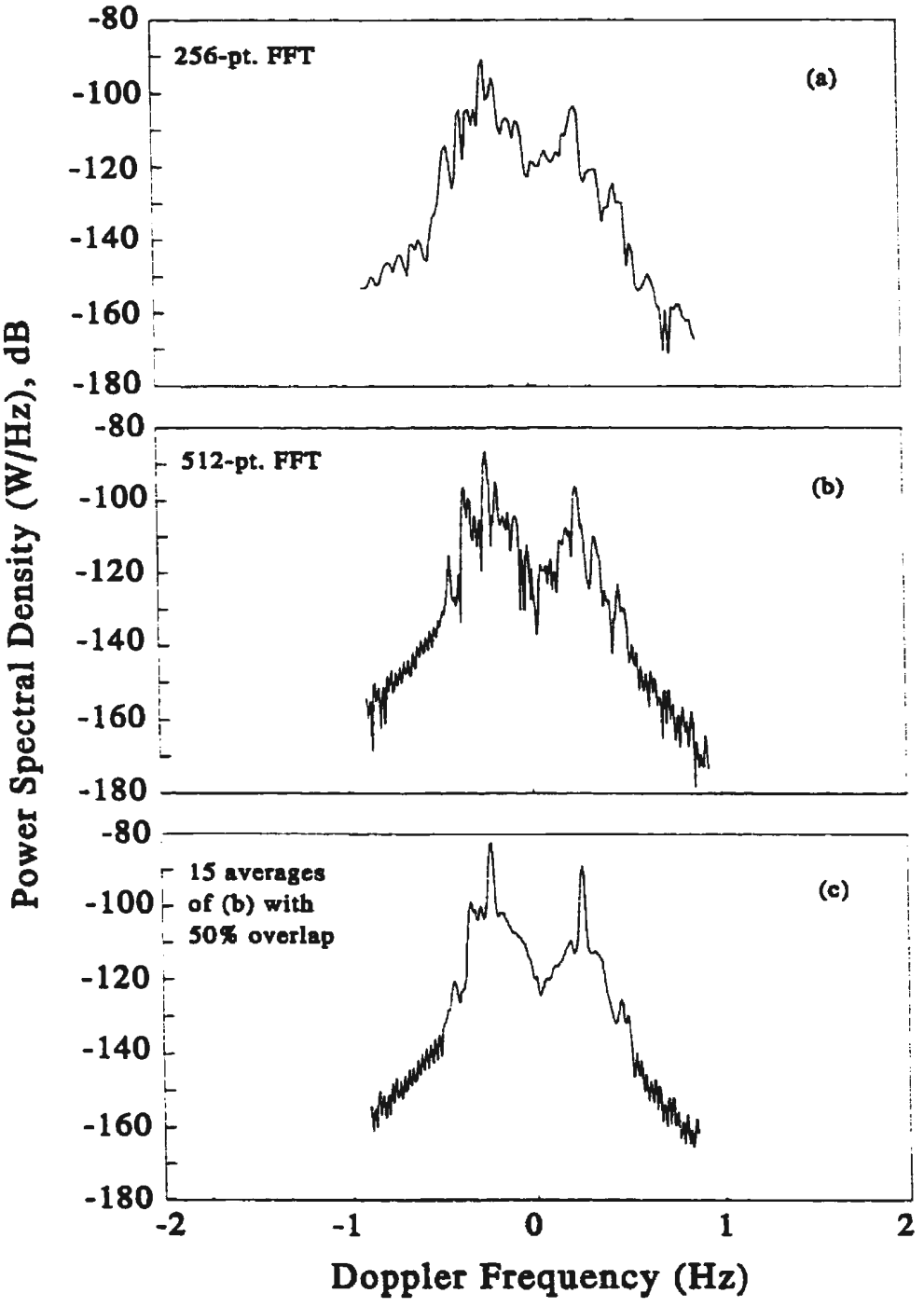

Figure 4.9: Sample results of taking the magnitude-squared of the Fourier transform of a time series modelled as discussed in the text. The clutter spectral density used in the model is from the 5.75 MHz case in Figure 4.8. The radar range is 50 km.

of 60° to the radar look direction was used. The result of this approximation shows that the apparent $(SNR)_c$ for the largest Bragg peak is approximately 70 dB. In the real data of Figure 3.10b, this value is greater than 60 dB. Given the fact that the system parameters and exact wind regime for the real data are unknown, this discrepancy between modelled and real data is quite reasonable. Furthermore, the time series lengths in each case are not the same. To indicate the effect of this parameter, Figure 4.9a–b presents the results for 256-pt and 512-pt transforms. Figure 4.9c shows the effect of taking a long time series. Cursory comparison of the latter with Figure 3.10b, which similarly uses a long time series, again serves to substantiate the model. Also, it must be remembered that median external noise values were employed in the simulations, and from [86] this could easily account for a 10 dB variation between measured and modelled spectra. Additionally, the time of day and season of the year are factors which according to [86] may significantly affect the F_a of equation (4.58). An example of an average value of F_a during summertime afternoon measurements at Cape Race, Newfoundland for a narrow range of operating frequencies is shown in Figure 4.10. At 5.75 MHz, a nominal value of F_a is just over 30 dB. The spectrum in Figure 3.10b, which was measured from a radar installation at Cape Race was obtained in late fall and could easily be subject to a different noise regime, again according to [86]. At the 50 km range used in Figures 3.10b and 4.9, the *apparent* noise floor is raised by the side lobes of the Blackman window (see Harris [83]) which was used in smoothing the results. Of course, as range increases, the spherical earth attenuation functions, $F(\cdot)$, used in the radar range equation decrease significantly, [72]. As a result, in the 5–6 MHz operating frequency interval, even the first-order clutter power will not be significantly above the noise floor when the range exceeds about 300 km, [32].

As a final note, it is obvious that the manifestation of the spectral peaks discussed throughout Section 3.6.6 will depend on the ocean conditions, the ambient noise

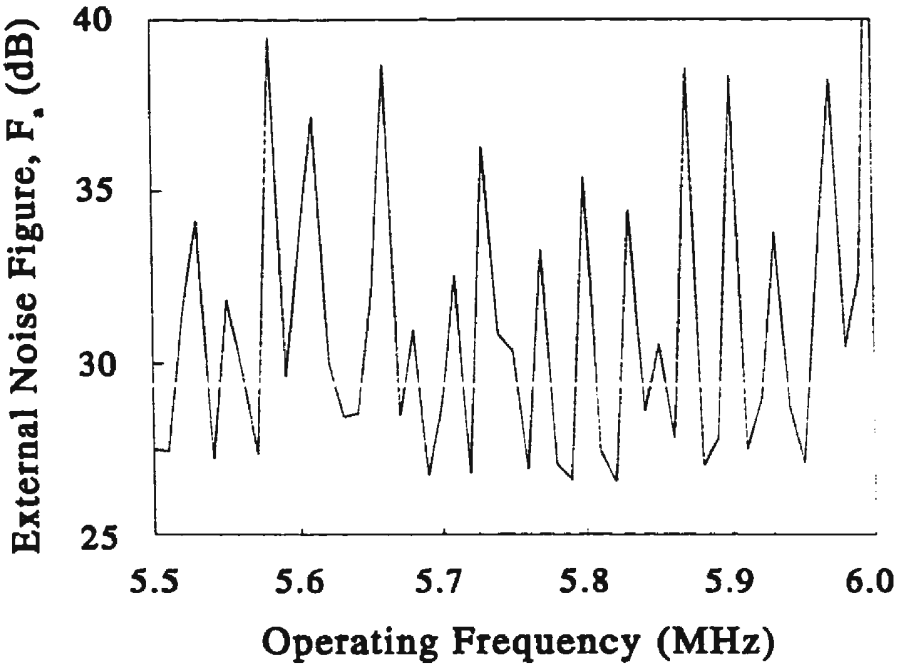

Figure 4.10: A plot of typical external noise figures for a small range in the lower HF band as measured at Cape Race, NF in July, 1998.

regime, the range at which the measurements are made, and even the signal processing schemes implemented. The simulations discussed here will provide a convenient model in setting the parameters of future experimentation for the purpose of examining the details of the theory.

4.6 General Chapter Summary

This chapter has been devoted to developing an appropriate noise model for pulsed HF radar measurements in an ocean environment. The condition of external noise limitation has been imposed, with no attempt being made to address any system noise features.

Initially, a finite number of radar pulses was considered. Later, extending this to infinitely many pulses, it was shown that the difference between the two cases was not significant. The noise model addressed the feature of the aliasing of broad band noise into the much narrower band Doppler echo from the ocean. Results were developed

for both stationary and non-stationary white Gaussian noise.

Consideration was also given to the effect of off-centre sampling of the pulses. It was shown that the effect on the noise spectral density was to multiply the on-centre result by a cosine factor whose argument was proportional to the time difference from the pulse centre.

Subsequently, it was shown that, for the pulse radar ocean clutter models developed in Chapter 3, the average, rather than peak, transmit power should be utilized when applying the results in the radar range equation. Then, using typical values for a pulsed HF radar system, plots of clutter and noise spectra were simulated. Initially, the results from ensemble averaging were illustrated. Then, using a time model for the sea echo and noise, the customary procedure of implementing the magnitude-squared of a fast Fourier transform of a data time series as an estimate of the power density spectrum was carried out. The results were seen to compare favourably with available monostatic field data.

Chapter 5

Conclusions

5.1 General Synopsis and Significant Results

The general aim of deriving a suitable model for the HF bistatic cross section of a good-conducting, random, time varying surface, with particular application to the ocean, has been accomplished. Earlier analyses by Walsh, especially [5] and [8], provided a general operator form for the various orders of scatter under the assumption of a vertical dipole source. These equations initially appear as two-dimensional spatial convolutions in the inverse Fourier transform (spatial) domain. The analysis implicitly assumes small height and small slope for the surface, the justification and limitations of which for ocean applications appear in Section 2.2. The small slope stipulation is shown from Phillips [64] to be always valid at HF for the gravity wave ocean spectrum. The legitimacy of the small height analysis is seen to be dependent on the operating frequency and ocean wave regime with the relevant condition being easily met for typical ocean conditions when operation occurs in the *lower* HF band. This, in fact, has been extensively verified experimentally by others (eg., Barrick [26]). The basic convolutions are presented in integral form to first and second order in scatter. After Rice [11], the surface is assumed to be representable as a Fourier series, the coefficients of whose terms are zero-mean Gaussian random variables. The source is initially assumed to be an elementary vertical dipole with an arbitrary current distribution. Unlike previous investigations, the reception point for all field components is

kept general – i.e. the fields are assumed to be received *bistatically*. For scatter from the non-time-varying surface, the field equations are simplified primarily via stationary phase techniques. In some cases of the second-order equations, these techniques required modification in order that they might produce tractable, yet meaningful, outcomes. The overall results are (1) a first-order field in which a single scatter occurs, in general, at a point remote from the transmitter and receiver before reception and (2) a second-order field arising from (a) two, essentially co-located, scatters at a remote point, (b) one scatter at the transmitter followed by another at a remote point before reception and (c) one scatter at a distance from both the transmitter and receiver followed by a second at the receiver immediately before reception. In all cases, the locus of the remote scattering region for a broad beam transmitter is an ellipse, any part of which may be interrogated by a narrow beam receiver if so desired. That this is the case is obvious since the transmit and receive positions are foci of an ellipse determined by the fixed sum of the distances from the transmitter and receiver to the remote scattering point. If the receiver is also broad beam, there is no way of distinguishing between the scatter from one portion of the ellipse and that from another as all of the scattered energy therefrom is received simultaneously.

There is, in fact, another stationary point arising from the second-order analysis which shows the possibility of energy from two points, neither of which is on the scattering ellipse, being received along with the other components. However, it is argued, based on the dependence of the second-order scatter on the bistatic angle, that this component will be relatively weak. Srivastava [54] shows that, even for monostatic operation, this is the case. Furthermore, if narrow beam transmission and reception are used, this component is not sensed.

With the final aim being the development of a model of the HF bistatic cross section of the ocean surface for pulsed Doppler radar, a pulsed sinusoidal current distribution is assumed for the vertical dipole following the preliminary analysis. Inverse

Fourier transformation and time convolution are then used to take the frequency-dependent fields of the basic analysis to the time domain appropriate for the task at hand. In this sense, the time parameter in the field equations dictates that the fields for a given time are being received from a particular scattering ellipse. The bistatic results are shown to contain the essential characteristics of their monostatic counterparts (where such exist) as a special case – i.e. when the bistatic angle, ϕ_0, is set to 0°.

In order to apply the field equation results of Chapter 2 to the ocean, it is necessary to allow the scattering surface to become time varying. This is accomplished in Chapter 3 by specifying an e^{jwt} time dependency for the surface components, thus allowing the Fourier surface coefficients to become time varying while maintaining their usual properties as zero-mean Gaussian random variables. The frequencies and wavenumbers of the first-order surface components are taken to be related through the linear deep-water dispersion relationship. Based on Hasselmann's theory [59] of energy transfer between constituents of the gravity wave spectrum, the Fourier coefficients of the second-order surface features are written in terms of products of the first-order coefficients and a so-called *hydrodynamic coupling coefficient* [8]. In this way, it is seen that second-order scattering actually arises from (1) single scatters from second-order surface elements and (2) a double scattering from first-order features. This compares with the standard conclusions reached in monostatic investigations (eg. [24, 54, 8]).

With the appropriate features of the time varying surface being substituted into the field equations, two time dependencies become apparent. One of these, arising from considerations in Chapter 2, dictates from where on the surface the radiation is being received. The other accounts for field changes due to the fact that the surface is varying with time. The standard procedure of ensemble averaging the various components of the bistatically received fields leads, upon temporal Fourier

transformation, to a Doppler power spectral density. Comparison with the bistatic radar range equation then allows a Doppler cross section per unit area of scattering surface to be derived.

An important feature of the first-order bistatic cross section is that its peaks are indicative of Bragg scatter, appropriately modified by the bistatic angle. The surface waves responsible for these spectral characteristics travel inward and outward along the scattering ellipse normal at the position(s) being interrogated and have a wavenumber of $2k_0 \cos\phi_0$ (i.e. a wavelength of $\frac{\lambda_0}{2\cos\phi_0}$, where λ_0 is the wavelength of the transmitted signal). These give rise to peaks in Doppler cross sections at radian frequencies of $\pm\sqrt{2k_0 g \cos\phi_0}$, the so-called Bragg frequencies, $\pm\omega_B$. This result was previously derived by Walsh and Dawe [9] and led to a convenient approach to development of the second-order bistatic effects presented in this work.

In the case of the double "patch" scatter phenomenon, the magnitude of the *sum* of the two wave vectors associated with the ocean waves responsible for the scattering must be $2k_0 \cos\phi_0$ and must likewise point along a normal to the scattering ellipse. The well known monostatic corner reflector spectral peaks which appear at $\pm 2^{\frac{3}{4}}\omega_B$ are seen to become $\pm 2^{\frac{3}{4}}\sqrt{\frac{[1 \pm \sin\phi_0]^{\frac{1}{2}}}{\cos\phi_0}}\,\omega_B$ for the bistatic case. Thus, there are four spectral peaks, rather than two as in the monostatic case, associated with the corner reflector phenomenon. The relative importance of these is largely dependent on the ocean surface conditions. Again, it may be noted that for monostatic operation, $\phi_0 = 0$ and this effect properly reduces to $\pm 2^{\frac{3}{4}}\omega_B$. The $\pm\sqrt{2}\,\omega_B$ peaks, which are familiar features of monostatic spectra, are again evident in the bistatic case. Of course, for a given frequency of operation, they will clearly appear at different frequency points for different modes of operation (i.e. monostatic or bistatic).

For double scattering where only one of the scatters occurs remotely from either the transmitter or receiver, the wavenumber of the distant scatterer must, as for other cases, be $2k_0 \cos\phi_0$. Spectral peaks due to these effects appear at $\pm 2\omega_B$ and, in

general, split peaks occur around zero Doppler. In the monostatic counterpart, the former also appear, but the latter degenerate to a single peak at zero Doppler.

The relative importance of the spectral phenomena associated with the various second-order bistatic fields is highly dependent on the particular ocean surface characteristics at the time of data collection as well as on the radar operating frequency. Furthermore, the cross sections depicted in Chapter 3 were based on idealized ensemble averaging and in every case assumed a fully developed sea. This last feature was imposed by the inclusion of the Pierson-Moskowitz result [60] as a model for the non-directional ocean spectrum.

In an attempt to more closely model what actually transpires in the collecting of Doppler power spectra from pulsed radars, the results of Chapter 3 for the idealized case were used in a time model of a stationary Gaussian process given by Pierson [61]. Additionally, this model was subjected to a typical noise environment as might be viewed by a pulse radar. External noise limitation was assumed. The noise, too, was modelled as a zero-mean Gaussian process. Initially, a model for stationary noise was developed considering finite and infinite numbers of pulses. Then, non-stationary noise results were derived. In all cases, the Doppler noise power spectral density was shown to be virtually independent of the number of pulses sampled, and this was *exactly* so for the non-stationary noise. For any duty cycle and any number of pulses the Doppler noise power spectral densities, when sampling occurred at the pulse centres, were seen to be within 3 dB of the ambient noise densities derived from noise figures found in [86]. This was independent of stationarity. Centre and off-centre pulse sampling were considered with the latter imposing a cosine variation, dependent on the sampling distance from the pulse centre, on the former.

It was shown that, for pulse radar interrogation of the sea surface, the average rather than peak transmit power should be used in the radar range equation. Using this fact and Pierson's model [61] for stationary Gaussian processes for both the

clutter (i.e. sea echo) and noise, a time series of a typical bistatic return from the ocean, including the noise regime, was developed. To simulate the usual procedure for obtaining Doppler power spectra, this time series was fast Fourier transformed. The magnitude-squared of the result was used as an *estimate* of the true Doppler power spectral density. It was illustrated that the result modelled available monostatic data reasonably well (no bistatic data were available). This model also demonstrated that the observation of the spectral features discussed in Chapter 3 for the idealized representations will definitely be dependent on the operating frequency, the sea state, and the noise regime. Also, given that for a typical observation period the noise content is unlikely to change significantly, the survival of the various second-order peaks will clearly be dependent on the range being monitored.

It is submitted that the main new feature of this work is the presentation of the various portions of the second-order bistatic HF cross sections of the ocean surface. Secondly, a useful theoretical basis for the introduction of noise into the cross section models has been derived. No dedicated experimentation has been undertaken to verify these models. However, it has been shown that the models do indeed collapse to their existing monostatic counterparts with the introduction of the appropriate parameter (namely, the bistatic angle set to zero). Furthermore, comparison with typical real monostatic data appears to validate the assertions herein. This being the case, a means of modelling the fields and related ocean cross sections and Doppler power spectral densities at HF for a general observation point is now available.

5.2 Suggestions for Future Work

The analyses which have culminated in this document have engendered many ideas and questions which could be pursued in future research. A few of the more obvious of these are briefly discussed here.

At the outset, it may be noted that the results presented in the thesis are founded

on the so-called "small height" approximation. However, Walsh's general formulations [57] do indeed account for surface heights which are not small (i.e. $k\xi \not\ll 1$), and this fact is intimated in equation (1.19). A development of (1.19) to produce corrections to the "small height" field equations would certainly appear to be a legitimate endeavour. It seems feasible that such corrections might give further insight into the saturation difficulties discussed in Section 2.2. Additionally, careful experimental investigation of this saturation phenomenon could indicate the proper limits to be placed on the definition of "small height" in the context of the bistatic models.

Also implicit in the present formulations is the assumption that the scattering surface is a good conductor. In fact, this condition was placed upon the developments by Walsh *et al.* [8] before imposition of the small-height constraint. While this considerably simplifies the ensuing analysis, it clearly restricts the class of surfaces which may be considered. The effects of relaxing this constraint would appear to be worthy of investigation.

In addition to the fundamental problems which may be pursued, there are several experimental possibilities arising from this work. One aspect which clearly requires empirical investigation is the significance of the singularities in the bistatic second-order cross section due to scattering at the transmitting and/or receiving antennas. It was pointed out that these singularities at (or near) zero Doppler and $\pm 2\omega_B$ are likely to be enhanced when the radar components are surrounded by sea water. This is especially important near zero Doppler. In fact, it was shown that for bistatic operation a split peak occurs in that region of the spectrum. If these effects are significant for certain operating parameters and surface conditions, they may obscure slowly moving targets.

Given that bistatic and monostatic radar operations are able to provide different views of the same patch of surface, it is reasonable to now assume that directional properties of surface phenomena (eg. waves and currents) may be obtained by using

a single transmitter and two receiving antennas. Of course, the reception would have to be synchronized. Experimentation to explore this possibility appears appropriate. Finally, it is noted that the real spectra presented for comparisons with the models of Chapters 3 and 4 were not produced from experiments designed for validation of ocean clutter phenomena. Consequently, it is felt that further dedicated experimentation would greatly aid in model validation and acceptance in the remote sensing community. It is deemed that the work presented here provides a solid basis warranting additional research in the context of bistatic operation of pulsed HF Doppler radar in the marine environment. It is expected that such exploration will prove fruitful in augmenting the role of HF radar as an ocean sensor as it has evolved during the last two decades.

References

[1] M. Tucker, *Waves in Ocean Engineering*. New York: Ellis Horwood, 1991.

[2] E. Gill, M. Khandekar, R. Howell, and J. Walsh, "Ocean surface wave measurement using a steerable high frequency narrow beam ground wave radar," *J. of Atmosphere and Oceanic Technology*, vol. 13, no. 3, 1996. Published by the American Meteorological Society.

[3] Antenna Standards Committee of the IEEE Antennas and Propagation Society, The Institute of Electrical and Electronics Engineers Inc., New York, *IEEE Standard Definitions of Terms for Antennas*, 145-1983 ed., 1983.

[4] M. Poon, R. Khan, and S. Le-Ngoc, "A singular value decomposition (SVD) based method for suppressing ocean clutter in high frequency radar," *IEEE Transactions on Signal Processing*, vol. 41, no. 3, pp. 1421–1425, 1993.

[5] J. Walsh, "On the theory of electromagnetic propagation across a rough surface and calculations in the VHF region," OEIC Report N00232, Memorial University of Newfoundland, St. John's, Newfoundland, 1980.

[6] D. Barrick, "Near-grazing illumination and shadowing of rough surfaces," *Radio Science*, vol. 30, no. 3, pp. 563–580, 1995.

[7] G. Valenzuela, "Theories for the interaction of electromagnetic and ocean waves – a review," *Boundary -Layer Meteorology*, no. 13, pp. 61–85, 1978.

[8] J. Walsh, R. Howell, and B. Dawe, "Model development for evaluation studies of ground wave radar," Contract Report 90-C14, Centre for Cold Ocean Resources Engineering, 1990. (Prepared for Department of National Defence, Government of Canada, DSS Contract Number W7714-8-5655/01-SS).

[9] J. Walsh and B. Dawe, "Development of a model for the first order bistatic ocean clutter radar cross section for ground wave radars," contract report, Northern Radar Systems Limited, 1994. (Contract Report Prepared for the Defence Research Establishment Ottawa, Department of National Defence, Government of Canada, DSS Contract Number W7714-1-9569/01-ST).

[10] J. Strutt, *The Theory of Sound*, vol. 2. New York: Dover, 1945.

[11] S. Rice, "Reflection of electromagnetic waves from a slightly rough surface," in *Theory of Electromagnetic Waves* (K. Kline, ed.), pp. 351–378, New York: Interscience, 1951.

[12] J. Wait, "Perturbation analysis for reflection from two-dimensional periodic sea waves," *Radio Science*, no. 6, pp. 387–391, 1971.

[13] A. Ishimaru, *Electromagnetic Wave Propagation, Radiation and Scattering.* Englewood Cliffs, New Jersey: Prentice-Hall Inc., 1991.

[14] D. Barrick, "Theory of HF and VHF propagation across the rough sea (Parts 1 and 2)," *Radio Science*, vol. 6, pp. 517–533, 1971.

[15] R. Rosich and J. Wait, "A general perturbation solution for reflection from two-dimensional periodic surfaces," *Radio Science*, vol. 12, pp. 719–729, 1977.

[16] K. Mitzner, "Effect of small irregularities on electromagnetic scattering from an interface of arbitrary shape," *Mathematical Physics*, vol. 5, pp. 1776–1786, 1964.

[17] E. Rodriguez and Y. Kim, "A unified perturbation expansion for surface scattering," *Radio Science*, vol. 27, no. 1, pp. 79–93, 1992.

[18] W. Peake, "Theory of radar return from terrain," in *IRE National Convention Record*, vol. 7, pp. 27–41, 1959.

[19] G. Valenzuela, "Depolarization of EM waves by slightly rough surfaces," *IEEE Transactions on Antennas and Propagation*, vol. 15, pp. 552–557, 1967.

[20] B. Kinsman, *Wind Waves.* New York: Dover Publications Inc., 1984.

[21] D. Barrick, "First-order theory and analysis of MF/HF/VHF scatter from the sea," *IEEE Transactions on Antennas and Propagation*, vol. 20, pp. 2–10, 1972.

[22] D. Crombie, "Doppler spectrum of sea echo at 13.56 mc./s.," *Nature*, vol. 175, pp. 681–682, 1955.

[23] K. Hasselmann, "Determination of ocean wave spectra from Doppler return from sea surface," *Nature Physical Science*, vol. 229, pp. 16–17, 1971.

[24] D. Barrick, "Remote sensing of sea state by radar," in *Remote Sensing of the Troposphere* (V. Derr, ed.), ch. 12, pp. 1–46, Washington, DC: U.S. Government Printing Office, 1972.

[25] E. Shearman, "Radio science and oceanography," *Radio Science*, vol. 18, no. 3, pp. 299–320, 1983.

[26] D. Barrick, "The role of the gravity-wave dispersion relation in HF radar measurements of the sea surface," *IEEE J. Oceanic Eng.*, vol. 11, no. 2, pp. 286–292, 1986.

[27] D. Barrick and B. Lipa, "The second-order shallow water hydrodynamic coupling coefficient in interpretation of HF radar sea echo," *IEEE J. Oceanic Eng.*, vol. 11, no. 2, pp. 310–315, 1986.

[28] B. Lipa and D. Barrick, "Extraction of sea state from HF radar sea echo: Mathematical theory and modeling," *Radio Science*, vol. 21, no. 1, pp. 81–100, 1986.

[29] L. Wyatt, J. Venn, G. Burrows, A. Ponsford, M. Moorhead, and J. Van Heteren, "HF radar measurements of ocean wave parameters during NURWEC," *IEEE J. Oceanic Eng.*, vol. OE-21, no. 2, pp. 219–234, 1986.

[30] E. Gill and J. Walsh, "Extraction of ocean wave parameters from HF backscatter received by a four-element array: Analysis and application," *IEEE J. Oceanic Eng.*, vol. 17, no. 4, pp. 376–386, 1992.

[31] R. Howell and J. Walsh, "Measurement of ocean wave spectra using narrow beam HF radar," *IEEE J. Oceanic Eng.*, vol. 18, no. 3, pp. 296–305, 1993.

[32] K. Hickey, E. Gill, J. Helbig, and J. Walsh, "Measurement of ocean surface currents using a long-range, high-frequency ground wave radar," *IEEE J. Oceanic Eng.*, vol. 19, no. 4, pp. 549–554, 1994.

[33] D. Johnstone, "Second-order electromagnetic and hydrodynamic effects in high-frequency radio wave scattering from the sea," Technical Report 3615-3, Stanford Electronics Laboratories, Stanford University, California, 1965.

[34] J. Stratton, *Electromagnetic Theory.* New York: McGraw-Hill, 1941.

[35] P. Beckman and A. Spizzichino, *The Scattering of Electromagnetic Waves from Rough Surfaces.* Norwood, Mass.: Artech House Inc., 1987.

[36] R. Kodis, "A note on the theory of scattering from an irregular surface," *IEEE Transactions on Antennas and Propagation*, vol. 14, pp. 77–82, 1966.

[37] D. Barrick, "Rough surface scattering based on specular point theory," *IEEE Transactions on Antennas and Propagation*, vol. 16, pp. 449–454, 1968.

[38] D. Barrick and E. Bahar, "Rough surface scattering using specular point theory," *IEEE Transactions on Antennas and Propagation*, vol. 29, pp. 798–800, 1981.

[39] D. Barrick, "Wind dependence of quasi-specular microwave sea scatter," *IEEE Transactions on Antennas and Propagation*, vol. 22, pp. 135–136, 1974.

[40] F. Ulaby and E. Elachi, *Radar Polarimetry for Geoscience Applications.* Norwood, Mass.: Artech House Inc., 1990.

[41] J. Wright, "A new model for sea clutter," *IEEE Transactions on Antennas and Propagation*, vol. 16, p. 2, 1968.

[42] G. Brown, "Backscattering from a Gaussian-distributed perfectly conducting rough surface," *IEEE Transactions on Antennas and Propagation*, vol. 26, pp. 472–482, 1978.

[43] G. Brown, "Application of the integral equation method of smoothing to random surface scattering," *IEEE Transactions on Antennas and Propagation*, vol. 32, pp. 1308–1312, 1984.

[44] G. Brown, "A scattering result for rough surfaces having small height but arbitrary slope," *Wave Motion*, vol. 12, pp. 475–483, 1990.

[45] G. Brown, "A new approach to the analysis of rough surface scattering," *IEEE Transactions on Antennas and Propagation*, vol. 39, pp. 943–948, 1991.

[46] E. Bahar, "Radio wave propagation in stratified media with nonuniform boundaries and varying electrical parameters – Full wave analysis," *Can. J. Physics*, vol. 50, no. 24, pp. 3132–3142, 1972.

[47] E. Bahar and G. Rajan, "Depolarization and scattering of electromagnetic waves by irregular boundaries for arbitrary incident and scatter angles – Full-wave solutions," *IEEE Transactions on Antennas and Propagation*, vol. 27, no. 2, pp. 214–225, 1979.

[48] R. Collin, "Electromagnetic scattering from perfectly conducting rough surfaces (A new full wave method)," *IEEE Transactions on Antennas and Propagation*, vol. 40, no. 12, pp. 1466–1477, 1992.

[49] E. Bahar, "Full-wave solutions for the scattered radiation field from rough surfaces with arbitrary slope and frequency," *IEEE Transactions on Antennas and Propagation*, vol. 28, pp. 11–21, 1980.

[50] E. Bahar, "Full-wave analysis for rough surface diffuse, incoherent radar cross sections with height-slope correlations included," *IEEE Transactions on Antennas and Propagation*, vol. 39, no. 9, pp. 1293–1304, 1991.

[51] E. Bahar and B. Lee, "Full-wave solutions for rough-surface bistatic radar cross sections: Comparison with small perturbation, physical optics, numerical and experimental results," *Radio Science*, vol. 29, no. 2, pp. 407–429, 1995.

[52] E. Bahar, B. Lee, G. Huang, and R. Kubik, "Like- and cross-polarized transmission scatter cross sections for random rough surfaces: Full wave solutions," *Radio Science*, vol. 30, no. 3, pp. 545–562, 1995.

[53] R. Collin, "Full wave theories for rough surface scattering: An updated assessment," *Radio Science*, vol. 29, no. 5, pp. 1237–1254, 1994.

[54] S. Srivastava, *Analysis of HF scattering from an ocean surface: An alternative approach incorporating a dipole source.* PhD thesis, Memorial University of Newfoundland, St. John's, Newfoundland, 1984.

[55] J. Walsh and R. Donnelly, "A consolidated approach to two-body electromagnetic scattering problems," *Phys. Review A*, vol. 36, no. 9, pp. 4474–4485, 1987.

[56] J. Walsh and S. Srivastava, "Rough surface propagation and scatter 1. General formulation and solution for periodic surfaces," *Radio Science*, vol. 22, no. 2, pp. 193–208, 1987.

[57] J. Walsh and B. Dawe, "Analytic model development for the study of ground wave radars as remote sensors in an ocean environment II," technical report, Centre for Cold Ocean Resources Engineering, 1988. (Prepared for Department of National Defence, Government of Canada, DSS File No. 20ST.W2207-6-AF04).

[58] R. Howell, "An algorithm for the extraction of ocean wave spectra from narrow beam HF radar backscatter," Master's thesis, Memorial University of Newfoundland, St. John's, Newfoundland, 1990.

[59] K. Hasselmann, "On the nonlinear energy transfer in a gravity wave spectrum, Part 1. General theory," *J. of Fluid Mechanics*, vol. 12, pp. 481–500, 1962.

[60] W. Pierson and L. Moskowitz, "A proposed spectral form for fully developed seas based upon the similarity theory of S.A. Kitaigorodskii," *J. Geophys. Res.*, vol. 69, no. 24, pp. 5181–5190, 1964.

[61] W. Pierson, "Wind generated gravity waves," *Advances in Geophysics*, vol. 2, pp. 93–178, 1955.

[62] M. Earle and J. Bishop, *A Practical Guide to Ocean Wave Measurement and Analysis.* ENDECO Inc., Marion, MA, U.S.A., 1984.

[63] R. Collin, *Antennas and Radio Wave Propagation.* New York: McGraw-Hill Book Company, 1985.

[64] O. Phillips, *The Dynamics of the Upper Ocean.* Cambridge, England: Cambridge University Press, 1977.

[65] R. King, "An introduction to electromagnetic surface wave propagation," *IEEE Transactions on Education*, pp. 59–61, 1966.

[66] N. Bleistein and R. Handelsman, *Asymptotic Expansion of Integrals.* New York: Holt, Rinehart and Winston, 1975.

[67] A. Jeffrey, *Handbook of Mathematical Formulas and Integrals.* New York: Academic Press, 1995.

[68] E. Gill and J. Walsh, "On the second-order high frequency bistatic ground wave radar cross section of the ocean surface," in *Proceedings of IEEE Canadian Conference on Electrical and Computer Engineering*, vol. 2, pp. 516–519, 1997.

[69] B. Friedman, *Lectures on Applications Oriented Mathematics.* San Francisco: Holden-Day, Inc., 1969.

[70] P. Derusso, R. Roy, and C. Close, *State Variables for Engineers.* New York: John Wiler and Sons, Inc., 1967.

[71] S. Haykin, *Communication Systems.* New York: John Wiley and Sons, Inc., 1994.

[72] B. Dawe, "Radio wave propagation over earth: Field calculations and an implementation of the roughness effect," Master's thesis, Memorial University of Newfoundland, St. John's, Newfoundland, 1988.

[73] A. Papoulis, *Probability, Random Variables and Stochastic Processes.* New York: McGraw-Hill Book Company, 1984.

[74] B. Weber and D. Barrick, "On the nonlinear theory for gravity waves on the ocean's surface. Part 1: Derivations," *Journal of Physical Oceanography*, vol. 7. no. 1, pp. 1–10, 1977.

[75] D. Barrick and J. Snider, "The statistics of HF sea-echo Doppler spectra," *IEEE Transactions on Antennas and Propagation*, vol. 25, pp. 19–28, 1977.

[76] J. Thomas, *An Introduction to Statistical Communication Theory.* New York: John Wiley and Sons, 1969.

[77] B. Lathi, *Random Signals and Communication Theory.* Scranton, Penn.: International Textbook Company, 1968.

[78] D. Trim, *Calculus and Analytic Geometry.* Reading, Mass.: Addison-Wesley Publishing Company, 1983.

[79] D. Barton, *Modern Radar Systems Analysis.* Norwood, Mass.: Artech House Inc., 1987.

[80] J. Ewing, "Some results from the Joint North Sea Wave Project of interest to engineers," in *The dynamics of marine vehicles and structures in waves* (R. Bishop and W. Price, eds.), London, Eng.: Mechanical Engineering Publications Ltd., 1975. Taken from reference[1].

[81] J. Walsh, "On the relationship between the Fourier coefficients for a random time varying surface and the Pierson-Moskowitz ocean model," 1998. Private correspondence.

[82] G. Tyler, C. Teague, R. Stewart, A. Peterson, W. Munk, and J. Joy, "Wave directional spectra from synthetic aperture observations of radio scatter," *Deep-Sea Research*, vol. 21, pp. 989–1016, 1974.

[83] F. Harris, "On the use of windows for harmonic analysis with the discrete Fourier transform," *IEEE Proceedings*, vol. 66, no. 1, pp. 51–83, 1978.

[84] B. Lipa and D. Barrick, "Analysis methods for narrow-beam high-frequency radar sea echo," Technical Report ERL 420-WPL 56, National Oceanic and Atmospheric Administration, U.S. Department of Commerce, 1982.

[85] E. Gill, "An alogorithm for the extraction of ocean wave parameters from wide beam HF radar (CODAR) backscatter," Master's thesis, Memorial University of Newfoundland, St. John's, Newfoundland, 1990.

[86] International Telecommunications Union, Geneva, *Propagation in Ionized Media (ITU-R Recommendations, 1994 PI Series Volume)*, 1994.

[87] J. Wait, *Electromagnetic Wave Theory*. New York: Harper and Row, 1985.

[88] S. Wolfram, *Mathematica, A System for Doing Mathematics by Computer*. New York: Addison-Wesley Publishing Company, 1991.

[89] M. Abramowitz and I. Stegun, eds., *Handbook of Mathematical Functions*. New York: Dover Publications, Inc., 9 ed., 1972.

[90] The MathWorks, Inc., Natick, Massachusetts, *MATLAB, version 4.2b*, 1994.

Appendix A

Scattering from a Time Invariant Surface

This appendix addresses many of the details associated with obtaining the first- and second-order electric field components for scattering from a non-time-varying surface when the source is an elementary vertical dipole. Section A.1 delineates the relevant procedures and assumptions necessary for providing a tractable form of the first-order bistatic component, while Section A.2 similarly treats the second-order problem.

A.1 The First-order Field

A.1.1 Asymptotic Integral Form for the First-order Field

In order to explicitly write the convolution of equation (2.15) in integral form, it is advantageous to express the surface gradient $\vec{\nabla}_{xy}$ in polar coordinates as

$$\vec{\nabla}_{xy} = \hat{\rho}\frac{\partial}{\partial\rho} + \hat{\theta}\frac{1}{\rho}\frac{\partial}{\partial\theta}\,. \tag{A.1}$$

Applying this to the bracketed factor in equation (2.15), while noting the absence of any θ dependence, gives

$$\begin{aligned}\vec{\nabla}_{xy}\left(C_0F(\rho)\frac{e^{-jk\rho}}{2\pi\rho}\right) &= \frac{\partial}{\partial\rho}\left(C_0F(\rho)\frac{e^{-jk\rho}}{2\pi\rho}\right)\hat{\rho} \\ &= \left(-jkC_0F(\rho)\frac{e^{-jk\rho}}{2\pi\rho}\right)\hat{\rho} + \mathbf{X}\hat{\rho}\end{aligned} \tag{A.2}$$

where $\mathbf{X}$ involves the derivatives of $F(\rho)$ and $\left(\frac{1}{2\pi\rho}\right)$. It is obvious that in the asymptotic sense (i.e. for large distances, ρ) the derivative involving $\left(\frac{1}{2\pi\rho}\right)$ will be much less than the leading term above. Also, Wait [87], Section 6.7, shows that for a highly conductive surface as is being considered here, $F(\rho)$ is roughly proportional to $\frac{1}{\rho}$ for large ρ. Thus, $\frac{\partial}{\partial\rho}F(\rho) << F(\rho)$ for large ρ and equation (A.2) may be approximated in the asymptotic sense as

$$\vec{\nabla}_{xy}\left(C_0F(\rho)\frac{e^{-jk\rho}}{2\pi\rho}\right) \approx \left(-jkC_0F(\rho)\frac{e^{-jk\rho}}{2\pi\rho}\right)\hat{\rho}\,. \tag{A.3}$$

Substituting (A.3) into equation (2.15), the asymptotic form of the latter is

$$\left(E^+_{0_n}\right)_1 \approx -jkC_0\left[\left(\hat{\rho}\cdot\vec{\nabla}_{xy}(\xi)F(\rho)\frac{e^{-jk\rho}}{2\pi\rho}\right) \overset{xy}{*} F(\rho)\frac{e^{-jk\rho}}{2\pi\rho}\right]\,. \tag{A.4}$$

From Figure 2.1, it may be seen that (A.4) may be cast as the double convolution integral

$$\begin{aligned}\left(E^+_{0_n}\right)_1 \;\approx\; & -jkC_0\int_{y_1}\int_{x_1}\hat{\rho}_1\cdot\vec{\nabla}_{x_1y_1}(\xi(x_1,y_1))F\left(\sqrt{x_1^2+y_1^2}\right)\\ & \cdot\frac{e^{-jk\sqrt{x_1^2+y_1^2}}}{2\pi\sqrt{x_1^2+y_1^2}}\cdot F\left(\sqrt{(x-x_1)^2+(y-y_1)^2}\right)\\ & \cdot\frac{e^{-jk\sqrt{(x-x_1)^2+(y-y_1)^2}}}{2\pi\sqrt{(x-x_1)^2+(y-y_1)^2}}dx_1dy_1\,.\end{aligned} \tag{A.5}$$

Recognizing, of course, that $\rho_1=\sqrt{x_1^2+y_1^2}$ and $\rho_2=\sqrt{(x-x_1)^2+(y-y_1)^2}$,

$$\begin{aligned}\left(E^+_{0_n}\right)_1 \;\approx\; & \frac{-jkC_0}{(2\pi)^2}\int_{y_1}\int_{x_1}\hat{\rho}_1\cdot\vec{\nabla}_{x_1y_1}(\xi(x_1,y_1))F(\rho_1)F(\rho_2)\\ & \cdot\frac{e^{-jk(\rho_1+\rho_2)}}{\rho_1\rho_2}dx_1dy_1\,,\end{aligned} \tag{A.6}$$

which is equation (2.16).

Considering $\hat{\rho}_1 \cdot \vec{\nabla}_{x_1 y_1}(\xi(x_1, y_1))$ of (A.6) in conjunction with equations (2.18) and (A.1), we have

$$\begin{aligned}
\hat{\rho}_1 \cdot \vec{\nabla}_{x_1 y_1}(\xi(x_1, y_1)) &= \hat{\rho}_1 \cdot \left\{ \hat{\rho}_1 \frac{\partial}{\partial \rho_1} \xi(x_1, y_1) + \hat{\theta}_1 \frac{1}{\rho_1} \frac{\partial}{\partial \theta_1} \xi(x_1, y_1) \right\} \\
&= \frac{\partial}{\partial \rho_1} \xi(x_1, y_1) \\
&= j \sum_{m,n} P_{\vec{K}_{mn}} K_{mn} \cos(\theta_{mn} - \theta_1) e^{j\rho_1 K_{mn} \cos(\theta_{mn} - \theta_1)} \qquad \text{(A.7)}
\end{aligned}$$

since $\hat{\rho}_1 \cdot \hat{\theta}_1 = 0$. Using equation (A.7) in (A.6) results in

$$\begin{aligned}
\left(E^+_{0_n}\right)_1 \approx \frac{kC_0}{(2\pi)^2} \sum_{m,n} P_{\vec{K}_{mn}} K_{mn} \int_{y_1} \int_{x_1} \cos(\theta_{mn} - \theta_1) F(\rho_1) F(\rho_2) \\
\cdot \frac{1}{\rho_1 \rho_2} \cdot e^{j\rho_1 [K_{mn} \cos(\theta_{mn} - \theta_1) - k]} \cdot e^{-jk\rho_2} \, dx_1 dy_1 \, , \qquad \text{(A.8)}
\end{aligned}$$

which is precisely equation (2.19).

A.1.2 Reduction of the First-order Field to a Single Integral

A.1.2.1 A Stationary Phase Form for the First-order Field

Under the conditions stated in Section 2.2.2, the δ-integral of equation (2.25) may be determined via a stationary phase approach. Bleistein and Handelsman [66] (or more recently, with application to scattering problems, Ishimaru [13], Appendix C) develop such an approach to a complex integral of the form

$$I = \int F(\delta) e^{jZf(\delta)} d\delta \, . \qquad \text{(A.9)}$$

Here, Z is a large positive real number and, in general, $f(\delta)$ and $F(\delta)$ are complex functions of the complex variable δ. Furthermore, $F(\delta)$ is slowly varying. The result of applying the stationary phase theory to (A.9) is

$$I \approx \sqrt{\frac{2\pi}{Z}} \frac{F(\delta_s)}{\sqrt{-j \frac{\partial^2 f(\delta_s)}{\partial \delta^2}}} e^{jZf(\delta_s)} \qquad \text{(A.10)}$$

where $\delta = \delta_s$ is the stationary phase point given by

$$\frac{\partial f(\delta)}{\partial \delta} = 0 \, .$$

As the name implies, (A.10) is the result of evaluating (A.9) along a contour where the phase of the exponential term is essentially constant, thus mitigating the oscillations which naturally occur in $e^{jZf(\delta)}$ for large Z.

The I_δ integral of equation (2.25) may now be considered in view of this stationary phase theory. For reference, the integral is repeated here as

$$\begin{aligned} I_\delta &= \int_0^{2\pi} \cos(\theta_{mn} - \theta_1) F(\rho_1) F(\rho_2) \\ &\quad \cdot e^{j\frac{\rho K_{mn}}{2}[\cosh\mu\cos\delta\cos(\theta_{mn}-\theta)+\sinh\mu\sin\delta\sin(\theta_{mn}-\theta)]} d\delta \ . \end{aligned} \tag{A.11}$$

Comparing equations (A.9) with (A.11), the following are easily identified:

$$\begin{aligned} Z &= \frac{\rho K_{mn}}{2} \\ f(\delta) &= [\cosh\mu\cos\delta\cos(\theta_{mn}-\theta) + \sinh\mu\sin\delta\sin(\theta_{mn}-\theta)] \\ F(\delta) &= \cos(\theta_{mn}-\theta_1) F(\rho_1) F(\rho_2) \ . \end{aligned}$$

Since the stationary points are required, the solution of

$$\frac{\partial f(\delta)}{\partial \delta} = -\cosh\mu\sin\delta\cos(\theta_{mn}-\theta) + \sinh\mu\cos\delta\sin(\theta_{mn}-\theta) = 0$$

must be found. These are obviously the points, δ_s, satisfying

$$\tan\delta_s = \tanh\mu\tan(\theta_{mn}-\theta) \ , \tag{A.12}$$

which is equation (2.27) of Section 2.2.2. For use in (A.10), it is seen that the second derivative of $f(\delta)$ is given by

$$\frac{\partial^2 f(\delta)}{\partial \delta^2} = -[\cosh\mu\cos\delta\cos(\theta_{mn}-\theta) + \sinh\mu\sin\delta\sin(\theta_{mn}-\theta)] \ . \tag{A.13}$$

Therefore, from equations (A.10), (A.11), and (A.13), the δ-integral may be approximated as

$$\begin{aligned} I_\delta &\approx \sqrt{2\pi}\cos(\theta_{mn}-\theta_1) F(\rho_1) F(\rho_2) \\ &\quad \cdot \frac{e^{j\frac{\rho K_{mn}}{2}[\cosh\mu\cos\delta\cos(\theta_{mn}-\theta)+\sinh\mu\sin\delta\sin(\theta_{mn}-\theta)]}}{\sqrt{j\frac{\rho K_{mn}}{2}[\cosh\mu\cos\delta\cos(\theta_{mn}-\theta)+\sinh\mu\sin\delta\sin(\theta_{mn}-\theta)]}} \ , \end{aligned} \tag{A.14}$$

it being understood that δ is subject to the constraint of equation (A.12). Also, from equation (2.21), it is clear that ρ_1, ρ_2, and θ_1 are functions of δ.

A.1.2.2 Interpretation of the Stationary Phase Result in Terms of the Bistatic Geometry

Since Figure 2.3 is used extensively in the analysis of this section, it is repeated here for reference as Figure A.1.

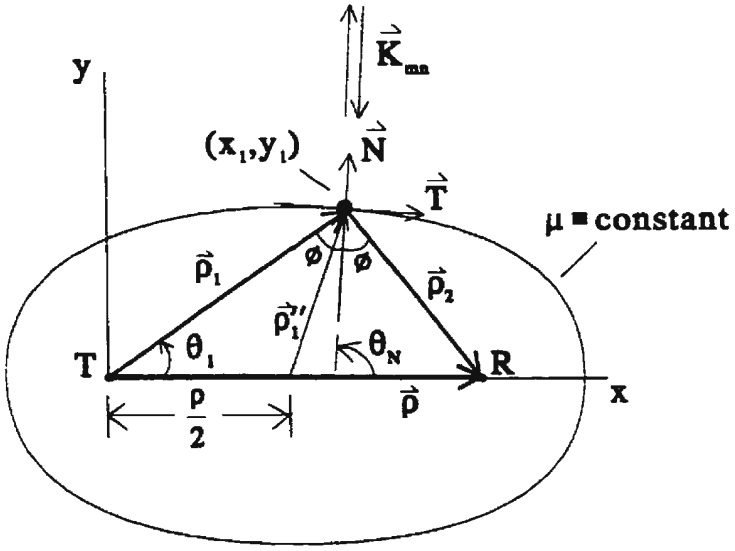

Figure A.1: Depiction of the geometry associated with the first-order stationary phase condition. R and T are receiver and transmitter, respectively.

With reference to Figure A.1, we will attempt to show that the surface wave vector, $\vec{K}_{mn}$, is perpendicular to the ellipse at the point of scatter. In Step 3 of the transformation to elliptical coordinates (Section 2.2.1.2), it transpired that

$$\begin{aligned} x_1'' &= \frac{\rho}{2}\cosh\mu\cos\delta \\ y_1'' &= \frac{\rho}{2}\sinh\mu\sin\delta\ . \end{aligned}$$

Relating this to Figure A.1, it is seen that

$$\vec{\rho}_1'' = \frac{\rho}{2}\cosh\mu\cos\delta\ \hat{x} + \frac{\rho}{2}\sinh\mu\sin\delta\ \hat{y} \qquad \text{(A.15)}$$

since for the stipulation of $\theta = 0$, the hat (unit) vectors are the same for the x–y system as they are for the x''–y'' system. From elementary vector analysis, the tangent, $\vec{T}$, to the $\mu \equiv$ constant curve at (x_1'', y_1'') is given by

$$\vec{T} = \frac{\partial x_1''}{\partial \delta}\,\hat{x} + \frac{\partial y_1''}{\partial \delta}\,\hat{y}\,,$$

and since μ and δ are orthogonal coordinates, the corresponding normal is

$$\begin{aligned} \vec{N} &= \frac{\partial x_1''}{\partial \mu}\,\hat{x} + \frac{\partial y_1''}{\partial \mu}\,\hat{y} \\ &= \frac{\rho}{2}\sinh\mu\cos\delta\,\hat{x} + \frac{\rho}{2}\cosh\mu\sin\delta\,\hat{y}\,. \end{aligned} \tag{A.16}$$

Letting θ_N be the direction of $\vec{N}$ (outward pointing), it is clear from (A.16) that

$$\tan\theta_N = \frac{\cosh\mu\sin\delta}{\sinh\mu\cos\delta} = \frac{\tan\delta}{\tanh\mu} \tag{A.17}$$

Also, the stationary phase condition from equation (A.12) with $\theta = 0$ as specified gives

$$\tan\theta_{mn} = \frac{\tan\delta}{\tanh\mu}\,. \tag{A.18}$$

Thus, (A.18) and (A.17) together show that the direction of $\vec{K}_{mn}$ is given by

$$\theta_{mn} = \theta_N \quad \text{or} \quad \theta_N + 180^\circ\,.$$

Therefore, it is established that the stationary values for δ correspond to points (δ, μ) on the ellipse of constant μ for which the surface wave vector responsible for scattering lies inward $(-)$ or outward $(+)$ along the ellipse normal at those points; i.e.,

$$\vec{K}_{mn} = \pm K_{mn}\,\hat{N} \tag{A.19}$$

where $\hat{N}$ is the unit vector along the *outward* ellipse normal.

Next, it will be established that $\vec{N}$ bisects the angle between the transmitter and receiver as viewed from the scattering point. Again, without loss of generality, θ is

chosen to be zero. In addition to equation (A.16) for the normal, $\vec{N}$, the following relationships are seen to exist (see Figure A.1):

$$\vec{\rho}_1 = x_1\,\hat{x} + y_1\,\hat{y}$$

$$\vec{\rho}_2 = (\rho - x_1)\,\hat{x} - y_1\,\hat{y}\,. \tag{A.20}$$

Using the transformation of equation (A.20), $\vec{\rho}_1$ and $\vec{\rho}_2$ may be converted to elliptic coordinate form. After some algebra, it is easily shown that

$$\vec{\rho}_2 \cdot \vec{N} = -\left(\frac{\rho_2}{\rho_1}\right)\vec{\rho}_1 \cdot \vec{N} \tag{A.21}$$

from whence

$$\hat{\rho}_2 \cdot \hat{N} = -\hat{\rho}_1 \cdot \hat{N} \tag{A.22}$$

where the hatted vectors have their usual meaning. Equation (A.22) immediately implies that the angle between $\hat{\rho}_2$ and $\hat{N}$ as measured from $\vec{N}$ is 180° minus the angle between $\hat{\rho}_1$ and $\hat{N}$ as measured from $\vec{N}$. Thus, if in Figure A.1 we label the latter angle ϕ, then the angle between $\hat{\rho}_2$ and $\hat{N}$ *inside* the vector triangle formed by $\vec{\rho}_1$, $\vec{\rho}_2$, and $\vec{\rho}$ must be ϕ also. Therefore, equation (A.22) proves that $\vec{N}$ bisects the angle between the transmitter and receiver as viewed from the scattering point.

To conclude this section, we seek a form of equation (A.14) for the δ integral which explicitly involves ρ_1, ρ_2, and ϕ of the bistatic scattering geometry. From the expression for $\vec{\rho}_1''$ in (A.15), it is immediately obvious that I_δ in (A.14) may be written (again, taking $\theta = 0$) as

$$I_\delta \approx \sqrt{2\pi}(\pm\cos\phi)F(\rho_1)F(\rho_2)\frac{e^{j\vec{\rho}_1''\cdot\vec{K}_{mn}}}{\sqrt{j\vec{\rho}_1''\cdot\vec{K}_{mn}}} \tag{A.23}$$

since

$$\cos(\theta_{mn} - \theta_1) = \hat{\rho}_1 \cdot \hat{K}_{mn} = \hat{\rho}_1 \cdot \pm\hat{N} = \pm\cos\phi\,.$$

Also, from Figure A.1,

$$\vec{\rho}_1'' = \vec{\rho}_1 - \frac{\vec{\rho}_2}{2} \text{ and } \vec{\rho}_1'' = \frac{\vec{\rho}_2}{2} - \vec{\rho}_2$$

or

$$2\vec{\rho}_1'' = \vec{\rho}_1 - \vec{\rho}_2 \,. \tag{A.24}$$

Therefore,

$$2\vec{\rho}_1'' \cdot \vec{N} = \vec{\rho}_1 \cdot \vec{N} - \vec{\rho}_2 \cdot \vec{N} \tag{A.25}$$

which, from (A.21), becomes

$$\vec{\rho}_1'' \cdot \hat{N} = \left(\frac{\rho_1 + \rho_2}{2}\right) \hat{\rho}_1 \cdot \hat{N} \,. \tag{A.26}$$

Combining the information in (A.26) with that in (A.19) and noting that $\hat{\rho}_1 \cdot \hat{N} = \cos\phi$, it readily follows that

$$\vec{\rho}_1'' \cdot \vec{K}_{mn} = K_{mn}\left(\frac{\rho_1 + \rho_2}{2}\right)(\pm\cos\phi) = K_{mn}\rho_s(\pm\cos\phi) \tag{A.27}$$

where

$$\rho_s = \frac{\rho_1 + \rho_2}{2} \,.$$

Finally, substituting (A.27) into (A.23) while observing $\frac{1}{\sqrt{\pm j}} = e^{\mp j\frac{\pi}{4}}$, the desired result,

$$I_\delta \approx \sqrt{2\pi}(\pm\sqrt{\cos\phi})\frac{F(\rho_1)F(\rho_2)}{\sqrt{K_{mn}\rho_s}} e^{\pm jK_{mn}\rho_s\cos\phi} e^{\mp j\frac{\pi}{4}} \,, \tag{A.28}$$

is reached. This is reported as equation (2.28) of Section 2.2.2.

A.2 The Second-order Field

A.2.1 The First Stationary Point (Patch Scatter) – Forward Analysis

A.2.1.1 Simplifying the Exponential in Equation (2.56) via a Change of Variables

In the course of evaluating the μ–δ integral of equation (2.56),

$$I_m = \int_0^{2\pi}\int_0^{\infty} \cos(\theta_{pq} - \theta_{12}) e^{j\frac{ka}{4}Q(\mu,\delta)} d\mu d\delta \tag{A.29}$$

with

$$Q(\mu,\delta) = [K_{mn}\cos(\theta_{mn}-\theta_2)-2k]\,\mu^2 + [2K_{mn}\sin(\theta_{mn}-\theta_2)]\,\mu\delta - [K_{mn}\cos(\theta_{mn}-\theta_2)]\,\delta^2 \,, \tag{A.30}$$

it would be convenient to eliminate the $\mu\delta$ term. This may be accomplished through a variable transformation. The technique applied here is that given by DeRusso *et al.* [70], Chapter 4.

The quantity, Q, is an example of a *quadratic form*, the general expression of which (in variables $x_1, x_2, \ldots, x_n$) is

$$q = \sum_{i=1}^{n}\sum_{j=1}^{n} a_{ij}x_i x_j \,,$$

a_{ij} being the coefficient of $x_i x_j$. In terms of this form,

$$Q = \sum_{i=1}^{2}\sum_{j=1}^{2} a_{ij}x_i x_j$$

where $x_1 = \mu$, $x_2 = \delta$, $a_{11} = K_{mn}\cos(\theta_{mn}-\theta_2) - 2k$, $a_{12} = a_{21} = K_{mn}\sin(\theta_{mn}-\theta_2)$, and $a_{22} = -K_{mn}\cos(\theta_{mn}-\theta_2)$. Clearly, in our case,

$$Q = \underline{x}^T \underline{\underline{A}}\, \underline{x} \tag{A.31}$$

with

$$\underline{x} = \begin{bmatrix} \mu \\ \delta \end{bmatrix} \quad , \quad \underline{\underline{A}} = \begin{bmatrix} a_{11} & a_{12} \\ a_{21} & a_{22} \end{bmatrix} \,,$$

and $\underline{x}^T$ is the transpose of $\underline{x}$.

The desire is to change the variables to

$$\underline{y} = \begin{bmatrix} \psi \\ \chi \end{bmatrix} \,,$$

say, such that Q may be written as

$$Q = \underline{y}^T \underline{\Delta}\, \underline{y} \tag{A.32}$$

where $\underline{\underline{\Lambda}}$ is a diagonal matrix. DeRusso *et al.* [70] show that the non-zero elements of $\underline{\underline{\Lambda}}$ are simply the eigenvalues, or characteristic values, of $\underline{\underline{A}}$. In our application, then, the eigenvalues, λ, are found in the usual manner from the characteristic equation

$$\left|\lambda \underline{\underline{I}} - \underline{\underline{A}}\right| = 0$$

where $\underline{\underline{I}}$ is the identity matrix and $|\cdot|$ is the determinant. Thus, here

$$\begin{vmatrix} \lambda - K_{mn}\cos(\theta_{mn} - \theta_2) - 2k & K_{mn}\sin(\theta_{mn} - \theta_2) \\ K_{mn}\sin(\theta_{mn} - \theta_2) & \lambda + K_{mn}\cos(\theta_{mn} - \theta_2) \end{vmatrix} = 0$$

which has solutions

$$\begin{aligned} \lambda_1 &= -k + \sqrt{k^2 + K_{mn}^2 - 2kK_{mn}\cos(\theta_{mn} - \theta_2)} \\ \lambda_2 &= -k - \sqrt{k^2 + K_{mn}^2 - 2kK_{mn}\cos(\theta_{mn} - \theta_2)}\,. \end{aligned} \tag{A.33}$$

From (A.32) and (A.33) since $\Lambda = \begin{bmatrix} \lambda_1 & 0 \\ 0 & \lambda_2 \end{bmatrix}$,

$$Q = \lambda_1 \psi^2 + \lambda_2 \chi^2\,. \tag{A.34}$$

Equations (A.33) and (A.34) are reported in Section 2.2.2.2 as equations (2.59) and (2.58), respectively.

Now, of course, the relationships between the ψ–χ and the μ–δ variables must be established. In order to accomplish this, the normalized modal matrix, $\underline{\underline{M}}$, must be examined. For the case of distinct eigenvalues such as encountered here, the columns of $\underline{\underline{M}}$ can be taken to be equal, or proportional, to any nonzero column of $\text{Adj}\left[\lambda_i \underline{\underline{I}} - \underline{\underline{A}}\right]$ where Adj means the adjoint matrix, which is simply the transpose of the matrix formed by replacing the elements of the matrix $\left[\lambda_i \underline{\underline{I}} - \underline{\underline{A}}\right]$ with their cofactors. For each λ_i, the columns of $\text{Adj}\left[\lambda_i \underline{\underline{I}} - \underline{\underline{A}}\right]$, which are eigenvectors, are linearly related so that each λ_i specifies only one column of $\underline{\underline{M}}$. Furthermore, for compactness, each column vector may be normalized by its magnitude. The problem here is particularly simple because $\underline{\underline{A}}$ is a 2×2 matrix. Therefore,

$$\text{Adj}\left[\lambda_i \underline{\underline{I}} - \underline{\underline{A}}\right] = \begin{bmatrix} \lambda - a_{22} & a_{21} \\ a_{12} & \lambda - a_{11} \end{bmatrix}\,. \tag{A.35}$$

Then, a normalized eigenvector, $\underline{u}_1$, associated with λ_1 may be given as

$$\underline{u}_1 = \begin{bmatrix} \lambda_1 - a_{22} \\ a_{12} \end{bmatrix} \cdot \frac{1}{\sqrt{(\lambda_1 - a_{22})^2 + (a_{12})^2}} . \tag{A.36}$$

It similarly follows for λ_2 that a normalized eigenvector, $\underline{u}_2$, is given by

$$\underline{u}_2 = \begin{bmatrix} a_{21} \\ \lambda_2 - a_{11} \end{bmatrix} \cdot \frac{1}{\sqrt{(\lambda_2 - a_{11})^2 + (a_{21})^2}} . \tag{A.37}$$

From (A.36) and (A.37), the modal matrix, $\underline{\underline{M}}$, can be immediately written as

$$\underline{\underline{M}} = \begin{bmatrix} \frac{\lambda_1 - a_{22}}{\sqrt{(\lambda_1 - a_{22})^2 + (a_{12})^2}} & \frac{a_{21}}{\sqrt{(\lambda_2 - a_{11})^2 + (a_{21})^2}} \\ \frac{a_{12}}{\sqrt{(\lambda_1 - a_{22})^2 + (a_{12})^2}} & \frac{\lambda_2 - a_{11}}{\sqrt{(\lambda_2 - a_{11})^2 + (a_{21})^2}} \end{bmatrix} . \tag{A.38}$$

It is straightforward to verify that $\underline{\underline{M}}$ is an orthogonal matrix, i.e. $\underline{\underline{M}}^{-1} = \underline{\underline{M}}^T$ where $\underline{\underline{M}}^{-1}$ and $\underline{\underline{M}}^T$ are the inverse and transpose, respectively. Now, in general, the linear transformation $\underline{x} = \underline{\underline{B}}\,\underline{y}$, where $\underline{\underline{B}}$ is an arbitrary $(n \times n)$ non-singular matrix, transforms the quadratic form of (A.30) in variables μ–δ to a quadratic form in ψ–χ, and, if $\underline{\underline{B}} = \underline{\underline{M}}$, the cross terms are eliminated.

Proof of Cross Term Elimination and Verification of the (μ, δ)–(ψ, χ) Relationships

From (A.31),

$$\begin{aligned} Q &= (\underline{\underline{B}}\,\underline{y})^T \underline{\underline{A}}\,(\underline{\underline{B}}\,\underline{y}) \\ &= \underline{y}^T \underline{\underline{B}}^T \underline{\underline{A}}\,\underline{\underline{B}}\,\underline{y} \end{aligned}$$

and if we set $\underline{\underline{B}} = \underline{\underline{M}}$ so that $\underline{\underline{B}}^T = \underline{\underline{B}}^{-1}$,

$$Q = \underline{y}^T \underline{\underline{M}}^{-1} \underline{\underline{A}}\,\underline{\underline{M}}\,\underline{y} . \tag{A.39}$$

It is not difficult to show that $\underline{\underline{M}}^{-1} \underline{\underline{A}}\,\underline{\underline{M}}$ is the diagonal matrix

$$\Lambda = \begin{bmatrix} \lambda_1 & 0 \\ 0 & \lambda_2 \end{bmatrix} ,$$

and, indeed,

$$\begin{aligned} Q &= \begin{bmatrix} \psi & \chi \end{bmatrix} \begin{bmatrix} \lambda_1 & 0 \\ 0 & \lambda_2 \end{bmatrix} \begin{bmatrix} \psi \\ \chi \end{bmatrix} \\ &= \lambda_1 \psi^2 + \lambda_2 \chi^2 . \end{aligned}$$

Therefore, we can write $\underline{x} = \underline{\underline{B}}\,\underline{y}$ or, more particularly,

$$\underline{x} = \underline{\underline{M}}\,\underline{y}\,, \tag{A.40}$$

which means that

$$\underline{y} = \underline{\underline{M}}^{-1}\,\underline{x} = \underline{\underline{M}}^{T}\,\underline{x}\,.$$

Then, from equation (A.38),

$$\begin{bmatrix} \psi \\ \chi \end{bmatrix} = \begin{bmatrix} \frac{\lambda_1 - a_{22}}{\sqrt{(\lambda_1 - a_{22})^2 + (a_{12})^2}} & \frac{a_{12}}{\sqrt{(\lambda_2 - a_{22})^2 + (a_{12})^2}} \\ \frac{a_{21}}{\sqrt{(\lambda_2 - a_{11})^2 + (a_{21})^2}} & \frac{\lambda_2 - a_{11}}{\sqrt{(\lambda_2 - a_{11})^2 + (a_{21})^2}} \end{bmatrix} \begin{bmatrix} \mu \\ \delta \end{bmatrix},$$

which, from the forms of a_{11}, a_{12}, a_{21}, and a_{22} given previously, means that

$$\begin{aligned} \psi &= \frac{[\lambda_1 + K_{mn}\cos(\theta_{mn} - \theta_2)]\,\mu + [K_{mn}\sin(\theta_{mn} - \theta_2)]\,\delta}{\sqrt{(\lambda_1 + K_{mn}\cos(\theta_{mn} - \theta_2))^2 + (K_{mn}\sin(\theta_{mn} - \theta_2))^2}} \\ \chi &= \frac{[K_{mn}\sin(\theta_{mn} - \theta_2)]\,\mu + [\lambda_2 - K_{mn}\cos(\theta_{mn} - \theta_2) + 2k]\,\delta}{\sqrt{(\lambda_2 - K_{mn}\cos(\theta_{mn} - \theta_2) + 2k)^2 + (K_{mn}\sin(\theta_{mn} - \theta_2))^2}}\,. \end{aligned} \tag{A.41}$$

Also, from equations (A.38) and (A.40) along with our definitions of the a_{ij}'s,

$$\begin{aligned} \mu &= \frac{[\lambda_1 + K_{mn}\cos(\theta_{mn} - \theta_2)]\,\psi}{\sqrt{(\lambda_1 + K_{mn}\cos(\theta_{mn} - \theta_2))^2 + (K_{mn}\sin(\theta_{mn} - \theta_2))^2}} \\ &\quad + \frac{[K_{mn}\sin(\theta_{mn} - \theta_2)]\,\chi}{\sqrt{(\lambda_2 - K_{mn}\cos(\theta_{mn} - \theta_2) + 2k)^2 + (K_{mn}\sin(\theta_{mn} - \theta_2))^2}} \\ \delta &= \frac{[K_{mn}\sin(\theta_{mn} - \theta_2)]\,\psi}{\sqrt{(\lambda_1 + K_{mn}\cos(\theta_{mn} - \theta_2))^2 + (K_{mn}\sin(\theta_{mn} - \theta_2))^2}} \\ &\quad + \frac{[\lambda_2 - K_{mn}\cos(\theta_{mn} - \theta_2) + 2k]\,\chi}{\sqrt{(\lambda_2 - K_{mn}\cos(\theta_{mn} - \theta_2) + 2k)^2 + (K_{mn}\sin(\theta_{mn} - \theta_2))^2}}\,. \end{aligned} \tag{A.42}$$

From equation (A.42), it is easy to show that the Jacobian of the transformation is unity, i.e.

$$J = \begin{vmatrix} \frac{\partial \mu}{\partial \psi} & \frac{\partial \mu}{\partial \chi} \\ \frac{\partial \delta}{\partial \psi} & \frac{\partial \delta}{\partial \chi} \end{vmatrix} = 1\,.$$

Therefore, $d\mu d\delta \equiv d\psi d\chi$. Also, from equation (A.41), it is clear that both integral limits in (A.29) will be from $-\infty$ to ∞ on changing to ψ, χ coordinates.

A.2.1.2 Expanding the Cosine Factor in Equation (2.56)

Another point which must be addressed in equation (A.29) is that, as seen in equation (2.51), θ_{12} is a function of μ and δ. Consequently, $\cos(\theta_{pq} - \theta_{12})$ must be presented in ψ, χ coordinates. To simplify the integral, we will approximate $\cos(\theta_{pq} - \theta_{12})$ by expanding its constituents to second order in μ and δ about the stationary point $(0, 0)$ using Taylor series. Noting that

$$\cos(\theta_{pq} - \theta_{12}) = \cos\theta_{pq}\cos\theta_{12} + \sin\theta_{pq}\sin\theta_{12}\ , \tag{A.43}$$

we write from Figure 2.4 and equations (2.43) and (2.44), after a little algebra,

$$\begin{aligned} \cos\theta_{12} = \frac{x_2 - x_1}{\rho_{12}} &= \frac{(1 - \cosh\mu\cos\delta)\cos\theta_2 + \sinh\mu\sin\delta\sin\theta_2}{\cosh\mu - \cos\delta} \\ \sin\theta_{12} = \frac{y_2 - y_1}{\rho_{12}} &= \frac{(1 - \cosh\mu\cos\delta)\sin\theta_2 - \sinh\mu\sin\delta\cos\theta_2}{\cosh\mu - \cos\delta}\ . \end{aligned} \tag{A.44}$$

The equations in (A.44) will be approximated by expanding each of the μ and δ functions separately (up to and including the $\frac{\partial^2}{\partial\mu^2}$ and $\frac{\partial^2}{\partial\delta^2}$ terms) about $\mu = 0$ and $\delta = 0$, respectively. The results are simply

$$\begin{aligned} \cosh\mu &\sim 1 + \frac{\mu^2}{2} \\ \sinh\mu &\sim \mu \\ \cos\delta &\sim 1 - \frac{\delta^2}{2} \\ \sin\delta &\sim \delta\ . \end{aligned}$$

These allow (A.44) to be written as

$$\begin{aligned} \cos\theta_{12} &\approx \frac{(\delta^2 - \mu^2)\cos\theta_2 + 2\mu\delta\sin\theta_2}{\mu^2 + \delta^2} \\ \sin\theta_{12} &\approx \frac{(\delta^2 - \mu^2)\sin\theta_2 - 2\mu\delta\cos\theta_2}{\mu^2 + \delta^2}\ . \end{aligned} \tag{A.45}$$

Substituting (A.45) into (A.43), it is easily shown that

$$\cos(\theta_{pq} - \theta_{12}) \approx \frac{(\delta^2 - \mu^2)\cos(\theta_{pq} - \theta_2) - 2\mu\delta\sin(\theta_{pq} - \theta_2)}{\mu^2 + \delta^2} \ . \tag{A.46}$$

Now, for compactness, we define the following:

$$\begin{aligned}
c_1 &= (\lambda_1 + K_{mn}\cos(\theta_{mn} - \theta_2))^2 + (K_{mn}\sin(\theta_{mn} - \theta_2))^2 \\
c_2 &= \left[(K_{mn}\sin(\theta_{mn} - \theta_2))^2 - (\lambda_1 + K_{mn}\cos(\theta_{mn} - \theta_2))^2\right]\cos(\theta_{pq} - \theta_2) \\
&\quad - [2(K_{mn}\sin(\theta_{mn} - \theta_2))(\lambda_1 + K_{mn}\cos(\theta_{mn} - \theta_2))]\sin(\theta_{pq} - \theta_2) \\
c_3 &= -2\{[2(K_{mn}\sin(\theta_{mn} - \theta_2))(\lambda_1 + K_{mn}\cos(\theta_{mn} - \theta_2))]\cos(\theta_{pq} - \theta_2) \\
&\quad + \left[(K_{mn}\sin(\theta_{mn} - \theta_2))^2 - (\lambda_1 + K_{mn}\cos(\theta_{mn} - \theta_2))^2\right]\sin(\theta_{pq} - \theta_2)\Big\} \ .
\end{aligned} \tag{A.47}$$

From equations (A.46), (A.42) and (A.47) it is then possible to show after some tedious algebra that

$$\cos(\theta_{pq} - \theta_{12}) \approx \frac{1}{c_1\left[\psi^2 + \chi^2\right]} \cdot \Big\{c_2(\psi^2 - \chi^2) + c_3\psi\chi\Big\} \ . \tag{A.48}$$

Taking (A.29), (A.34) and (A.48) together, an approximation of equation (2.56) may be written as

$$I_m \approx \int_{-\infty}^{\infty}\int_{-\infty}^{\infty} \frac{c_2(\psi^2 - \chi^2) + c_3\psi\chi}{c_1\left[\psi^2 + \chi^2\right]} e^{j\frac{\rho_2}{4}\left[\lambda_1\psi^2 + \lambda_2\chi^2\right]} d\psi d\chi \ . \tag{A.49}$$

Thus, equation (2.62) has been derived.

A.2.1.3 A Final Form for Equation (2.54)

The form of the exponential in equation (A.49) suggests that the integration may be facilitated by a change of variables from (ψ, χ) to polar coordinates, (r, ν), say. To this end,

$$\begin{aligned}
\psi &= r\cos\nu \\
\chi &= r\sin\nu \\
d\psi d\chi &\equiv r dr d\nu \ ,
\end{aligned}$$

which imply

$$\begin{aligned} \psi^2 + \chi^2 &= r^2 \\ \psi^2 - \chi^2 &= r^2 \cos(2\nu) \\ \psi\chi &= \frac{r^2}{2}\sin(2\nu)\,. \end{aligned} \tag{A.50}$$

If we further write

$$\lambda_1 = c_4 + c_5 \quad \text{and} \quad \lambda_2 = c_4 - c_5 \tag{A.51}$$

where, from (A.33), $c_4 = -k$ and $c_5 = \sqrt{k^2 + K_{mn}^2 - 2kK_{mn}\cos(\theta_{mn} - \theta_2)}$, it is not difficult to show that from (A.49) and (A.50)

$$I_m \approx \frac{-2j}{c_1\rho_2}\int_0^{2\pi} \frac{c_2\cos\theta_c + \frac{c_3}{2}\sin\theta_c}{c_4 + c_5\cos\theta_c} d\theta_c$$

with $\theta_c = 2\nu$. The second term of the integrand, containing the $\sin\theta_c$, evaluates to 0 and, using Mathematica [88] and equations (A.33) and (A.51), the remaining term evaluates to

$$I_m \approx \frac{-4\pi j}{\rho_2} \frac{c_2\sqrt{\lambda_1\lambda_2} + c_2 k}{c_1\sqrt{k^2 + K_{mn}^2 - 2kK_{mn}\cos(\theta_{mn} - \theta_2)}\sqrt{\lambda_1\lambda_2}}\,. \tag{A.52}$$

Again, after a large amount of algebraic detail, it can be shown that, on using equations (A.33), (A.47), (A.51) and (A.52),

$$\begin{aligned} K_{pq}K_{mn}\cos(\theta_{mn} - \theta_2)I_m &\approx \frac{4\pi}{\rho_2}\left\{\frac{\left(\vec{K}_{mn}\cdot\hat{\rho}_2\right)\left[\vec{K}_{pq}\cdot\left(\vec{K}_{mn} - k\hat{\rho}_2\right)\right]}{\sqrt{\vec{K}_{mn}\cdot\left(\vec{K}_{mn} - 2k\hat{\rho}_2\right)}}\right\} \\ &\quad \cdot\left\{\frac{k + j\sqrt{\vec{K}_{mn}\cdot\left(\vec{K}_{mn} - 2k\hat{\rho}_2\right)}}{k^2 + \vec{K}_{mn}\cdot\left(\vec{K}_{mn} - 2k\hat{\rho}_2\right)}\right\} \\ &= \frac{4\pi}{\rho_2}\gamma_{E12F,1} \end{aligned} \tag{A.53}$$

where the definition of $\gamma_{E12F,1}$ is obvious. The quantity $\gamma_{E12F,1}$ will be referred to as an *electromagnetic coupling coefficient*. Later, it will become part of a larger expression and will be discussed in detail in Section 3.6.3.

Considering equation (2.54), (2.56), and (A.53), the former is clearly given by

$$I_{12F,1} = -2\pi \sum_{m,n} \sum_{p,q} P_{\vec{K}_{mn}} P_{\vec{K}_{pq}} \frac{F(\rho_2)}{\rho_2} \gamma_{E12F,1} \cdot e^{j\rho_2 K_{pq} \cos(\theta_{pq}-\theta_2)} \cdot e^{j\frac{\rho_2}{2}[2K_{mn}\cos(\theta_{mn}-\theta_2)-2k]} \quad \text{(A.54)}$$

with the attenuation function $F(0) = 1$ in equation (2.54). Thus, the left hand member of the convolution in equation (2.66) as applied to the "patch" scatter stationary point has been developed.

A.2.2 The First Stationary Point (One Scatter Near the Receiver) – Backward Analysis

We wish to apply a two-dimensional stationary phase technique (Bleistein and Handelsmann [66] or Friedman [69]) to equation (2.102) for the stationary point $(0,0)$. We have

$$I_{23B} = j \sum_{p,q} P_{\vec{K}_{pq}} K_{pq} e^{jK_{pq}\rho\cos(\theta_{pq}-\theta)} \cdot \int_0^{2\pi} \int_0^{\infty} \cos(\theta_{pq}-\theta_{12}) F(\rho_{12}) F(\rho_{20}) e^{j\frac{\rho_4}{2}\Phi_{23}(\mu,\delta)} d\mu d\delta \quad \text{(A.55)}$$

it being understood that ρ_{12}, ρ_{20}, and θ_{12} are functions of μ and δ, in general. Let us consider the double integral separately as

$$I_{B,1} = \int_0^{2\pi} \int_0^{\infty} \cos(\theta_{pq}-\theta_{12}) F(\rho_{12}) F(\rho_{20}) e^{j\frac{\rho_4}{2}\Phi_{23}(\mu,\delta)} d\mu d\delta \quad \text{(A.56)}$$

where $\Phi_{23}(\mu,\delta)$ is defined in equation (2.99). Again, using Bleistein and Handelsmann [66], Section 8.4, and our notation, equation (A.56) may be structured as

$$I_{B,1} = \int_0^{2\pi} \int_0^{\infty} f(\mu,\delta) e^{j\frac{\rho_4}{2}\Phi_{23}(\mu,\delta)} d\mu d\delta \quad \text{(A.57)}$$

where the distance parameter, $\frac{\rho_4}{2}$, is a large parameter and $f(\mu,\delta) = \cos(\theta_{pq} - \theta_{12}) F(\rho_{12}) F(\rho_{20})$. For a stationary point, (μ_s, δ_s), which lies on the boundary of the integration region, (A.57) may be approximated as

$$I_{B,1} \approx \frac{1}{2} \frac{f(\mu_s,\delta_s) \left[\frac{2\pi}{\frac{\rho_4}{2}}\right] e^{j\frac{\rho_4}{2}\Phi_{23}(\mu_s,\delta_s)} e^{j\frac{\pi}{4}\mathrm{sig}[\Phi_{23}(\mu_s,\delta_s)]_{\mu\delta}}}{\sqrt{\left|\det\left[\Phi_{23}(\mu_s,\delta_s)\right]_{\mu\delta}\right|}} . \quad \text{(A.58)}$$

Here, $[\Phi_{23}(\mu_s, \delta_s)]_{\mu\delta}$ is the matrix

$$\begin{bmatrix} \frac{\partial^2 \Phi_{23}(\mu,\delta)}{\partial \mu^2} & \frac{\partial^2 \Phi_{23}(\mu,\delta)}{\partial \mu \partial \delta} \\ \frac{\partial^2 \Phi_{23}(\mu,\delta)}{\partial \delta \partial \mu} & \frac{\partial^2 \Phi_{23}(\mu,\delta)}{\partial \delta^2} \end{bmatrix} \tag{A.59}$$

evaluated at (μ_s, δ_s), $\left|\det [\Phi_{23}(\mu_s, \delta_s)]_{\mu\delta}\right|$ is the absolute value of the determinant of the matrix and

$$\begin{aligned} \operatorname{sig} [\Phi_{23}(\mu_s, \delta_s)]_{\mu\delta} \;=\; & (\text{number of positive eigenvalues of matrix}) \\ & -(\text{number of negative eigenvalues of matrix}) \; . \end{aligned} \tag{A.60}$$

Since from equation (2.99)

$$\begin{aligned} \Phi_{23}(\mu, \delta) \;=\; & K_{pq} \{ [\cosh \mu \cos \delta - 1] \cos(\theta_{pq} - \theta_4) \\ & + [\sinh \mu \sin \delta \sin(\theta_{pq} - \theta_4)] - 2k \cosh \mu \} \; , \end{aligned} \tag{A.61}$$

carrying out the derivatives of (A.59) and evaluating at the $(0,0)$ stationary point gives

$$[\Phi_{23}(0,0)]_{\mu\delta} = \begin{bmatrix} K_{pq} \cos(\theta_{pq} - \theta_4) - 2k & K_{pq} \sin(\theta_{pq} - \theta_4) \\ K_{pq} \sin(\theta_{pq} - \theta_4) & -K_{pq} \cos(\theta_{pq} - \theta_4) \end{bmatrix} . \tag{A.62}$$

From (A.62) it is readily shown that

$$\det [\Phi_{23}(0,0)]_{\mu\delta} = 2kK_{pq} \cos(\theta_{pq} - \theta_4) - K_{pq}^2 \; . \tag{A.63}$$

The matrix eigenvalues are

$$\lambda = -k \pm \sqrt{k^2 + \left[K_{pq}^2 - 2kK_{pq} \cos(\theta_{pq} - \theta_4)\right]} \; , \tag{A.64}$$

and they must be real since the discriminant, $d_{0,0}$, has the property

$$d_{0,0} = K_{pq}^2 - 2kK_{pq} \cos(\theta_{pq} - \theta_4) + k^2 \geq (K_{pq} - k)^2 \geq 0 \; .$$

Clearly, if $d_{0,0} > k$, the matrix has one positive and one negative eigenvalue, while if $d_{0,0} < k$, there are two negative eigenvalues. In the first case,

$$\operatorname{sig} [\Phi_{23}(0,0)]_{\mu\delta} = 0 \;\text{ and }\; 2kK_{pq} \cos(\theta_{pq} - \theta_4) - K_{pq}^2 < 0 \; ,$$

while in the second case,

$$\text{sig}\left[\Phi_{23}(0,0)\right]_{\mu\delta} = -2 \text{ and } 2kK_{pq}\cos(\theta_{pq}-\theta_4) - K_{pq}^2 > 0\,.$$

Noting, finally, that

$$e^{j\frac{\pi}{4}\text{sig}[\Phi_{23}(0,0)]_{\mu\delta}} = \begin{cases} 1, & \text{sig}[\cdot] = 0 \\ j, & \text{sig}[\cdot] = -2 \end{cases},$$

the absolute value in the expression for (A.53) may be removed and from (2.100), (A.61)–(A.64) and the discussion following the latter, the integral result is

$$I_{B,1} \approx \frac{2\pi\cos(\theta_{pq}-\theta_{12})F(\rho_{12})F(0)e^{-jk\rho_{12}}}{\rho_{12}\sqrt{K_{pq}^2 - 2kK_{pq}\cos(\theta_{pq}-\theta_{12})}}\,. \tag{A.65}$$

Then, for the stationary point $(0,0)$ (indicated by the subscript, 1, on $I_{23B,1}$), equation (A.55) becomes

$$\begin{aligned} I_{23B,1} \approx\ & j2\pi\sum_{p,q} P_{\vec{K}_{pq}} K_{pq} \frac{\cos(\theta_{pq}-\theta_{12})F(\rho_{12})}{\sqrt{K_{pq}^2 - 2kK_{pq}\cos(\theta_{pq}-\theta_{12})}} \\ & \cdot \frac{e^{-jk\rho_{12}}}{\rho_{12}} e^{jK_{pq}\rho\cos(\theta_{pq}-\theta)}\,. \end{aligned} \tag{A.66}$$

Thus, the convolution in equation (2.91) has been approximated for the case when the second scatter, before reception, occurs near the receiving antenna. This result is reported as equation (2.103).

A.3 Application to a Pulsed Radar

A.3.1 The Relationship Between the Bistatic Angle and the Scattering Ellipse Normal

Consider Figure A.2 which is simply Figure 2.3 appropriately labelled for the task at hand. It will be shown that

$$\cos\phi = \sqrt{1 - \left(\frac{\frac{\rho}{2}}{\rho_s}\right)^2 \sin^2\theta_N}$$

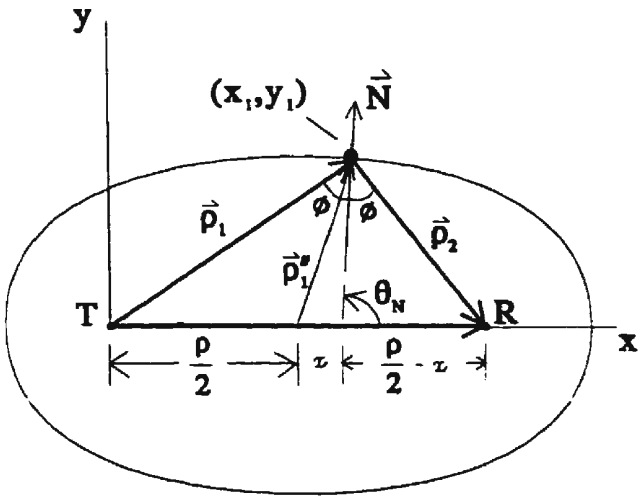

Figure A.2: Depiction of the geometry associated with the first-order stationary phase condition. R and T are receiver and transmitter, respectively.

where ϕ is the bistatic angle, ρ is the distance between the transmitter (T) and the receiver (R), and

$$\rho_s = \frac{\rho_1 + \rho_2}{2}$$

with ρ_1 and ρ_2 being the distances from the transmitter and receiver, respectively, to the scatter point. The angle, θ_N, is the direction of the normal to the scattering ellipse at the point of scatter.

Simply, from the law of sines,

$$\frac{\sin\phi}{\frac{\rho}{2} + x} = \frac{\sin\theta_N}{\rho_1} \quad (\text{since} \quad \sin\theta_N = \sin(\pi - \theta_N))$$

and

$$\frac{\sin\phi}{\frac{\rho}{2} - x} = \frac{\sin\theta_N}{\rho_2} ,$$

from which

$$x = \frac{\rho}{2}\left(\frac{\rho_1 - \rho_2}{\rho_1 + \rho_2}\right) .$$

From the second sine law expression, it then follows that

$$\frac{\sin\theta_N}{\rho_2} = \frac{\sqrt{1 - \cos^2\phi}}{\frac{\rho}{2}\left[1 - \frac{\rho_1 - \rho_2}{\rho_1 + \rho_2}\right]} .$$

A little algebra and substitution of $\rho_s = \frac{\rho_1 + \rho_2}{2}$ into the last expression readily yields

$$\cos\phi = \sqrt{1 - \left(\frac{\frac{\rho}{2}}{\rho_s}\right)^2 \sin^2\theta_N} \tag{A.67}$$

as required. This result was also derived by Walsh and Dawe [9], but in a more complex fashion using a transformation to elliptic coordinates and an application of vector algebra.

A.3.2 Proof of Equivalence Between "Patch" Scatter Fields from Forward and Backward Analyses

It was suggested in Section 2.2.3.3 that the equivalence between the "forward" and "backward" convolution process used in obtaining the electric field component as a result of both scatters occurring at the same position on the scattering ellipse could be verified by proving that

$$\gamma_{E12B,2} = -\gamma_{E12F,1} \tag{A.68}$$

where the γ's are defined in equations (2.109) and (2.64), respectively.

To emphasize that a pulse radar is being used, based on the analysis in equations (2.114) to (2.118), the k in the expressions for γ may be replaced by k_0, the wavenumber of the pulsed dipole radiation. Rewriting (2.64) and (2.109) then gives

$$\begin{aligned} -\gamma_{E12F,1} &= -\left\{\frac{j\sqrt{\vec{K}_{mn}\cdot\left[\vec{K}_{mn} - 2k_0\hat{\rho}_2\right]} + k_0}{k_0^2 + \vec{K}_{mn}\cdot\left[\vec{K}_{mn} - 2k_0\hat{\rho}_2\right]}\right\} \\ &\quad \cdot \left\{\frac{\left(\vec{K}_{mn}\cdot\hat{\rho}_2\right)\left[\vec{K}_{pq}\cdot\left(\vec{K}_{mn} - k_0\hat{\rho}_2\right)\right]}{\sqrt{\vec{K}_{mn}\cdot\left[\vec{K}_{mn} - 2k_0\hat{\rho}_2\right]}}\right\}, \end{aligned} \tag{A.69}$$

$$\begin{aligned} \gamma_{E12B,2} &= \left\{\frac{j\sqrt{\vec{K}_{pq}\cdot\left[\vec{K}_{pq} + 2k_0\hat{\rho}_{20}\right]} + k_0}{k_0^2 + \vec{K}_{pq}\cdot\left[\vec{K}_{pq} + 2k_0\hat{\rho}_{20}\right]}\right\} \\ &\quad \cdot \left\{\frac{\left(\vec{K}_{mn}\cdot\hat{\rho}_2\right)\left[\vec{K}_{pq}\cdot\left(\vec{K}_{pq} + k_0\hat{\rho}_{20}\right)\right]}{\sqrt{\vec{K}_{pq}\cdot\left[\vec{K}_{pq} + 2k_0\hat{\rho}_{20}\right]}}\right\}. \end{aligned}$$

If it can be shown that

$$\vec{K}_{pq}\cdot\left[\vec{K}_{pq}+2k_0\hat{\rho}_{20}\right]=\vec{K}_{mn}\cdot\left[\vec{K}_{mn}-2k_0\hat{\rho}_2\right]\quad\text{AND}\quad\left(\vec{K}_{pq}+k_0\hat{\rho}_{20}\right)=-\left(\vec{K}_{mn}-k_0\hat{\rho}_2\right),$$

it is clear that the proof of equivalence is complete.

STEP 1 The relationship between the unit vectors, $\hat{\rho}_2$ and $\hat{\rho_{20}}$ must be established. Figure A.3 is the same as Figure 2.6 appropriately labelled for the discussion which follows. The bistatic angle ϕ_0 is of the form given in (2.133) with due regards given to replacing ρ_{0s} with $\rho_{0s12,1}=\left(\frac{\rho_{02}+\rho_{020}}{2}\right)$. Also, since the variation in $\vec{\rho}_2$ and $\vec{\rho}_{20}$ over a pulse length is very small compared with the magnitude of the quantities themselves,

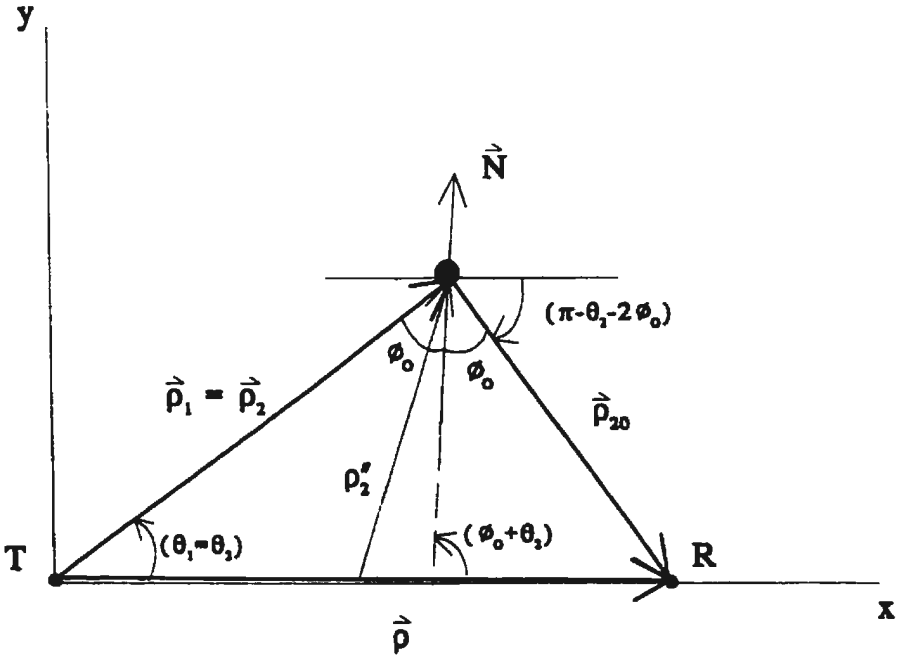

Figure A.3: Depiction of the geometry associated with the second-order stationary phase condition. R and T are receiver and transmitter, respectively.

the unit vectors $\hat{\rho}_{02}$ and $\hat{\rho}_{020}$ are certainly adequately represented by $\hat{\rho}_2$ and $\hat{\rho}_{20}$. Then,

$$\begin{aligned}\hat{\rho}_2 &= \hat{x}\cos\theta_2+\hat{y}\sin\theta_2\\ \hat{N} &= \hat{x}\cos(\theta_2+\phi_0)+\hat{y}\sin(\theta_2+\phi_0)\\ \hat{\rho}_{20} &= -\hat{x}\cos(\theta_2+2\phi_0)-\hat{y}\sin(\theta_2+2\phi_0)\\ \hat{\theta}_N &= -\hat{x}\sin(\theta_2+\phi_0)+\hat{y}\cos(\theta_2+\phi_0)\,.\end{aligned}\tag{A.70}$$

It is easy to show from (A.70) that

$$\hat{\rho}_2 = \cos\phi_0 \hat{N} - \sin\phi_0 \hat{\theta}_N$$

and

$$\hat{\rho}_{20} = -\cos\phi_0 \hat{N} - \sin\phi_0 \hat{\theta}_N \ ,$$

from which

$$\hat{\rho}_{20} = \hat{\rho}_2 - 2\cos\phi_0 \hat{N} \ . \tag{A.71}$$

It was deduced in Section 2.2.5.2 that the surface wave vector $\vec{K}_{rs}$ can be written to a very good approximation as

$$\vec{K}_{rs} \approx 2k_0 \cos\phi_0 \hat{N}$$

$$\Rightarrow \ \hat{N} \approx \frac{\vec{K}_{rs}}{2k_0 \cos\phi_0} \ .$$

Then, (A.71) can be written as

$$\hat{\rho}_{20} = \hat{\rho}_2 - \frac{\vec{K}_{rs}}{k_0} = \hat{\rho}_2 - \frac{\vec{K}_{mn} + \vec{K}_{pq}}{k_0} \ , \tag{A.72}$$

it being understood that the equality suggested is restricted by the approximation on $\vec{K}_{rs}$.

STEP 2 Next, $\vec{K}_{pq} \cdot \left[\vec{K}_{pq} + 2k_0\hat{\rho}_{20}\right]$ is considered. Since $\vec{K}_{rs} = \vec{K}_{mn} + \vec{K}_{pq}$, we have, using (A.72),

$$\begin{aligned}
\vec{K}_{pq} \cdot \left[\vec{K}_{pq} + 2k_0\hat{\rho}_{20}\right] &= \left(\vec{K}_{rs} - \vec{K}_{mn}\right) \cdot \left[\vec{K}_{rs} - \vec{K}_{mn} + 2k_0\hat{\rho}_2 - 2\vec{K}_{rs}\right] \\
&= \left(\vec{K}_{mn} - \vec{K}_{rs}\right) \cdot \left\{\left[\vec{K}_{mn} - 2k_0\hat{\rho}_2\right] + \vec{K}_{rs}\right\} \\
&= \vec{K}_{mn} \cdot \left[\vec{K}_{mn} - 2k_0\hat{\rho}_2\right] + \vec{K}_{mn} \cdot \vec{K}_{rs} - \vec{K}_{rs} \cdot \vec{K}_{mn} \\
&\quad + \vec{K}_{rs} \cdot 2k_0\hat{\rho}_2 - \vec{K}_{rs} \cdot \vec{K}_{rs} \\
&= \vec{K}_{mn} \cdot \left[\vec{K}_{mn} - 2k_0\hat{\rho}_2\right] + \vec{K}_{rs} \cdot 2k_0 \left[\cos\phi_0 \hat{N} - \sin\phi_0 \hat{\theta}_N\right] \\
&\quad - \vec{K}_{rs} \cdot \vec{K}_{rs} \\
&= \vec{K}_{mn} \cdot \left[\vec{K}_{mn} - 2k_0\hat{\rho}_2\right] + \left(\vec{K}_{rs} \cdot \vec{K}_{rs}\right) - \left(\vec{K}_{rs} \cdot \vec{K}_{rs}\right) \\
&= \vec{K}_{mn} \cdot \left[\vec{K}_{mn} - 2k_0\hat{\rho}_2\right]
\end{aligned}$$

where, in the second last line, we have used the fact that, essentially,

$$\vec{K}_{rs} = 2k_0 \cos\phi_0 \hat{N} \text{ and } \hat{N} \cdot \hat{\theta}_N = 0 .$$

Therefore, within the approximation on the magnitude of $\vec{K}_{rs}$ (i.e. $K_{rs} \approx 2k_0 \cos\phi_0$), it has been shown that

$$\vec{K}_{pq} \cdot \left[\vec{K}_{pq} + 2k_0\hat{\rho}_{20}\right] = \vec{K}_{mn} \cdot \left[\vec{K}_{mn} - 2k_0\hat{\rho}_2\right]$$

STEP 3 It remains to be shown that $\left(\vec{K}_{pq} + 2k_0\hat{\rho}_{20}\right) = -\left(\vec{K}_{mn} - k_0\hat{\rho}_2\right)$. From (A.72) we have

$$\begin{aligned} \vec{K}_{pq} + k_0\hat{\rho}_{20} &= \vec{K}_{pq} + k_0\left(\hat{\rho}_2 - \frac{\vec{K}_{mn} + \vec{K}_{pq}}{k_0}\right) \\ &= -\vec{K}_{mn} + k_0\hat{\rho}_2 \\ &= -(\vec{K}_{mn} - k_0\hat{\rho}_2) \end{aligned}$$

as required.

Thus, all requirements for the equality of $\gamma_{E12B,2}$ and $-\gamma_{E12F,1}$ have been verified within the approximation $\vec{K}_{rs} = 2k_0 \cos\phi_0 \hat{N}$. Consequently, too, the equivalence of electric fields obtained by forward and backward analysis of the convolution equations for two scatters at a point remote from the transmitter and receiver, has been established.

Appendix B

Derivations Pertinent to the Bistatic Cross Sections of the Ocean Surface

Here, a detailed analysis of the auto- and cross-correlations appearing in equation (3.35) is carried out. From these correlations, Doppler power spectra are derived. Subsequently, high frequency Doppler cross sections per unit area of surface are determined. Also, a few other details related to the cross section calculations and discussions of Chapter 3 are addressed.

B.1 The Cross-correlations and Spectra of the First- and Second-order Field Components

The definitions of the cross-correlations of the first- and second-order electric field components are detailed in equation (3.47). They are of the form

$$\begin{aligned} \mathcal{R}_{11,2J}(\tau) &= < \left(E_{0_n}^{+}\right)_{11}(t_0, t+\tau) \left(E_{0_n}^{+}\right)_{2J}^{*}(t_0, t) > \\ &\text{or} \\ \mathcal{R}_{2J,11}(\tau) &= < \left(E_{0_n}^{+}\right)_{2J}(t_0, t+\tau) \left(E_{0_n}^{+}\right)_{11}^{*}(t_0, t) > \end{aligned} \tag{B.1}$$

where, for the second-order fields, the subscript, $J \equiv P,\ T$ or R, is for double scatter on the remote patch, one scatter on the patch and one near the transmitter, or one scatter on the patch and one near the receiver, respectively.

In exactly the same way as $< {}_1P_{\vec{K},\omega}\, {}_1P^*_{\vec{K}',\omega'} >$ entered equation (3.39) for the autocorrelation of the first-order field, there will be in $\mathcal{R}_{11,2J}(\tau)$ an average of the form

$$< {}_1P_{\vec{K}_1,\omega_1}\, {}_1P^*_{\vec{K}_2,\omega_2}\, {}_1P^*_{\vec{K}_3,\omega_3} > ,$$

and, in $\mathcal{R}_{2J,11}(\tau)$, one of the form

$$< {}_1P_{\vec{K}_2,\omega_2}\, {}_1P_{\vec{K}_3,\omega_3}\, {}_1P^*_{\vec{K}_1,\omega_1} > .$$

In either case, the averages involve the product of three zero-mean Gaussian random variables, and, therefore, being a special case of the product of an *odd* number of such variables, must vanish (Thomas [76]); i.e.

$$\mathcal{R}_{11,2J}(\tau) = \mathcal{R}_{2J,11}(\tau) = 0 . \tag{B.2}$$

This immediately implies that the Doppler power spectral densities corresponding to these correlations must also vanish; i.e.

$$\mathcal{P}_{11,2J}(\omega_d) = \mathcal{P}_{2J,11}(\omega_d) = 0 . \tag{B.3}$$

Thus, equations (3.48) and (3.49) are valid and the first- and second-order fields are uncorrelated.

B.2 The Autocorrelation and Spectrum for Double Scatter on the Remote Patch

Next, the autocorrelation in equation (3.50),

$$\mathcal{R}_{2P}(\tau) = \frac{A_r}{2\eta_0} < \left(E^+_{0_n}\right)_{2P}(t_0, t+\tau) \left(E^+_{0_n}\right)^*_{2P}(t_0, t) > \tag{B.4}$$

for the so-called (elliptical) patch scatter is considered. Referencing equation (3.25) and noting that the randomness is associated only with the first-order surface coefficients, equation (B.4) becomes

$$\mathcal{R}_{2P}(\tau) = \frac{A_r}{2\eta_0} \left\{ \frac{\eta_0^2 k_0^4 \left|I_0 \Delta\ell\right|^2 (\Delta\rho_s)^2}{(2\pi)^3 \rho_{0s} \left[\rho_{0s}^2 - \left(\frac{\rho}{2}\right)^2\right]} \right\} \sum_{\vec{K}_1,\omega_1} \sum_{\vec{K}'_1,\omega'_1} \sum_{\vec{K}_2,\omega_2} \sum_{\vec{K}'_2,\omega'_2} \Gamma_P \Gamma'^*_P$$

$$\cdot e^{j\frac{\vec{\rho}}{2}\cdot\vec{K}} e^{-j\frac{\vec{\rho}}{2}\cdot\vec{K}'} e^{j\rho_{0s}K\cos\phi_0} e^{-j\rho_{0s}K'\cos\phi_0'} < {}_1P_{\vec{K}_1,\omega_1}\, {}_1P_{\vec{K}_2,\omega_2}\, {}_1P^*_{\vec{K}_1',\omega_1'}\, {}_1P^*_{\vec{K}_2',\omega_2'} >$$

$$\cdot e^{j(\omega_1+\omega_2)(t+\tau)} e^{-j(\omega_1'+\omega_2')(t)} \sqrt{K\cos\phi_0}\sqrt{K'\cos\phi_0'}\, F(\rho_{01},\omega_0) F(\rho_{02},\omega_0)$$

$$\cdot F^*(\rho_{01}',\omega_0) F^*(\rho_{02}',\omega_0) \mathrm{Sa}\left[\frac{\Delta\rho_s}{2}\left(\frac{K}{\cos\phi_0}-2k_0\right)\right] \mathrm{Sa}\left[\frac{\Delta\rho_s}{2}\left(\frac{K'}{\cos\phi_0'}-2k_0\right)\right] \quad \text{(B.5)}$$

where the primes throughout are associated with wave vectors $\vec{K}_1'$ and $\vec{K}_2'$.

As a first step in analyzing (B.5), the average represented by $< \cdot >$ is considered. For zero-mean Gaussian random variables,

$$\begin{aligned} < {}_1P_{\vec{K}_1,\omega_1}\, {}_1P_{\vec{K}_2,\omega_2}\, {}_1P^*_{\vec{K}_1',\omega_1'}\, {}_1P^*_{\vec{K}_2',\omega_2'} > \;=\; & < {}_1P_{\vec{K}_1,\omega_1}\, {}_1P_{\vec{K}_2,\omega_2} >< {}_1P^*_{\vec{K}_1',\omega_1'}\, {}_1P^*_{\vec{K}_2',\omega_2'} > \\ & + < {}_1P_{\vec{K}_1,\omega_1}\, {}_1P^*_{\vec{K}_1',\omega_1'} >< {}_1P_{\vec{K}_2,\omega_2}\, {}_1P^*_{\vec{K}_2',\omega_2'} > \\ & + < {}_1P_{\vec{K}_1,\omega_1}\, {}_1P^*_{\vec{K}_2',\omega_2'} >< {}_1P_{\vec{K}_2,\omega_2}\, {}_1P^*_{\vec{K}_1',\omega_1'} > \;. \quad \text{(B.6)} \end{aligned}$$

Using equations (3.4) and (3.6), the first term in (B.6) becomes

$$\begin{aligned} & < {}_1P_{\vec{K}_1,\omega_1}\, {}_1P_{\vec{K}_2,\omega_2} >< {}_1P^*_{\vec{K}_1',\omega_1'}\, {}_1P^*_{\vec{K}_2',\omega_2'} > \\ & \qquad = < {}_1P_{\vec{K}_1,\omega_1}\, {}_1P^*_{-\vec{K}_2,-\omega_2} >< {}_1P_{-\vec{K}_1',-\omega_1'}\, {}_1P^*_{\vec{K}_2',\omega_2'} > \\ & \qquad = \begin{cases} < \left|{}_1P_{\vec{K}_1,\omega_1}\right|^2 >< \left|{}_1P_{\vec{K}_1',\omega_1'}\right|^2 >; & \begin{array}{l}\vec{K}_1 = -\vec{K}_2 \\ \vec{K}_1' = -\vec{K}_2' \\ \omega_1 = -\omega_2 \\ \omega_1' = -\omega_2'\end{array} \\ 0;\ \text{otherwise.} \end{cases} \quad \text{(B.7)} \end{aligned}$$

However, in the last paragraph of Section 2.2.5.2, it was pointed out that $\vec{K} = \vec{K}_1 + \vec{K}_2$ (i.e. $\vec{K}_{rs} = \vec{K}_{mn} + \vec{K}_{pq}$) and that essentially all of the contribution to the second-order patch scatter occurs when $\vec{K} = 2k_0\cos\phi_0\hat{N}$, $\hat{N}$ being the unit vector along the outward ellipse normal. In equation (B.7), which is constrained such that $\vec{K}_1 = -\vec{K}_2$, $\vec{K} = \vec{0}$. This obviously violates the known scatter condition. Therefore, it is necessary to consider only the last two terms in equation (B.6), the results of which, based again on equations (3.4) and (3.6), reduce to

$$< {}_1P_{\vec{K}_1,\omega_1}\, {}_1P_{\vec{K}_2,\omega_2} >< {}_1P^*_{\vec{K}_1',\omega_1'}\, {}_1P^*_{\vec{K}_2',\omega_2'} >$$

$$= \begin{cases} 2 < \left|{}_1P_{\vec{K}_1,\omega_1}\right|^2 >< \left|{}_1P_{\vec{K}_2,\omega_2}\right|^2 >; & \begin{array}{l}\vec{K}_1 = \vec{K}_1' \\ \vec{K}_2 = \vec{K}_2' \\ \omega_1 = \omega_1' \\ \omega_2 = \omega_2'\end{array} \\ 0; \text{ otherwise.} \end{cases} \tag{B.8}$$

The restrictions on (B.8) also show that $\vec{K}' = \vec{K}_1' + \vec{K}_2' = \vec{K}_1 + \vec{K}_2 = \vec{K}$. The final form of (B.8), then, using the first-order part of equation (3.7) is

$$< {}_1P_{\vec{K}_1,\omega_1}\, {}_1P_{\vec{K}_2,\omega_2}\, {}_1P^*_{\vec{K}_1',\omega_1'}\, {}_1P^*_{\vec{K}_2',\omega_2'} >$$

$$= \begin{cases} 2N^4W^2 S_1(\vec{K}_1,\omega_1)S_1(\vec{K}_2,\omega_2); & \begin{array}{l}\vec{K}_1 = \vec{K}_1' \\ \vec{K}_2 = \vec{K}_2' \\ \omega_1 = \omega_1' \\ \omega_2 = \omega_2'\end{array} \\ 0; \text{ otherwise.} \end{cases} \tag{B.9}$$

Conveniently, along with the other possible simplifications, (B.9) reduces all of the exponential factors in (B.5) to $e^{j\omega\tau}$ where $\omega = \omega_1 + \omega_2$. However, since $\Gamma_P = {}_H\Gamma + {}_E\Gamma_P$, it is clear from equations (2.64) and (2.142), with the appropriate notation change on the wave vectors, that Γ_P is not symmetric in $\vec{K}_1$, $\vec{K}_2$; i.e.

$$\Gamma_P(\vec{K}_1, \vec{K}_2) \neq \Gamma_P(\vec{K}_2, \vec{K}_1) \ .$$

To this end, we note the identity

$$\sum_{\vec{K}_1}\sum_{\vec{K}_2} \Gamma_P(\vec{K}_1, \vec{K}_2) = \sum_{\vec{K}_1}\sum_{\vec{K}_2} \frac{1}{2}\left[\Gamma_P(\vec{K}_1, \vec{K}_2) + \Gamma_P(\vec{K}_2, \vec{K}_1)\right] \tag{B.10}$$

and define a *symmetric* coupling coefficient as

$${}_s\Gamma_P = \frac{1}{2}\left[\Gamma_P(\vec{K}_1, \vec{K}_2) + \Gamma_P(\vec{K}_2, \vec{K}_1)\right] \ . \tag{B.11}$$

Then, inside the summations of equation (B.5), $\Gamma_P\Gamma_P'^*$ may be written as $|{}_s\Gamma_P|^2$. This reduction could be effected only via (B.11) because the last term in (B.6) required that $\vec{K}_1' = \vec{K}_2$ and $\vec{K}_2' = \vec{K}_1$. Now, the autocorrelation in (B.5) becomes

$$\mathcal{R}_{2P}(\tau) = \frac{A_r}{2\eta_0}\left\{\frac{\eta_0^2 k_0^4 \left|I_0 \Delta\ell\right|^2 (\Delta\rho_s)^2}{(2\pi)^3 \rho_{0s}\left[\rho_{0s}^2 - \left(\frac{\rho}{2}\right)^2\right]}\right\} \sum_{\vec{K}_1,\omega_1}\sum_{\vec{K}_2,\omega_2} |{}_s\Gamma_P|^2 \cdot \left[2N^4W^2\right.$$

$$\cdot\ S_1(\vec{K}_1,\omega_1)S_1(\vec{K}_2,\omega_2)\Big]\, e^{j\omega\tau}(K\cos\phi_0)$$
$$\cdot\ |F(\rho_{01},\omega_0)F(\rho_{02},\omega_0)|^2\,\mathrm{Sa}^2\left[\frac{\Delta\rho_s}{2}\left(\frac{K}{\cos\phi_0}-2k_0\right)\right]\ . \qquad \text{(B.12)}$$

If, as following equation (3.40), the fundamental spatial and temporal periods become very large (i.e., $N, W \to 0$), and if $S_1(\cdot)$ is cast in the form of (3.10), equation (B.12) may be written as

$$\begin{aligned}\mathcal{R}_{2P}(\tau) \;=\; & \frac{A_r}{2\eta_0}\left\{\frac{\eta_0^2k_0^4\,|I_0\Delta\ell|^2\,(\Delta\rho_s)^2}{2\cdot(2\pi)^3\rho_{0s}\left[\rho_{0s}^2-\left(\frac{\rho}{2}\right)^2\right]}\right\}\sum_{m_1=\pm1}\sum_{m_2=\pm1}\int_{\vec{K}_2}\int_{\vec{K}_1}\\ & \Big\{S_1(m_1\vec{K}_1)S_1(m_2\vec{K}_2)\,|{}_s\Gamma_P|^2\,e^{j\omega\tau}(K\cos\phi_0)\\ & \cdot\,|F(\rho_{01},\omega_0)F(\rho_{02},\omega_0)|^2\,\mathrm{Sa}^2\left[\frac{\Delta\rho_s}{2}\left(\frac{K}{\cos\phi_0}-2k_0\right)\right]\Big\}\,d^2\vec{K}_1d^2\vec{K}_2\ . \qquad \text{(B.13)}\end{aligned}$$

The ω-integrals have been evaluated via the delta functions entering through the first-order part of equation (3.10). Therefore, in analogy to equation (3.43),

$$\begin{aligned}\omega_1 &= -m_1\sqrt{gK_1}\\ \omega_2 &= -m_2\sqrt{gK_2}\\ \Rightarrow\ \omega &= -m_1\sqrt{gK_1}-m_2\sqrt{gK_2}\ .\end{aligned} \qquad \text{(B.14)}$$

Also, it is understood that

$$\begin{aligned}d^2\vec{K}_1 &= K_1dK_1d\theta_{\vec{K}_1}\\ \text{and}\qquad\qquad\\ d^2\vec{K}_2 &= K_2dK_2d\theta_{\vec{K}_2}\ .\end{aligned} \qquad \text{(B.15)}$$

It will be useful to convert the $\vec{K}_2$ integration to an integral over $\vec{K}$. With the stipulation that $\vec{K}_2=\vec{K}-\vec{K}_1$, it is easy to show that the Jacobian of the transformation is unity so that

$$\begin{aligned}\mathcal{R}_{2P}(\tau) \;=\; & \frac{A_r}{2\eta_0}\left\{\frac{\eta_0^2k_0^4\,|I_0\Delta\ell|^2\,(\Delta\rho_s)^2}{2\cdot(2\pi)^3\rho_{0s}\left[\rho_{0s}^2-\left(\frac{\rho}{2}\right)^2\right]}\right\}\sum_{m_1=\pm1}\sum_{m_2=\pm1}\int_{-\pi}^{\pi}\int_0^{\infty}\int_{-\pi}^{\pi}\int_0^{\infty}\\ & \Big\{S_1(m_1\vec{K}_1)S_1(m_2\vec{K}_2)\,|{}_s\Gamma_P|^2\,e^{j\omega\tau}(K^2\cos\phi_0)\,|F(\rho_{01},\omega_0)F(\rho_{02},\omega_0)|^2\\ & \cdot\mathrm{Sa}^2\left[\frac{\Delta\rho_s}{2}\left(\frac{K}{\cos\phi_0}-2k_0\right)\right]K_1\Big\}\,dK_1\,d\theta_{\vec{K}_1}\,dK\,d\theta_{\vec{K}}\ . \qquad \text{(B.16)}\end{aligned}$$

The resemblance of (B.16) to equation (3.42) for the first order is clear, so that Fourier transforming it immediately yields the Doppler power spectral density as

$$\begin{aligned}\mathcal{P}_{2P}(\omega_d) &= \left\{\frac{A_r\eta_0 k_0^4\left|I_0\Delta\ell\right|^2(\Delta\rho_s)^2}{4\cdot(2\pi)^2\rho_{0s}\left[\rho_{0s}^2-\left(\frac{\rho}{2}\right)^2\right]}\right\}\sum_{m_1=\pm1}\sum_{m_2=\pm1}\int_{-\pi}^{\pi}\int_0^{\infty}\int_{-\pi}^{\pi}\int_0^{\infty}\\ &\left\{S_1(m_1\vec{K}_1)S_1(m_2\vec{K}_2)\left|{}_s\Gamma_P\right|^2(K^2\cos\phi_0)\left|F(\rho_{01},\omega_0)F(\rho_{02},\omega_0)\right|^2\right.\\ &\cdot\mathrm{Sa}^2\left[\frac{\Delta\rho_s}{2}\left(\frac{K}{\cos\phi_0}-2k_0\right)\right]\delta\left(\omega_d+m_1\sqrt{gK_1}+m_2\sqrt{gK_2}\right)K_1\Big\}\\ &dK_1d\theta_{\vec{K}_1}dKd\theta_{\vec{K}}\,. \end{aligned}\tag{B.17}$$

Again, it is emphasized that ω_d is the transform variable for τ and ω is given in (B.14). At this stage, equation (B.17) represents the power spectral density due to the field being received from all double scatters occurring on a fixed elliptical patch of the time varying surface of width $\Delta\rho_s$ $(=\frac{c\tau_0}{2})$.

B.3 The Autocorrelation and Spectrum when One of Two Scatters Occurs Near the Transmitting Antenna

The autocorrelation given by equation (3.53),

$$\mathcal{R}_{2T}(\tau)=\frac{A_r}{2\eta_0}<\left(E_{0_n}^{+}\right)_{2T}(t_0,t+\tau)\left(E_{0_n}^{+}\right)_{2T}^{*}(t_0,t)>\,,\tag{B.18}$$

is now considered. The appropriate electric field is given in equation (3.28) making (B.18)

$$\begin{aligned}\mathcal{R}_{2T}(\tau) &= \frac{A_r}{2\eta_0}\left\{\frac{\eta_0^2k_0^4\left|I_0\Delta\ell\right|^2(\Delta\rho_s)^2}{(2\pi)^3\rho_{0s}\left[\rho_{0s}^2-\left(\frac{\rho}{2}\right)^2\right]}\right\}\sum_{\vec{K}_1,\omega_1}\sum_{\vec{K}_1',\omega_1'}\sum_{\vec{K}_2,\omega_2}\sum_{\vec{K}_2',\omega_2'}{}_E\Gamma_T\,{}_E\Gamma_T'^{*}\\ &\cdot e^{j\frac{\vec{\rho}}{2}\cdot\vec{K}_2}e^{-j\frac{\vec{\rho}}{2}\cdot\vec{K}_2'}e^{j\rho_{0s}K_2\cos\phi_0}e^{-j\rho_{0s}K_2'\cos\phi_0'}<{}_1P_{\vec{K}_1,\omega_1}\,{}_1P_{\vec{K}_2,\omega_2}\,{}_1P_{\vec{K}_1',\omega_1'}\,{}_1P_{\vec{K}_2',\omega_2'}^{*}>\\ &\cdot e^{j(\omega_1+\omega_2)(t+\tau)}e^{-j(\omega_1'+\omega_2')(t)}\sqrt{K_2\cos\phi_0}\sqrt{K_2'\cos\phi_0'}\,F(\rho_{01},\omega_0)F(\rho_{02},\omega_0)\\ &\cdot F^{*}(\rho_{01}',\omega_0)F^{*}(\rho_{02}',\omega_0)\,\mathrm{Sa}\left[\frac{\Delta\rho_s}{2}\left(\frac{K_2}{\cos\phi_0}-2k_0\right)\right]\mathrm{Sa}\left[\frac{\Delta\rho_s}{2}\left(\frac{K_2'}{\cos\phi_0'}-2k_0\right)\right]\end{aligned}\tag{B.19}$$

It is to be understood that $\vec{K}_1$, $\vec{K}_1'$, ω_1, and ω_1' are associated with surface waves near the transmitter while $\vec{K}_2$, $\vec{K}_2'$, ω_2, and ω_2' are similarly the wavenumbers and frequencies for the scatterers on the distant elliptical patch. As in the previous section, the ensemble average indicated by the angular brackets in (B.19) must be determined. The initial expansion has exactly the same form as equation (B.6).

1. The Second Term of $\mathcal{R}_{2T}(\tau)$ and the Related Power Spectral Density

It will be seen from what follows that the second term in (B.6) as it is applied here is the most significant. Thus, we consider that term firstly, and recalling equation (3.6) and (3.7), we define

$$< {}_1P_{\vec{K}_1,\omega_1}\, {}_1P^*_{\vec{K}_1',\omega_1'} >< {}_1P_{\vec{K}_2,\omega_2}\, {}_1P^*_{\vec{K}_2',\omega_2'} >$$

$$= \begin{cases} N^4 W^2 S_1(\vec{K}_1,\omega_1) S_1(\vec{K}_2,\omega_2); & \begin{array}{l}\vec{K}_1 = \vec{K}_1' \\ \vec{K}_2 = \vec{K}_2' \\ \omega_1 = \omega_1' \\ \omega_2 = \omega_2'\end{array} \\ 0; \text{ otherwise.} \end{cases} \tag{B.20}$$

As before, equation (3.10) for $S(\cdot)$ is invoked and the fundamental spatial and temporal periods are extended to infinity. Then, using the subscript 2 on $\mathcal{R}_{2T}(\tau)$ to emphasize that only the second term of the ensemble average is being considered, equation (B.19) becomes

$$\mathcal{R}_{2T,2}(\tau) = \frac{A_\tau}{2\eta_0}\left\{\frac{\eta_0^2 k_0^4 \left|I_0 \Delta\ell\right|^2 (\Delta\rho_s)^2}{4\cdot(2\pi)^3 \rho_{0s}\left[\rho_{0s}^2 - \left(\frac{\varrho}{2}\right)^2\right]}\right\} \sum_{m_1=\pm1}\sum_{m_2=\pm1} \int_{-\pi}^{\pi}\int_0^{\infty}\int_{-\pi}^{\pi}\int_0^{\infty}$$

$$\left\{S_1(m_1\vec{K}_1) S_1(m_2\vec{K}_2) \left|{}_E\Gamma_T\right|^2 e^{j(\omega_1+\omega_2)\tau} (K_2^2 \cos\phi_0) \left|F(\rho_{01},\omega_0) F(\rho_{02},\omega_0)\right|^2\right.$$

$$\left.\cdot \mathrm{Sa}^2\left[\frac{\Delta\rho_s}{2}\left(\frac{K_2}{\cos\phi_0} - 2k_0\right)\right] K_1\right\} dK_1 d\theta_{\vec{K}_1} dK_2 d\theta_{\vec{K}_2} \,. \tag{B.21}$$

In (B.21), the differentials are formally defined by equation (B.15). Also, the ω-integrals have again yielded to the delta functions of equation (3.10). It is also clear from the fact that $\vec{K}_1 = \vec{K}_1'$ and $\vec{K}_2 = \vec{K}_2'$ that the coupling coefficient factors,

${}_E\Gamma_T\,{}_E\Gamma_T'^*$, as defined by equations (2.87) and (2.146) (recalling $\vec{K}_{mn} \equiv \vec{K}_1$ and $\vec{K}_{pq} \equiv \vec{K}_2$), reduce to $|{}_E\Gamma_T|^2$. It should be recalled from Section 2.2.5.2, that to a very good approximation, $\vec{K}_2 = 2k_0 \cos\phi_0 \hat{N}$ where $\hat{N}$ is the unit normal at any position on the scattering ellipse; that is, $\vec{K}_2$ lies along the "outward" normal to the remote scattering ellipse. No such constraint, either in magnitude or direction, is placed upon the wave vector, $\vec{K}_1$, associated with the first scatter near the transmitter. Comparing equation (B.21) with (B.16), we may immediately write, by analogy with (B.17), that the Doppler power spectral density contribution from the second term of the average in (B.19) is

$$\begin{aligned}
\mathcal{P}_{2T,2}(\omega_d) \;=\; & \left\{ \frac{A_\tau \eta_0 k_0^4 \,|I_0 \Delta\ell|^2 \,(\Delta\rho_s)^2}{8\cdot(2\pi)^2 \rho_{0s} \left[\rho_{0s}^2 - \left(\frac{\ell}{2}\right)^2\right]} \right\} \sum_{m_1=\pm 1} \sum_{m_2=\pm 1} \int_{-\pi}^{\pi}\int_{0}^{\infty}\int_{-\pi}^{\pi}\int_{0}^{\infty} \\
& \left\{ S_1(m_1\vec{K}_1) S_1(m_2\vec{K}_2)\,|{}_E\Gamma_T|^2\,(K_2^2\cos\phi_0) \right. \\
& \cdot\, |F(\rho_{01},\omega_0)F(\rho_{02},\omega_0)|^2\,\mathrm{Sa}^2\left[\frac{\Delta\rho_s}{2}\left(\frac{K_2}{\cos\phi_0} - 2k_0\right)\right] \\
& \left. \cdot\, \delta\left(\omega_d + m_1\sqrt{gK_1} + m_2\sqrt{gK_2}\right) K_1 \right\}\; dK_1 d\theta_{\vec{K}_1} dK_2 d\theta_{\vec{K}_2} \,. \qquad \text{(B.22)}
\end{aligned}$$

Here, ω_1 and ω_2 are defined as in (B.14) and ω_d is the usual transform variable for τ. Since $\vec{K}_1$ is not constrained, (B.22) represents a continuum in ω_d. Implications of the specific conditions on $\vec{K}_2$ will be discussed further when the cross section corresponding to this portion of the power density spectrum is developed in Sections 3.5–3.6.

2. The First Term of $\mathcal{R}_{2T}(\tau)$ and the Related Power Spectral Density

The first term of the ensemble average in equation (B.19) may be written as

$$\begin{aligned}
&< {}_1P_{\vec{K}_1,\omega_1}\,{}_1P_{\vec{K}_2,\omega_2} >< {}_1P^*_{\vec{K}_1',\omega_1'}\,{}_1P^*_{\vec{K}_2',\omega_2'} > \\
&\qquad\qquad = < {}_1P^*_{-\vec{K}_1,-\omega_1}\,{}_1P_{\vec{K}_2,\omega_2} >< {}_1P_{-\vec{K}_1',-\omega_1'}\,{}_1P^*_{\vec{K}_2',\omega_2'} >
\end{aligned}$$

$$= \begin{cases} N^4 W^2 S_1(\vec{K}_2, \omega_2) S_1(\vec{K}_2', \omega_2'); & \begin{array}{l} \vec{K}_1 = -\vec{K}_2 \\ \vec{K}_2' = -\vec{K}_1' \\ \omega_1 = -\omega_2 \\ \omega_2' = -\omega_1' \end{array} \\ 0; \text{ otherwise.} \end{cases} \quad \text{(B.23)}$$

The ideas encountered in determining a power spectral density corresponding to this part of the average are important in the sense that they may be applied frequently in the subsequent analysis. Thus, so that direct comparison may be used to write down many of the later results, we proceed with some detail in this section.

Converting the sums to integrals, as in equation (B.21), and evaluating the ω-integrals using the delta functions appearing in equation (3.10), equation (B.19) for the term corresponding to (B.23) may be written

$$\begin{aligned} \mathcal{R}_{2T,1}(\tau) = \frac{A_r}{2\eta_0} & \left\{ \frac{\eta_0^2 k_0^4 \left| I_0 \Delta\ell \right|^2 (\Delta\rho_s)^2}{4 \cdot (2\pi)^3 \rho_{0s} \left[\rho_{0s}^2 - \left(\frac{\rho}{2}\right)^2 \right]} \right\} \sum_{m_1=\pm 1} \sum_{m_2=\pm 1} \int_{-\pi}^{\pi} \int_0^{\infty} \int_{-\pi}^{\pi} \int_0^{\infty} \left\{ S_1(m_1 \vec{K}_2) \right. \\ & \cdot S_1(m_2 \vec{K}_2') \left({}_E\Gamma_T(-\vec{K}_2, \hat{\rho}_2) {}_E\Gamma_T^*(-\vec{K}_2', \hat{\rho}_2') \right) e^{j\vec{0}\cdot\vec{\tau}} \sqrt{K_2 K_2' \cos\phi_0 \cos\phi_0'} \\ & \cdot F(\rho_{01}, \omega_0) F(\rho_{02}, \omega_0) F^*(\rho_{01}', \omega_0) F^*(\rho_{02}', \omega_0) e^{j\frac{\vec{\rho}}{2}\cdot(\vec{K}_2 - \vec{K}_2')} \\ & \cdot e^{j\rho_{0s}(K_2 \cos\phi_0 - K_2' \cos\phi_0')} \mathrm{Sa}\left[\frac{\Delta\rho_s}{2} \left(\frac{K_2}{\cos\phi_0} - 2k_0 \right) \right] \\ & \left. \mathrm{Sa}\left[\frac{\Delta\rho_s}{2} \left(\frac{K_2'}{\cos\phi_0'} - 2k_0 \right) \right] K_2 K_2' \right\} dK_2 d\theta_{\vec{K}_2} dK_2' d\theta_{\vec{K}_2'} \, . \end{aligned} \quad \text{(B.24)}$$

In writing this form, the constraint on the ω's in (B.23) has been used to write the time exponentials in (B.19) as $e^{j\vec{0}\cdot\vec{\tau}}$. This feature has been left explicit so that the transition to the power density spectrum may be effected in an obvious manner. Also, for reference purposes, the arguments of the coupling coefficient, ${}_E\Gamma_T$, have been made explicit using equations (2.87) and (2.146) and the fact that $\vec{K}_2 \approx 2k_0 \cos\phi_0 \hat{N}$. It must be realized, however, that equation (B.24) still applies to a complete elliptical scattering patch as emphasized by the limits on the angle integrations. This means, then, that here $\hat{N}$, the unit normal to the ellipse, changes with position during the integration.

Fourier transformation of equation (B.24) gives for the Doppler power spectral density of this component for the entire elliptical patch

$$\begin{aligned}
\mathcal{P}_{2T,1}(\omega_d) &= \left\{ \frac{A_r \eta_0 k_0^4 \left| I_0 \Delta\ell \right|^2 (\Delta\rho_s)^2}{8 \cdot (2\pi)^2 \rho_{0s} \left[\rho_{0s}^2 - \left(\frac{\rho}{2}\right)^2 \right]} \right\} \sum_{m_1=\pm 1} \sum_{m_2=\pm 1} \int_{-\pi}^{\pi} \int_0^{\infty} \int_{-\pi}^{\pi} \int_0^{\infty} \left\{ S_1(m_1 \vec{K}_2) \right. \\
&\cdot S_1(m_2 \vec{K}_2') \left({}_E\Gamma_T(-\vec{K}_2, \hat{\rho}_2) {}_E\Gamma_T^*(-\vec{K}_2', \hat{\rho}_2') \right) \sqrt{K_2 K_2' \cos\phi_0 \cos\phi_0'} \\
&\cdot F(\rho_{01}, \omega_0) F(\rho_{02}, \omega_0) F^*(\rho_{01}', \omega_0) F^*(\rho_{02}', \omega_0) e^{j\frac{\vec{\rho}}{2} \cdot (\vec{K}_2 - \vec{K}_2')} \\
&\cdot e^{j\rho_{0s}(K_2 \cos\phi_0 - K_2' \cos\phi_0')} \operatorname{Sa}\left[\frac{\Delta\rho_s}{2} \left(\frac{K_2}{\cos\phi_0} - 2k_0 \right) \right] \\
&\left. \operatorname{Sa}\left[\frac{\Delta\rho_s}{2} \left(\frac{K_2'}{\cos\phi_0'} - 2k_0 \right) \right] \delta(\omega_d)\ K_2 K_2' \right\} dK_2 d\theta_{\vec{K}_2} dK_2' d\theta_{\vec{K}_2'} \,. \qquad \text{(B.25)}
\end{aligned}$$

The Dirac delta function, $\delta(\omega_d)$, implies a power spike at zero Doppler. We will now examine (B.25) and outline the important steps used to show that the fourth-order integral multiplying the delta function is practically zero. Initially, the exponential factors may be combined using equation (2.133) to give

$$e^{j\frac{\rho K_2}{2} f_1(\theta_{\vec{K}_2})} e^{j\frac{\rho K_2'}{2} f_2(\theta_{\vec{K}_2'})} \qquad \text{(B.26)}$$

where

$$\begin{aligned}
f_1(\theta_{\vec{K}_2}) &= \cos\theta_{\vec{K}_2} + \sqrt{\left(\frac{\rho_{0s}}{\frac{\rho}{2}} \right)^2 - \sin^2\theta_{\vec{K}_2}} \\
f_2(\theta_{\vec{K}_2'}) &= -\left[\cos\theta_{\vec{K}_2'} + \sqrt{\left(\frac{\rho_{0s}}{\frac{\rho}{2}} \right)^2 - \sin^2\theta_{\vec{K}_2'}} \right] .
\end{aligned}$$

This allows the angle integrals in equation (B.25) to be done via the stationary phase technique. The analysis leads to stationary points at $(\theta_{\vec{K}_2}, \theta_{\vec{K}_2'}) \equiv (0,0),\ (0,\pi),\ (\pi,0)$ or (π,π). By way of example, for the point $(0,0)$ it may be readily shown from equations (2.87) and (2.146) that

$${}_E\Gamma_T(-\vec{K}_2, \hat{\rho}_2) = \frac{-2k_0^2}{\sqrt{K_2^2 - 2k_0 K_2}}$$

and

$${}_E\Gamma_T^*(-\vec{K}_2', \hat{\rho}_2') = \frac{-2k_0^2}{\sqrt{K_2'^2 - 2k_0 K_2'}} \,.$$

As well,

$$F(\rho_{01},\omega_0)F(\rho_{02},\omega_0)F^*(\rho'_{01},\omega_0)F^*(\rho'_{02},\omega_0) = |F(\rho_{01},\omega_0)F(\rho_{02},\omega_0)|^2$$

and

$$\cos\phi_0 = \cos\phi'_0 = 1$$

since $\vec{K}_2$ and $\vec{K}'_2$, in this case, are in the same direction as $\hat{\rho}_2$. These results give for (B.24) evaluated at $\theta_{\vec{K}_2} = \theta_{\vec{K}'_2} = 0$

$$\begin{aligned}\mathcal{P}_{2T,1}(\omega_d)|_{\theta_{\vec{K}_2}=\theta_{\vec{K}'_2}=0} \approx & \left\{\frac{A_r\eta_0 k_0^4\,|I_0\Delta\ell|^2\,(\Delta\rho_s)^2\,|F(\rho_{01},\omega_0)F(\rho_{02},\omega_0)|^2}{8\cdot(2\pi)^2\rho_{0s}\left[\rho_{0s}^2-\left(\frac{\rho}{2}\right)^2\right]}\right\} \\ & \cdot\frac{(2^7k_0^5\pi)}{\rho\left[1+\left(\frac{(\rho/2)}{\rho_{0s}}\right)\right]}\sum_{m_1=\pm1}\sum_{m_2=\pm1}\int_{2k_0-\Delta K}^{2k_0+\Delta K}\int_{2k_0-\Delta K}^{2k_0+\Delta K} S_1(m_1\vec{K}_2) \\ & \cdot S_1(m_2\vec{K}'_2)\frac{e^{j\frac{\rho}{2}K_2\left[1+\left(\frac{(\rho_{0s}}{\rho/2}\right)\right]}}{\sqrt{K_2-2k_0}}\frac{e^{-j\frac{\rho}{2}K'_2\left[1+\left(\frac{(\rho_{0s}}{\rho/2}\right)\right]}}{\sqrt{K'_2-2k_0}}\delta(\omega_d)dK_2dK'_2\,. \qquad \text{(B.27)}\end{aligned}$$

Here, too, we have approximated K_2 and K'_2 by $2k_0$ except where such approximations would lead to singularities in the integrand. Additionally, in the $2\Delta K$ interval of integration, the respective sampling functions have been approximated by unity. The remaining integrals were executed using Mathematica [88] with the result being

$$\begin{aligned}\mathcal{P}_{2T,1}(\omega_d)|_{\theta_{\vec{K}_2}=\theta_{\vec{K}'_2}=0} \approx & \left\{\frac{A_r\eta_0 2^2k_0^9\,|I_0\Delta\ell|^2\,(\Delta\rho_s)^2\,|F(\rho_{01},\omega_0)F(\rho_{02},\omega_0)|^2}{\pi\rho\left[\rho_{0s}^2-\left(\frac{\rho}{2}\right)^2\right]\left[\rho_{0s}+\left(\frac{\rho}{2}\right)\right]}\right\} \\ & \cdot\sum_{m_1=\pm1}\sum_{m_2=\pm1} S_1\left(2k_0,\left(\frac{1-m_1}{2}\right)\pi\right)S_1\left(2k_0,\left(\frac{1-m_2}{2}\right)\pi\right) \\ & \cdot\left\{(-1)^{\frac{1}{4}}\,e^{jk_0[\rho+2\rho_{0s}|}\sqrt{\frac{\pi}{\left[\frac{\rho}{2}+\rho_{0s}\right]}}\right. \\ & \left.\cdot\left[\mathrm{Erf}\left[(-1)^{\frac{3}{4}}\sqrt{\frac{\rho}{2}+\rho_{0s}}\,\sqrt{-\Delta K}\right]-\mathrm{Erf}\left[(-1)^{\frac{3}{4}}\sqrt{\frac{\rho}{2}+\rho_{0s}}\,\sqrt{\Delta K}\right]\right]\right\} \\ & \cdot\left\{(-1)^{\frac{3}{4}}\,e^{-jk_0[\rho+2\rho_{0s}|}\sqrt{\frac{\pi}{\left[\frac{\rho}{2}+\rho_{0s}\right]}}\right. \\ & \left.\cdot\left[\mathrm{Erf}\left[(-1)^{\frac{1}{4}}\sqrt{\frac{\rho}{2}+\rho_{0s}}\,\sqrt{-\Delta K}\right]-\mathrm{Erf}\left[(-1)^{\frac{1}{4}}\sqrt{\frac{\rho}{2}+\rho_{0s}}\,\sqrt{\Delta K}\right]\right]\right\}\delta(\omega_d) \qquad \text{(B.28)}\end{aligned}$$

where Erf(·) is the error function (eg., Ambromowitz and Stegun [89], Chapter 7) of the form

$$\mathrm{Erf}(z_0) = \frac{2}{\sqrt{\pi}} \int_0^{z_0} e^{-\frac{z^2}{2}} dz \ .$$

It may be readily shown that the arguments of each pair of error functions has the form $(a+ja)$ and $(ja-a)$ with a being large by virtue of the parameter $\left(\frac{\rho}{2} + \rho_{0s}\right)$. In fact, a does not have to be large for the real part in (B.28) to be negligible, but should be $\gtrapprox 10$ for the imaginary part to become small. This may be determined numerically using any suitable computational package such as Mathematica [88]. These observations, in addition to the factors containing ρ and ρ_{0s} arising from the stationary phase procedure, will cause the multiplier on $\delta(\omega_d)$ to be very small compared to, say, that on the sampling functions which are associated with the first-order return in equation (3.46).

The above procedure may be repeated for $(\theta_{\vec{K}_2}, \theta_{\vec{K}_2'}) \equiv (0, \pi)$, $(\pi, 0)$ or (π, π) with essentially the same form of $\mathcal{P}_{2T,1}(\omega_d)$ resulting as in equation (B.28). The sum of these results is still insignificant compared with the power spectral density, $\mathcal{P}_{2T,2}(\omega_d)$, of equation (B.22).

As a final observation, we note that if, as is typically the case in HF radar operation, a narrow beam receiver is used, the $\vec{K}_2$ and $\vec{K}_2'$ wave vectors are essentially coincident on the patch of surface under interrogation. This also means that $\phi_0 = \phi_0'$, and these facts together would immediately remove the exponentials from equation (B.24). The resulting derivation of the power spectral density would be much less complicated than presented here for a general receiver, but the end result reveals that the power density spike at zero Doppler still has a much smaller multiplier than that of the first order. Consequently, further calculation associated with this minor power point will not be pursued here.

3. The First Term of $\mathcal{R}_{2T}(\tau)$ and the Related Power Spectral Density

Finally, in equation (B.19) we consider the term associated with

$$< {}_1P_{\vec{K}_2,\omega_2}\, {}_1P^*_{\vec{K}_1',\omega_1'} >< {}_1P_{\vec{K}_1,\omega_1}\, {}_1P^*_{\vec{K}_2',\omega_2'} >$$

$$= \begin{cases} N^4W^2S_1(\vec{K}_2,\omega_2)S_1(\vec{K}_2',\omega_2'); & \vec{K}_2=\vec{K}_1' \\ & \vec{K}_1=\vec{K}_2' \\ & \omega_2=\omega_1' \\ & \omega_1=\omega_2' \\ 0;\ \text{otherwise.} \end{cases} \tag{B.29}$$

Thus, on changing from sums to integrals and using equation (3.10), we write for the remaining part of (B.19)

$$\begin{aligned} \mathcal{R}_{2T,3}(\tau) \;=\; & \frac{A_r}{2\eta_0}\left\{\frac{\eta_0^2k_0^4\,|I_0\Delta\ell|^2\,(\Delta\rho_s)^2}{4\cdot(2\pi)^3\rho_{0s}\left[\rho_{0s}^2-\left(\frac{\rho}{2}\right)^2\right]}\right\}\sum_{m_1=\pm1}\sum_{m_2=\pm1}\int_{-\pi}^{\pi}\int_0^{\infty}\int_{-\pi}^{\pi}\int_0^{\infty}\Big\{S_1(m_1\vec{K}_2) \\ & \cdot S_1(m_2\vec{K}_2')\left({}_E\Gamma_T(\vec{K}_2',\hat{\rho}_2)\,{}_E\Gamma_T^*(\vec{K}_2,\hat{\rho}_2')\right)e^{j(\omega_2+\omega_2')\tau}\sqrt{K_2K_2'\cos\phi_0\cos\phi_0'} \\ & \cdot F(\rho_{01},\omega_0)F(\rho_{02},\omega_0)F^*(\rho_{01}',\omega_0)F^*(\rho_{02}',\omega_0)e^{j\frac{\vec{\rho}}{2}\cdot(\vec{K}_2-\vec{K}_2')} \\ & \cdot e^{j\rho_{0s}(K_2\cos\phi_0-K_2'\cos\phi_0')}\mathrm{Sa}\left[\frac{\Delta\rho_s}{2}\left(\frac{K_2}{\cos\phi_0}-2k_0\right)\right] \\ & \cdot \mathrm{Sa}\left[\frac{\Delta\rho_s}{2}\left(\frac{K_2'}{\cos\phi_0'}-2k_0\right)\right]K_2\,K_2'\Big\}\,dK_2d\theta_{\vec{K}_2}dK_2'd\theta_{\vec{K}_2'}\,. \end{aligned} \tag{B.30}$$

Here, the constraints on $\vec{K}$'s and ω's have been taken from (B.29). The Fourier transform of (B.30) then gives the power spectral density associated with term (B.29) of equation (B.19) as

$$\begin{aligned} \mathcal{P}_{2T,3}(\omega_d) \;=\; & \frac{A_r\eta_0k_0^4\,|I_0\Delta\ell|^2\,(\Delta\rho_s)^2}{8\cdot(2\pi)^2\rho_{0s}\left[\rho_{0s}^2-\left(\frac{\rho}{2}\right)^2\right]}\sum_{m_1=\pm1}\sum_{m_2=\pm1}\int_{-\pi}^{\pi}\int_0^{\infty}\int_{-\pi}^{\pi}\int_0^{\infty}\Big\{S_1(m_1\vec{K}_2) \\ & \cdot S_1(m_2\vec{K}_2')\left({}_E\Gamma_T(\vec{K}_2',\hat{\rho}_2)\,{}_E\Gamma_T^*(\vec{K}_2,\hat{\rho}_2')\right)\sqrt{K_2K_2'\cos\phi_0\cos\phi_0'} \\ & \cdot F(\rho_{01},\omega_0)F(\rho_{02},\omega_0)F^*(\rho_{01}',\omega_0)F^*(\rho_{02}',\omega_0)e^{j\frac{\vec{\rho}}{2}\cdot(\vec{K}_2-\vec{K}_2')} \\ & \cdot e^{j\rho_{0s}(K_2\cos\phi_0-K_2'\cos\phi_0')}\,\mathrm{Sa}\left[\frac{\Delta\rho_s}{2}\left(\frac{K_2}{\cos\phi_0}-2k_0\right)\right] \\ & \cdot \mathrm{Sa}\left[\frac{\Delta\rho_s}{2}\left(\frac{K_2'}{\cos\phi_0'}-2k_0\right)\right]\delta\left(\omega_d+m_1\sqrt{gK_2}+m_2\sqrt{gK_2'}\right)K_2\,K_2'\Big\} \\ & dK_2\,d\theta_{\vec{K}_2}\,dK_2'\,d\theta_{\vec{K}_2'}\,. \end{aligned} \tag{B.31}$$

With the exception of the delta function argument, equation (B.31) has the same form as equation (B.25) and may, therefore, be treated in the same manner. For example, for the $(0,0)$ stationary point arising from this analysis it transpires that we may let $K_2 = K_2' \approx 2k_0 \cos\phi_0$ so that the delta function gives rise to three discrete power spikes – one at $\omega_d = 0$ and others at $\omega_d = \pm\sqrt{2gk_0\cos\phi_o}$. However, the multiplier on these spikes may be handled in exactly the same manner as that on $\delta(\omega_d)$ in the discussion following (B.25). Making all of the same arguments as previously, it may be immediately concluded that the power spectral density associated with those discrete values of ω_d will be unimportant in comparison to other portions of the spectrum. Thus, this component of $\mathcal{P}_{2T}(\omega_d)$ will not be further considered.

This completes the power spectral density derived from the autocorrelation of the second-order field arising from one scatter near the transmitter followed by a second on a remote elliptical patch. Given that only the second term in equation (B.6), as it applies to this autocorrelation, produces a result which is significantly different from zero, the power spectral density associated with the elliptical surface patch may be written from equation (B.22) as

$$\mathcal{P}_{2T}(\omega_d) \approx \mathcal{P}_{2T,2}(\omega_d)\ . \tag{B.32}$$

This component, unlike $\mathcal{P}_{2T,1}(\omega_d)$ and $\mathcal{P}_{2T,3}(\omega_d)$ is a continuum in ω_d associated with each position on the remote scattering ellipse. It is used to determine the related cross section in Section 3.5.

B.4 The Autocorrelation and Spectrum when One of Two Scatters Occurs Near the Receiving Antenna

The autocorrelation and power spectral densities associated with second-order scattering involving a single scatter at the remote elliptical scattering patch preceding a scatter near the receiving antenna follows very closely that of Appendix B.3. This

time, however, it is the $\vec{K}_1$ vector which is associated with the remote scatter while $\vec{K}_2$ is near the receiver. Thus, $\vec{K}_1 \approx 2k_0 \cos\phi_0 \hat{N}$, while, in general, $\vec{K}_2$ is not constrained in magnitude or direction. Formally, the autocorrelation is given in equation (3.56) as

$$\mathcal{R}_{2R}(\tau) = \frac{A_r}{2\eta_0} < \left(E^+_{0_n}\right)_{2R}(t_0, t+\tau) \left(E^+_{0_n}\right)^*_{2R}(t_0, t) > \ . \tag{B.33}$$

Using the electric field from equation (3.29) in (B.33) yields

$$\begin{aligned}
\mathcal{R}_{2R}(\tau) \ = \ & \frac{A_r}{2\eta_0} \left\{ \frac{\eta_0^2 k_0^4 \left|I_0 \Delta\ell\right|^2 (\Delta\rho_s)^2}{(2\pi)^3 \rho_{0s} \left[\rho_{0s}^2 - \left(\frac{\ell}{2}\right)^2\right]} \right\} \sum_{\vec{K}_1,\omega_1} \sum_{\vec{K}'_1,\omega'_1} \sum_{\vec{K}_2,\omega_2} \sum_{\vec{K}'_2,\omega'_2} {}_E\Gamma_R \, {}_E\Gamma'^*_R \\
& \cdot e^{j\frac{\vec{\ell}}{2}\cdot(\vec{K}_1 - \vec{K}'_1)} e^{j\rho_{0s} K_1 \cos\phi_0} e^{-j\rho_{0s} K'_1 \cos\phi'_0} < {}_1P_{\vec{K}_1,\omega_1} \, {}_1P_{\vec{K}_2,\omega_2} \, {}_1P^*_{\vec{K}'_1,\omega'_1} \, {}_1P^*_{\vec{K}'_2,\omega'_2} > \\
& \cdot e^{j\vec{\rho}\cdot(\vec{K}_2 - \vec{K}'_2)} e^{j(\omega_1+\omega_2)(t+\tau)} e^{-j(\omega'_1+\omega'_2)(t)} \sqrt{K_1 \cos\phi_0} \sqrt{K'_1 \cos\phi'_0} \\
& \cdot F(\rho_{01}, \omega_0) F(\rho_{02}, \omega_0) F^*(\rho'_{01}, \omega_0) F^*(\rho'_{02}, \omega_0) \\
& \cdot \mathrm{Sa}\left[\frac{\Delta\rho_s}{2}\left(\frac{K_1}{\cos\phi_0} - 2k_0\right)\right] \mathrm{Sa}\left[\frac{\Delta\rho_s}{2}\left(\frac{K'_1}{\cos\phi'_0} - 2k_0\right)\right] \ .
\end{aligned} \tag{B.34}$$

The expansion of the ensemble average, $< \cdot >$, follows from equation (B.6), and these results are given by equations (B.20), (B.23) and (B.29). All that was discussed with respect to $\vec{K}_1$, $\vec{K}_2$, $\vec{K}'_1$, and $\vec{K}'_2$ in Appendix B.3 now holds for $\vec{K}_2$, $\vec{K}_1$, $\vec{K}'_2$, and $\vec{K}'_1$, respectively. Therefore, the various terms of the autocorrelations and their respective power spectral densities may be written immediately with reference to equations (B.21), (B.22), (B.24), (B.25), (B.30), and (B.31) as:

1. Result for $< {}_1P_{\vec{K}_1,\omega_1} {}_1P^*_{\vec{K}'_1,\omega'_1} >< {}_1P_{\vec{K}_2,\omega_2} {}_1P^*_{\vec{K}'_2,\omega'_2} >$ - i.e. $\mathcal{R}_{2R,2}(\tau)$

$$\begin{aligned}
\mathcal{R}_{2T,2}(\tau) \ = \ & \frac{A_r}{2\eta_0} \left\{ \frac{\eta_0^2 k_0^4 \left|I_0 \Delta\ell\right|^2 (\Delta\rho_s)^2}{4 \cdot (2\pi)^3 \rho_{0s} \left[\rho_{0s}^2 - \left(\frac{\ell}{2}\right)^2\right]} \right\} \sum_{m_1=\pm 1} \sum_{m_2=\pm 1} \int_{-\pi}^{\pi} \int_0^{\infty} \int_{-\pi}^{\pi} \int_0^{\infty} \\
& \left\{ S_1(m_1\vec{K}_1) S_1(m_2\vec{K}_2) \left|{}_E\Gamma_R\right|^2 e^{j(\omega_1+\omega_2)\tau} (K_1^2 \cos\phi_0) \left|F(\rho_{01}, \omega_0) F(\rho_{02}, \omega_0)\right|^2 \right. \\
& \left. \cdot \mathrm{Sa}^2\left[\frac{\Delta\rho_s}{2}\left(\frac{K_1}{\cos\phi_0} - 2k_0\right)\right] K_2 \right\} dK_1 d\theta_{\vec{K}_1} \, dK_2 \, d\theta_{\vec{K}_2} \ .
\end{aligned} \tag{B.35}$$

The Doppler power spectral density, $\mathcal{P}_{2R,2}(\omega_d)$, is then given by

$$\begin{aligned}\mathcal{P}_{2R,2}(\omega_d) &= \frac{A_r \eta_0 k_0^4 \left|I_0 \Delta\ell\right|^2 (\Delta\rho_s)^2}{8\cdot(2\pi)^2 \rho_{0s}\left[\rho_{0s}^2 - \left(\frac{\rho}{2}\right)^2\right]} \sum_{m_1=\pm 1}\sum_{m_2=\pm 1}\int_{-\pi}^{\pi}\int_{0}^{\infty}\int_{-\pi}^{\pi}\int_{0}^{\infty} \\ &\left\{S_1(m_1\vec{K}_1)S_1(m_2\vec{K}_2)\left|{}_E\Gamma_R\right|^2 (K_1^2\cos\phi_0)\left|F(\rho_{01},\omega_0)F(\rho_{02},\omega_0)\right|^2\right. \\ &\cdot \mathrm{Sa}^2\left[\frac{\Delta\rho_s}{2}\left(\frac{K_1}{\cos\phi_0} - 2k_0\right)\right]\delta\left(\omega_d + m_1\sqrt{gK_1} + m_2\sqrt{gK_2}\right)K_2\Big\} \\ &dK_1\, d\theta_{\vec{K}_1}\, dK_2\, d\theta_{\vec{K}_2}\,. \end{aligned} \tag{B.36}$$

While the $\vec{K}_1$ vector is constrained in magnitude and direction, the $\vec{K}_2$ vector is not. Therefore, (B.36) represents a continuum in ω_d analogous to that for $\mathcal{P}_{2T,2}(\omega_d)$ in equation (B.22). At the moment, $\mathcal{P}_{2R,2}(\omega_d)$ is associated with the complete remote elliptical scattering region. It is used in Section 3.5 to determine the cross section associated with a single scatter on the remote elliptical patch followed by a second near the receiver.

For the sake of completeness, we shall write down the autocorrelations and power spectral densities associated with the remaining two parts of the ensemble average as dictated by equations (B.23) and (B.29). It was seen that these averages provided essentially no content to the overall power density for a single scatter at the transmitter followed by a single scatter at the patch. Now the power spectral densities involving these averages for a single scatter at the patch followed by a single scatter at the receiver will be essentially zero also.

2. Result for $< {}_1P_{\vec{K}_1,\omega_1}\,{}_1P_{\vec{K}_2,\omega_2} >< {}_1P^*_{\vec{K}_1',\omega_1'}\,{}_1P^*_{\vec{K}_2',\omega_2'} >$ – i.e. $\mathcal{R}_{2R,1}(\tau)$

The first term of the ensemble average in equation (B.34) may be written as

$$\begin{aligned}\mathcal{R}_{2R,1}(\tau) &= \frac{A_r}{2\eta_0}\left\{\frac{\eta_0^2 k_0^4 \left|I_0\Delta\ell\right|^2 (\Delta\rho_s)^2}{4\cdot(2\pi)^3\rho_{0s}\left[\rho_{0s}^2 - \left(\frac{\rho}{2}\right)^2\right]}\right\}\sum_{m_1=\pm 1}\sum_{m_2=\pm 1}\int_{-\pi}^{\pi}\int_{0}^{\infty}\int_{-\pi}^{\pi}\int_{0}^{\infty}\Big\{S_1(m_1\vec{K}_1) \\ &\cdot S_1(m_2\vec{K}_1')\left({}_E\Gamma_R(-\vec{K}_1,\hat{\rho}_{12})\,{}_E\Gamma_R^*(-\vec{K}_1',\hat{\rho}_{12}')\right)e^{j0\cdot\tau}\sqrt{K_1K_1'\cos\phi_0\cos\phi_0'} \\ &\cdot F(\rho_{01},\omega_0)F(\rho_{02},\omega_0)F^*(\rho_{01}',\omega_0)F^*(\rho_{02}',\omega_0)e^{j\frac{\vec{\rho}}{2}\cdot(\vec{K}_1'-\vec{K}_1)}e^{j\rho_{0s}(K_1\cos\phi_0 - K_1'\cos\phi_0')} \\ &\cdot \mathrm{Sa}\left[\frac{\Delta\rho_s}{2}\left(\frac{K_1}{\cos\phi_0} - 2k_0\right)\right]\mathrm{Sa}\left[\frac{\Delta\rho_s}{2}\left(\frac{K_1'}{\cos\phi_0'} - 2k_0\right)\right]K_1\,K_1'\Big\}\,dK_1\,d\theta_{\vec{K}_1}\,dK_1'\,d\theta_{\vec{K}_1'} \end{aligned} \tag{B.37}$$

with corresponding power spectral density

$$\mathcal{P}_{2R,1}(\omega_d) = \frac{A_r \eta_0 k_0^4 \left|I_0 \Delta\ell\right|^2 (\Delta\rho_s)^2}{8\cdot(2\pi)^2 \rho_{0s}\left[\rho_{0s}^2 - \left(\frac{\varrho}{2}\right)^2\right]} \sum_{m_1=\pm1}\sum_{m_2=\pm1}\int_{-\pi}^{\pi}\int_{0}^{\infty}\int_{-\pi}^{\pi}\int_{0}^{\infty}\Big\{S_1(m_1\vec{K}_1)$$
$$\cdot S_1(m_2\vec{K}_1')\left({}_E\Gamma_R(-\vec{K}_1,\hat{\rho}_{12}){}_E\Gamma_R^*(-\vec{K}_1',\hat{\rho}_{12}')\right)\sqrt{K_1 K_1' \cos\phi_0 \cos\phi_0'}$$
$$\cdot F(\rho_{01},\omega_0)F(\rho_{02},\omega_0)F^*(\rho_{01}',\omega_0)F^*(\rho_{02}',\omega_0)e^{j\frac{\vec{\varrho}}{2}\cdot(\vec{K}_1'-\vec{K}_1)}$$
$$\cdot e^{j\rho_{0s}(K_1\cos\phi_0 - K_1'\cos\phi_0')}\mathrm{Sa}\left[\frac{\Delta\rho_s}{2}\left(\frac{K_1}{\cos\phi_0}-2k_0\right)\right]$$
$$\cdot \mathrm{Sa}\left[\frac{\Delta\rho_s}{2}\left(\frac{K_1'}{\cos\phi_0'}-2k_0\right)\right]\delta(\omega_d)K_1\ K_1'\Big\}\,dK_1 d\theta_{\vec{K}_1} dK_1' d\theta_{\vec{K}_1'} \qquad \text{(B.38)}$$

where $\omega_1 = -\omega_2$ and $\omega_1' = -\omega_2'$, as dictated by the ensemble averages, have been used. The coupling coefficient arguments have been written explicitly using equations (2.106) and (2.149) and the fact that $\vec{K}_1 \approx 2k_0\cos\phi_0\hat{N}$. Now, the similarities between (B.38) and (B.25) are obvious. Thus, an analysis here could follow that which led to equation (B.28), with the result being that the multiplier on the zero-Doppler power density spike would again be essentially zero. As for (B.28), therefore, this discrete spike is not included in the overall power density. Also, for narrow beam reception, the exponential factors in (B.38) would be unity, but subsequent analysis again leads to a negligible result.

3. Result for $< {}_1P_{\vec{K}_2,\omega_2}\,{}_1P^*_{\vec{K}_1',\omega_1'} > < {}_1P_{\vec{K}_1,\omega_1}\,{}_1P^*_{\vec{K}_2',\omega_2'} >$ – i.e. $\mathcal{R}_{2R,3}(\tau)$

The third term of the ensemble average in equation (B.34) may be written as

$$\mathcal{R}_{2R,3}(\tau) = \frac{A_r}{2\eta_0}\left\{\frac{\eta_0^2 k_0^4 \left|I_0\Delta\ell\right|^2(\Delta\rho_s)^2}{4\cdot(2\pi)^3\rho_{0s}\left[\rho_{0s}^2-\left(\frac{\varrho}{2}\right)^2\right]}\right\}\sum_{m_1=\pm1}\sum_{m_2=\pm1}\int_{-\pi}^{\pi}\int_{0}^{\infty}\int_{-\pi}^{\pi}\int_{0}^{\infty}\Big\{S_1(m_1\vec{K}_1)$$
$$\cdot S_1(m_2\vec{K}_1')\left({}_E\Gamma_R(\vec{K}_1',\hat{\rho}_{12}){}_E\Gamma_R^*(\vec{K}_1,\hat{\rho}_{12}')\right)e^{j(\omega_1+\omega_1')\tau}\sqrt{K_1 K_1'\cos\phi_0\cos\phi_0'}$$
$$\cdot F(\rho_{01},\omega_0)F(\rho_{02},\omega_0)F^*(\rho_{01}',\omega_0)F^*(\rho_{02}',\omega_0)e^{j\frac{\vec{\varrho}}{2}\cdot(\vec{K}_1'-\vec{K}_1)}$$
$$\cdot e^{j\rho_{0s}(K_1\cos\phi_0-K_1'\cos\phi_0')}\mathrm{Sa}\left[\frac{\Delta\rho_s}{2}\left(\frac{K_1}{\cos\phi_0}-2k_0\right)\right]$$
$$\cdot \mathrm{Sa}\left[\frac{\Delta\rho_s}{2}\left(\frac{K_1'}{\cos\phi_0'}-2k_0\right)\right]K_1\ K_1'\Big\}\,dK_1\,d\theta_{\vec{K}_1}\,dK_1'\,d\theta_{\vec{K}_1'}\,. \qquad \text{(B.39)}$$

Here, the constraints on $\vec{K}$'s and ω's have been taken again from (B.29). The power

spectral density associated with (B.39) is then

$$\begin{aligned}\mathcal{P}_{2R,3}(\omega_d) \;=\; & \frac{A_r\eta_0 k_0^4\,|I_0\Delta\ell|^2\,(\Delta\rho_s)^2}{8\cdot(2\pi)^2\rho_{0s}\left[\rho_{0s}^2-\left(\frac{\ell}{2}\right)^2\right]}\sum_{m_1=\pm1}\sum_{m_2=\pm1}\int_{-\pi}^{\pi}\int_{0}^{\infty}\int_{-\pi}^{\pi}\int_{0}^{\infty}\Big\{S_1(m_1\vec{K}_1)\\ & \cdot S_1(m_2\vec{K}_1')\left({}_E\Gamma_R(\vec{K}_1',\hat{\rho}_{12})\,{}_E\Gamma_R^*(\vec{K}_1,\hat{\rho}_{12}')\right)\sqrt{K_1K_1'\cos\phi_0\cos\phi_0'}\\ & \cdot F(\rho_{01},\omega_0)F(\rho_{02},\omega_0)F^*(\rho_{01}',\omega_0)F^*(\rho_{02}',\omega_0)e^{j\frac{\vec{\ell}}{2}\cdot(\vec{K}_1'-\vec{K}_1)}\\ & \cdot e^{j\rho_{0s}(K_1\cos\phi_0-K_1'\cos\phi_0')}\mathrm{Sa}\left[\frac{\Delta\rho_s}{2}\left(\frac{K_1}{\cos\phi_0}-2k_0\right)\right]\\ & \cdot \mathrm{Sa}\left[\frac{\Delta\rho_s}{2}\left(\frac{K_1'}{\cos\phi_0'}-2k_0\right)\right]\delta\left(\omega_d+m_1\sqrt{gK_1}+m_2\sqrt{gK_1'}\right)K_1\;K_1'\Big\}\\ & dK_1\,d\theta_{\vec{K}_1}\,dK_1'\,d\theta_{\vec{K}_1'}\;. \end{aligned}\tag{B.40}$$

Comparison with $\mathcal{P}_{2T,3}(\omega_d)$ of equation (B.31) shows that (B.40) exhibits the same features. Thus, at each position on the scattering ellipse, (B.40) will produce three power spikes – at $\omega_d = 0$ and at $\omega_d = \pm\sqrt{2gk_0\cos\phi_o}$. Again, however, the fourth-order integral is essentially zero. For this reason, $\mathcal{P}_{2R,3}(\omega_d)$ will not be included further in the components of the overall power spectral density. We note that the analysis for narrow beam reception could be effected more easily than the case of a general receiver presented here. However, the conclusion of the insignificance of $\mathcal{P}_{2R,1}(\omega_d)$ and $\mathcal{P}_{2R,3}(\omega_d)$ would be unaltered.

This concludes the discussion of the autocorrelation and subsequent power spectral density for the case of a single scatter on a remote elliptical patch being followed by a scatter near the receiving antenna. On the basis of the arguments given, the power density, $\mathcal{P}_{2R}(\omega_d)$, here may be written with reference to equation (B.36) as

$$\mathcal{P}_{2R}(\omega_d) \approx \mathcal{P}_{2R,2}(\omega_d)\;. \tag{B.41}$$

Again it is emphasized that this power spectral density is a continuum in ω_d at each position on the scattering ellipse. The relevant cross section is discussed in Sections 3.5–3.6.

B.5 The Cross-correlation of the "Patch" Field with Other Second-order Field Components

From equation (3.35), and using notation similar to that in (3.47), we wish to consider $\mathcal{R}_{2P,2T}(\tau)$, $\mathcal{R}_{2P,2R}(\tau)$, $\mathcal{R}_{2T,2P}(\tau)$, and $\mathcal{R}_{2R,2P}(\tau)$. These represent the cross-correlations of the field from a double scatter at the remote elliptical scattering patch with fields involving a single scatter at the transmitter or receiver and another on the patch. In fact, it will be seen that, based on the scattering constraints and ocean surface features previously discussed, these terms are negligible.

B.5.1 The Cross-correlations $\mathcal{R}_{2P,2T}(\tau)$ and $\mathcal{R}_{2T,2P}(\tau)$

Formally, the cross-correlation of the second-order field from a double scatter on the remote patch with that involving a scatter near the transmitter may be written as

$$\mathcal{R}_{2P,2T}(\tau) = \frac{A_r}{2\eta_0} < \left(E^+_{0_n}\right)_{2P}(t_0, t+\tau)\left(E^+_{0_n}\right)^*_{2T}(t_0, t) > \tag{B.42}$$

or

$$\begin{aligned}\mathcal{R}_{2P,2T}(\tau) = {} & \frac{A_r}{2\eta_0}\left\{\frac{\eta_0^2 k_0^4 \left|I_0 \Delta\ell\right|^2 (\Delta\rho_s)^2}{(2\pi)^3 \rho_{0s}\left[\rho_{0s}^2 - \left(\frac{\rho}{2}\right)^2\right]}\right\} \sum_{\vec{K}_1,\omega_1}\sum_{\vec{K}_2,\omega_2}\sum_{\vec{K}_3,\omega_3}\sum_{\vec{K}_4,\omega_4} \Gamma_P(\vec{K}_3,\vec{K}_4)_E \Gamma_T^*(\vec{K}_1,\vec{\rho}_2') \\ & \cdot e^{j\frac{\vec{\rho}}{2}\cdot(\vec{K}-\vec{K}_2)} e^{j\rho_{0s}K\cos\phi_0} e^{-j\rho_{0s}K_2\cos\phi_0'} < {}_1P_{\vec{K}_3,\omega_3}\, {}_1P_{\vec{K}_4,\omega_4}\, {}_1P^*_{\vec{K}_1,\omega_1}\, {}_1P^*_{\vec{K}_2,\omega_2} > \\ & \cdot e^{j(\omega_3+\omega_4)(t+\tau)} e^{-j(\omega_1+\omega_2)(t)} \sqrt{K\cos\phi_0}\sqrt{K_2\cos\phi_0'} F(\rho_{01},\omega_0) F(\rho_{02},\omega_0) \\ & \cdot F^*(\rho_{01}',\omega_0) F^*(\rho_{02}',\omega_0) \mathrm{Sa}\left[\frac{\Delta\rho_s}{2}\left(\frac{K}{\cos\phi_0} - 2k_0\right)\right] \mathrm{Sa}\left[\frac{\Delta\rho_s}{2}\left(\frac{K_2}{\cos\phi_0'} - 2k_0\right)\right] .\end{aligned} \tag{B.43}$$

In equation (B.43), $\vec{K}_3$ and $\vec{K}_4$ represent wave vectors associated with double patch scatter (i.e. two scatters near each other on the remote scattering ellipse) and $\vec{K}_1$ and $\vec{K}_2$ are similarly linked to surface waves at the transmitter and patch, respectively. The various ω's are, as usual, related to the K's via the dispersion relationship of equation (3.9). On the basis of equation (B.6), the object to be considered here is

$$< {}_1P_{\vec{K}_3,\omega_3}\, {}_1P_{\vec{K}_4,\omega_4}\, {}_1P^*_{\vec{K}_1,\omega_1}\, {}_1P^*_{\vec{K}_2,\omega_2} > \;=\; < {}_1P_{\vec{K}_3,\omega_3}\, {}_1P_{\vec{K}_4,\omega_4} >< {}_1P^*_{\vec{K}_1,\omega_1}\, {}_1P^*_{\vec{K}_2,\omega_2} >$$
$$+ < {}_1P_{\vec{K}_3,\omega_3}\, {}_1P^*_{\vec{K}_1,\omega_1} >< {}_1P_{\vec{K}_4,\omega_4}\, {}_1P^*_{\vec{K}_2,\omega_2} >$$
$$+ < {}_1P_{\vec{K}_4,\omega_4}\, {}_1P^*_{\vec{K}_1,\omega_1} >< {}_1P_{\vec{K}_3,\omega_3}\, {}_1P^*_{\vec{K}_2,\omega_2} > \;. \quad \text{(B.44)}$$

1. Result for $< {}_1P_{\vec{K}_3,\omega_3}\, {}_1P_{\vec{K}_4,\omega_4} >< {}_1P^*_{\vec{K}_1,\omega_1}\, {}_1P^*_{\vec{K}_2,\omega_2} >$ – i.e. $\mathcal{R}_{2P,2T,1}(\tau)$

From equations (3.4) and (3.6), the first factor on the right hand side (r.h.s.) of (B.44) is non-zero only if $\vec{K}_3 = -\vec{K}_4$. However, $\vec{K}_3$ and $\vec{K}_4$ are associated with the double scatter such that, as seen in Section 2.2.5.2,

$$\vec{K}_3 + \vec{K}_4 = \vec{K} \approx 2k_0 \cos\phi_0 \hat{N} \;. \quad \text{(B.45)}$$

This condition is obviously violated if $\vec{K}_3 = -\vec{K}_4$ so that the first term on the r.h.s of (B.44) must vanish. Thus,

$$\mathcal{R}_{2P,2T,1}(\tau) = 0 \implies \mathcal{P}_{2P,2T,1}(\omega_d) = 0 \quad \text{(B.46)}$$

where $\mathcal{P}_{2P,2T,1}(\omega_d)$ is the corresponding power spectral density.

At this point, it is useful to comment that, in addition to $\mathcal{R}_{2P,2T,1}(\tau)$ of equation (B.43), there will also be an average from equation (3.35) which may be denoted by

$$\mathcal{R}_{2T,2P}(\tau) = \frac{A_r}{2\eta_0} < \left(E^+_{0_n}\right)_{2T}(t_0, t+\tau) \left(E^+_{0_n}\right)^*_{2P}(t_0, t) > \;. \quad \text{(B.47)}$$

Since the process under consideration is assumed to be stationary (in fact, the less stringent *wide sense* stationary condition would suffice here (see Papoulis [73], Chapter 10),

$$\mathcal{R}_{2T,2P,1}(\tau) = \mathcal{R}^*_{2P,2T,1}(-\tau) \;. \quad \text{(B.48)}$$

Now, since $\mathcal{R}_{2P,2T,1}(\tau)$ is identically zero, it follows that its counterpart from (B.47), along with the power spectral density is also zero, i.e.

$$\mathcal{R}_{2T,2P,1}(\tau) = 0 \implies \mathcal{P}_{2T,2P,1}(\omega_d) = 0 \;. \quad \text{(B.49)}$$

2. Result for $< {}_1P_{\vec{K}_3,\omega_3}\, {}_1P^*_{\vec{K}_1,\omega_1} > < {}_1P_{\vec{K}_4,\omega_4}\, {}_1P^*_{\vec{K}_2,\omega_2} >$ - i.e. $\mathcal{R}_{2P,2T,2}(\tau)$

Next, the second factor of the second term on the r.h.s. of (B.44) is non-zero only for $\vec{K}_3 = \vec{K}_1$, $\omega_3 = \omega_1$, $\vec{K}_4 = \vec{K}_2$, and $\omega_4 = \omega_2$. From (B.43), this part of the average gives, with the usual changes from sums to integrals,

$$\begin{aligned}
\mathcal{R}_{2P,2T,2}(\tau) \;=\; & \frac{A_r}{2\eta_0}\left\{\frac{\eta_0^2 k_0^4\,|I_0\Delta\ell|^2\,(\Delta\rho_s)^2}{4\cdot(2\pi)^3\rho_{0s}\left[\rho_{0s}^2-\left(\frac{\rho}{2}\right)^2\right]}\right\}\sum_{m_1=\pm1}\sum_{m_2=\pm1}\int_{-\pi}^{\pi}\int_0^{\infty}\int_{-\pi}^{\pi}\int_0^{\infty} \\
& \Big\{S_1(m_1\vec{K}_1)S_1(m_2\vec{K}_2)\Gamma_P(\vec{K}_1,\vec{K}_2)_E\Gamma_T^*(\vec{K}_1,\hat{\rho}_2')\sqrt{KK_2\cos\phi_0\cos\phi_0'} \\
& \cdot e^{j\frac{\vec{\rho}}{2}\cdot(\vec{K}-\vec{K}_2)}e^{j\rho_{0s}(K\cos\phi_0-K_2\cos\phi_0')}e^{j(\omega_1+\omega_2)\tau} \\
& \cdot F(\rho_{01},\omega_0)F(\rho_{02},\omega_0)F^*(\rho_{01}',\omega_0)F^*(\rho_{02}',\omega_0) \\
& \cdot \mathrm{Sa}\left[\frac{\Delta\rho_s}{2}\left(\frac{K}{\cos\phi_0}-2k_0\right)\right]\mathrm{Sa}\left[\frac{\Delta\rho_s}{2}\left(\frac{K_2}{\cos\phi_0'}-2k_0\right)\right]KK_2\Big\} \\
& dK\,d\theta_{\vec{K}}\,dK_2\,d\theta_{\vec{K}_2}
\end{aligned} \tag{B.50}$$

where it must be understood that $\vec{K} = \vec{K}_3 + \vec{K}_4 = \vec{K}_1 + \vec{K}_2$. The K_1 integration has been changed to a K integration with the understanding that $\vec{K}_1 = \vec{K} - \vec{K}_2$. Then, given the fact that $\mathcal{R}_{2T,2P,2}(\tau) = \mathcal{R}^*_{2P,2T,2}(-\tau)$, the Doppler power spectral density from $\mathcal{R}_{2T,2P,2}(\tau)$ and $\mathcal{R}_{2P,2T,2}(\tau)$ is

$$\begin{aligned}
\mathcal{P}_{2P,2T,2}(\omega_d)+\mathcal{P}_{2T,2P,2}(\omega_d) \;=\; & \frac{A_r\eta_0 k_0^4\,|I_0\Delta\ell|^2\,(\Delta\rho_s)^2}{4\cdot(2\pi)^2\rho_{0s}\left[\rho_{0s}^2-\left(\frac{\rho}{2}\right)^2\right]}\sum_{m_1=\pm1}\sum_{m_2=\pm1}\int_{-\pi}^{\pi}\int_0^{\infty}\int_{-\pi}^{\pi}\int_0^{\infty} \\
& \Big\{S_1(m_1\vec{K}_1)S_1(m_2\vec{K}_2)\mathrm{Re}\Big[\Gamma_P(\vec{K}_1,\vec{K}_2)_E\Gamma_T^*(\vec{K}_1,\hat{\rho}_2')e^{j\frac{\vec{\rho}}{2}\cdot(\vec{K}-\vec{K}_2)} \\
& \cdot e^{j\rho_{0s}(K\cos\phi_0-K_2\cos\phi_0')}\Big]\sqrt{KK_2\cos\phi_0\cos\phi_0'} \\
& \cdot F(\rho_{01},\omega_0)F(\rho_{02},\omega_0)F^*(\rho_{01}',\omega_0)F^*(\rho_{02}',\omega_0) \\
& \cdot \mathrm{Sa}\left[\frac{\Delta\rho_s}{2}\left(\frac{K}{\cos\phi_0}-2k_0\right)\right]\mathrm{Sa}\left[\frac{\Delta\rho_s}{2}\left(\frac{K_2}{\cos\phi_0'}-2k_0\right)\right] \\
& \cdot \delta\left(\omega_d+m_1\sqrt{gK_1}+m_2\sqrt{gK_2}\right)K\,K_2\Big\}\,dK\,d\theta_{\vec{K}}\,dK_2\,d\theta_{\vec{K}_2}\,.
\end{aligned} \tag{B.51}$$

Here, both $\vec{K}$ and $\vec{K}_2$ are normal to the scattering ellipse. However, for the moment, the positions on the ellipse need not be the same for these two wave vectors. Further

comment on (B.51) is reserved until the last pieces of $\mathcal{R}_{2P,2T}(\tau)$ and $\mathcal{R}_{2T,2P}(\tau)$ are developed below.

3. Result for $< {}_1P_{\vec{K}_4,\omega_4}\, {}_1P^*_{\vec{K}_1,\omega_1} >< {}_1P_{\vec{K}_3,\omega_3}\, {}_1P^*_{\vec{K}_2,\omega_2} >$ – i.e. $\mathcal{R}_{2P,2T,3}(\tau)$

The component of (B.43) corresponding to the final product from (B.44) may be written similarly to (B.50) as

$$\mathcal{R}_{2P,2T,3}(\tau) = \frac{A_r}{2\eta_0}\left\{\frac{\eta_0^2 k_0^4 \left|I_0\Delta\ell\right|^2 (\Delta\rho_s)^2}{4\cdot(2\pi)^3\rho_{0s}\left[\rho_{0s}^2-\left(\frac{\rho}{2}\right)^2\right]}\right\}\sum_{m_1=\pm1}\sum_{m_2=\pm1}\int_{-\pi}^{\pi}\int_0^{\infty}\int_{-\pi}^{\pi}\int_0^{\infty}$$
$$\left\{S_1(m_1\vec{K}_1)S_1(m_2\vec{K}_2)\Gamma_P(\vec{K}_2,\vec{K}_1)_E\Gamma_T^*(\vec{K}_1,\vec{\rho}_2')\sqrt{KK_2\cos\phi_0\cos\phi_0'}\right.$$
$$\cdot\, e^{j\frac{\vec{\rho}}{2}\cdot(\vec{K}-\vec{K}_2)}e^{j\rho_{0s}(K\cos\phi_0-K_2\cos\phi_0')}e^{j(\omega_1+\omega_2)\tau}F(\rho_{01},\omega_0)F(\rho_{02},\omega_0)$$
$$\left.\cdot\, F^*(\rho_{01}',\omega_0)F^*(\rho_{02}',\omega_0)\mathrm{Sa}\left[\frac{\Delta\rho_s}{2}\left(\frac{K}{\cos\phi_0}-2k_0\right)\right]\mathrm{Sa}\left[\frac{\Delta\rho_s}{2}\left(\frac{K_2}{\cos\phi_0'}-2k_0\right)\right]K\,K_2\right\}$$
$$dK\,d\theta_{\vec{K}}\,dK_2\,d\theta_{\vec{K}_2} \qquad \text{(B.52)}$$

where it is to be understood that $\vec{K}_1 = \vec{K}_4$, $\omega_1 = \omega_4$, $\vec{K}_2 = \vec{K}_3$ and $\omega_2 = \omega_3$ have been used. In a way similar to (B.51), the power spectral density from (B.52) and its counterpart, $\mathcal{R}_{2T,2P,3}(\tau)$, may be written as

$$\mathcal{P}_{2P,2T,3}(\omega_d)+\mathcal{P}_{2T,2P,3}(\omega_d) = \frac{A_r\eta_0 k_0^4\left|I_0\Delta\ell\right|^2(\Delta\rho_s)^2}{4\cdot(2\pi)^2\rho_{0s}\left[\rho_{0s}^2-\left(\frac{\rho}{2}\right)^2\right]}\sum_{m_1=\pm1}\sum_{m_2=\pm1}\int_{-\pi}^{\pi}\int_0^{\infty}\int_{-\pi}^{\pi}\int_0^{\infty}$$
$$\left\{S_1(m_1\vec{K}_1)S_1(m_2\vec{K}_2)\mathrm{Re}\left[\Gamma_P(\vec{K}_2,\vec{K}_1)_E\Gamma_T^*(\vec{K}_1,\hat{\rho}_2')e^{j\frac{\vec{\rho}}{2}\cdot(\vec{K}-\vec{K}_2)}\right.\right.$$
$$\left.\cdot\, e^{j\rho_{0s}(K\cos\phi_0-K_2\cos\phi_0')}\right]\sqrt{KK_2\cos\phi_0\cos\phi_0'}$$
$$\cdot\, F(\rho_{01},\omega_0)F(\rho_{02},\omega_0)F^*(\rho_{01}',\omega_0)F^*(\rho_{02}',\omega_0)$$
$$\cdot\,\mathrm{Sa}\left[\frac{\Delta\rho_s}{2}\left(\frac{K}{\cos\phi_0}-2k_0\right)\right]\mathrm{Sa}\left[\frac{\Delta\rho_s}{2}\left(\frac{K_2}{\cos\phi_0'}-2k_0\right)\right]$$
$$\left.\cdot\,\delta\left(\omega_d+m_1\sqrt{gK_1}+m_2\sqrt{gK_2}\right)KK_2\right\}dK\,d\theta_{\vec{K}}\,dK_2\,d\theta_{\vec{K}_2}\,. \qquad \text{(B.53)}$$

Again, it is important to realize that $\vec{K}_1 = \vec{K} - \vec{K}_2$ and that both $\vec{K}$ and $\vec{K}_2$ are normal to the scattering ellipse, howbeit not at the same positions, in general.

On the basis of equations (B.44), (B.51), and (B.53), the Doppler power spectral density arising from the cross-correlations of the second-order fields, one of which involves a double scatter at the remote elliptical patch and the other of which involves a single scatter at the transmitter and another at the patch, may be written as

$$\mathcal{P}_{2P,2T}(\omega_d) + \mathcal{P}_{2T,2P}(\omega_d) = \mathcal{P}_{2P,2T,2}(\omega_d) + \mathcal{P}_{2T,2P,2}(\omega_d) + \mathcal{P}_{2P,2T,3}(\omega_d) + \mathcal{P}_{2T,2P,3}(\omega_d) \,. \tag{B.54}$$

It will now be shown that, in fact, this power spectral density is approximately zero. Consideration of equations (B.51) and (B.53) reveals that the only difference is that, in the former, $\Gamma_P(\vec{K}_1, \vec{K}_2)$ $(\equiv \Gamma_P\left((\vec{K} - \vec{K}_2), \vec{K}_2\right))$ appears, while in the latter this factor is replaced by $\Gamma_P(\vec{K}_2, \vec{K}_1)$ $(\equiv \Gamma_P\left(\vec{K}_2), (\vec{K} - \vec{K}_2)\right))$. As a first step in showing the insignificance of the sum in (B.54) it will be verified that the electromagnetic portion of this coupling coefficient makes the portions of the sum containing it vanish. To do this, it must be shown that at the places of major contribution to the integrals here

$$_E\Gamma_P(\vec{K}_1, \vec{K}_2) = -{}_E\Gamma_P(\vec{K}_2, \vec{K}_1) \,, \tag{B.55}$$

where ${}_E\Gamma_P(\cdot)$ is found in equations (2.64) and (2.142).

To begin, it may be noted that exponential factors,

$$e^{j\frac{\vec{\rho}}{2}\cdot(\vec{K}-\vec{K}_2)} e^{j\rho_{0s}\left[K\cos\phi_0 - K_2\cos\phi_0'\right]} \,,$$

in equations (B.51) and (B.53) take the same form as in (B.25). In the latter, a stationary phase approach gave the angles from which most of the contribution to the integral resulted. Using exactly the same approach here gives the stationary values of the $\vec{K}_1$ and $\vec{K}_2$ directions as

$$\left(\theta_{\vec{K}}, \theta_{\vec{K}_2}\right)_{\text{stationary}} = (0,0), \ (0,\pi), \ (\pi,0), \text{ and } (\pi,\pi) \,. \tag{B.56}$$

Thus, the points of major contribution referred to above have been established.

Next, consider that to a good approximation as dictated by the sampling functions in (B.51) and (B.53),

$$\begin{aligned} K &\approx 2k_0 \cos\phi_0 \\ K_2 &\approx 2k_0 \cos\phi_0' \,. \end{aligned} \tag{B.57}$$

Furthermore,

$$\begin{aligned} \vec{K} &= \vec{K}_3 + \vec{K}_4 \quad \text{(from Section 2.2.2.2)} \\ &= \vec{K}_1 + \vec{K}_2 \quad \text{(from the ensemble average conditions)} \,. \end{aligned} \tag{B.58}$$

When $\left(\theta_{\vec{K}}, \theta_{\vec{K}_2}\right) = (0,0)$ or (π,π), $\vec{K}$ and $\vec{K}_2$ have the same direction and by (B.57) they have approximately the same magnitude. From equation (B.58), this implies $\vec{K}_1 \approx \vec{0}$ which is not possible on the actual ocean (i.e. there are no infinitely long waves). Alternately, $S\left(m_1(\vec{K}-\vec{K}_2)\right) = S\left(m_1\vec{K}_1\right) \approx S\left(\vec{0}\right) = 0$ in the integrands of (B.51) and (B.53).

At the remaining stationary points, $\left(\theta_{\vec{K}}, \theta_{\vec{K}_2}\right) \equiv (0,\pi)$ or $(\pi,0)$, $\vec{K}_2 = -\vec{K} \Longrightarrow \vec{K} - \vec{K}_2 = 2\vec{K} = \vec{K}_1$. At these points, $\vec{K}$ is in the same direction as $\hat{\rho}_2$. From these observations, and equations (2.64) and (2.142), it easily follows that

$$\begin{aligned} {}_E\Gamma_P(\vec{K}-\vec{K}_2, \vec{K}_2) &= \tfrac{-3K^2}{\sqrt{2}} \cdot \tfrac{k_0 + j\sqrt{2}K}{k_0^2 + 2K^2} \\ \text{and} \qquad & \\ {}_E\Gamma_P(\vec{K}_2, \vec{K}-\vec{K}_2) &= \tfrac{+3K_2^2}{\sqrt{2}} \cdot \tfrac{k_0 + j\sqrt{2}K_2}{k_0^2 + 2K_2^2} \,. \end{aligned} \tag{B.59}$$

However, from (B.57) and noting that, at the stationary points, $\phi_0 = \phi_0' = 0$, we have

$$K \approx K_2 \,.$$

Thus, from (B.59), equation (B.55) is established and the contribution from the "electromagnetic" portion of (B.54) vanishes.

Next the hydrodynamic effects, entering (B.55) firstly by virtue of the hydrodynamic coupling coefficient, ${}_H\Gamma$ found in the overall coupling coefficient, Γ_P, of the various power spectral densities, must be addressed. It is easy to show for the stipulations on the K's given above that the magnitude of ${}_H\Gamma$ is in fact k_0, which is the maximum that this parameter can be. However, it must be remembered that the ocean spectra, $S(\cdot)$'s, appear as products in each of the power density expressions.

For the stationary points, only $S(\pm\vec{k}_0)$ and $S(\pm 2\vec{k}_0)$ appear. At HF, k_0 is of sufficient size that the ocean waves with the same wavenumber carry very little energy in comparison to the spectral maximum. Therefore, the contribution of the hydrodynamic effects to the Doppler spectral densities in (B.54) may be neglected. This argument could have been used for the electromagnetic portion of these spectral densities also as long as it could be verified that the electromagnetic coupling coefficient did not contain singularities at the points in question.

On the basis of the foregoing, it is clear that from equation (B.54),

$$\mathcal{P}_{2P,2T}(\omega_d) + \mathcal{P}_{2T,2P}(\omega_d) \approx 0 \; . \tag{B.60}$$

The discussion presented above was necessary because no constraints were placed on the receiving antenna. As usual, for a narrow beam receiver, equation (B.60) can be deduced very simply. For all parts of the ensemble average given in (B.44). narrow beam reception dictates that one of the wavevectors vanish. The first piece of the average leads to zero result as discussed in conjunction with equation (B.46). The second piece requires $\vec{K}_4 = \vec{K}_2 \approx 2k_0 \cos\phi_0 \hat{N}$ rather than $2k_0 \cos\phi_0' \hat{N}'$ when the receiving beam is narrow. Equation (B.45) then gives $\vec{K}_3 = \vec{K}_1 \approx \vec{0}$ and $S(m_1 \vec{K}_1) = \vec{0}$ which violates the surface assumptions. Similarly, in the third piece of the average found in (B.44), $\vec{K}_3 = \vec{K}_2 \approx 2k_0 \cos\phi_0 \hat{N}$, and again $\vec{K}_1 \approx \vec{0}$, which as before is not physically realizable.

On the basis of the preceding arguments, it must be concluded that, irrespective of the receiving system, the field due to double "patch" scatter and that due to a single scatter near the transmitter followed by another at the remote elliptical surface patch are essentially uncorrelated.

B.5.2 The Cross-correlations $\mathcal{R}_{2P,2R}(\tau)$ and $\mathcal{R}_{2R,2P}(\tau)$

By analogy to equations (B.42) and (B.47), the cross-correlation of the field from a double patch scatter with that produced by a single scatter at the patch followed by

another at the receiver may be written as

$$\mathcal{R}_{2P,2R}(\tau) = \frac{A_r}{2\eta_0} < \left(E_{0_n}^+\right)_{2P}(t_0, t+\tau)\left(E_{0_n}^+\right)_{2R}^*(t_0, t) >$$
and
$$\mathcal{R}_{2R,2P}(\tau) = \frac{A_r}{2\eta_0} < \left(E_{0_n}^+\right)_{2R}(t_0, t+\tau)\left(E_{0_n}^+\right)_{2P}^*(t_0, t) > \ . \tag{B.61}$$

The wave vectors $\vec{K}_3$ and $\vec{K}_4$ may be allowed to retain their meaning as in Appendix B.5.1, while $\vec{K}_1$ is taken as a surface wave vector on the remote patch and $\vec{K}_2$ is near the receiver. Then, equations completely analogous to the power spectral densities of (B.49), (B.51), and (B.53) may be written for the present case. The only significant differences in the results are that $\vec{K}_1$ replaces $\vec{K}_2$ and $\Gamma_R^*(\vec{K}_1, \hat{\rho}'_{12})$ replaces $\Gamma_T^*(\vec{K}_1, \hat{\rho}'_2)$. For all of the same reasons as outline in Appendix B.5.1, it transpires that for a general receiving system

$$\mathcal{P}_{2P,2R}(\omega_d) + \mathcal{P}_{2R,2P}(\omega_d) \approx 0 \ . \tag{B.62}$$

As before, if narrow beam reception is imposed, equation (B.62) follows more readily. Since no new insights manifest themselves in writing down the complete power spectral densities for this situation, they are omitted here.

B.6 The Cross-correlation of the Second-order Fields Due to Scatter at the Transmitter and Receiver

The final portions of $\mathcal{R}(\tau)$ in equation (3.35) involve the second-order fields in which for one case one of the two scatters occurs near the transmitter and in the other case one of the scatters occurs near the receiver. In each instance, the other scatter occurs on the remote patch. In keeping with the notation throughout this appendix, we write

$$\mathcal{R}_{2T,2R}(\tau) = \frac{A_r}{2\eta_0} < \left(E_{0_n}^+\right)_{2T}(t_0, t+\tau)\left(E_{0_n}^+\right)_{2R}^*(t_0, t) >$$
and
$$\mathcal{R}_{2R,2T}(\tau) = \frac{A_r}{2\eta_0} < \left(E_{0_n}^+\right)_{2R}(t_0, t+\tau)\left(E_{0_n}^+\right)_{2T}^*(t_0, t) > \ . \tag{B.63}$$

If it is agreed to use $\vec{K}_1$ and $\vec{K}_4$ for the wave vectors of the scatterers near the transmitter and receiver, respectively, and $\vec{K}_2$ and $\vec{K}_3$ as similar quantities at the remote patch, equation (B.63), based on appropriately modified equations (3.28) and (3.29), becomes

$$\mathcal{R}_{2T,2R}(\tau) = \frac{A_r}{2\eta_0}\left\{\frac{\eta_0^2 k_0^4 \left|I_0 \Delta\ell\right|^2 (\Delta\rho_s)^2}{(2\pi)^3 \rho_{0s}\left[\rho_{0s}^2 - \left(\frac{\rho}{2}\right)^2\right]}\right\} \sum_{\vec{K}_1,\omega_1}\sum_{\vec{K}_2,\omega_2}\sum_{\vec{K}_3,\omega_3}\sum_{\vec{K}_4,\omega_4} {}_E\Gamma_T(\vec{K}_1,\hat{\rho}_2)\,{}_E\Gamma_R^*(\vec{K}_3,\hat{\rho}_{12})$$
$$\cdot\, e^{j\frac{\vec{d}}{2}\cdot(\vec{K}_2-\vec{K}_3)} e^{j\rho_{0s}(K_2\cos\phi_0 - K_3\cos\phi_0')} e^{-j\vec{\rho}\cdot\vec{K}_4} < {}_1P_{\vec{K}_1,\omega_1}\,{}_1P_{\vec{K}_2,\omega_2}\,{}_1P^*_{\vec{K}_3,\omega_3}\,{}_1P^*_{\vec{K}_4,\omega_4} >$$
$$\cdot\, e^{j(\omega_1+\omega_2)(t+\tau)} e^{-j(\omega_3+\omega_4)(t)} \sqrt{K_2\cos\phi_0}\sqrt{K_3\cos\phi_0'}\, F(\rho_{01},\omega_0) F(\rho_{02},\omega_0)$$
$$\cdot\, F^*(\rho_{01}',\omega_0) F^*(\rho_{02}',\omega_0) \mathrm{Sa}\left[\frac{\Delta\rho_s}{2}\left(\frac{K_2}{\cos\phi_0} - 2k_0\right)\right] \mathrm{Sa}\left[\frac{\Delta\rho_s}{2}\left(\frac{K_3}{\cos\phi_0'} - 2k_0\right)\right] \quad \text{(B.64)}$$

The ensemble average in this equation may be expanded as

$$< {}_1P_{\vec{K}_1,\omega_1}\,{}_1P_{\vec{K}_2,\omega_2}\,{}_1P^*_{\vec{K}_3,\omega_3}\,{}_1P^*_{\vec{K}_4,\omega_4} > = < {}_1P_{\vec{K}_1,\omega_1}\,{}_1P_{\vec{K}_2,\omega_2} >< {}_1P^*_{\vec{K}_3,\omega_3}\,{}_1P^*_{\vec{K}_4,\omega_4} >$$
$$+ < {}_1P_{\vec{K}_1,\omega_1}\,{}_1P^*_{\vec{K}_3,\omega_3} >< {}_1P_{\vec{K}_2,\omega_2}\,{}_1P^*_{\vec{K}_4,\omega_4} >$$
$$+ < {}_1P_{\vec{K}_1,\omega_1}\,{}_1P^*_{\vec{K}_4,\omega_4} >< {}_1P_{\vec{K}_2,\omega_2}\,{}_1P^*_{\vec{K}_3,\omega_3} > \quad \text{(B.65)}$$

After the manner of Appendices (B.3)–(B.5), the three terms of equation (B.65) may be treated separately. The first two terms will produce power spectral densities at discrete values of ω_d exactly as was seen in equations (B.25) and (B.31) for $\mathcal{P}_{2T,1}(\omega_d)$ and $\mathcal{P}_{2T,3}(\omega_d)$, respectively. In the same way as was done for those expressions, it may be shown that here

$$\begin{aligned} &\mathcal{P}_{2T,2R,1}(\omega_d) + \mathcal{P}_{2R,2T,1}(\omega_d) \approx 0 \\ \text{and} \quad &\\ &\mathcal{P}_{2T,2R,2}(\omega_d) + \mathcal{P}_{2R,2T,2}(\omega_d) \approx 0\,. \end{aligned} \quad \text{(B.66)}$$

However, the third average in (B.65) leads to a power spectral density expression which is different enough from the first two to warrant further comment. Implementing the usual procedures for obtaining Doppler power spectral densities, it transpires that

$$\mathcal{P}_{2T,2R,3}(\omega_d) + \mathcal{P}_{2R,2T,3}(\omega_d) = \frac{A_r \eta_0 k_0^4 \left|I_0 \Delta\ell\right|^2 (\Delta\rho_s)^2}{4\cdot(2\pi)^2 \rho_{0s}\left[\rho_{0s}^2 - \left(\frac{\rho}{2}\right)^2\right]} \sum_{m_1=\pm1}\sum_{m_2=\pm1} \int_{-\pi}^{\pi}\int_{0}^{\infty}\int_{-\pi}^{\pi}\int_{0}^{\infty}$$

$$\Big\{S_1(m_1\vec{K}_1)S_1(m_2\vec{K}_2)\mathrm{Re}\left[{}_E\Gamma_T(\vec{K}_1,\hat{\rho}_2)\,{}_E\Gamma_R^*(\vec{K}_1,\hat{\rho}_{12})e^{-j\vec{\rho}\cdot\vec{K}_1}\right]$$
$$\cdot K_2^2\cos\phi_0\,|F(\rho_{01},\omega_0)F(\rho_{02},\omega_0)|^2\cdot \mathrm{Sa}^2\left[\frac{\Delta\rho_s}{2}\left(\frac{K_2}{\cos\phi_0}-2k_0\right)\right]$$
$$\cdot\,\delta\left(\omega_d+m_1\sqrt{gK_1}+m_2\sqrt{gK_2}\right)K_1\Big\}\,dK_1d\theta_{\vec{K}_1}dK_2d\theta_{\vec{K}_2}\,. \qquad \text{(B.67)}$$

The integrand here is similar to that for $\mathcal{P}_{2T,2}(\omega_d)$ in equation (B.22). As such, the Doppler power spectral density here is a continuum in ω_d. There are, however, two very important differences between (B.22) and (B.67), they being (1) the factor $e^{-j\vec{\rho}\cdot\vec{K}}$ appearing in the latter and (2) the product of the coupling coefficients is ${}_E\Gamma_T\,{}_E\Gamma_R^*$ rather than $|{}_E\Gamma_T|^2$. These differences cause this component of the power spectral density to be oscillatory and permit it to assume both positive and negative values. However, it may be shown numerically that these values are not significant, even at their maxima, when compared to the other pieces of the power spectral density. As well, the average power content obtained from $\int_{\omega_d}\mathcal{P}(\omega_d)d\omega_d$ is negligible. This is true for both monostatic and bistatic operation and, consequently, this component is not pursued further here.

B.7 The Relationship Between $S_1(K)$ and the Pierson-Moskowitz Spectrum

The first-order portion of the scattering surface, ${}_1\xi(x,y,t)$, was characterized in equation (3.12) as

$${}_1\xi(x,y,t)=\sum_{\vec{K},\omega}{}_1P_{\vec{K},\omega}e^{j\vec{K}\cdot\vec{\rho}}e^{j\omega t} \qquad \text{(B.68)}$$

where the various quantities are defined throughout Section 3.2.1. The relationship between the first-order Fourier coefficients, ${}_1P_{\vec{K},\omega}$, and the power spectral density, $S_1(\vec{K},\omega)$, is given by equation (3.7) provided the two quantities under discussion are appropriately subscripted. However, in Section 3.6.1, the Pierson-Moskowitz [60] model, $S_{PM}(K)$, for the non-directional part of the ocean power spectrum given in equation (3.78) was implemented in calculating the HF Doppler cross section of the

ocean surface. The question as to how the general form, $S_1(K)$, used throughout the *derivation* of the cross section equations is related to $S_{PM}(K)$ used in the *calculation* of those cross sections must, therefore, be addressed. The basis of the relationship has been formulated by Walsh [81] and is repeated here to give continuity to the final steps of the process derived below.

At the outset, in our notation, Pierson [61] defines the random surface, ${}_1\xi(x,y,t)$, as

$$ {}_1\xi(x,y,t) = \int_0^{\infty}\int_{-\pi}^{\pi} \cos\left[\frac{\omega^2}{g}(x\cos\theta + y\sin\theta) - \omega t + \epsilon(\omega,\theta)\right] \sqrt{S'_{PM}(\omega,\theta)d\omega d\theta}\,. \tag{B.69} $$

Here, the randomness is introduced through the phase term, $\epsilon(\omega,\theta)$, which is uniformly distributed on $0 < \theta < 2\pi$, and the surface spectrum is $S'_{PM}(\omega,\theta)$ where $\theta = \tan^{-1}\left(\frac{y}{x}\right)$. Pierson argues that (B.69) represents a zero-mean stationary Gaussian process as was also imposed in (B.68) via the definition of the Fourier surface coefficients in Section 3.2.1. It might be noted that Pierson's $S'_{PM}(\omega,\theta)\,d\omega$ is the equivalent of $S_{PM}(K,\theta)\,dK$ where $S_{PM}(K,\theta)$ is Pierson's spectrum expressed in terms of wavenumber. The aim is, then, to relate our $S_1(K,\theta)\,dK$ to $S_{PM}(K,\theta)\,dK$.

It is not difficult to verify that, for a real surface, the Fourier surface coefficients in equation (B.68) may be cast as

$$ {}_1P_{\vec{K},\omega} = \frac{1}{2}\left[P_{\vec{K}}e^{j\epsilon(\vec{K})}\delta_K\left(\omega + \sqrt{gK}\right) + P_{-\vec{K}}e^{-j\epsilon(-\vec{K})}\delta_K\left(\omega - \sqrt{gK}\right)\right] \tag{B.70} $$

with $P_{\vec{K}} = P^*_{\vec{K}}$ where $*$ denotes the complex conjugate (i.e. $P_{\vec{K}}$ is real), $\epsilon(\vec{K})$ is a random phase term and $\delta_K(\cdot)$ is the Kronecker delta defined such that

$$ \delta_K\left(\omega \pm \sqrt{gK}\right) = \begin{cases} 1, & \omega = \mp\sqrt{gK} \\ 0, & \text{otherwise.} \end{cases} $$

Also, implicit in (B.70) is the fact that the linear dispersion relationship of equation (3.9) has been invoked to give this result for ${}_1P_{\vec{K},\omega}$. This expression will now be used to determine the relationship between the $S_1(K,\theta)$ used throughout this work and $S_{PM}(K,\theta)$.

Substituting (B.70) into (B.68) and carrying out the necessary algebra leads, for the surface to first order, to

$$ {}_1\xi(x,y,t) = \sum_{\vec{K}} P_{\vec{K}} \cos\left[\vec{K}\cdot\vec{\rho} - \sqrt{gK}t + \epsilon(\vec{K})\right] . \tag{B.71} $$

Allowing the fundamental spatial period to approach infinity, as in Section 3.4.2.1 following equation (3.40), the Fourier coefficients become

$$ P_{\vec{K}} = \sqrt{S_1(K_x K_y) dK_x dK_y} \tag{B.72} $$

and the summation of (B.71) reduces to the integral form

$$ {}_1\xi(x,y,t) = \int_{-\infty}^{\infty}\int_{-\infty}^{\infty} \cos\left[\vec{K}\cdot\vec{\rho} - \sqrt{gK}t + \epsilon(\vec{K})\right] \sqrt{S_1(K_x K_y) dK_x dK_y} . \tag{B.73} $$

it being understood that $S_1(K_x, K_y)$ is the first-order surface spectrum. Before comparing this result to Pierson's formulation in (B.69), a change to polar coordinates is effected via

$$ \begin{aligned} dK_x dK_y &= K dK d\theta \\ \vec{\rho} &= x\hat{x} + y\hat{y} \\ \vec{K} &= K\cos\theta\hat{x} + K\sin\theta\hat{y} . \end{aligned} $$

Then, equation (B.73) may be equivalently presented as

$$ {}_1\xi(x,y,t) = \int_0^{\infty}\int_{-\pi}^{\pi} \cos\left[K(x\cos\theta + y\sin\theta) - \sqrt{gK}\,t + \epsilon(K,\theta)\right] \sqrt{S_1(K_x K_y) K dK d\theta} . \tag{B.74} $$

Finally, it is noted that since $\omega = \sqrt{gK}$,

$$ dK = 2\sqrt{\frac{K}{g}} d\omega , $$

which means that

$$ \begin{aligned} {}_1\xi(x,y,t) \;=\; & \int_0^{\infty}\int_{-\pi}^{\pi} \cos\left[\frac{\omega^2}{g}(x\cos\theta + y\sin\theta) - \omega t + \epsilon(\omega,\theta)\right] \\ & \cdot \sqrt{2K\sqrt{\frac{K}{g}} S_1(K_x, K_y) d\omega d\theta} . \end{aligned} \tag{B.75} $$

Clearly, our representation of the surface in (B.75) agrees with Pierson's model in (B.69) provided

$$2K\sqrt{\frac{K}{g}}S_1(K_x, K_y) = S'_{PM}(\omega, \theta)$$

or

$$S_1(K_x, K_y) = \frac{1}{2}\frac{g^{\frac{1}{2}}}{K^{\frac{3}{2}}}S'_{PM}(\omega, \theta)\ .$$

That is, from (B.72), the two models agree if our Fourier coefficients are written as

$$P_{\vec{K}} = \sqrt{\frac{1}{2}\frac{g^{\frac{1}{2}}}{K^{\frac{3}{2}}}S'_{PM}(\omega, \theta)dK_x dK_y}\ . \tag{B.76}$$

This provides the necessary starting point for comparing our non-directional ocean spectrum with the Pierson-Moskowitz model.

In the usual manner of developing the surface spectral density, the ensemble average, $< \cdot >$, of the Fourier coefficients is considered. Using equation (B.70),

$$\begin{aligned} < {}_1P_{\vec{K},\omega 1}P^*_{\vec{K}',\omega'} > \ = \ & \frac{1}{4} < \left\{ P_{\vec{K}}\, e^{j\epsilon(\vec{K})}\delta_K\left(\omega + \sqrt{gK}\right) + P_{-\vec{K}}\, e^{-j\epsilon(-\vec{K})}\delta_K\left(\omega - \sqrt{gK}\right)\right\} \\ & \cdot \left\{ P_{\vec{K}'}\, e^{j\epsilon(\vec{K}')}\delta_K\left(\omega' + \sqrt{gK'}\right) + P_{-\vec{K}'}e^{-j\epsilon(-\vec{K}')}\delta_K\left(\omega' - \sqrt{gK'}\right)\right\} > . \end{aligned}$$

and, given that the randomness lies in the phase factors,

$$\begin{aligned} < {}_1P_{\vec{K},\omega 1}P^*_{\vec{K}',\omega'} > \ = \ & \frac{1}{4}\left\{ P_{\vec{K}}P_{\vec{K}'}\delta_K\left(\omega + \sqrt{gK}\right)\delta_K\left(\omega' + \sqrt{gK'}\right) < e^{j\left[\epsilon(\vec{K}) - \epsilon(\vec{K}')\right]} > \right. \\ & + P_{-\vec{K}}P_{-\vec{K}'}\delta_K\left(\omega - \sqrt{gK}\right)\delta_K\left(\omega' - \sqrt{gK'}\right) < e^{-j\left[\epsilon(-\vec{K}) - \epsilon(-\vec{K}')\right]} > \\ & + P_{\vec{K}}P_{-\vec{K}'}\delta_K\left(\omega + \sqrt{gK}\right)\delta_K\left(\omega' - \sqrt{gK'}\right) < e^{j\left[\epsilon(\vec{K}) + \epsilon(-\vec{K}')\right]} > \\ & \left. + P_{-\vec{K}}P_{\vec{K}'}\delta_K\left(\omega - \sqrt{gK}\right)\delta_K\left(\omega' + \sqrt{gK'}\right) < e^{-j\left[\epsilon(-\vec{K}) + \epsilon(\vec{K}')\right]} > \right\}\ . \end{aligned} \tag{B.77}$$

As usual, (see equation (3.7)) the only non-zero contributions in (B.77) occur when the exponentials become unity everywhere. The last two terms cannot meet this stipulation leaving

$$< {}_1P_{\vec{K},\omega 1}P^*_{\vec{K}',\omega} >= \frac{1}{4}\left\{ P^2_{\vec{K}}\delta_K\left(\omega + \sqrt{gK}\right) + P^2_{-\vec{K}}\delta_K\left(\omega - \sqrt{gK}\right)\right\}\ .$$

Then, from (B.76)

$$< {}_1P_{\vec{K},\omega}\,{}_1P^*_{\vec{K}',\omega'} > \;=\; \frac{1}{4}\left\{\frac{1}{2}\frac{g^{\frac{1}{2}}}{K^{\frac{3}{2}}}S_{PM}(\omega,\theta)\delta_K\left(\omega+\sqrt{gK}\right)\right.$$
$$\left.+\,\frac{1}{2}\frac{g^{\frac{1}{2}}}{K^{\frac{3}{2}}}S_{PM}(\omega,\theta+\pi)\delta_K\left(\omega-\sqrt{gK}\right)\right\}dK_xdK_y\;. \quad \text{(B.78)}$$

Using the differential form of equation (3.7), along with the last result, gives

$$S_1(K_x,K_y,\omega)dK_xdK_yd\omega \;=\; \frac{1}{4}\left\{\frac{1}{2}\frac{g^{\frac{1}{2}}}{K^{\frac{1}{2}}}\sum_{m=\pm1}S_{PM}\left(\omega,\theta+\left(\frac{1-m}{2}\right)\pi\right)\right.$$
$$\left.\cdot\;\delta_K\left(\omega+m\sqrt{gK}\right)\right\}dK_xdK_y\;.$$

Since

$$S_1(K_x,K_y,\omega)=\frac{S_1(K,\theta,\omega)}{K}\;,$$

(see, for example, Tucker [1]) and $dK_xdK_y = KdKd\theta$, it follows that

$$S_1(\vec{K},\omega)dKd\theta d\omega \;=\; \frac{1}{4}\left\{\frac{1}{2}\frac{g^{\frac{1}{2}}}{K^{\frac{1}{2}}}\sum_{m=\pm1}S_{PM}\left(\omega,\theta+\left(\frac{1-m}{2}\right)\pi\right)\right.$$
$$\left.\cdot\;\delta_K\left(\omega+m\sqrt{gK}\right)\right\}dKd\theta\;. \quad \text{(B.79)}$$

Then, using equation (3.10) and the fact that

$$S_{PM}(\omega,\theta)=S_{PM}(K,\theta)\frac{dK}{d\omega}=S_{PM}(K,\theta)\cdot\left(2\sqrt{\frac{K}{g}}\right)\;,$$

$$\frac{1}{2}\sum_{m=\pm1}S_1(m\vec{K})\delta\left(\omega+m\sqrt{gK}\right)d\omega=\frac{1}{4}\left\{\sum_{m=\pm1}S_{PM}(m\vec{K})\delta_K\left(\omega+m\sqrt{gK}\right)\right\} \quad \text{(B.80)}$$

where

$$S_1(m\vec{K})=S_1\left(K,\theta+\left(\frac{1-m}{2}\right)\pi\right)$$

and $\delta(\cdot)$ on the left of (B.80) is the Dirac delta function. Invoking the identity

$$\delta\left(\omega+m\sqrt{gK}\right)d\omega=\delta_K\left(\omega+m\sqrt{gK}\right)\;,$$

we finally reach the conclusion that

$$S_1(m\vec{K})=\frac{1}{2}S_{PM}(m\vec{K})\;. \quad \text{(B.81)}$$

Given the directional spectrum characteristic of equation (3.76), the non-directional parts of (B.81) are related as

$$S_1(K) = \frac{1}{2} S_{PM}(K) \; . \tag{B.82}$$

The significance of this result is that everywhere that $S_1(K)$ appears in the cross section expressions, $\frac{1}{2}S_{PM}(K)$ should be used for illustrative purposes. It therefore transpires that the first-order cross section will be 3 dB lower than that appearing in the literature for the monostatic case ([24], [54], [8]). Similarly, the second-order monostatic cross section model will be 6 dB lower than previously reported since all of its components contain a product of $S_1(\cdot)$ functions (see equations (3.102), (3.126) and (3.134)).

B.8 A Note on the High-Doppler Tails of $\sigma_{2T}(\omega_d)$, $\sigma_{2R}(\omega_d)$, and Srivastava's Model

Srivastava [54] developed a monostatic result for the second-order cross section component involving a single scatter at the transmitter followed by another on a distant surface patch corresponding to $\sigma_{2T}(\omega_d)$ of this work. However, the high-Doppler tails of Srivastava's model are very flat beyond the $\pm 2\omega_d$ singularities. While here the $\sigma_{2T}(\omega_d)$ and the $\sigma_{2R}(\omega_d)$ tails also enhance the overall second-order result beyond that of the $\sigma_{2P}(\omega_d)$ patch scatter portion, the fall-off of the tails is much more rapid than in Srivastava's presentation. This difference is addressed here and may be attributed to the forms of the coupling coefficient.

Using the notation presented throughout this work, the magnitude square of Srivastava's coupling coefficient, Γ_S, for what corresponds to the $\sigma_{2T}(\omega_d)$ cross section component, may be written as

$$|\Gamma_S|^2 = \frac{\left[(\vec{K}_2 + 2\vec{K}_1)\cdot\vec{K}_1\right]^2}{\left|(\vec{K}_2 + \vec{K}_1)\cdot\vec{K}_1\right|} \tag{B.83}$$

where $\left|\vec{K}_2\right| = K_2 = 2k_0$. Using $\theta_{\vec{K}_1}$ and $\theta_{\vec{K}_2}$ as the directions of the wave vectors $\vec{K}_1$ and $\vec{K}_2$, respectively,

$$|\Gamma_S|^2 = \frac{\left[2k_0K_1\cos(\theta_{\vec{K}_2} - \theta_{\vec{K}_1}) + 2K_1^2\right]^2}{\left|2k_0K_1\cos(\theta_{\vec{K}_2} - \theta_{\vec{K}_1}) + K_1^2\right|} ,$$

and this can be written as

$$|\Gamma_S|^2 = \frac{\left[2k_0\cos(\theta_{\vec{K}_2} - \theta_{\vec{K}_1}) + 2K_1\right]^2}{\left|\frac{2k_0\cos(\theta_{\vec{K}_2} - \theta_{\vec{K}_1})}{K_1} + 1\right|} . \tag{B.84}$$

Now, in the high-Doppler tails, K_1 increases without bound, theoretically. This means that $|\Gamma_S|^2$, as given in (B.84), similarly increases without bound; i.e. for large K_1,

$$|\Gamma_S|^2 \longrightarrow \left[2k_0\cos(\theta_{\vec{K}_2} - \theta_{\vec{K}_1}) + 2K_1\right]^2 . \tag{B.85}$$

The effect of this ever-increasing factor for large $|\omega_d|$ is mitigated by the reducing ocean spectrum, $S_1(\vec{K}_1)$, and the overall effect is to produce spectral tails which fall off more slowly than actual radar spectra would indicate.

From equations (2.87) and (2.146), it is not difficult to show that, for $\phi_0 = 0$ (i.e. the monostatic case)

$$|_E\Gamma_T|^2 = \frac{k_0^2\left[K_1^2 + k_0K_1\cos(\theta_{\vec{K}_2} - \theta_{\vec{K}_1})\right]^2}{\left\{\left[K_1^2 + 2k_0K_1\cos(\theta_{\vec{K}_2} - \theta_{\vec{K}_1})\right]\cdot\left[K_1^2 + 2k_0K_1\cos(\theta_{\vec{K}_2} - \theta_{\vec{K}_1})\right.\right.} \\ \left.\left. -2k_0\sqrt{\left|K_1^2 + 2k_0K_1\cos(\theta_{\vec{K}_2} - \theta_{\vec{K}_1})\right| - k_0^2}\right]\right\} . \tag{B.86}$$

Dividing numerator and denominator of the last equation by K_1^4,

$$|_E\Gamma_T|^2 = \frac{k_0^2\left[1 + \frac{k_0}{K_1}\cos(\theta_{\vec{K}_2} - \theta_{\vec{K}_1})\right]^2}{\left\{\left[1 + \frac{2k_0\cos(\theta_{\vec{K}_2} - \theta_{\vec{K}_1})}{K_1}\right]\left[1 + \frac{2k_0\cos(\theta_{\vec{K}_2} - \theta_{\vec{K}_1})}{K_1}\right.\right.} \\ \left.\left. -2k_0\sqrt{\left|\frac{1}{K_1^2} + \frac{2k_0\cos(\theta_{\vec{K}_2} - \theta_{\vec{K}_1})}{K_1^3}\right| - \left(\frac{k_0}{K_1}\right)^2}\right]\right\} . \tag{B.87}$$

In this form, it is easily seen that as K_1 becomes unbounded

$$|_E\Gamma_T|^2 \longrightarrow k_0^2 . \tag{B.88}$$

Thus, as K_1, and consequently ω_d, increases, $|_E\Gamma_T|^2$ has an upper limit unlike Srivastava's coefficient. The ocean spectrum is, as before, decreasing rapidly so that the combined effect is that the high Doppler tails of $\sigma_{2T}(\omega_d)$ should essentially follow that of the $S_1(K_1)$. This concludes the explanation of the difference between $\sigma_{2T}(\omega_d)$ and Srivastava's corresponding monostatic model.

As a concluding remark, it may be noted that in the $\sigma_{2R}(\omega_d)$ cross section component of equation (3.134), it is readily shown that, for $\phi_0 = 0$

$$\lim_{K_2 \to \infty} |_E\Gamma_R|^2 = k_0^2 \cos(\theta_{\vec{K}_2} + \theta_{\vec{K}_1}) \leq k_0^2 \, .$$

Clearly, from (B.88),

$$\lim_{K_2 \to \infty} |_E\Gamma_R|^2 \leq \lim_{K_1 \to \infty} |_E\Gamma_T|^2 \, ,$$

so that over the whole angle integration intervals for $\theta_{\vec{K}_2}$ and $\theta_{\vec{K}_1}$, the tails of $\sigma_{2T}(\omega_d)$ will, in our formulation, be higher than those of $\sigma_{2R}(\omega_d)$. This is really a result of the different approximations used in determining these two portions of the cross section and should not be taken to have physical significance. As was depicted in Section 3.6.6, even though this effect is evident, the differences in the $\sigma_{2T}(\omega_d)$ and $\sigma_{2R}(\omega_d)$ are minimal.

B.9 The Hasselmann Coupling Coefficient – Near-Forward Scattering

The hydrodynamic coupling coefficient for deep water waves arising from Hasselmann's [59] analysis is given in equation (3.18) as

$$_H\Gamma = \frac{1}{2}\left\{K_1 + K_2 + \frac{g}{\omega_1\omega_2}\left(K_1K_2 - \vec{K}_1 \cdot \vec{K}_2\right)\left(\frac{gK + (\omega_1 + \omega_2)^2}{gK - (\omega_1 + \omega_2)^2}\right)\right\} \qquad \text{(B.89)}$$

where $\omega_1 = m_1\sqrt{gK_1}$ and $\omega_2 = m_2\sqrt{gK_2}$ as in equations (3.10) and (3.94). As usual, m_1, $m_2 = \pm 1$. Also, from the scatter analysis,

$$\vec{K} = \vec{K}_1 + \vec{K}_2 \approx 2k_0 \cos\phi_0 \hat{N} \, . \qquad \text{(B.90)}$$

Suppose that a scatter occurs very nearly on the line joining the transmitter to the receiver as depicted in Figure B.1a. Since for this situation, $\phi_0 \longrightarrow 90°$,

$$\vec{K} \longrightarrow 0\hat{N} ,$$

which means that the wavelength associated with K must be approaching infinity.

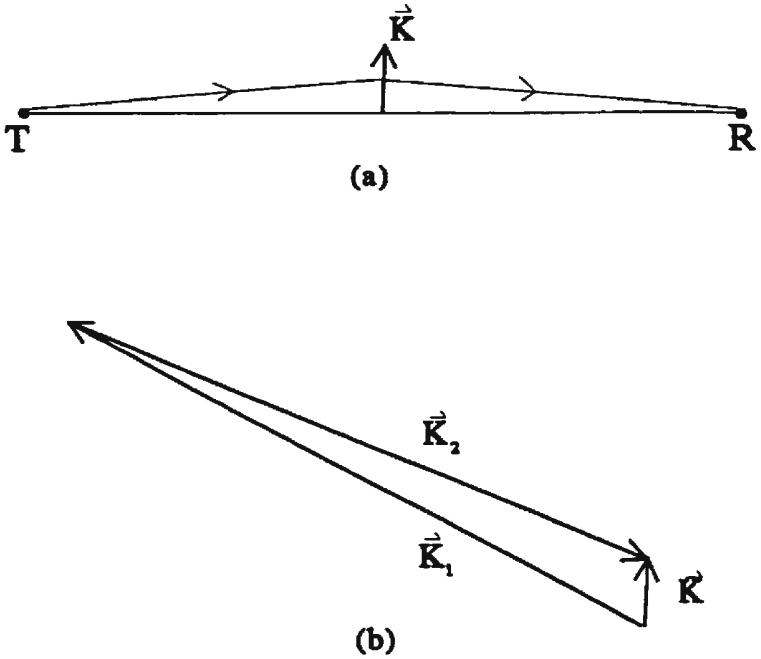

Figure B.1: (a) indicates the geometry of near-forward scattering. (b) indicates the relationship of typical wave vectors of the surface components responsible for the scatter.

Now, the individual waves which are capable of providing significant energy to the Doppler cross section must be very much shorter than this – i.e. K_1 and K_2 must both be very much greater than K. Thus, as depicted in Figure B.1b, for near-forward scatter, to a very good approximation,

$$\begin{aligned} \vec{K}_1 \approx -\vec{K}_2 &= \vec{K}_r , \text{ say,} \\ K_1 \approx K_2 &= K_r , \\ \text{and} \quad \vec{K}_1 \cdot \vec{K}_2 &\approx -K_r^2 . \end{aligned} \tag{B.91}$$

Using equation (B.91) in (B.89) along with the ω_1 and ω_2 definitions,

$$_H\Gamma = \frac{1}{2}\left\{ K_r + K_r + \frac{m_1 m_2 (K_r^2 + K_r^2)}{\sqrt{K_r^2}} \left(\frac{g(K + (2 + 2m_1 m_2)K_r)}{g(K - (2 + 2m_1 m_2)K_r)} \right) \right\}$$

$$= \frac{1}{2}\left\{2K_r + 2m_1m_2K_r\left(\frac{(K+(2+2m_1m_2)K_r)}{(K-(2+2m_1m_2)K_r)}\right)\right\} . \qquad \text{(B.92)}$$

Case 1: $m_1m_2 = +1$: Using the fact that $K_r \gg K$ for the forward scattering condition.

$$\begin{aligned} {}_H\Gamma &\approx \frac{1}{2}\left\{2K_r + 2K_r\left(\frac{4K_r}{-4K_r}\right)\right\} \\ &= 0 . \end{aligned} \qquad \text{(B.93)}$$

Case 2: $m_1m_2 = -1$: Now, (B.92) becomes

$$\begin{aligned} {}_H\Gamma &\approx \frac{1}{2}\left\{2K_r - 2K_r\left(\frac{K+0}{K-0}\right)\right\} \\ &= 0 . \end{aligned} \qquad \text{(B.94)}$$

Combining Case 1 and Case 2, it is thus established that as $\phi_0 \longrightarrow 90°$, ${}_H\Gamma \longrightarrow 0$, and the hydrodynamic contribution to $\sigma_{2P}(\omega_d)$ must be negligible for forward scatter.

Appendix C

Alternate Considerations of the Noise and Clutter Power Spectral Density Problem

In Section 4.2.2, the noise power spectral density for infinitely many pulses was developed using the results for a finite pulse train given in Section 4.2.1 In this appendix, an alternate approach is presented and is shown to lead to identical results. Some features of this analysis are used directly in Section 4.4 to determine the proper form of the transmit power spectral density to be used when calculating the received power spectral density for sea echo (clutter).

C.1 An Alternate Approach to the Noise Power Spectral Density Assuming Infinitely Many Pulses

The desire is to apply the expression in equation (4.1) to a pulse radar system. It is considered that pulse repetition period is T_L while the temporal width of the pulse is τ_0 as depicted in Figure 4.1. The pulse train is unbounded.

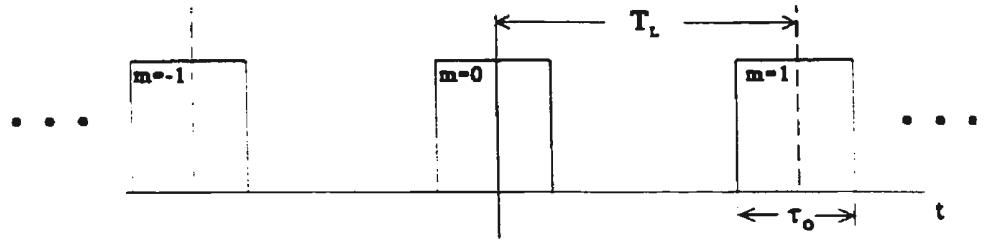

Figure C.1: An infinitely long pulse train, with pulse width τ_0 and repetition period T_L.

Thus, the noise, $n(t)$, at any time sampled by the receiving system may be characterized, using (4.1), as

$$\begin{aligned} n(t) &= \sum_{m=-\infty}^{\infty} \left[h\left(t - mT_L + \frac{\tau_0}{2}\right) - h\left(t - mT_L - \frac{\tau_0}{2}\right) \right] n_a(t) \\ &= \sum_{m=-\infty}^{\infty} \left[h\left(t - mT_L + \frac{\tau_0}{2}\right) - h\left(t - mT_L - \frac{\tau_0}{2}\right) \right] \\ &\quad \cdot \int_{\omega'} \left[h\left(\omega' + \frac{B}{2}\right) - h\left(\omega' - \frac{B}{2}\right) \right] e^{j\omega' t}\, e^{j\epsilon(\omega')} \\ &\quad \cdot \sqrt{S_N(\omega') \frac{d\omega'}{2\pi}} \ . \end{aligned} \tag{C.1}$$

A power spectral density for $n(t)$ may now be sought. Keeping in mind that the autocorrelation, $\mathcal{R}(t_1, t_2)$, for $n(t)$ is given in the usual sense by

$$\begin{aligned} \mathcal{R}_N(t_1, t_2) = < n(t_1) n^*(t_2) > &= \frac{1}{(2\pi)^2} \int_{\omega_2} \int_{\omega_1} e^{j\omega_1 t_1} e^{-j\omega_2 t_2} \\ &\quad \cdot < N(\omega_1) N^*(\omega_2) > d\omega_1 d\omega_2 \ , \end{aligned} \tag{C.2}$$

where $N(\cdot)$ is the Fourier transform of $n(\cdot)$, we first seek $N(\omega)$ – i.e. the Fourier transform of $n(t)$ in (C.1). Formally, because of the Heaviside functions in the summations

of (C.1),

$$N(\omega) = \sum_{m=-\infty}^{\infty} \int_{\omega'} \left[h\left(\omega' + \frac{B}{2}\right) - h\left(\omega' - \frac{B}{2}\right) \right] e^{j\epsilon(\omega')} \cdot \int_{mT_L - \frac{\tau_0}{2}}^{mT_L + \frac{\tau_0}{2}} e^{j(\omega' - \omega)t} dt \sqrt{S_N(\omega') \frac{d\omega'}{2\pi}} \quad . \tag{C.3}$$

The time integral in the transform, on changing the variable to $t' = t - mT_L$, becomes

$$\begin{aligned} \int_{\frac{-\tau_0}{2}}^{\frac{\tau_0}{2}} e^{j(\omega' - \omega)(t' + mT_L)} dt' &= e^{j(\omega' - \omega)mT_L} \cdot \frac{\left[e^{j(\omega' - \omega)\frac{\tau_0}{2}} - e^{-j(\omega' - \omega)\frac{\tau_0}{2}} \right]}{j(\omega' - \omega)} \\ &= \tau_0 e^{j(\omega' - \omega)mT_L} \cdot \frac{\left[e^{j(\omega' - \omega)\frac{\tau_0}{2}} - e^{-j(\omega' - \omega)\frac{\tau_0}{2}} \right]}{2j\left[(\omega' - \omega) \cdot \frac{\tau_0}{2} \right]} \\ &= \tau_0 e^{j(\omega' - \omega)mT_L} \mathrm{Sa}\left[(\omega' - \omega)\frac{\tau_0}{2} \right] \end{aligned} \tag{C.4}$$

where $\mathrm{Sa}[\cdot] = \dfrac{\sin[\cdot]}{[\cdot]}$. Substituting (C.4) into (C.3) leads to

$$N(\omega) = \tau_0 \int_{\omega'} \left[h\left(\omega' + \frac{B}{2}\right) - h\left(\omega' - \frac{B}{2}\right) \right] e^{j\epsilon(\omega')} \mathrm{Sa}\left[(\omega' - \omega)\frac{\tau_0}{2} \right] \cdot \sum_{m=-\infty}^{\infty} e^{j(\omega' - \omega)mT_L} \sqrt{S_N(\omega') \frac{d\omega'}{2\pi}} \quad . \tag{C.5}$$

Lathi [77] (Chapter 1) presents the identity

$$\sum_{m=-\infty}^{\infty} e^{jm\frac{2\pi}{T_P}t_d} = T_P \sum_{m=-\infty}^{\infty} \delta(t_d - mT_P) \tag{C.6}$$

where $\delta(\cdot)$ is the Dirac delta function, T_P is a fixed period and t_d is time. Examining the summation in (C.5) in view of (C.6) and identifying t_d as $(\omega' - \omega)$ and T_P as $\dfrac{2\pi}{T_L}$, the form of the sum is

$$\sum_{m=-\infty}^{\infty} e^{j(\omega' - \omega)mT_L} = \frac{2\pi}{T_L} \sum_{m=-\infty}^{\infty} \delta\left[(\omega' - \omega) - \frac{m2\pi}{T_L} \right] \quad .$$

The Fourier transform in equation (C.5) is then given by

$$N(\omega) = \frac{2\pi\tau_0}{T_L} \sum_{m=-\infty}^{\infty} \int_{\omega'} \left[h\left(\omega' + \frac{B}{2}\right) - h\left(\omega' - \frac{B}{2}\right) \right] e^{j\epsilon(\omega')} \delta\left[\omega' - \omega - \frac{m2\pi}{T_L} \right] \sqrt{S_N(\omega') \frac{d\omega'}{2\pi}} \cdot \mathrm{Sa}\left[(\omega' - \omega)\frac{\tau_0}{2} \right] \quad . \tag{C.7}$$

From (C.7) and given the usual argument that

$$< e^{j\epsilon(\omega_1')} e^{-j(\omega_2')} >= \begin{cases} 1, & \omega_1' = \omega_2' = \omega', \text{ say} \\ 0, & \text{otherwise,} \end{cases}$$

the autocorrelation in the integrand of equation (C.2) becomes

$$< N(\omega_1)N^*(\omega_2) > = 2\pi \left(\frac{\tau_0}{T_L}\right)^2 \sum_{m=-\infty}^{\infty} \sum_{n=-\infty}^{\infty} \int_{\omega'} \left[h\left(\omega' + \frac{B}{2}\right) - h\left(\omega' - \frac{B}{2}\right)\right]$$

$$\cdot \delta\left[\omega' - \omega_1 - \frac{m2\pi}{T_L}\right] \delta\left[\omega' - \omega_2 - \frac{n2\pi}{T_L}\right]$$

$$\cdot \mathrm{Sa}\left[(\omega' - \omega_1)\frac{\tau_0}{2}\right] \mathrm{Sa}\left[\omega' - \omega_2)\frac{\tau_0}{2}\right] S_N(\omega')d\omega' \,. \qquad \text{(C.8)}$$

The delta function constraint immediately requires that

$$\omega_1 - \omega_2 = (n - m)\frac{2\pi}{T_L}$$

so that, using one of the delta functions to evaluate the ω' integral, equation (C.8) may be written as

$$< N(\omega_1)N^*(\omega_2) > = 2\pi \left(\frac{\tau_0}{T_L}\right)^2 \sum_{m=-\infty}^{\infty} \sum_{n=-\infty}^{\infty}$$

$$\left[h\left(\omega_1 + \frac{m2\pi}{T_L} + \frac{B}{2}\right) - h\left(\omega_1 + \frac{m2\pi}{T_L} - \frac{B}{2}\right)\right]$$

$$\cdot \delta\left[\omega_1 - \omega_2 + (m - n)\frac{2\pi}{T_L}\right] \mathrm{Sa}\left[\frac{m2\pi\tau_0}{2T_L}\right]$$

$$\cdot \mathrm{Sa}\left[\left(\omega_1 - \omega_2 + \frac{m2\pi}{T_L}\right)\frac{\tau_0}{2}\right] S_N\left(\omega_1 + \frac{m2\pi}{T_L}\right) \,. \qquad \text{(C.9)}$$

Using the inverse Fourier transform expression given in equation (C.2), the autocorrelation function is

$$\mathcal{R}_N(t_1,t_2) = \frac{1}{2\pi}\left(\frac{\tau_0}{T_L}\right)^2 \int_{\omega_1} \sum_{m=-\infty}^{\infty}\sum_{n=-\infty}^{\infty}\left[h\left(\omega_1+\frac{m2\pi}{T_L}+\frac{B}{2}\right)\right.$$

$$\left.-h\left(\omega_1+\frac{m2\pi}{T_L}-\frac{B}{2}\right)\right]\cdot \ \mathrm{Sa}\left[m\pi\frac{\tau_0}{T_L}\right]\mathrm{Sa}\left[n\pi\frac{\tau_0}{T_L}\right]$$

$$\cdot\ S_N\left(\omega_1+\frac{m2\pi}{T_L}\right)e^{j\omega_1 t_1}e^{-jt_2\left[\omega_1+(m-n)\frac{2\pi}{T_L}\right]}d\omega_1 \qquad \text{(C.10)}$$

where the ω_2 integral has been executed via the delta function of (C.9). Defining

$$\tau = t_1 - t_2$$

and setting $\omega_1 = \omega$, this autocorrelation finally appears as

$$\mathcal{R}_N(\tau+t_2,t_2) = \left(\frac{\tau_0}{T_L}\right)^2\cdot\frac{1}{2\pi}\int_{\omega}\left[\sum_{m=-\infty}^{\infty}\left[h\left(\omega+\frac{m2\pi}{T_L}+\frac{B}{2}\right)-h\left(\omega+\frac{m2\pi}{T_L}-\frac{B}{2}\right)\right]\right.$$

$$\left.\cdot\,\mathrm{Sa}\left(m\pi\frac{\tau_0}{T_L}\right)S_N\left(\omega+\frac{m2\pi}{T_L}\right)\right]$$

$$\cdot\left[\sum_{n=-\infty}^{\infty}\mathrm{Sa}\left(\frac{n\pi\tau_0}{T_L}\right)e^{j(n-m)\frac{2\pi}{T_L}t_2}\right]\cdot e^{j\omega\tau}d\omega\,. \qquad \text{(C.11)}$$

The noise power spectral density, $\mathcal{P}_N(\omega,t)$, clearly follows from the Fourier transform of $\mathcal{R}_N(\tau+t_2,t_2)$ as

$$\mathcal{P}_N(\omega,t) = \left(\frac{\tau_0}{T_L}\right)^2\sum_{m=-\infty}^{\infty}\left\{\left[h\left(\omega+\frac{m2\pi}{T_L}+\frac{B}{2}\right)-h\left(\omega+\frac{m2\pi}{T_L}-\frac{B}{2}\right)\right]\right.$$

$$\left.\cdot\,\mathrm{Sa}\left(m\pi\frac{\tau_0}{T_L}\right)S_N\left(\omega+\frac{m2\pi}{T_L}\right)\right.$$

$$\left.\cdot\sum_{n=-\infty}^{\infty}\left\{\mathrm{Sa}\left(\frac{n\pi\tau_0}{T_L}\right)e^{j(n-m)\frac{2\pi}{T_L}t}\right\}\right\} \qquad \text{(C.12)}$$

where $t = t_2$. Therefore, as in Section 4.2.2, the power spectral density for the noise appears as a time dependent quantity.

In order to reduce the complexity of (C.12), an alternate form is sought for the second summation. To this end, it is noted that a periodic train of impulses, like that in Figure C.1, may be written as a Fourier series in the form

$$\sum_{n=-\infty}^{\infty}\left[h\left(t+nT_L+\frac{\tau_0}{2}\right)-h\left(t+nT_L-\frac{\tau_0}{2}\right)\right]=\sum_{n=-\infty}^{\infty}c_n e^{jn\frac{2\pi}{T_L}t} \qquad \text{(C.13)}$$

where c_n are the Fourier coefficients. These are given by

$$c_n=\frac{1}{T_L}\int_{\frac{-\tau_0}{2}}^{\frac{\tau_0}{2}} e^{-jn\frac{2\pi}{T_L}tdt}dt\ ,$$

which easily gives

$$c_n=\frac{\tau_0}{T_L}\mathrm{Sa}\left(n\pi\frac{\tau_0}{T_L}\right)\ . \qquad \text{(C.14)}$$

From equations (C.13) and (C.14), the noise power spectral density in (C.12) simplifies to

$$\begin{aligned}\mathcal{P}_N(\omega,t) \;=\; & \frac{\tau_0}{T_L}\sum_{m=-\infty}^{\infty}\left\{\left[h\left(\omega+\frac{m2\pi}{T_L}+\frac{B}{2}\right)-h\left(\omega+\frac{m2\pi}{T_L}-\frac{B}{2}\right)\right]\right.\\ & \left.\cdot\,\mathrm{Sa}\left(m\pi\frac{\tau_0}{T_L}\right)S_N\left(\omega+\frac{m2\pi}{T_L}\right)e^{-jm\frac{2\pi}{T_L}t}\right\}\\ & \cdot\sum_{n=-\infty}^{\infty}\left[h\left(t+nT_L+\frac{\tau_0}{2}\right)-h\left(t+nT_L-\frac{\tau_0}{2}\right)\right]\ . \qquad \text{(C.15)}\end{aligned}$$

Equation (C.15) is identical to that for infinitely many pulses given in equation (4.16). The equivalence of the two procedures is thus established. As noted earlier, some of the approach used here is implemented in Section 4.4 for the ocean clutter to allow a power spectral density for that quantity to be written down directly.

C.2 An Estimate of the Doppler Power Spectral Density for Sea Echo in the Presence of Noise

Using Pierson's model [61] of a one-dimensional stationary Gaussian process for a time function, $f(t)$, of limited bandwidth, B, (4.1) may be written as

$$f(t)=\int_B e^{j\omega t}e^{j\epsilon(\omega)}\sqrt{F_s(\omega)\frac{d\omega}{2\pi}} \qquad \text{(C.16)}$$

where

$$-\frac{B}{2} \leq \omega \leq \frac{B}{2}$$

and $F_s(\omega)$ is the power spectral density of $f(t)$. Now,

$$f(t) = \begin{cases} n(t), & \text{for the noise process} \\ c(t), & \text{for the clutter process} \end{cases} \tag{C.17}$$

where $n(t)$ and $c(t)$ are defined in equations (4.2) and (4.52), respectively, and a large number of pulses is assumed. Similarly,

$$F_s(\omega) = \begin{cases} \mathcal{P}_N(\omega), & \text{for the noise process} \\ \mathcal{P}_c(\omega), & \text{for the clutter process} \end{cases} \tag{C.18}$$

and sampling at the pulse centres is assumed. $\mathcal{P}_N(\omega)$ and $\mathcal{P}_c(\omega)$ are then given by equations (4.31) and (4.62), respectively. Since $\mathcal{P}_N(\omega)$ and $\mathcal{P}_c(\omega)$ are developed from ensemble averages using ideal conditions, they represent the "true" (i.e. best possible) power spectral densities of the noise and clutter.

The integral in equation (C.16) may be represented by the limit of a partial sum [61] as given by

$$f(t) = \lim_{\substack{\omega_{2p} \to \infty \\ (\omega_{2q+2} - \omega_{2q}) \to 0}} \sum_{q=0}^{p} e^{j(\omega_{2q+1}t)} e^{j\epsilon(\omega_{2q+1})} \sqrt{F_s(\omega_{2q+1}) \cdot \frac{\omega_{2q+2} - \omega_{2q}}{2\pi}} \; . \tag{C.19}$$

Equation (C.19) is then used to approximate a time series for the noise, $n(t)$, and the clutter, $c(t)$. The time function, $s(t)$, representing the sum of the clutter and noise signals received by the pulsed radar system is simply

$$s(t) = c(t) + n(t) \; . \tag{C.20}$$

The signal, $s(t)$, may be fast-Fourier-transformed (FFT) using any suitable algorithm (eg., the nfft$(\cdot)$ function from MATLAB [90] was used for the plots in Section 4.5.3). The magnitude-squared of FFT algorithm is a normalized estimate of the power spectral density, $S(f)$, and may be divided by the time series "length" to give the proper units of W/Hz. This is the so-called *periodogram* or sample spectrum.